PB83-238725

Modeling of Simulated Photochemical Smog with Kinetic Mechanisms

Systems Applications, Inc., San Rafael, CA

Prepared for

Environmental Sciences Research Lab.
Research Triangle Park, NC

May 83

U.S. Department of Commerce
National Technical Information Service
NTIS

TECHNICAL REPORT DATA
(Please read Instructions on the reverse before completing)

1. REPORT NO. EPA-600/3-83-043	2.	3. RECIPIENT'S ACCESSION NO. PB8 3 238725
4. TITLE AND SUBTITLE MODELING OF SIMULATED PHOTOCHEMICAL SMOG WITH KINETIC MECHANISMS		5. REPORT DATE May 1983
		6. PERFORMING ORGANIZATION CODE
7. AUTHOR(S) G. Z. Whitten, J. P. Killus and R. G. Johnson		8. PERFORMING ORGANIZATION REPORT NO.
9. PERFORMING ORGANIZATION NAME AND ADDRESS Systems Applications, Inc. 101 Lucas Valley Road San Rafael, CA 94903		10. PROGRAM ELEMENT NO. CDWA1A/01-0301 (FY-83)
		11. CONTRACT/GRANT NO. Contract No. 68-02-3281
12. SPONSORING AGENCY NAME AND ADDRESS Environmental Sciences Research Laboratory-RTP, NC Office of Research and Development U.S. Environmental Protection Agency Research Triangle Park, NC 27711		13. TYPE OF REPORT AND PERIOD COVERED Final Report (9/79-8/82)
		14. SPONSORING AGENCY CODE EPA/600/09

15. SUPPLEMENTARY NOTES

16. ABSTRACT

This report supplements the following two journal articles: (1) J. P. Killus and G. Z. Whitten, "A Mechanism Describing the Photochemical Oxidation of Toluene in Smog," Atmos. Environ., 16, 1973-1988 (1982) and (2) J. P. Killus and G. Z. Whitten, "A New Carbon-Bond Mechanism," submitted to Environ. Sci. Technol., 1982. The supplemental material contained in this report describes the computer modeling of smog chamber data performed in three stages. First, a mechanism was developed to describe the inorganic chemistry and the chemistries of formaldehyde, acetaldehyde and PAN. The aldehyde mechanisms were verified independently, using data from experiments covering both formaldehyde and acetaldehyde. Second, a series of mechanisms for specific compounds was added to the standard mechanism and experiments involving those compounds were simulated. Those compounds included ethene, propene, m-xylene, biacetyl, methylglyoxal, methylethyl ketone, and acetone. Third, a study of the background reactivity of smog chambers and unpolluted tropospheric air was under taken to assess the biases inherent in smog chamber experiments and to supply information for use in atmospheric modeling studies.

17. KEY WORDS AND DOCUMENT ANALYSIS

a. DESCRIPTORS	b. IDENTIFIERS/OPEN ENDED TERMS	c. COSATI Field/Group

18. DISTRIBUTION STATEMENT RELEASE TO PUBLIC	19. SECURITY CLASS *(This Report)* UNCLASSIFIED	21. NO. OF PAGES 329
	20. SECURITY CLASS *(This page)* UNCLASSIFIED	22. PRICE

EPA Form 2220-1 (Rev. 4-77) PREVIOUS EDITION IS OBSOLETE

PB83-238725

EPA-600/3-83-043
May 1983

MODELING OF SIMULATED PHOTOCHEMICAL SMOG WITH KINETIC MECHANISMS

by

G. Z. Whitten
J. P. Killus
R. G. Johnson

Systems Applications, Inc.
101 Lucas Valley Road
San Rafael, California 94903

Contract No. 68-02-3281

Project Officer

Marcia C. Dodge
Atmospheric Chemistry and Physics Division
Environmental Sciences Research Laboratory
Research Triangle Park, North Carolina 27711

ENVIRONMENTAL SCIENCES RESEARCH LABORATORY
OFFICE OF RESEARCH AND DEVELOPMENT
U.S. ENVIRONMENTAL PROTECTION AGENCY
RESEARCH TRIANGLE PARK, NORTH CAROLINA 27711

NOTICE

This document has been reviewed in accordance with U.S. Environmental Protection Agency policy and approved for publication. Mention of trade names or commercial products does not constitute endorsement or recommendation for use.

ABSTRACT

This report supplements several publications in the open literature that were submitted under this contract. The supplemental material describes the computer modeling of smog chamber data performed in three stages. First, a mechanism was developed to describe the inorganic chemistry and the chemistries of formaldehyde, acetaldehyde and PAN. The aldehyde mechanisms were verified independently, using data from experiments covering both formaldehyde and acetaldehyde. Second, a series of mechanisms for specific compounds was added to the standard mechanism and experiments involving those compounds were simulated. Those compounds included ethene, propene, m-xylene, biacetyl, methylglyoxal, methylethyl ketone, and acetone. Third, a study of the background reactivity of smog chambers and unpolluted tropospheric air was undertaken to assess the biases inherent in smog chamber experiments and to supply information for use in atmospheric modeling studies.

This report has been submitted to the U.S. Environmental Protection Agency in fulfillment of contract No. 68-02-3281, by Systems Applications, Inc. The studies reported here are part of a three-year effort to elucidate the fundamental chemistry of smog formation. The period from 24 September 1980 to 24 September 1982 is covered in this report.

CONTENTS

Abstract.. iii
Figures... vii
Tables.. xii

1. Introduction... 1
2. Summary of Results, Conclusions, and Recommendations......... 3
    General Conclusions....................................... 3
    Summary of Results and Conclusions........................ 4
    Recommendations... 6
3. The Standard Mechanism...................................... 11
    Introduction.. 11
    Analysis of Submodels..................................... 11
    Discussion.. 18
4. The Explicit Mechanisms for Individual Compounds............ 95
    Introduction.. 95
    Olefin Chemistry.. 96
    Ethene Simulations.. 100
    m-Xylene.. 102
    Dicarbonyls... 105
    Acetone and Methyl Ethyl Ketone........................... 106
5. Background Effects... 196
    Background Reactivity for Atmospheric Modeling Studies.... 196
    Background Reactivity in Smog Chambers.................... 218

Radical Sources in the UCR Chamber.................. 227
UNC Solar Light Studies............................ 241
References... 260
Appendix... 268

FIGURES

Number		Page
1a.	Simulation results for UNCB 51877	23
1b.	Simulation results for UNCR 71677	25
1c.	Simulation results for UNCR 72877	27
1d.	Simulation results for UNCB 91477	29
1e.	Simulation results for UNCR 91477	31
1f.	Simulation results for UNCB 91977	33
1g.	Simulation results for UNCR 91977	35
1h.	Simulation results for UNCB 90878	37
1i.	Simulation results for UNCR 90878	39
1j.	Simulation results for UNCB 91578	41
1k.	Simulation results for UNCB 92178	43
1l.	Simulation results for UNCB 73079	45
1m.	Simulation results for UNCR 73079	47
1n.	Simulation results for UNCR 73179	49
1o.	Simulation results for UNCB 80179	51
1p.	Simulation results for UNCB 80279	52
1q.	Simulation results for UNCB 80479	54
1r.	Simulation results for UNCB 80579	55

1s. Simulation results for UNCB 90779........................... 56

1t Simulation results for UNCR 90779........................... 58

2a. Simulation results for UNCR 51877........................... 60

2b. Simulation results for UNCB 71877........................... 62

2c. Simulation results for UNCB 111277........................... 64

2d. Simulation results for UNCB 112077........................... 65

2e. Simulation results for UNCB 22778........................... 67

2f. Simulation results for UNCB 30678........................... 69

2g. Simulation results for UNCB 33178........................... 70

2h. Simulation results for UNCB 80878........................... 71

2i. Simulation results for UNCR 80878........................... 73

2j. Simulation results for UNCB 81778........................... 75

2k. Simulation results for UNCR 81778........................... 77

2l. Simulation results for UNCR 101278........................... 79

2m. Simulation results for UNCR 101378........................... 81

2n. Simulation results for UNCR 101378........................... 83

2o. Simulation results for UNCR 102578........................... 85

2p. Simulation results for UNCR 72179........................... 87

2q. Simulation results for UNCR 80179........................... 89

2r. Simulation results for UNCB 81679........................... 91

2s. Simulation results for UNCR 80880........................... 93

3. Simulation results for NIES 780705........................... 117

4. Simulation results for NIES 780707........................... 119

5. Prophylene glycol dinitrate isopleth........................ 121
6. Simulation results for UNCR 101877.......................... 122
7. Simulation results for UNCB 101877.......................... 123
8. Simulation results for UNCR 111277.......................... 125
9. Simulation results for UNCR 111977.......................... 126
10. Simulation results for UNCR 112077.......................... 128
11. Simulation results for UNCB 11078........................... 130
12. Simulation results for UNCR 61678........................... 132
13. Simulation results for UNCB 63078........................... 134
14. Simulation results for UNCR 70178........................... 136
15. Simulation results for UNCR 73078........................... 138
16. Simulation results for UNCB 80678........................... 140
17. Simulation results for UNCR 81078........................... 141
18. Simulation results for UNCB 81078........................... 142
19. Simulation results for UNCB 81578........................... 143
20. Simulation results for UNCR 82878........................... 145
21. Simulation results for UNCB 82378........................... 147
22. Simulation results for UNCB 91478........................... 149
23. Simulation results for UNCR 91578........................... 151
24. Simulation results for UNCR 91878........................... 153
25. Simulation results for UNCR 91978........................... 155
26. Simulation results for UNCR 92178........................... 156
27. Simulation results for UNCB 100278.......................... 158

28. Simulation results for UNCR 100378.......................... 160

29. Simulation results for UNCR 80479........................... 162

30. Simulation results for UNCR 80579........................... 164

31. Simulation results for UNCR 103179.......................... 166

32. Simulation results for UNCB 103179.......................... 167

33. Simulation results for UNCR 70860........................... 168

34. Simulation results for EC-344............................... 169

35. Simulation results for EC-345............................... 170

36. Ring opening of m-xylene.................................... 171

37. Simulation results for UNCR 70980........................... 172

38. Simulation results for UNCB 80880........................... 174

39. Simulation results for UNCB 70980 using methylygloyoxal photolysis equal to 0.15 k_1................................ 176

40. Simulation results for UNCB 70960........................... 178

41. Simulation results for UNCB 60480........................... 180

42. Simulation results for UNCR 81380........................... 182

43. Simulation results for UNCB 81380........................... 184

44. Simulation results for UNCB 62079........................... 186

45. Simulation results for UNCR 102079.......................... 188

46. Simulation results for UNCR 60480........................... 190

47. Simulation results for UNCB 80980........................... 192

48. Simulation results for UNCR 80980........................... 194

49. Special CBM-EKMA isopleth with low-range background levels (NO_x emissions).................................. 214

50. Special CBM-EKMA isopleth with mid-range background levels (NO_x emissions)........ 215

51. Special CBM-EKMA isopleth with high-range background levels (NO_x emissions)........ 216

52. Special CBM-EKMA isopleth with high-range background levels........ 217

53. Simulation results for UNC experiments........ 222

54. Simulation results for experiment EC-253........ 228

55. Plot of (radical source/K_1 against NO_2 concentration at 303 K........ 230

56. Simulation results for NIES........ 236

57. Estimated equilibrium profiles for NO_x species versus aerosol acidity (established for an initial condition of NO_2 in equilibrium with H_2SO_4)........ 238

58. Data points taken from Stedman, Harvey, and Dickerson (1977)........ 243

59. Data points taken from Zafonte, Rieger, and Holmes (1976)........ 244

60. Daily average atmospheric turbidity (500nm)........ 247

61. Diurnal NO_2 photolysis for the UNC smog chamber........ 248

62. Specific photolysis rate of nitrogen dioxide and incident total solar radiation and ultraviolet radiation as a function of time for 13 October 1976. Solid line is total solar radiation; dashed line is ultraviolet radiation (full scale is 64.64 x 10^{-3} al-cm^{-2}-min^{-1}); 0 are ambient k_1, + k_1 inside the smog chamber. Sky conditions were clear........ 259

TABLES

Number Page

1 The Standard Mechanism.. 12

2 Initial Conditions for Acetaldehyde Experiments.............. 19

3 Results of Acetaldehyde Simulations.......................... 20

4 Propene Reactions.. 109

5 Ethene Reactions... 111

6 Initial Conditions for Olefin Experiments.................... 112

7 m-Xylene Mechanism... 114

8 Mechanism for Acetone and MEK.................................. 116

9 PG&E Hydrocarbon Data for ERT Project A029.................. 203

10 PG&E Hydrocarbon Data for ERT Project A029.................. 205

11 Hydrocarbon Concentrations in Clean and Perturbed Rural Air... 207

12 Typical Values and Ranges of Observed Hydrocarbon Concentrations.. 208

13 Recommended Background of Reactive Hydrocarbons............. 211

14 Experiments for Which Hydrocarbon Contamination Can Be Estimated From Pitts et al. (1977; 1979).................. 232

15 Typical Emissions of Hydrocarbons from the UCR EC Wall....... 231

16 UCR Experiments Involving the Addition of Benzaldehyde to an Air/NO_x System.. 240

SECTION 1

INTRODUCTION

For several years the Environmental Protection Agency (EPA) has been sponsoring a series of coordinated studies directed toward the development and refinement of mathematical models capable of simulating the chemical transformations occurring in urban atmospheres. In addition to advancing the state of knowledge of the smog phenomenon, these chemical models can be used in condensed form as part of large, comprehensive air quality simulation models, which can then be used to evaluate various smog abatement programs.

The series of coordinated programs sponsored by the EPA has included the following types of studies: fundamental investigations of individual chemical reactions, evaluations of such investigations, smog chamber experiments, computer modeling of chamber data to develop accurate chemical models, and the development and testing of the comprehensive atmospheric models. This report is part of a three-year computer modeling effort using the smog chamber data. It is not intended, however, as a comprehensive summary of the entire three-year study, since the following key findings have already appeared in the open literature:

> A detailed mechanism for toluene oxidation in smog (published in Atmospheric Environment).

> A revised condensed smog mechanism for use in atmospheric models (published as an EPA Report; also to appear in Environmental Science and Technology).

> A critical study of smog chamber radical sources (excerpts published in International Journal of Chemical Kinetics).

Material presented in this report involves those portions of the three-year computer modeling study not found in these publications, and is intended to supplement the published material.

The computer modeling effort reported here used smog chamber data obtained primarily from the outdoor chamber of the University of North Carolina (UNC). In previous studies (e.g., Whitten, Killus, and Hogo, 1980), primary attention was given to the refinement of mechanisms that describe the chemistry of propene and butane. Some emphasis was also directed toward extending the olefin and paraffin chemistry, refining a condensed mechanism to include the extended chemistry, and developing a parameterized scheme for aromatics oxidation. Whereas previous work was directed towards the development of a practical condensed mechanism known as the Carbon Bond Mechanism (CBM), which was based on the detailed chemical mechanisms and the parameterized aromatics scheme, the major focus of this study concerns the fundamental details of explicit chemistry. The study has been directed (1) towards the development of a detailed chemical mechanism for aromatics and (2) a careful assessment of the previously developed and reported on detailed chemical mechanisms. CBM revisions performed to refine the aromatics chemistry and to update and extend the inorganic chemistry are given in Killus and Whitten (1982).

Although the smog phenomenon has long been known to be sensitive to sunlight intensity and temperature, the details of this sensitivity are still somewhat uncertain. Much of the present study has therefore been directed towards its elucidation. However, the smog chamber data contain uncertainties caused by the instrumentation, the walls of the chambers, impurities in the air, dilution effects, and the use of natural sunlight. Hence a careful investigation of sunlight and temperature effects must also involve the minimization of these smog chamber uncertainties.

Section 2 of this report presents a summary of results, conclusions, and recommendations. Section 3 describes the smog chemistry of acetaldehyde, which includes formaldehyde and inorganic smog chemistry, and which forms a basic set of reactions common to all the other explicit mechanisms. Section 4 describes the explicit chemistry of several molecules that we have not yet published in the open literature. Section 5 discusses recent studies on background effects performed under this contract. The Appendix describes the use of the Carbon Bond Mechanism and the testing of the steady state species it employs.

SECTION 2

SUMMARY OF RESULTS, CONCLUSIONS, AND RECOMMENDATIONS

As noted in Section 1, the major findings of this three-year study have already been published. Topics summarized in this section are supplemental to the published findings and have not yet been published in the open literature. The following three topics are summarized here:

(1) The development and validation of a standard mechanism common to virtually all smog systems.

(2) Current refinements added to several explicit mechanisms for individual organic compounds.

(3) Some recent studies of background effects caused by the rural air used to fill the UNC chamber and effects due to the chamber walls.

Before presenting specific results and conclusions, the overall accomplishments of the study are briefly summarized.

GENERAL CONCLUSIONS

In computer modeling studies such as the one reported here, many ideas are tried, and large quantities of computer output are produced. The implicit conclusion in the descriptions of the modeling activity that produced the current closest agreement between simulations and observational data is that the steps taken were both unique and necessary. However, experience has shown that equally close agreement is possible as a result of several combinations of adjustments to physical conditions and mechanisms. Hence, the conclusions presented here must be qualified with the caveat that the results are subject to change in accordance with new data and further modeling efforts.

During the past three years, there has been a different kind of progress in the development and refinement of the knowledge of smog chemistry. In the past, a rapid growth in understanding and in the quality of models designed to simulate the chemistry seen in smog chambers was often associated with empiricism and speculation, in addition to a heavy reliance on a small number of scientific experiments. The past three years can be characterized as a period of confirmation, evaluation, and refinement of our knowledge of smog chemistry. Although the agreement between chemical model simulations and observed data may not be substantially improved as yet, the scientific basis of such agreement has been more firmly established.

At the beginning of this study, the explicit chemistry of aromatics was rudimentry and highly empirical; assumed amounts of initial nitrous acid were necessary to simulate virtually all smog chamber experiments, and very little was known about the subtle effects of lighting, temperature, humidity, and background contamination. We now have a refined explicit aromatics mechanism especially for toluene, and initial amounts of nitrous acid have been observed at the concentration level previously assumed. Work still remains to be done in all areas, but a clear understanding is now emerging that should soon provide satisfactory explanations for the observed effects of changes in lighting, temperature, humidity, and background levels.

SUMMARY OF RESULTS AND CONCLUSIONS

The explicit chemistry of aromatics has been developed for toluene and to some extent for the xylenes. Central to this chemistry are three features not seen in the explicit chemistry of olefins and alkanes:

(1) Dicarbonyl intermediates, some of which can photolyse rapidly.

(2) Stable hydroxy-substituted intermediates (cresols), which react rapidly with the NO_3 radical.

(3) A large fraction of fairly unreactive intermediates.

In contrast, the olefin and alkane explicit chemistries tend to generate large fractions of highly reactive monocarbonyls that photolyse rather slowly and apparently do not react rapidly with NO_3.

The second version of the condensed atmospheric scheme known as the Carbon Bond Mechanism (CBM-II) treated the features of aromatics chemistry empirically. In the present study, the CBM was updated, primarily to serve as a condensed version of the explicit aromatics chemistry. For the benefit of CBM users, the updated version (CBM-III) was also more thoroughly validated and documented than the previous versions.

A central issue that must be addressed when a mechanism developed from smog chamber data is used for atmospheric modeling concerns the radical sources necessary to drive the chemical simulations. The CBM was developed using a minimal source of radicals from chamber walls and therefore should be reliable for use in atmospheric applications. Nevertheless, the issue of chamber-dependent radical sources remains controversial, in spite of a recent progression towards acceptance of more minimal levels by the proponents of the concept of wall-related radical sources.

Discussions of the initial conditions, mechanisms, and physical conditions used to simulate the experiments shown in this report are included in the text. Occasionally, special asumptions (e.g., NO_x or hydrocarbon emissions from the chamber walls) were employed to simulate the data. Such cases are explained in the text. In general, the simulations did not use the walls as a source of radicals. However, some experiments could be simulated only by assuming some extra source of reactivity. In such cases (which are also noted in the text) some extra level of contamination was simulated using assumed amounts of formaldehyde or ethene.

As mentioned previously, most of the study conclusions just summarized have been documented through recent publications in the open literature. The following study results and conclusions, which are not contained in these publications, are documented in this report:

> Kinetic mechanisms for formaldehyde, acetaldehyde, and peroxyacetyl nitrate are now at approximately the same level of refinement as basic inorganic reaction kinetics. Accordingly, we have added these reactions to our standard mechanism. Some uncertainty still exists concerning the products of radical-radical reactions, particularly those involving peroxyacetyl. However, the rate constants for these reactions are reported in the open literature and appear to be compatible with observed phenomena in smog chamber experiments (e.g., PAN decay).

> The explicit mechanisms for propene and ethene have been revised. The remaining uncertainties in the kinetics of these compounds, having little effect on ozone and NO_x behavior, appear to be minor.

> Our knowledge of aromatic photooxidation has been extended to m-xylene. Xylene oxidation appears to differ from toluene chemistry in several respects that are easily interpreted on the basis of the standard ring opening

mechanism. Because of a greater yield of alkyl dicarbonyls, the radical yield (and PAN production) is greater for xylenes than for toluene, whereas the $NO_3^{\cdot}$-related NO_x sink is reduced because of a lower yield of hydroxy compounds relative to toluene.

- Experiments involving biacetyl, methyl glyoxal, acetone, and methyl ethyl ketone have been simulated. The dicarbonyl experiments are consistent with dicarbonyl dominance in the oxidation of aromatic hydrocarbons.
- We have made a thorough study of background reactivity effects in smog chambers and the expected photochemical background of the lower atmosphere. Radical initiation and oxidation reactivity in the atmosphere appears to be similar to that found in smog chambers (within a factor of three), thus verifying the utility of smog chambers at high to intermediate concentration levels. The greatest difference between trace smog chamber contaminants and the atmosphere appears to be a relatively high NO_x emission rate (equivalent to 40 to 120 ppb NO_x during the course of an experiment) from smog chamber walls.

RECOMMENDATIONS

The recommendations offered here have been divided into three general areas: smog chamber experiments, analytical measurements, and laboratory studies. We also wish to emphasize the need for continued support in all phases of smog research. The effectiveness of money spent on modeling can often be enhanced considerably if more money is set aside for improved analytical capabilities. Smog chamber data that exhibit good carbon and nitrogen mass balance might require the modeler to simulate more species, but the margin for speculation and concomitant uncertainties is diminished.

We recommend the performance of the following smog chamber experiments:

- A series of experiments should be performed to help characterize the effects of carry-over contamination, which has been identified as an uncertain aspect of smog chambers. For example, the use of acetaldehyde or biacetyl as the only initial precursor provides a sensitive means of assessing the amount of NO_x emitted from chamber walls. PAN measurements give a direct assessment of NO_x off-gassing, and ozone measurements combined with modeling offer an indirect and confirmatory assessment. Thus a high NO_x experiment, followed by several successive days of experiments using only biacetyl, should provide a picture of the carry-over effect for NO_x. Similarly, a series of experiments using 0.5 ppm NO only can provide a measure of the organic reactivity carry-over. In this case, the rate of NO to NO_2 conversion monitors one aspect of the background reactivity, and the height of the NO_2 peak, if any, monitors the competition for OH between the background organic and NO_2.

- A large number of organic compounds should be studied, one at a time, so that rudimentary mechanisms for each can be constructed. Three advantages are seen from such a program: the generalization assumptions of mechanisms such as the Carbon Bond Mechanism can be tested, the reactivities of many organics known to be emitted or generated as secondary products in the atmosphere can be assessed, and information potentially helpful in the current mechanism development can be gained. A classic example of the last advantage is the rapid advance in toluene chemistry that resulted from the discovery of biacetyl as a secondary product in a smog chamber experiment using o-xylene and NO_x. This recommendation is also made because of recent advances in analytic techniques, to take advantage of the skill some modelers have developed in rapidly working out rudimentary mechanisms.

- The chemistry of hydroxy-containing compounds requires investigation. The phenomenon of alkoxy radical isomerization (tail biting) suggests that hydroxy compounds are formed in alkane systems, and there is some reason to believe that OH addition to olefins may sometimes yield dysfunctional hydroxides as well. Toluene hydroxide (cresol) is now known to react rapidly with NO_3 and is an important NO_x sink in toluene systems. It is reasonable to speculate that other hydroxides may have important effects in olefin and paraffin systems.

- The radical balance in alkane systems should be more accurately assessed. At present, the question of radical sources in the butane system is obscured by the question of chamber reactivity and unknown radical sources. However, it should be possible to design dual chamber runs in the UNC chamber (perhaps involving high levels of CO as a radical chain length amplifier) to estimate the overall radical balance in paraffin oxidation systems.

The following analytical studies and tasks should be performed:

> Since certain effects of clouds and haze are probably linked to changes in the ratio of aldehyde photolysis to K_1, spectral measurements are needed at 310-330 nm and at 370-400 nm (or total UV) to assess these effects. Light measurements should be spherically integrated, if possible.

> A total gas phase organics detector, especially one that includes carbonyl compounds, would be useful.

> Instruments that are used in urban pollution field studies should at least occasionally be used in smog chamber studies to provide a cross reference.

> An alternate NO_2-specific instrument is needed, since many intermediate nitrates (such as PAN) interfere with the present measurements.

> Measurement of peroxy radicals would be useful for mechanism validation. These radicals are more sensitive to light and hydrocarbon reactivity than the OH radical. At present, peroxy radical levels can be tested only via modeling, and only at high levels of NO, assuming exclusive NO to NO_2 conversion reacting channels.

> Sample line delays from the chamber to the monitoring devices need to be precisely known and, if possible, minimized. The present study indicates that subtle lighting effects are hidden behind the sample line delay, which allows reaction of O_3 with NO.

> Direct NO_3 measurements are possible at night using long path absorption techniques. Such measurements should be conducted, if resources permit.

> Atmospheric measurements that include breakdowns of hydrocarbons, nitrogen oxides and acids, peroxides, and carbonyl compounds made in both urban and rural environments, at ground level and at higher altitudes.

Our recommendations for laboratory studies are as follows:

- More studies of the NO_3 radical are needed. This species is now known to react with olefins, cresols, and to some extent with aldehydes. At nighttime, NO_3 concentrations can be a significant fraction of the total gas phase NO_x. Knowledge of the chemistry of NO_3 under such conditions, however, is rudimentary, since many possible reactions have not been studied. The specific reactions requiring further study should become more clearly identified as nighttime modeling of smog chamber data containing NO_3 is completed.

- The chemistry of hydroxy-substituted compounds needs further study. Such compounds, especially hydroxy-substituted carbonyls, have been suggested as the reaction products in a variety of different reaction schemes. However little has been done in the laboratory to verify the reaction rates, photolysis rates, and reaction channels of such species. Specific species that need study are glycolaldehyde, 4-hydroxy-butyraldehyde, hydroxy-acetone, and methyl cresols.

- Recent speculation in modeling has identified α-hydroxy nitrates as a possible product in olefin chemistry if the initial α-hydroxy peroxy radical reacts with NO to form nitrates. Hydrogen bonding from the hydroxyl hydrogen to nitrate oxygen creates the potential for photolysis or some other decomposition pathway to HONO and carbonyl compounds:

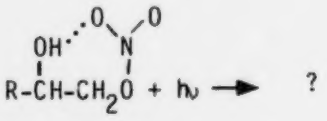

$$\text{R-CH(OH}\cdots\text{O-N(=O)-)}\text{-CH}_2\text{O} + h\nu \longrightarrow ?$$

- There is a need for photolysis data for organic compounds under atmospheric conditions at realistic concentrations. Present reference sources (e.g., Calvert and Pitts, 1966) offer a wide range of information, but the data is often out of date, not taken at wavelengths appropriate to tropospheric sunlight, not done in air at atmospheric pressure, and the concentrations used were so high that secondary attack by original radical products dominates the primary process.

Specific species that require immediate investigation on the basis of the work reported here are as follows:

> Acetaldehyde--Several recent studies are now providing conflicting information regarding the channel to radical production. Some studies indicate methyl and formyl radical production, whereas other studies point to production of the acetyl radical and a hydrogen atom; however, none of the studies appears to relate directly to smog chemistry conditions.

> Glycolaldehyde--this has been identified in the ethene oxidation chemistry, but its own subsequent chemistry is uncertain.

> Glyoxal--Although many studies have been reported, the fate of this species under dilute atmospheric conditions is still uncertain.

> Methacrolein--this appears to be a key intermediate in the oxidation of isoprene.

> Methylvinylketone--another key to the oxidation of isoprene.

> Hydroxy-acetone--a propene analog to the glycolaldehyde channel that occurs in ethene oxidation.

> α-hydroxy-propionaldehyde--the other analog to glycolaldehye expected to occur in propene oxidation.

> Benzaldehyde--an intermediate in toluene chemistry that is known to inhibit smog chemistry; however, the specific reactions are uncertain.

Section 3

THE STANDARD MECHANISM

3.1 INTRODUCTION

The idea of a standard mechanism stems from the concept of a hierarchical series of mechanisms originally described in Whitten et al. (1979). In reality, the name reflects our latest method of implementing the hierarchical concept on our computer system. The present standard mechanism consists of all the smog chemistries involved with acetaldehyde (see Table 1). Hence the inorganic chemistry and formaldehyde chemistry are also included. This standard mechanism is stored in the computer in a special file common to any modeling simulation involving explicit chemistry. For instance, a simulation of an ethene experiment would involve the standard mechanism plus the few reactions that involve ethene only and the reactions of the special intermediate species found in the ethene system.

The standard mechanism has been assembled from the latest evaluated rate constants and the simulations involve our latest assessments of chamber effects. The mechanism has been tested against all available UNC experiments involving clean air, carbon monoxide, nitrogen oxides, formaldehyde, and acetaldehyde, and all available combinations of these species. This validation set encompasses several years of experiments over wide ranges of seasons, temperatures, sky conditions, humidity, and concentrations of precursors. Therefore, any attempt to alter one of the reactions in either the standard mechanism or the present simulation treatments so as to improve the agreement between simulation and experimental observation must first consider the extent of the present overall validation.

3.2 ANALYSIS OF SUBMODELS

Formaldehyde Chemistry

Formaldehyde represents one of the simplest precursors for photochemical smog and it appears to be an intermediate product in the oxidation of almost all organics. Our current standard mechanism contains four reactions involving formaldehyde: the reactions with hydroxyl, hydroperoxyl, and oxygen atoms

TABLE 1. THE STANDARD MECHANISM

	Reaction	Rate Constant at 298 K $(ppm^{-1}min^{-1})^*$	E/R E/R (degK)	Notes
1	$NO_2 \rightarrow NO + O$	1.0		2
2	$O + O_2 + M \rightarrow O_3$	2.29-5	-590	1
3	$O_3 + NO \rightarrow NO_2$	26.6	1450	1
4	$O + NO_2 \rightarrow NO$	1.38+4		1
5	$O + NO_2 + M \rightarrow NO_3$	3.26-3	-575	1
6	$NO_2 + O_3 \rightarrow NO_3$	4.74-2	2450	1
7	$O_3 \rightarrow O1D$	1.-3		2
8	$O_3 \rightarrow O$	4.2-2		2
9	$O1D + M \rightarrow O$	4.44+4	-106	1, 3
10	$O1D + H_2O \rightarrow OH + OH$	3.4+5		1
11	$O_3 + OH \rightarrow HO_2$	100	940	1
12	$O_3 + HO_2 \rightarrow OH$	2.4	580	1
13	$NO_3 + NO \rightarrow NO_2 + NO_2$	2.8+4	-250	1
14	$NO_3 + NO_2 + M \rightarrow N_2O_5$	2.66-3	1110.	1
15	$N_2O_5 + H_2O \rightarrow HNO_3 + HNO_3$	1.5-5		4
16	$N_2O_5 + M \rightarrow NO_3 + NO_2$	4.50-6	12300.	1
17	$NO + NO_2 + H_2O \rightarrow HNO_2 + HNO_2$	1.6-11		1
18	$HNO_2 + HNO_2 \rightarrow NO + NO_2 + H_2O$	1.5-5		1
19	$HNO_2 \rightarrow NO + OH$	0.300		2
20	$NO_2 + OH + M \rightarrow HNO_3$	1.63-2	-500	1
21	$NO + OH + M \rightarrow HNO_2$	9.77-3	-500	1
22	$HO_2 + NO \rightarrow OH + NO_2$	1.2+4	-200	1
23	$NO + NO + O_2 \rightarrow NO_2 + NO_2$	7.28-10	-530	1
24	$H_2O_2 \rightarrow OH + OH$	1.4-3		2
25	$OH + H_2O_2 \rightarrow HO_2$	2470	143	1
26	$OH + HNO_2 \rightarrow NO_2$	9770		1

TABLE 1 (Continued)

	Reaction	Rate Constant at 298 K ($ppm^{-1}min^{-1}$)	E/R (degK)	Notes
27	$NO_3 \rightarrow NO_2 + O$	10.8		3
28	$NO_3 \rightarrow NO$	1.32		3
29	$HO_2 + HO_2 \rightarrow H_2O_2$	4590	-1100	1
30	$HO_2 + HO_2 + H_2O \rightarrow H_2O_2 + HO_2$	0.182	-5800	1
31	$HO_2 + NO_2 + M \rightarrow PNA$	1.63-3	-850	1
32	$PNA + M \rightarrow HO_2 + NO_2$	5.12-6	10418	1
33	$OH + CO + M \rightarrow HO_2$	4.3-4		1
34	$HO_2 + FORM \rightarrow FROX$	14.8		1
35	$OH + FORM \rightarrow HO_2 + CO$	1.5+4		1
36	$FORM \rightarrow HO_2 + HO_2 + CO$	0.9		6
37	$FORM \rightarrow CO$	0.9		6
38	$O + FORM \rightarrow OH + HO_2 + CO$	237		1
39	$FROX + NO \rightarrow FACD + NO_2 + HO_2$	10400		1
40	$FROX \rightarrow HO_2 + FORM$	90		1
41	$OH + HNO_3 \rightarrow NO_3$	160		7
42	$ALD_2 + O \rightarrow C_2O_3 + OH$	636	986	1
43	$ALD_2 + OH \rightarrow C_2O_3$	24000	-250	1
44	$ALD_2 + NO_3 \rightarrow C_2O_3 + HNO_3$	2.52		1
45	$ALD_2 \rightarrow STAR$	1.3		6
46	$STAR \rightarrow C_2O_3 + HO_2$	90	10000	6
47	$STAR \rightarrow ALD_2$	10		6
48	$C_2O_3 + NO \rightarrow MEO_2 + NO_2$	16500	-250	8
49	$C_2O_3 + NO_2 \rightarrow PAN$	9000	-250	8
50	$PAN \rightarrow C_2O_3 + NO_2$	0.0222	14000	1
51	$MEO_2 + NO_2 + M \rightarrow MPNA$	6.36-3	-1000	1
52	$MPNA + M \rightarrow MEO_2 + NO_2$	8.1-5	11600	1, 9
53	$MEO_2 + NO \rightarrow MEO + NO_2$	10400	-250	1

TABLE 1 (Concluded)

	Reaction	Rate Constant at 298 K ($ppm^{-1}min^{-1}$)	E/R (degK)	Notes
54	$MEO + NO \rightarrow MNIT$	44400	-200	1
55	$MEO + NO \rightarrow FORM + HO_2 + NO$	1920		1, 10
56	$MEO + NO_2 \rightarrow MEN_3$	22200		1
57	$MEO + O_2 \rightarrow FORM + HO_2$	1.48	2220	1
58	$MEN_3 + OH \rightarrow FORM + NO_2$	2220	360	1
59	$MNIT + OH \rightarrow FORM + NO$	2370	340	1
60	$MNIT \rightarrow MEO + NO$	0.3		2
61	$NO_3 + NO_2 \rightarrow NO + NO_2$	0.59	1230	1
62	$MEO_2 + MEO_2 \rightarrow MEO + MEO$	160		1
63	$MEO_2 + MEO_2 \rightarrow FORM + MEOH$	300		1
64	$MEO_2 + C_2O_3 \rightarrow MEO + MEO_2$	4400		11
65	$C_2O_3 + C_2O_3 \rightarrow MEO_2 + MEO_2$	3700		11
66	$MEO_2 + HO_2 \rightarrow FORM$	9600		11
67	$C_2O_3 + HO_2 \rightarrow PROX$	9600		11
68	$HO_2 + ALD_2 \rightarrow MEO_2 + FORM$	5		12
69	$O + NO + M \rightarrow NO_2$	2.6-3		13
70	$OH + CH_4 \rightarrow MEO_2$	11.4	1710	13

---

* Unimolecular and photolysis reactions are in min^{-1}; termolecular reactions are in $ppm^{-2}min^{-1}$; numbers following a + or - are powers of ten.

Notes for Table 1

1. Atkinson and Lloyd, (1982)
2. Ratio to photolysis of NO_2
3. NASA (1981)
4. H. Jeffries (private communication, 1982)
5. Magnotta and Johnston (1980)
6. See text
7. Nelson, Marinelli, and Johnston (1981)
8. Addison et al. (1980)
9. Bahta, Simonaitis, and Heicklen (1982)
10. HNO chemistry assumed fast according to Carter et al. (1979)
11. Addison et al. (1980); see text
12. Analogy with reactions 34 and 40 assuming a partial hydrogen exchange; confirmation needed
13. Baulch et al. (1980).

plus photolysis. The main decay pathway for formaldehyde in typical urban atmospheres is the reaction with hydroxyl. However, the photolysis of formaldehyde is much more important to the overall smog chemistry because a major photolysis pathway involves the generation of radicals, which can drive the overall oxidation of all organics.

Presently, all UNC smog chamber formaldehyde experiments for which we have received data (21 experiments) can be simulated with the current standard mechanism (see Figure 1*). However, some of the simulations must invoke a means of simulating the loss and reappearance of formaldehyde to and from the condensed water (if any) on the chamber walls.

3.2.2 Acetaldehyde Chemistry

Some recent developments in the literature have prompted us to reevaluate the atmospheric chemistry of acetaldehyde. Our present inventory of smog chamber data has approximately 20 experiments from the UNC chamber that feature acetaldehyde as the primary organic. Acetaldehyde chemistry brings the chemistry of PAN and methylperoxy radicals into the formaldehyde and NO_x chemistry. Methylglyoxyl and biacetyl also add these two features, but we do not yet have the range of experimental conditions to test the chemistry of these compounds as well as we can test that of acetaldehyde. A major problem remaining in the chemistry of acetaldehyde (formaldehyde appearance) is also seen in the dicarbonyl experiments. Since the peroxacetyl radical appears in methylglyoxyl, biacetyl, and acetaldehyde chemistry, the peroxyacetyl radical should be the source of formaldehyde. Perhaps experiments with propionaldehyde will show high yields of acetaldehyde. Such experiments, however, are not yet available.

The first noteworthy development recorded in the literature was the study by Gill, Johnson, and Atkinson (1981). Their experiments utilized a time-resolved intracavity laser detection (TRILD) method, which suggested that the primary photodissociation of acetaldehyde produces $CH_3\dot{C}O$ and $H\cdot$. They hypothesized that all previous studies that had reported $CH_3\cdot$ and $HC\dot{O}$ as the primary products were confounded by an attack of the original $CH_3\dot{C}O$ radical on the parent acetaldehyde molecules. In the atmosphere, immediate scavenging by O_2 and the low concentration of acetaldehyde would presumably preclude such secondary reactions with the parent acetaldehyde molecules. This new development provides an extra NO-to-NO_2 conversion from the photolysis of acetaldehyde. However, as this report is being written there appears to be much controversy over the work by Gill, Johnson, and Atkinson (1981), so our use of their scheme is tentative.

---

* All figures are included at the end of the chapter.

According to our understanding of the peroxyacetyl chemistry, this new photolysis mechanism would lead to 4 NO-to-NO_2 conversions at low NO_2-to-NO_x ratios (PAN formation competes with the NO reaction at high NO_2-to-NO_x ratios).

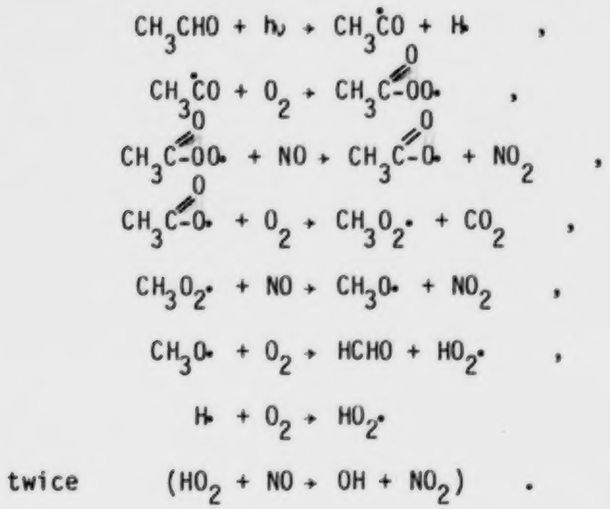

$$CH_3CHO + h\nu \rightarrow CH_3\dot{C}O + H\cdot \quad ,$$

$$CH_3\dot{C}O + O_2 \rightarrow CH_3\overset{O}{\overset{\|}{C}}\text{-}OO\cdot \quad ,$$

$$CH_3\overset{O}{\overset{\|}{C}}\text{-}OO\cdot + NO \rightarrow CH_3\overset{O}{\overset{\|}{C}}\text{-}O\cdot + NO_2 \quad ,$$

$$CH_3\overset{O}{\overset{\|}{C}}\text{-}O\cdot + O_2 \rightarrow CH_3O_2\cdot + CO_2 \quad ,$$

$$CH_3O_2\cdot + NO \rightarrow CH_3O\cdot + NO_2 \quad ,$$

$$CH_3O\cdot + O_2 \rightarrow HCHO + HO_2\cdot \quad ,$$

$$H\cdot + O_2 \rightarrow HO_2\cdot$$

$$\text{twice} \qquad (HO_2 + NO \rightarrow OH + NO_2) \quad .$$

The previous mechanism yielded only three conversions from the initial photolysis of acetaldehyde:

$$CH_3CHO + h\nu \rightarrow CH_3\cdot + HCO\cdot \quad ,$$

$$HCO\cdot + O_2 \rightarrow HO_2\cdot + CO \quad ,$$

$$CH_3\cdot + O_2 \rightarrow CH_3O_2\cdot \quad .$$

This new development in photolysis may explain a problem we previously encountered. In our earlier studies with acetaldehyde systems, the diurnal changes in photolysis seemed too great (more conversions of NO to NO_2 were needed in the morning hours). At that time, we switched from a scheme in which acetaldehyde photolysis was essentially varied independent to the photolysis of NO_2 to a scheme using a constant ratio of acetaldehyde-to-NO_2 photolysis. Now, we have reinstituted the older scheme, which is based on the change in solar spectra that occurs with zenith angle. Thus, the photolysis of acetaldehyde, like formaldehyde, is slower relative to NO_2 photolysis in the morning (high zenith angle) than it is at noon (lowest zenith angle). Although some atmospheric models such as the Systems Applications' Urban

Airshed Model use a constant ratio of aldehyde-to-NO_2 photolysis, we feel that our present approach is more correct.

Another development affecting acetaldehyde chemistry appeared in a paper by Addison et al. (1980) that addressed the kinetics of the acetylperoxy radical. Specific estimates of several reactions were made in this paper and have been incorporated into our most recent mechanism. The kinetics of the acetylperoxy radical that we had been using came from the evaluation of Atkinson and Lloyd (1982). The adjustments to the kinetics of acetaldehyde we have recently made involve the PAN formation rate and radical-radical chemistry. PAN decay can now be simulated in many experiments to agree more closely with observations by using a rather high value for the reaction of the acetylperoxy radical with the hydroperoxy radical, as suggested by Addison et al. (1980). This subject is discussed further in the next subsection.

3.2.3 Radical-Radical Reactions and Pan Decay

Under conditions of high reactivity and low NO_x (e.g., after the primary ozone peak), PAN shows a peak and begins to decay. This process seems to be due to radical-radical reactions:

Radical-radical Reactions	Rate Constant $ppm^{-1}min^{-1}$
$C_2O_3 + HO_2 \rightarrow CH_3COO_2H$	9600
$C_2O_3 + C_2O_3 \rightarrow MEO_2 + MEO_2$	3700
$C_2O_3 + MEO_2 \rightarrow MEO_2 + MEO$	4400
$MEO_2 + MEO_2 \rightarrow HCHO + MEOH$	300
$MEO_2 + MEO_2 \rightarrow MEO + MEO$	160
$MEO_2 + HO_2 \rightarrow CH_3O_2H$	9600

The reactions involving peroxyacetyl are taken from Addison et al. (1980). The self reactions of methylperoxy are taken from Niki et al (1981c), whose findings are in close agreement with Sander and Watson (1981) and Kan, Calvert, and Shaw (1980). A minor pathway (~ 8 percent) to $CH_3O_2CH_3$ has been neglected.

The reaction rate constant for MEO_2 with HO_2 is taken from Addison et al. (1980) to be consistent with the important peroxyacetyl reaction rates. However, this rate constant is five times that reported by Kan, Calvert, and Shaw (1980).

The products of the peroxylacetyl reactions are not known with certainty, and errors in their specification could have biased the work of Addison et al. Our analysis of MEK and other PAN decomposition systems leads us to suspect that the radical-peroxyacetyl reactions do not lead to formaldehyde. Clearly, additional work is needed.

3.3 DISCUSSION

Tables 2 and 3 present the initial conditions for the acetaldehyde experiments and the results of the acetaldehyde simulations, respectively. The current set of simulations must not be regarded as definitive because the final tape of UNC data arrived as this report was being written; therefore, many of the experiments will need to be reinvestigated because the revised data could be significantly different from that presented in this report: In addition, the formaldehyde experiments were, for the most part, affected by formaldehyde adsorption and desorption from the chamber walls. Since such physical phenomena are poorly characterized by the available UNC data, the simulation latitude was great. Furthermore, there is still little available data with which to completely characterize the formaldehyde photolysis pathways as they change with time on cloudy days. Hence, the validation of the simplest chemical systems (formaldehyde and nitrogen oxides) remains somewhat uncertain as a result of these physical problems.

Nevertheless, the match between observations and simulations is encouraging because no elaborate schemes were used to solve the problems of wall adsorption and solar spectra. The simulation of each experiment was optimized to the observed data using only the following set of parameters:

> Initial HONO--The initial rates of precursor behavior were adjusted to the observed data by varying the amount of initial HONO. No upper or lower limit was assumed; therefore, the consistency of the "best fit" HONO values is very encouraging. The occasional extra-high values tend to highlight experiments that need repeating or further investigation, such as the two experiments on 8 September 1978, for which a value of 0.02 ppm HONO was used in the simulations.

TABLE 2. INITIAL CONDITIONS FOR ACETALDEHYDE EXPERIMENTS

Date	Chamber Side	Beginning Temperature (K°)	Sky Conditions	Beginning Time	Acetaldehyde	NO	NO_2	HONO*	H_2O	FORM*	CO	O_3	NX*	Ethylene	Formaldehyde Wall Effects*
5/18/77	Red	297	Clear	6:00	0.95	0.2818	0.077	0.001	2.0×10^4	0.0	0.0	0.0017	0.00	0.00	0.00
7/18/77	Blue	303.6	Cloudy	6:08	0.50	0.392	0.141	0.035	2×10^4	0.02	0.45	0.0	0.00	0.00	0.00
11/12/77	Blue	269.4	Cloudy	7:44	0.85	0.340	0.120	0.002	2×10^4	0.00	0.00	0.00	0.00	0.00	0.00
11/20/77	Blue	272.3	Clear	7:30	1.95	0.7821	0.180	0.006	2×10^4	0.00	0.00	0.00	0.00	0.00	0.200
2/27/78	Blue	264.6	Cloudy	8:00	0.9650	0.268	0.086	0.00	1.2×10^4	0.00	0.22	0.00	0.00	0.00	0.06
3/06/78	Blue	270.6	Cloudy	7:36	0.900	0.291	0.083	0.006	1.4×10^4	0.00	0.285	0.0	0.00	0.00	0.100
3/31/78	Blue	273.5	Overcast	6:48	1.000	0.327	0.066	0.001	2×10^4	0.00	0.300	0.0	0.00	0.00	0.00
8/08/78	Red	294.9	Cloudy	6:20	0.455	0.424	0.093	0.020	2×10^4	0.00	0.346	0.001	0.00	0.00	0.00
8/08/78	Blue	294.9	Cloudy	6:20	1.950	0.424	0.103	0.005	2×10^4	0.00	0.330	0.00	0.00	0.00	0.00
8/17/78	Blue	294.8	Cloudy	5:40	2.00	0.614	0.091	0.020	1.5×10^4	0.00	0.400	0.00	0.00	0.00	0.00
8/17/78	Red	294.8	Cloudy	6:40	0.480	0.609	0.087	0.025	1.5×10^4	0.00	0.380	0.00	0.00	0.00	0.00
10/13/78	Red	283.1	Cloudy	7:13	0.400	0.378	0.115	0.001	2×10^4	0.00	0.300	0.00	0.00	0.00	0.00
10/13/78	Blue	283.1	Cloudy	7:13	1.050	0.770	0.136	0.00	2×10^4	0.00	0.300	0.00	0.00	0.00	0.00
7/21/79	Red	294.8	Cloudy	5:40	1.00	0.0	0.013	0.004	2.9×10^4	0.00	0.00	0.00	0.070	0.00	0.00
7/21/79	Blue	294.8	Cloudy	5:40	1.00	0.0	0.020	0.006	2.9×10^4	0.00	0.00	0.00	0.120	0.00	0.00
8/01/79	Red	299.3	Clear	6:32	0.940	0.274	0.079	0.005	3.3×10^4	0.00	0.320	0.00	0.00	0.00	0.00
8/08/80	Red	294.5	Clear	6:18	1.00	0.322	0.097	0.011	1×10^4	0.01	0.00	0.00	0.00	0.00	0.200
10/12/78	Red	280.2	Clear	7:24	0.630	0.364	0.115	0.00	2×10^4	0.00	0.300	0.00	0.00	0.0985	0.00
10/25/78	Red	272.9	Clear	7:14	0.580	0.341	0.103	0.00	2×10^4		0.580	0.00	0.00	0.0985	0.00
8/16/79	Blue	287.1	Overcast	6:40	0.610	0.304	0.130	0.00	1×10^4	0.00	0.270	0.00	0.00	0.083	0.00

---

* These values were all assumed to optimize agreement between data and simulations; see text for further discussion.

TABLE 3. RESULTS OF ACETALDEHYDE SIMULATIONS

Date	Chamber Side	Initial NO_x (ppm)	Initial NO_2/NO_x Ratio	Initial HC/NO_x Ratio (ppmC/ppm)	Maximum O_3 (ppm)		Difference in O_3 Maxima (percent)	Time to Maximum O_3 (minimum)		Difference in Time to Max. O_3 (percent)	Maximum NO_2 (ppm)		Difference in NO_2 Maximum (percent)	Time to Maximum NO_2 (minimum)		Difference in Time to Maximum NO_2 (percent)
					Sim.	Meas.		Sim.	Meas.		Sim.	Meas.		Sim.	Meas.	
5/18/77	Red	0.359	0.215	5.29	0.88	0.93	-6	>700	>700	--	0.27	0.33	-22	250	270	-8
7/18/77	Blue	0.533	0.265	1.88	0.52	0.72	-38	>640	>640	--	0.40	0.42	-5	280	270	4
11/12/77	Blue	0.460	0.260	3.04	0.07	0.03	57	410	400	2	0.30	0.28	7	420	420	0
11/20/77	Blue	0.962	0.187	4.05	0.062	0.062	0	480	490	-2	0.60	0.59	2	420	400	5
2/27/78	Blue	0.354	0.243	5.45	0.120	0.148	-23	490	560	-14	0.20	0.24	-20	290	350	-21
3/06/78	Blue	0.374	0.222	4.81	0.20	0.26	-30	550	570	-4	0.23	0.33	-43	320	360	-13
3/31/78	Blue	0.393	0.168	5.09	0.41	0.49	-22	>600	>600	--	0.24	0.34	-42	290	340	-17
8/08/78	Red	0.517	0.180	1.76	0.34	0.51	-50	>640	>640	--	0.36	0.40	-11	325	320	2
8/08/78	Blue	0.527	0.195	7.40	1.00	1.11	-11	>640	>640	--	0.36	0.50	-39	220	280	-27
8/17/78	Blue	0.707	0.129	5.67	1.12	1.28	-14	>640	>640	--	0.54	0.51	6	200	210	-5
8/17/78	Red	0.696	0.125	1.38	0.19	0.17	10	>640	>640	--	0.48	0.48	0	350	320	-6
10/12/78	Red	0.479	0.240	2.63	0.25	0.23	8	>560	>480	--	0.31	0.33	-6	300	300	0
10/13/78	Red	0.493	0.233	1.62	0.075	0.080	7	460	480	-4	0.33	0.34	-3	490	440	10
10/13/78	Blue	0.906	0.150	2.32	0.148	0.148	0	460	470	-2	0.58	0.64	-10	360	360	0
10/25/78	Red	0.444	0.232	2.61	0.13	0.13	-0	>540	>540	--	0.24	0.28	-17	360	380	-6
7/21/79	Red	--	--	--	0.23	0.37	-61	>660	660	--	0.036	0.038	-6	180	180	0
7/21/79	Blue	--	--	--	0.325	0.463	-42	>660	660	--	0.066	0.068	-3	190	190	0
8/01/79	Red	0.353	0.224	5.33	1.00	0.93	7	>540	>540	--	0.26	0.29	-12	185	200	-8
8/16/79	Blue	0.434	0.300	2.81	0.59	0.53	10	>640	>640	--	0.28	0.30	-7	280	320	-14
8/08/80	Red	0.419	0.232	4.77	0.96	1.05	-9	640	630	2	0.31	0.31	0	250	250	0

- Formaldehyde desorption--Because the temperature invariably increases during the first few hours, there is always a net desorption of formaldehyde in the UNC chamber. Therefore, we treated only the desorption process. For simplicity, we always used the same rate of first-order decay of 0.005 min^{-1} for the initial wall-to-gas-phase desorption rate. The only adjustable parameter used for the desorption was the ratio of initial wall-to-gas-phase concentration of formaldehyde.

Individual experiments in the acetaldehyde series (see Figure 2) were similarly adjusted with the following exceptions:

- Wall source of NO_x--The UNC experiments of 21 July 1979 were run without initial NO_x; however, the observed PAN verifies a chamber source of NO_x (Figure 2p). The simulations were generated by assuming an NO_x value of NX 0.07 and 0.12 ppm (NX in Table 2) on the red and the blue wall, respectively, decayed into the gas phase with a first-order decay constant of 0.005 min^{-1}. The observed UNC PAN and ozone data show a decided delay in ozone appearance when compared with that for PAN. We believe this delay was caused by PAN formation near the walls rather than in the bulk gas phase. We hope to use a special two-cell model to simulate this phenomenon if time and funds are available.

- Wall source of formaldehyde--Three experiments (20 November 1977, 6 March 1978, and 8 August 1980; Figures 2d, 2f, and 2s) were simulated using extra formaldehyde (0.2, 0.1, and 0.2 ppm, respectively) that was assumed to decay from the walls into the gas phase with a first-order decay constant of 0.002 min^{-1}; this was done to help simulate the observed formaldehyde and CO data, though the simulations still failed to generate the reported amounts.

- Additional ethene--Slightly less than 0.1 ppm initial ethene was reported for three experiments (12 October 1978, 25 October 1978, and 16 August 1979; Figures 2ℓ, 2o, and 2r). These experiments were simulated by adding the observed amounts of ethene along with an ethene mechanism.

Overall adjustment of the formaldehyde mechanism was accomplished by reducing formaldehyde photolysis slightly (10 percent) from previous photolysis constants published in Whitten, Killus, and Hogo (1980).

Overall adjustment of the acetaldehyde mechanism was accomplished primarily by the adoption of a temperature-dependent photolysis rate for acetaldehyde as suggested by Kamens et al. (1981). Temperatures range from 264 K in the 27 February 1978 acetaldehyde experiment to 314 K in the 1 August 1979 acetaldehyde experiment. The temperature dependence is handled by assuming an exited state (STAR) for the initial absorption reaction. The photolytic rate of this initial reaction is taken to be 30 percent more rapid than our previous acetaldehyde rate (Whitten, Killus, and Hogo, 1980). The stabilization rate of STAR back to acetaldehyde is taken to be 10 percent of the total reaction rate at 298 K and is independent of temperature. The unimolecular decomposition rate is taken to be 90 percent of the total STAR reaction rate at 298 K, with an E/R of 10,000 K.

This approach provides only a modest increase in the net photolysis rate at temperatures above 298 K (30 percent maximum), but a considerable reduction in the photolysis rate is provided at the coldest temperatures. For example, this scheme reduces the photolysis rate of acetaldehyde by almost a factor of 12 at 264 K compared with the photolysis rate at 298 K. It is also noteworthy that the coldest experiment--27 February 1978--was optimized using zero HONO. Unfortunately, the data for acetaldehyde and CO for that day were incomplete; hence the quality of the simulation is uncertain, even though PAN and O_3 were reasonably well simulated.

The simulation for 1 August 1979 was made at the other end of the temperature range. In this case, the simulated rate of acetaldehyde decay seems a little too rapid at midday, yet the observed appearance rate of formaldehyde is more rapid than the simulated curve. It is unfortunate that the CO data are incomplete, since such data are often helpful in judging the quality of the simulation. Nevertheless, the agreement between simulated and observed ozone and PAN is reasonable and supports the concept of a temperature dependence in the acetaldehyde photolysis rate. Presently, laboratory confirmation of this concept is lacking, and the actual temperature-sensitive chemistry may yet be found in the inorganic chemistry.

An alternate system such as biacetyl with NO_x might be studied across a range of temperatures. Biacetyl photolyses more rapidly and at longer wavelengths than acetaldehyde, which would eliminate the sensitivity to changes in solar spectra. Biacetyl, however, would emphasize the temperature dependence of PAN chemistry. Another possibility is methylnitrite; however, the rapidly generated formaldehyde within this system could adhere to the chamber walls.

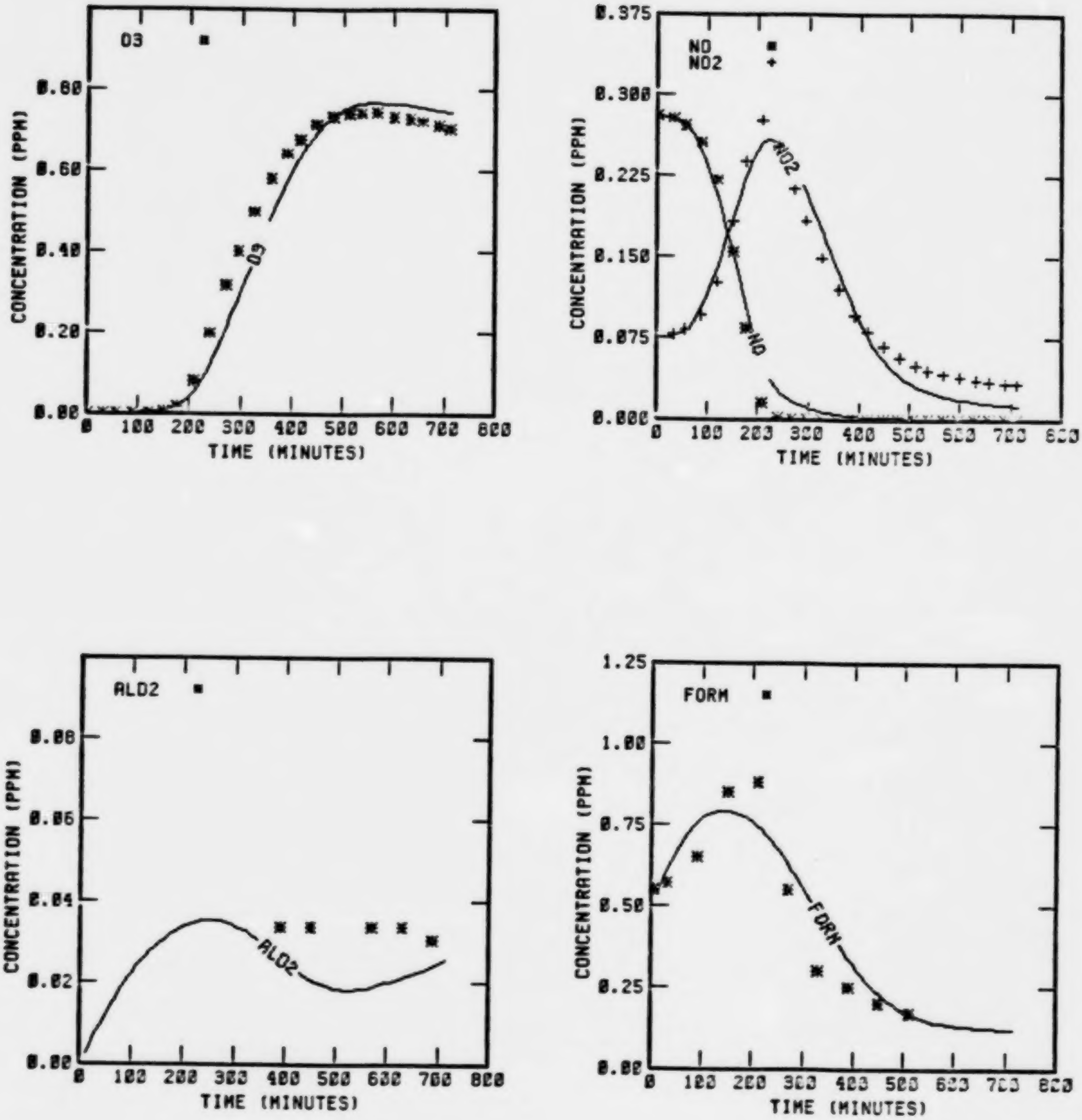

FIGURE 1a. SIMULATION RESULTS FOR
UNCB 51877

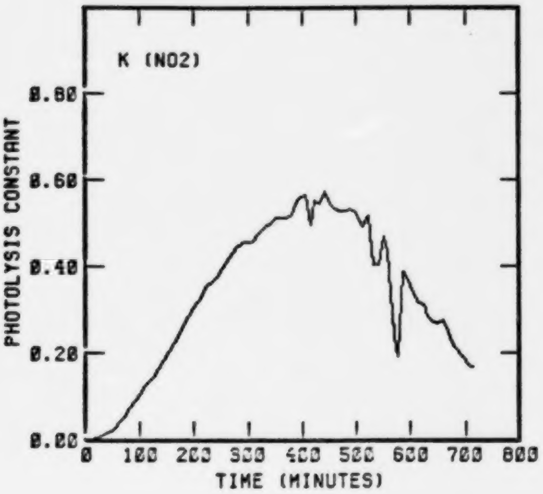

FIGURE 1a. SIMULATION RESULTS FOR
UNCB 51677

(concluded)

Reproduced from
best available copy.

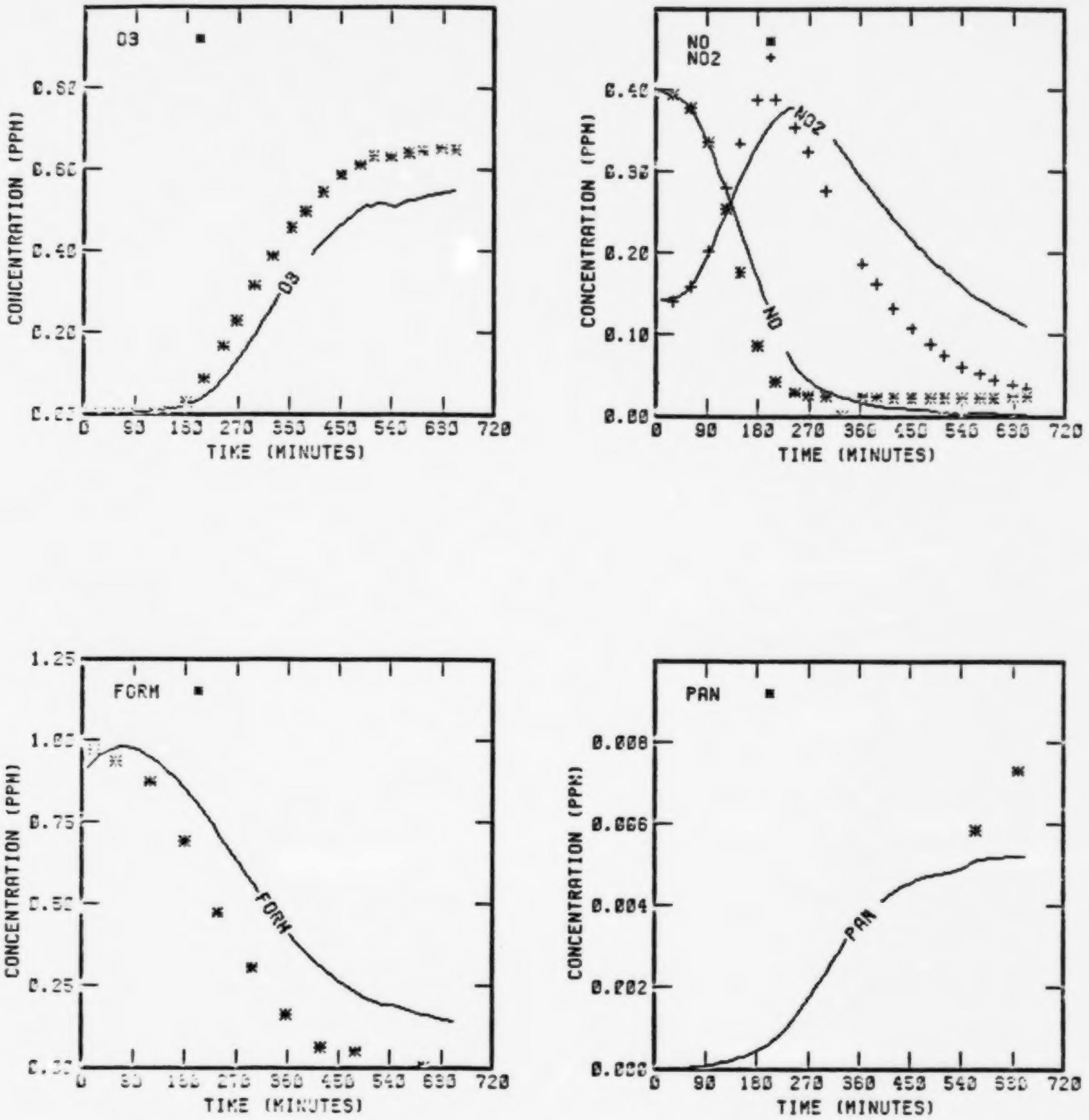

FIGURE 1b. SIMULATION RESULTS FOR
UNCR 71677

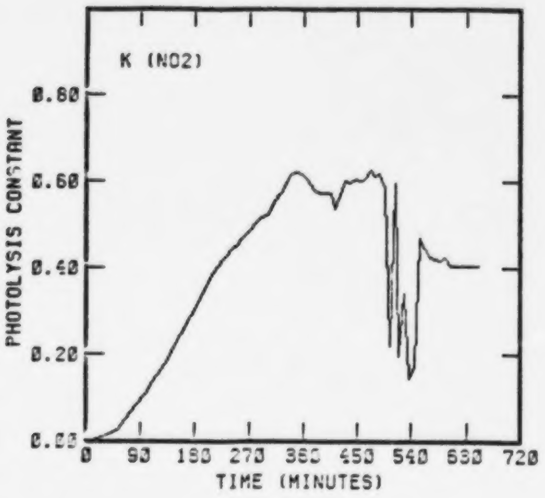

FIGURE 1b. SIMULATION RESULTS FOR
UNCR 71877

(concluded)

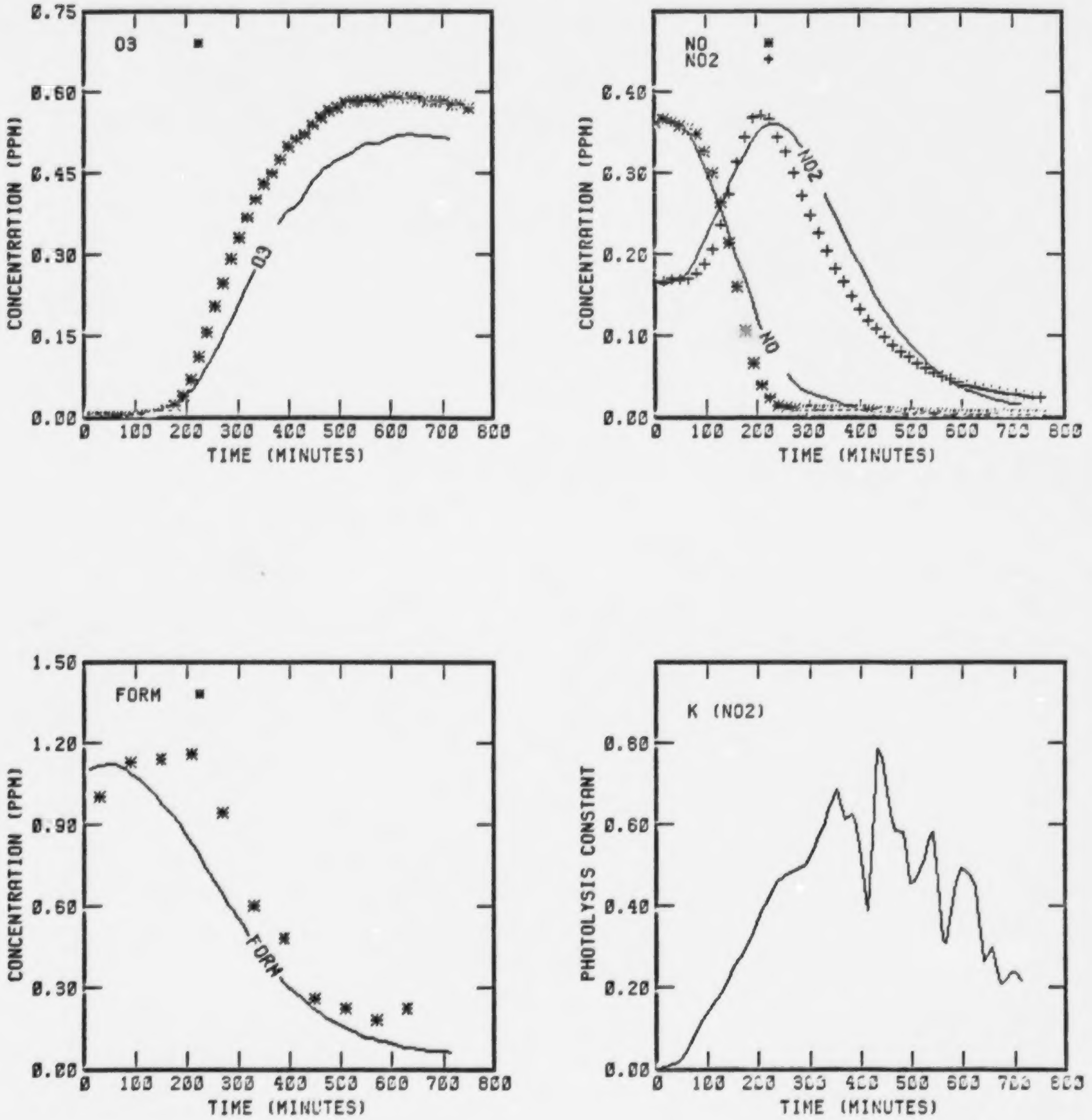

FIGURE 1c. SIMULATION RESULTS FOR
UNCR 72877

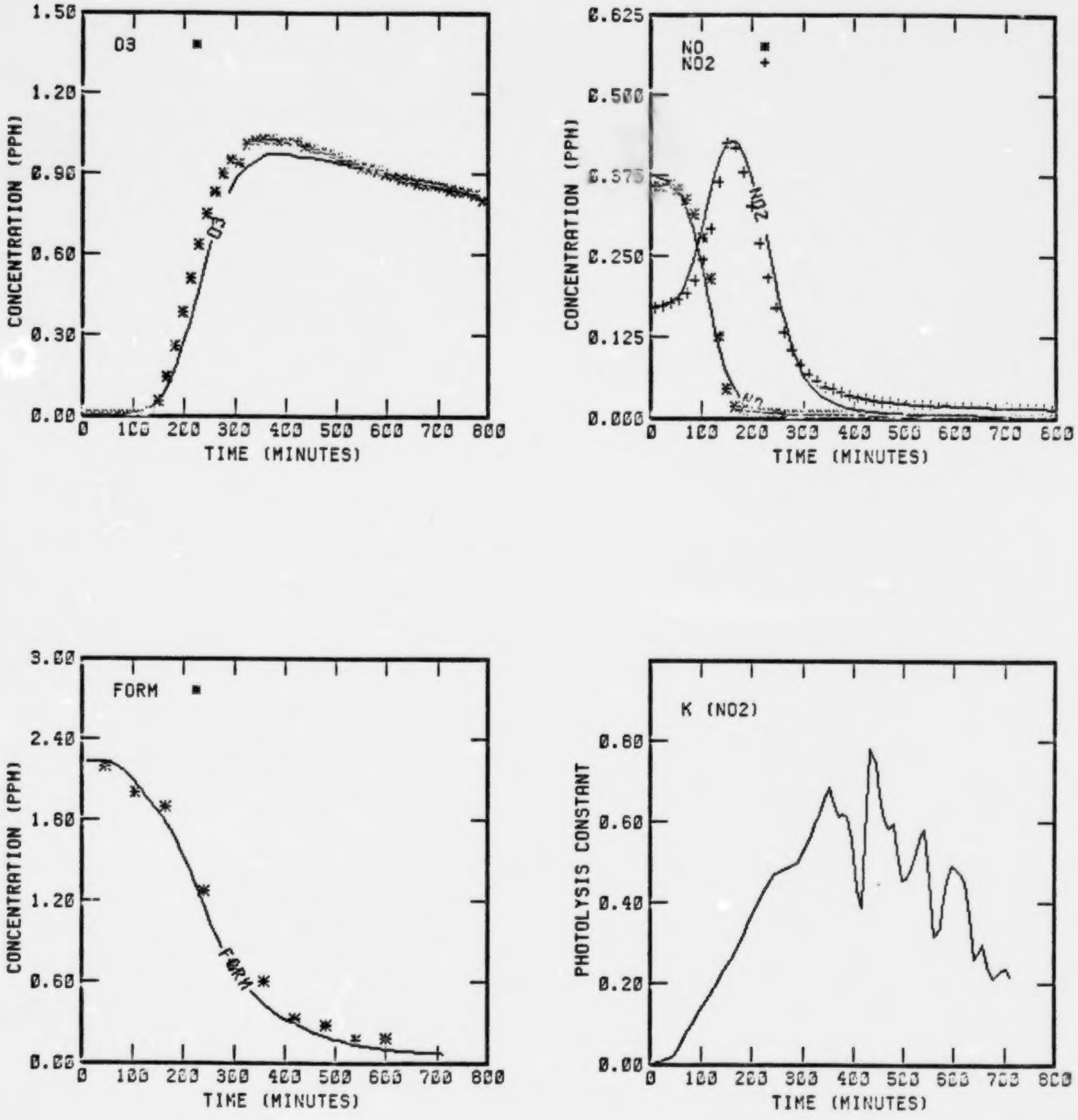

FIGURE 1c. SIMULATION RESULTS FOR UNCB 72877

(concluded)

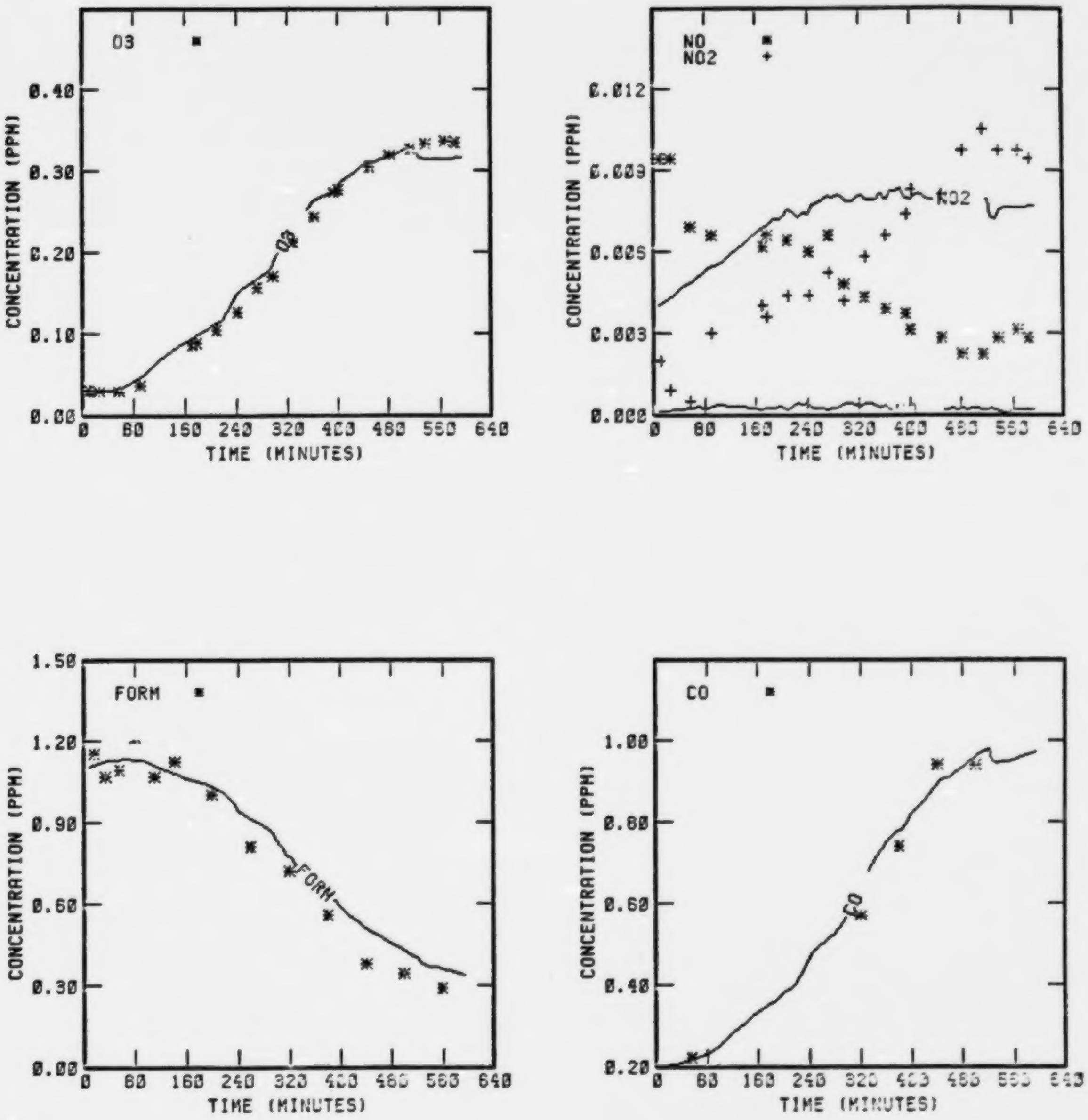

FIGURE 1d. SIMULATION RESULTS FOR
UNCB 91477

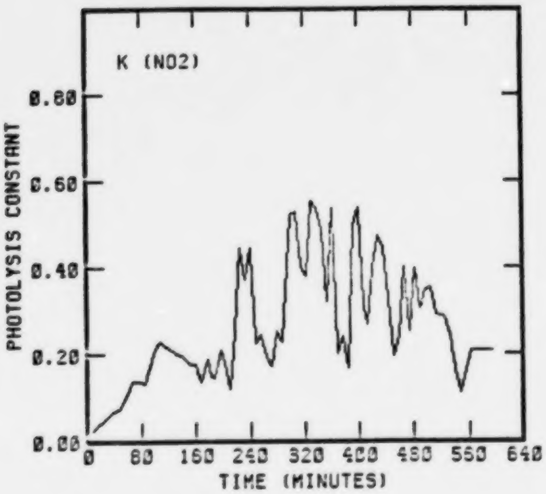

FIGURE 1d. SIMULATION RESULTS FOR
UNCB 91477

(concluded)

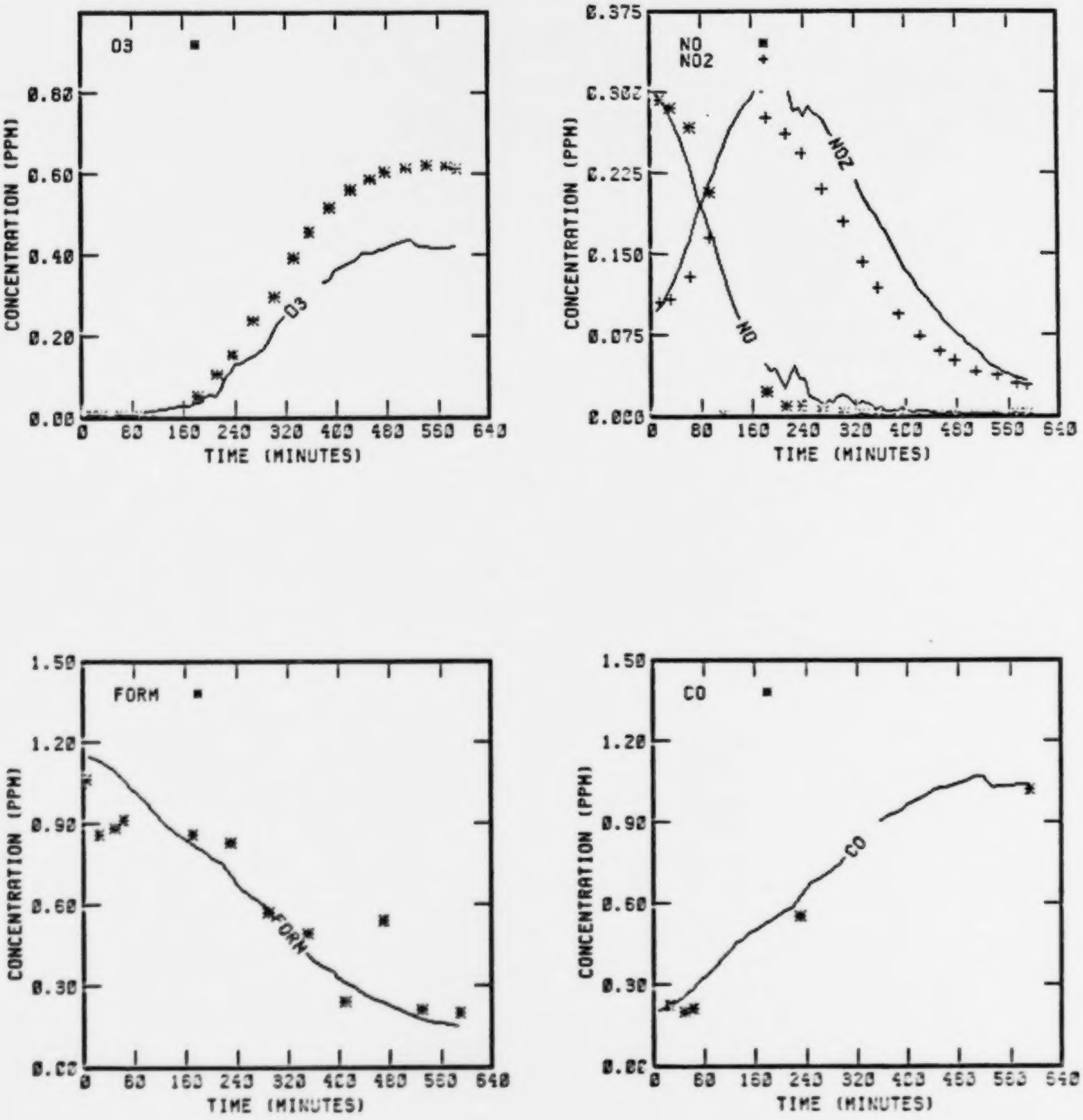

FIGURE 1e. SIMULATION RESULTS FOR
UNCR 91477

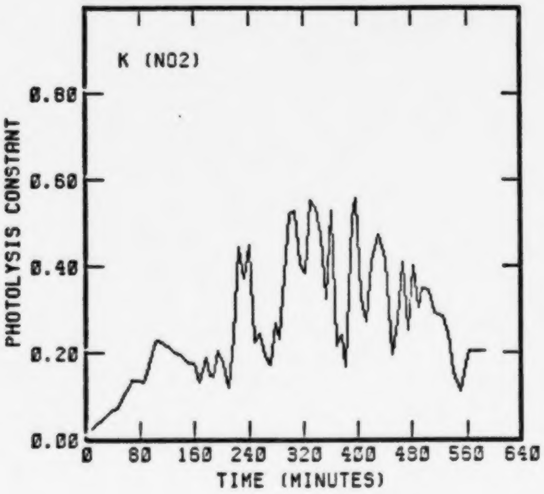

FIGURE 1e. SIMULATION RESULTS FOR
UNCR 91477

(concluded)

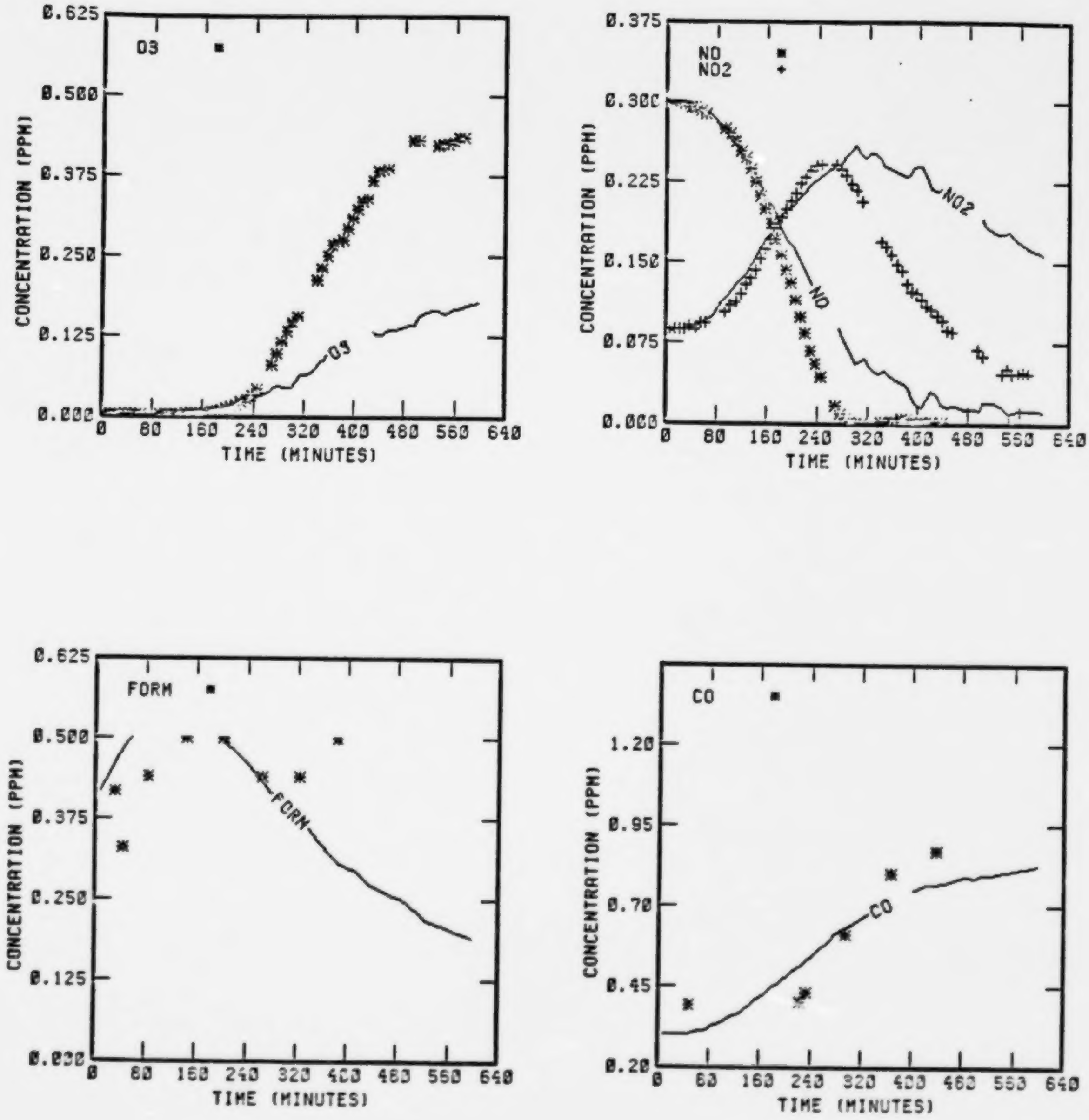

FIGURE 1f. SIMULATION RESULTS FOR
UNCB 91977

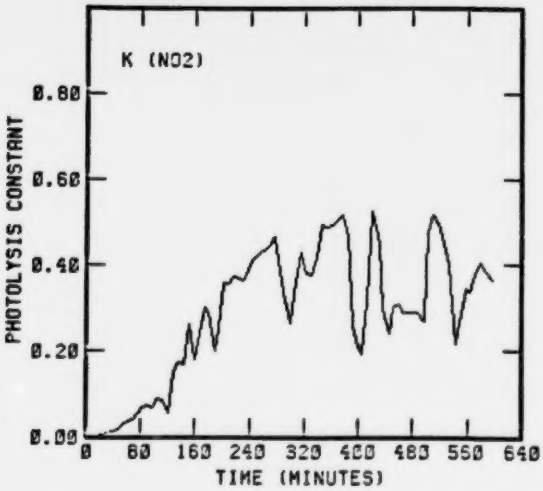

FIGURE 1f. SIMULATION RESULTS FOR
UNCB 91977

(concluded)

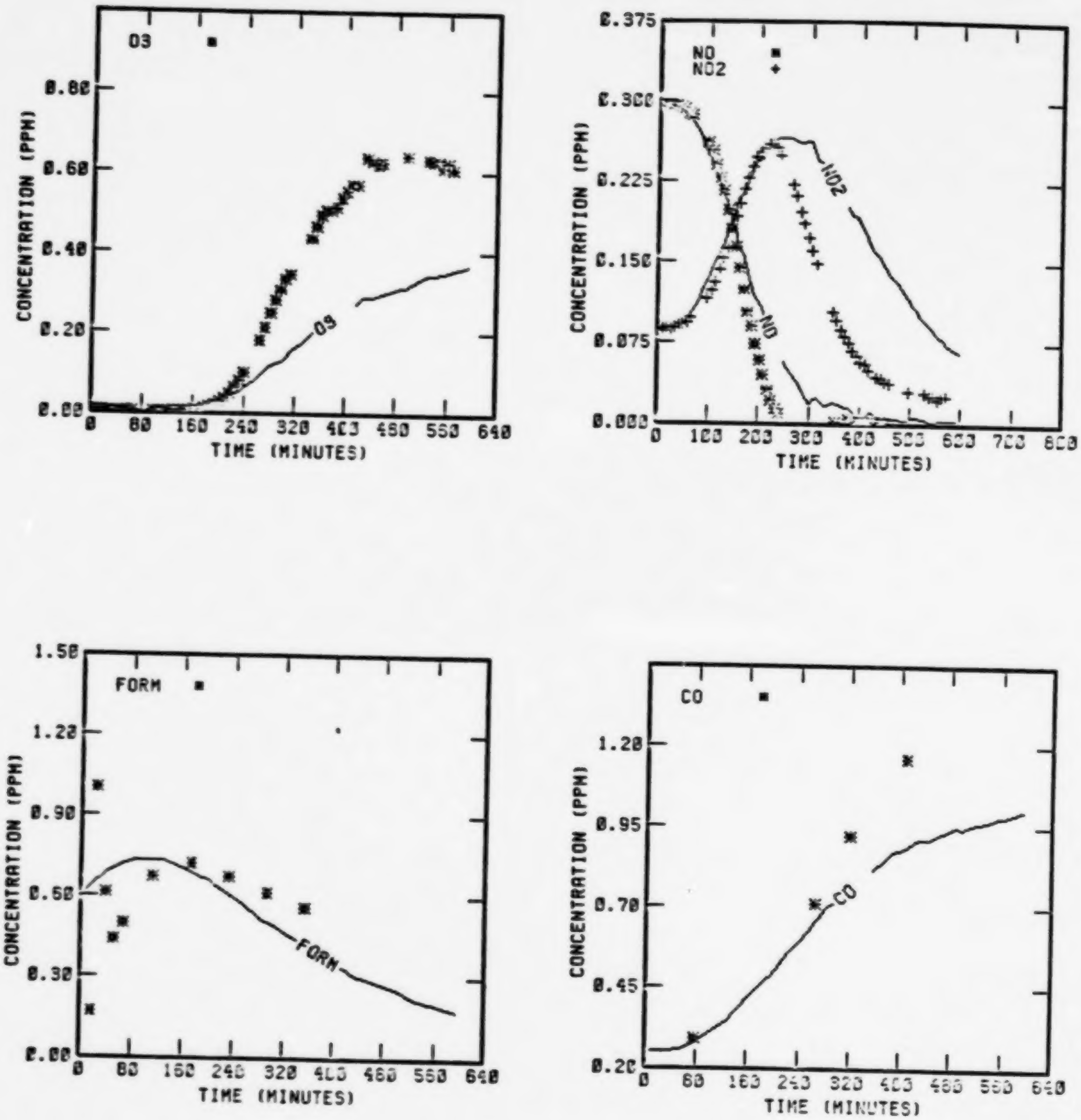

FIGURE 1g. SIMULATION RESULTS FOR UNCR 91977

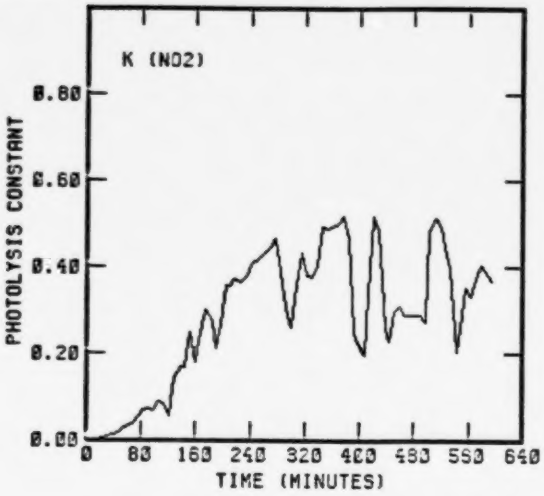

FIGURE 1g. SIMULATION RESULTS FOR
UNCR 91977

(concluded)

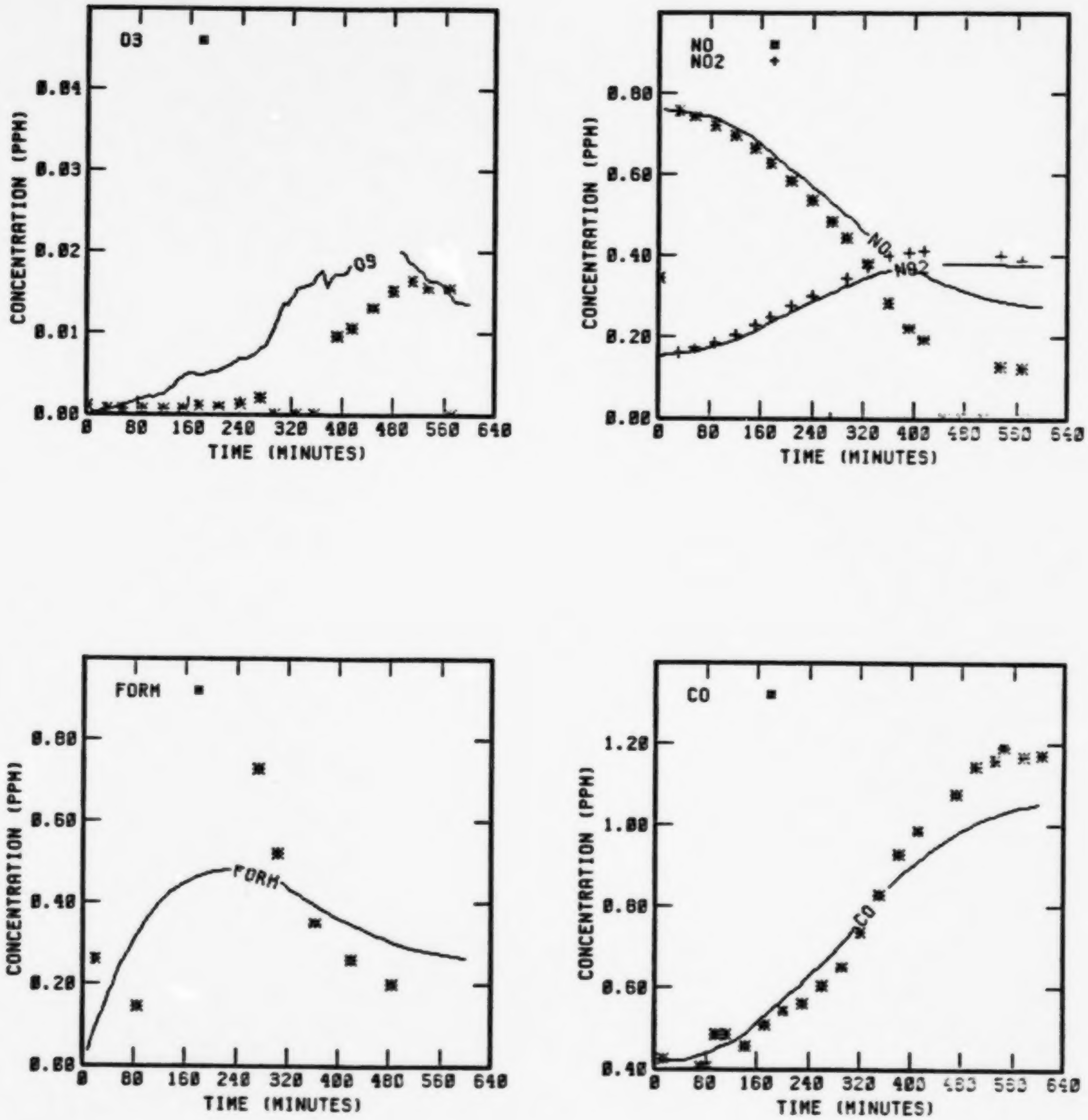

FIGURE 1h. SIMULATION RESULTS FOR
UNCB 90878

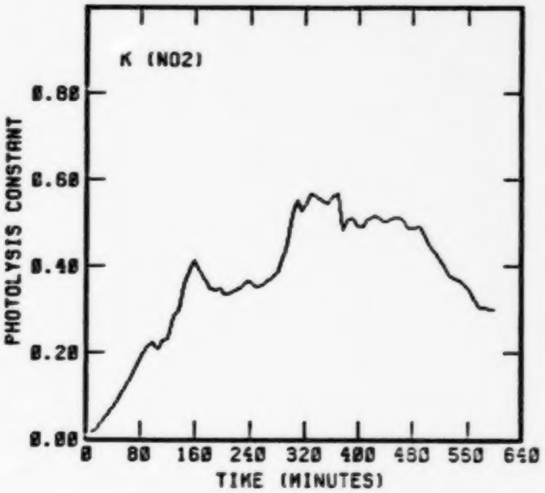

FIGURE 1h. SIMULATION RESULTS FOR
UNCB 90678

(concluded)

Reproduced from
best available copy.

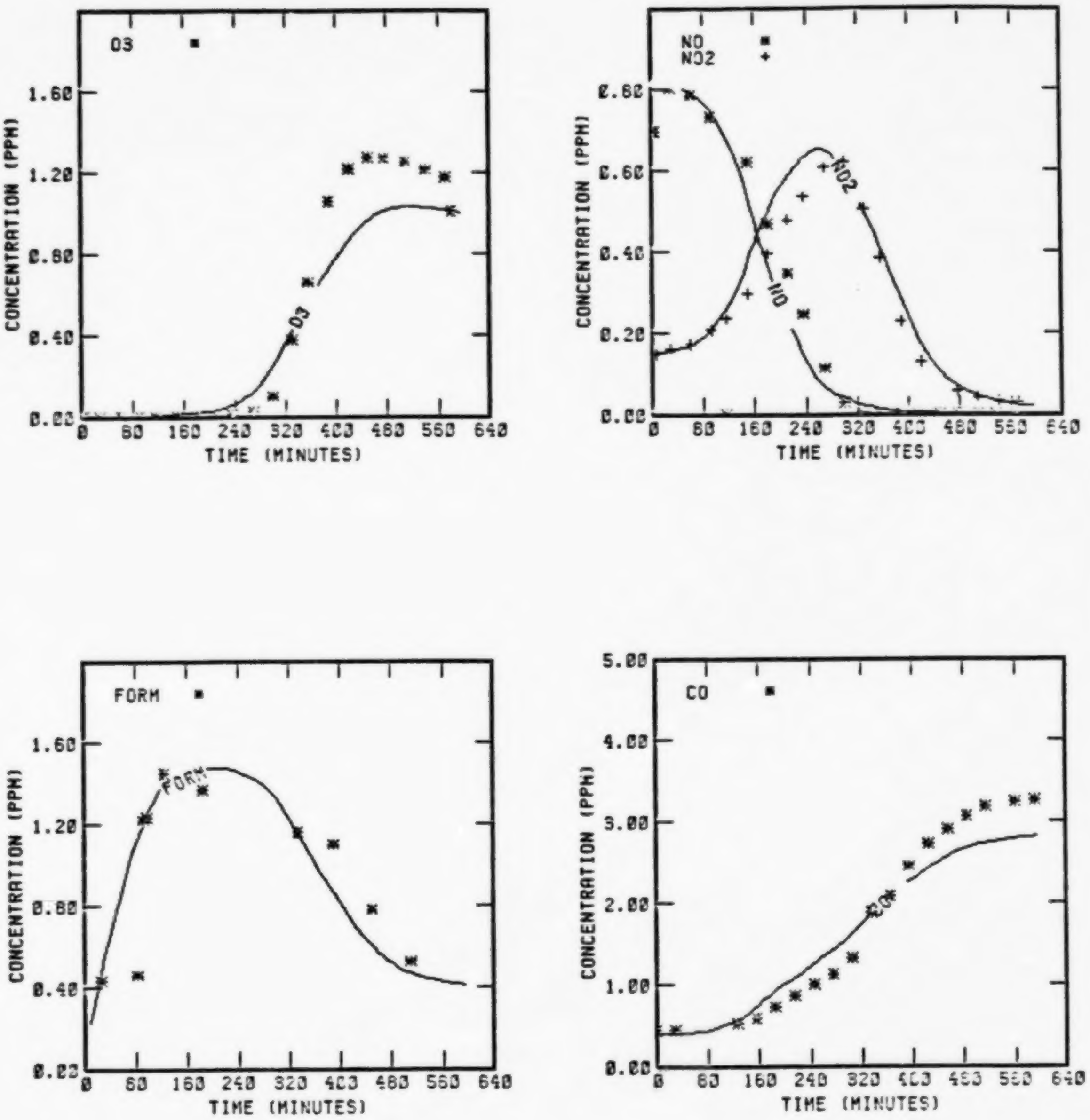

FIGURE 1i. SIMULATION RESULTS FOR
UNCR 90878

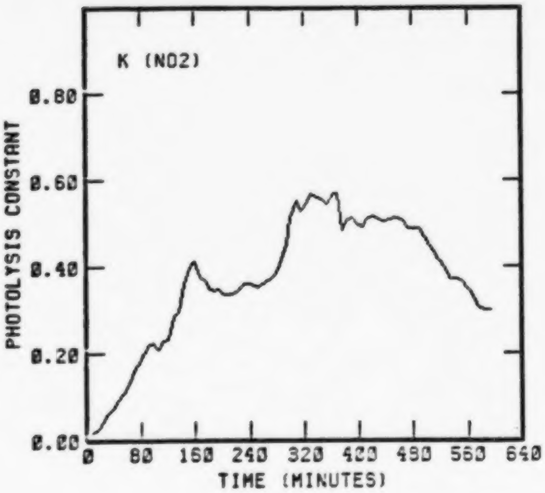

FIGURE 1i. SIMULATION RESULTS FOR
UNCR 90378

(concluded)

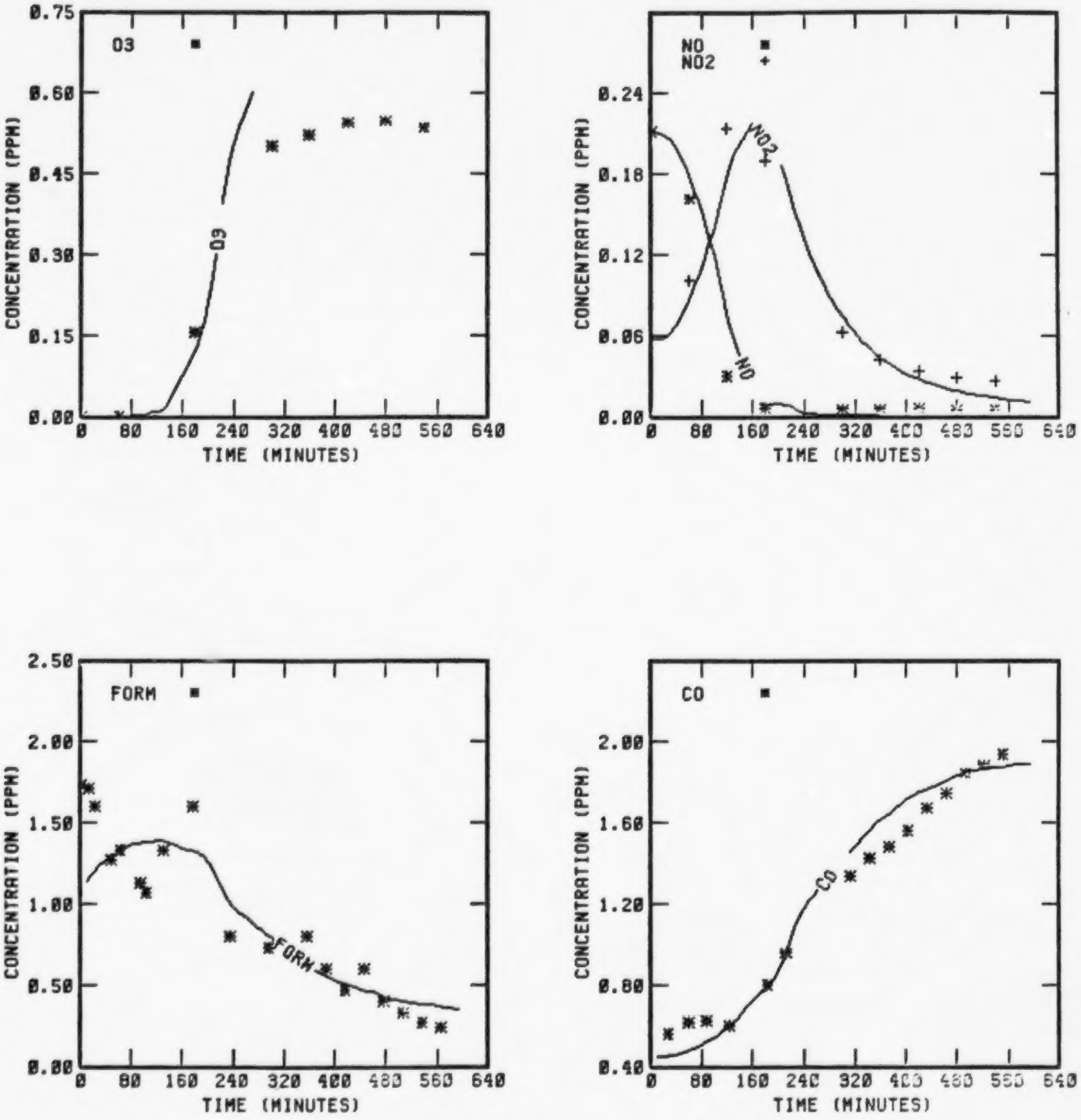

FIGURE 1j. SIMULATION RESULTS FOR
UNCB 91578

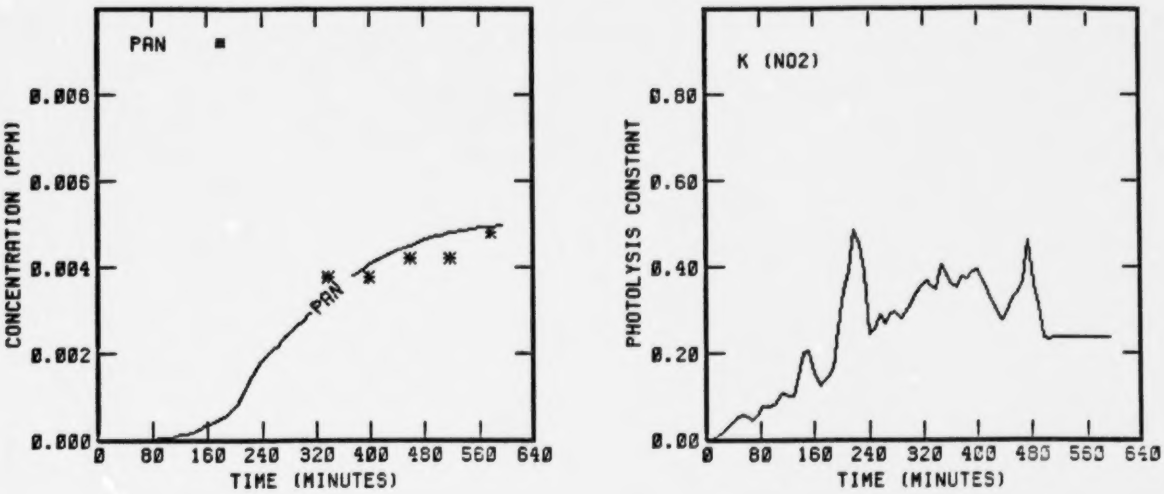

FIGURE 1j. SIMULATION RESULTS FOR
UNCB 9157B

(concluded)

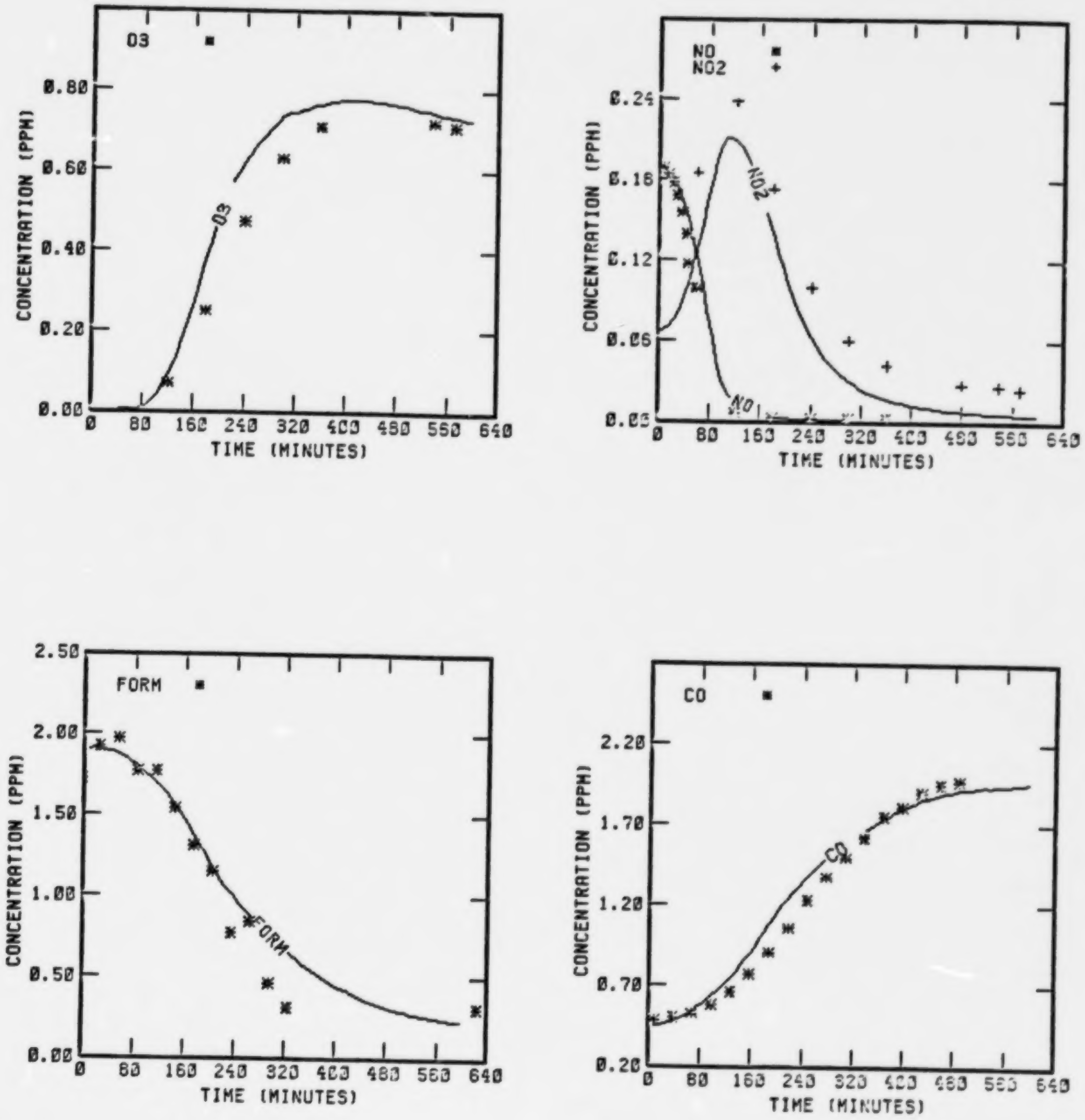

FIGURE 1k. SIMULATION RESULTS FOR
UNCB 92178

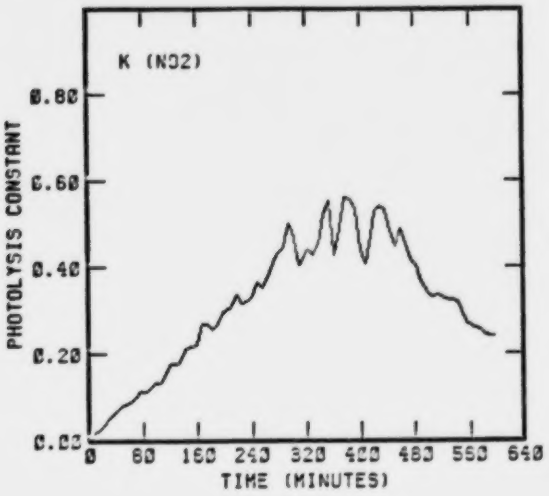

FIGURE 1k. SIMULATION RESULTS FOR
UNCB 92178

(concluded)

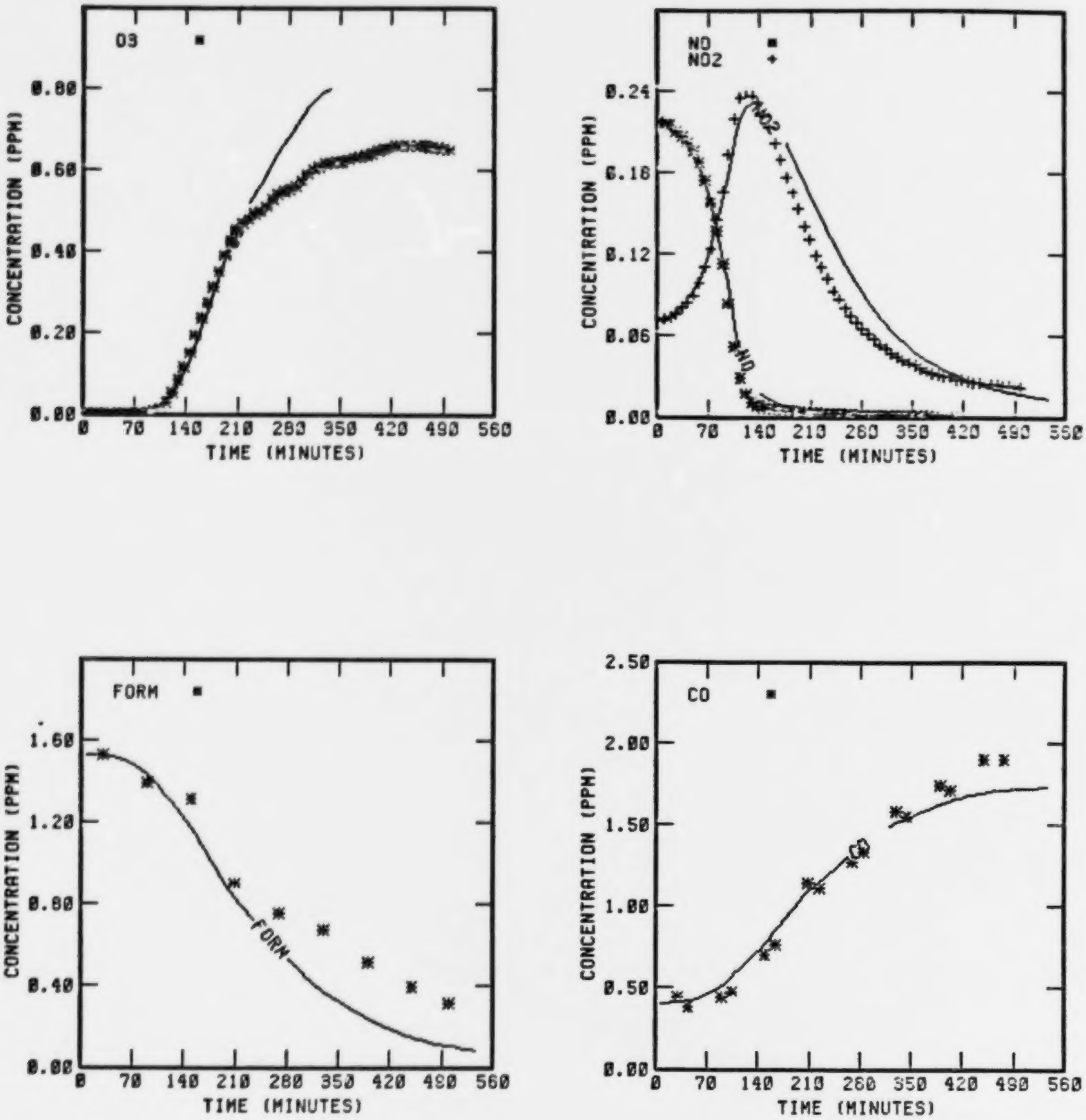

FIGURE 1ℓ. SIMULATION RESULTS FOR
UNCB 73079

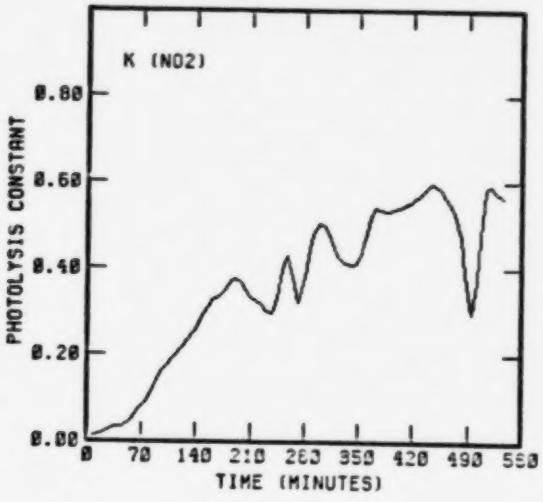

FIGURE 1ℓ . SIMULATION RESULTS FOR
UNCB 73079

(concluded)

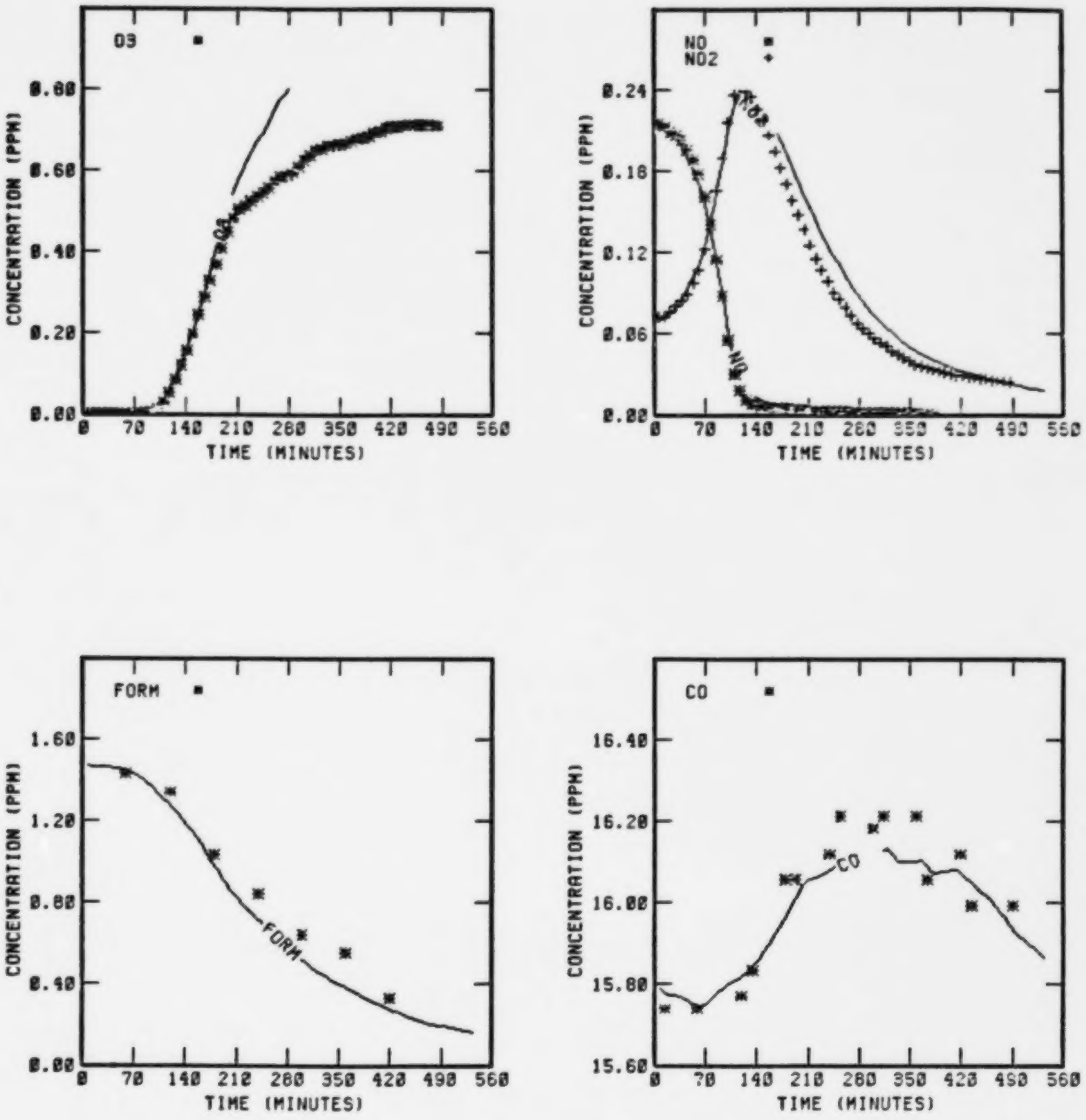

FIGURE 1m. SIMULATION RESULTS FOR
UNCR 73079

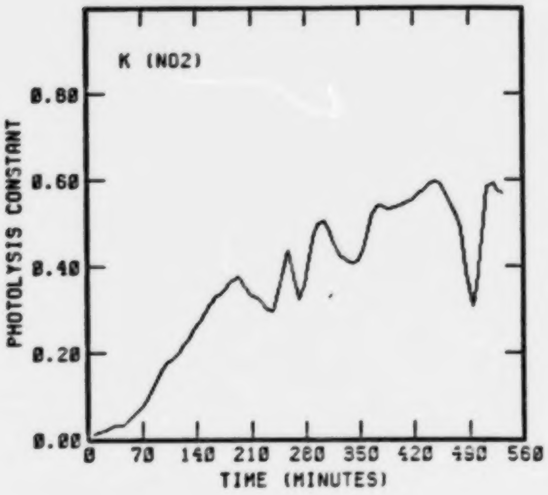

FIGURE 1m. SIMULATION RESULTS FOR
UNCR 73079

(concluded)

Reproduced from
best available copy.

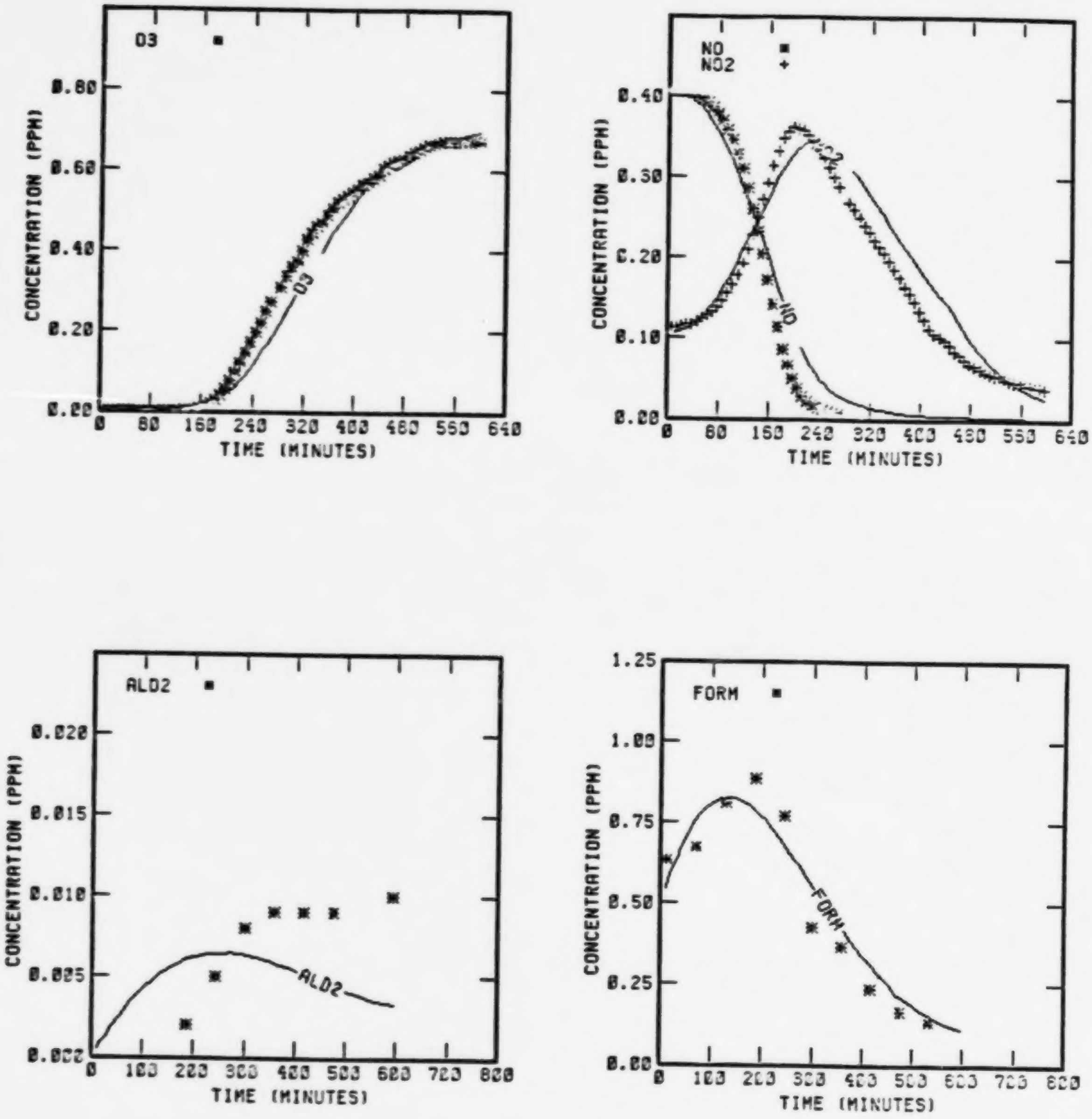

FIGURE 1n. SIMULATION RESULTS FOR
UNCR 73179

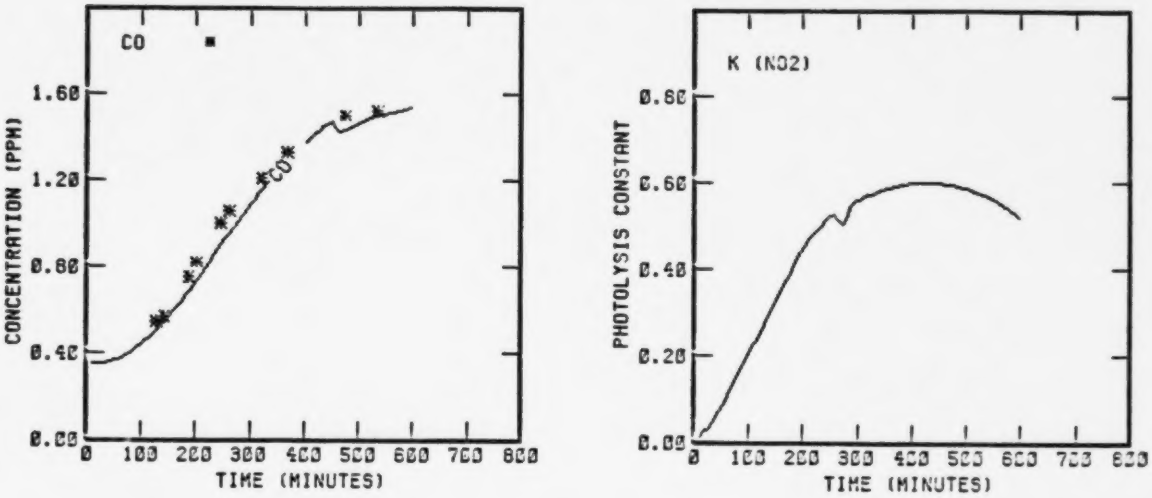

FIGURE 1n. SIMULATION RESULTS FOR
UNCR 73179

(concluded)

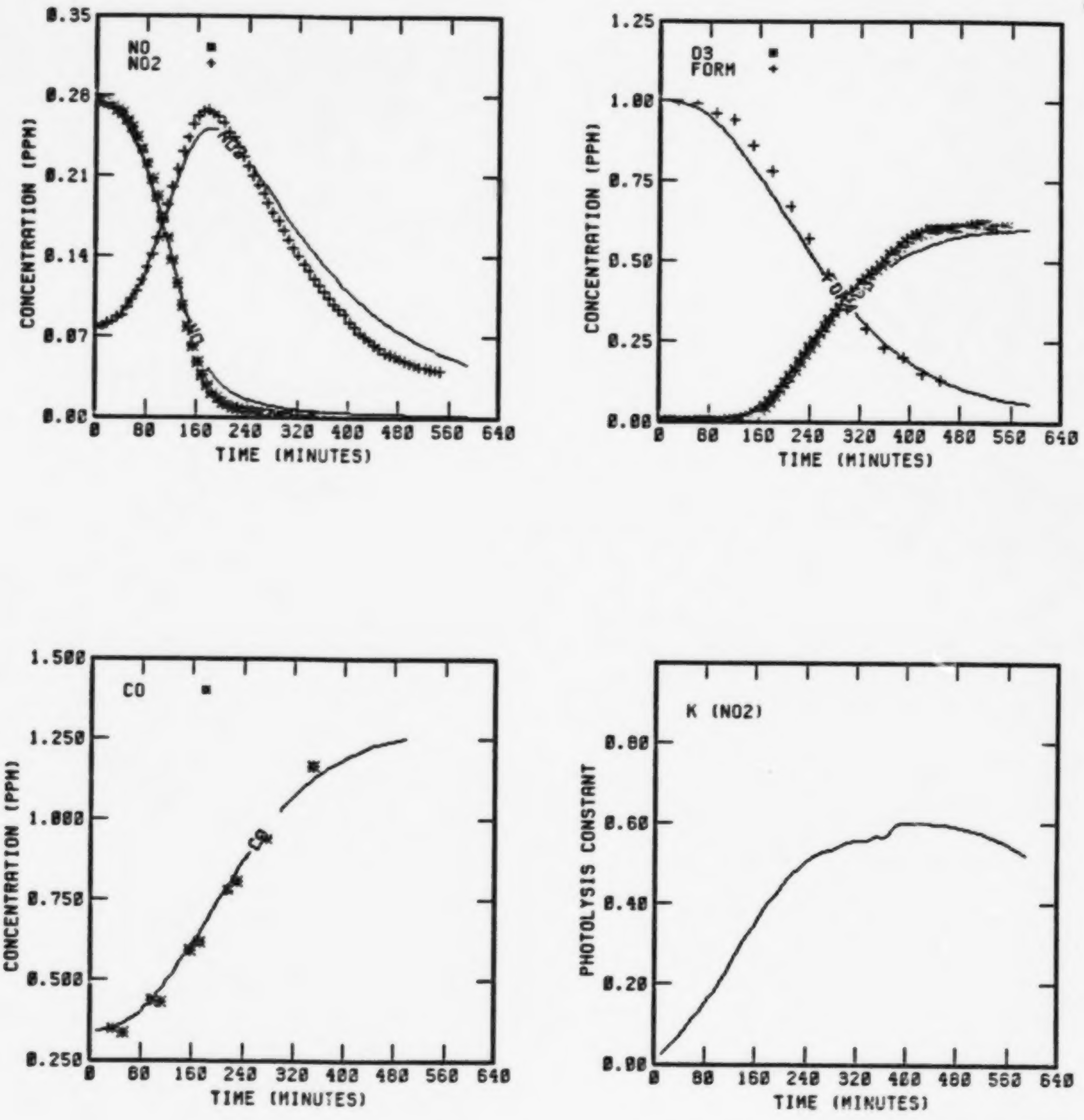

FIGURE 10. SIMULATION RESULTS FOR
UNCB 80179

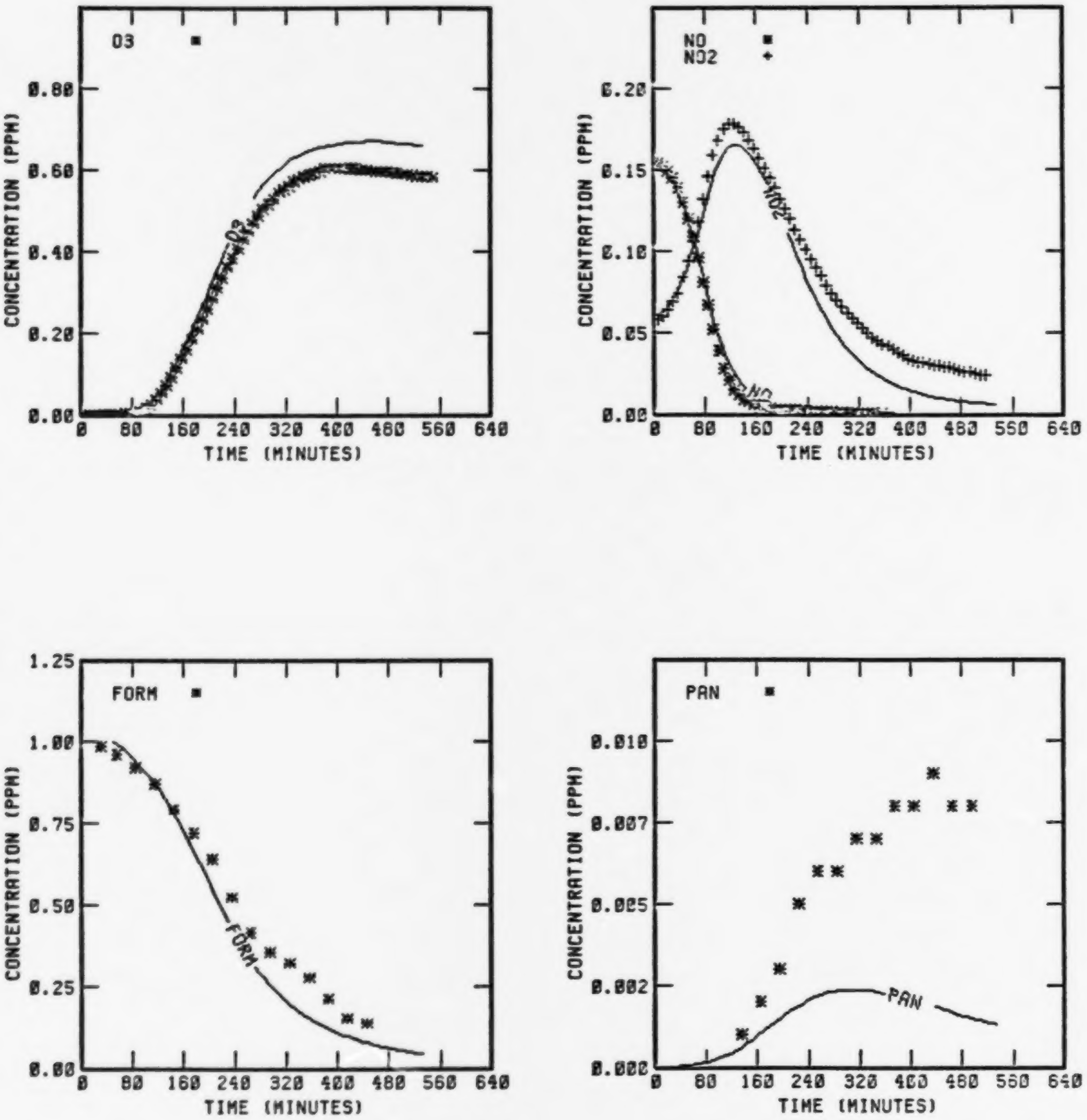

FIGURE 1p. SIMULATION RESULTS FOR
UNCB 80279

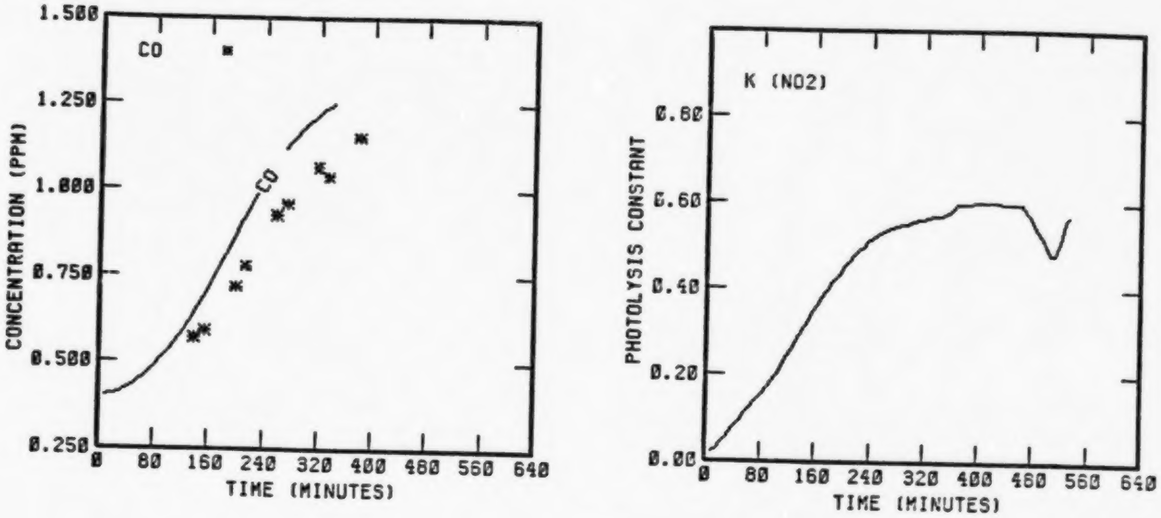

FIGURE 1p. SIMULATION RESULTS FOR
UNCB 80279

(concluded)

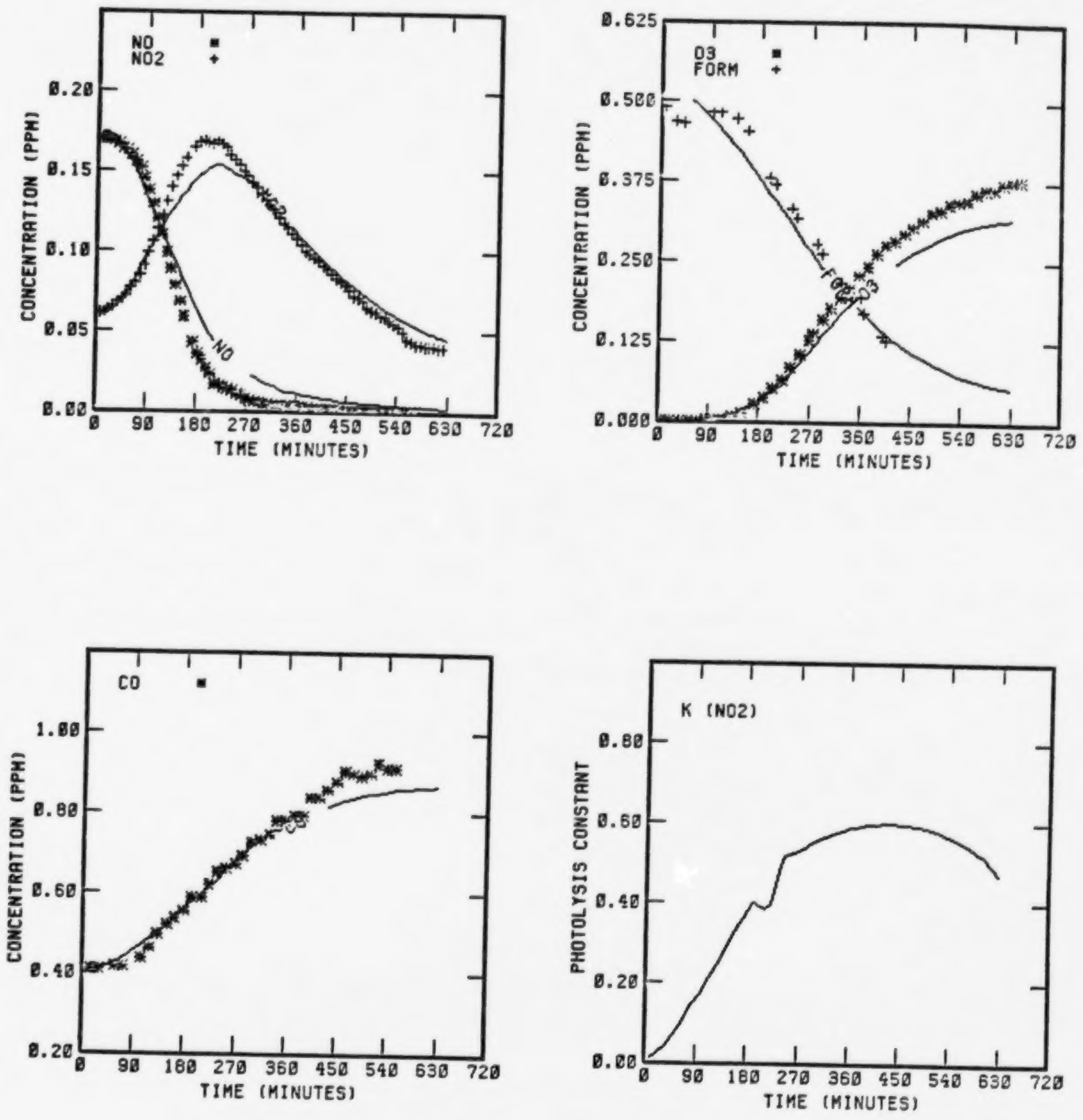

FIGURE 1q. SIMULATION RESULTS FOR UNCB 80479

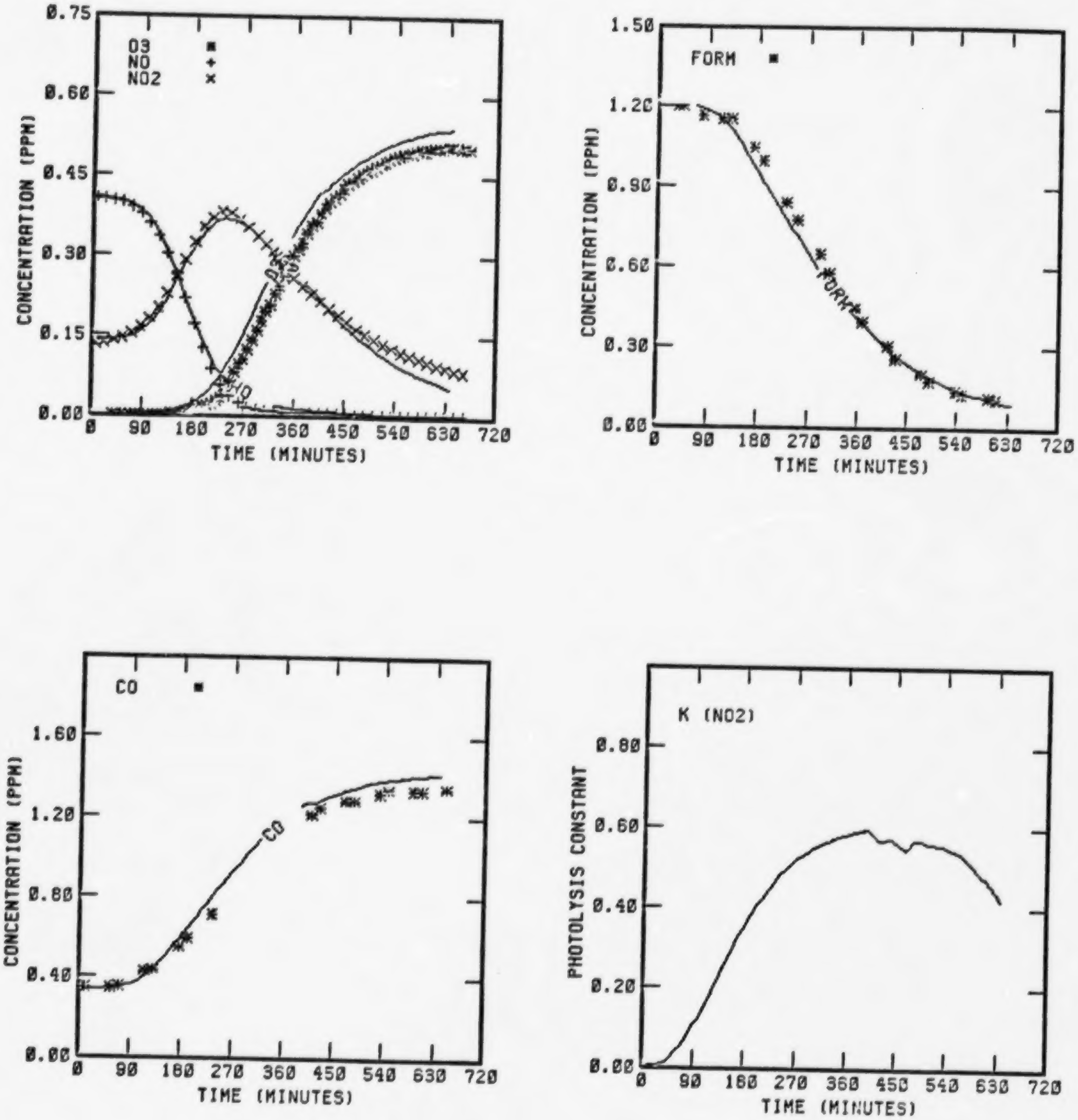

FIGURE 1r. SIMULATION RESULTS FOR
UNCB 80579

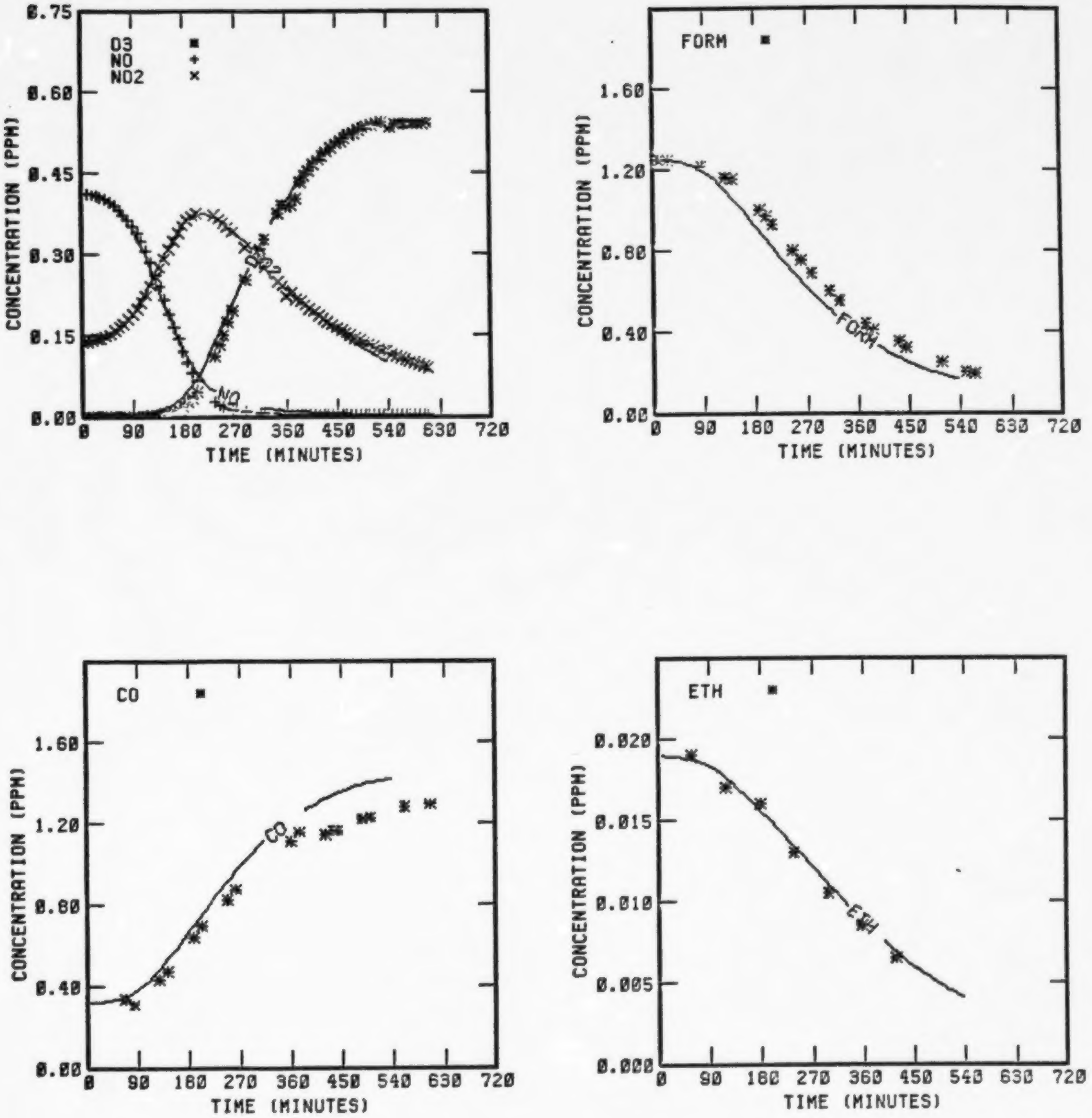

FIGURE 1s. SIMULATION RESULTS FOR
UNCB 90779

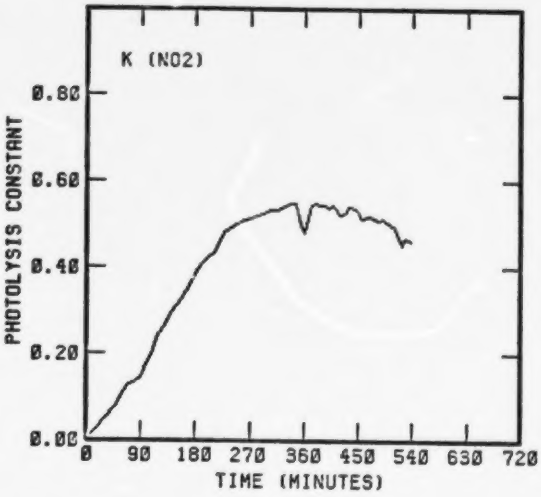

FIGURE 1s. SIMULATION RESULTS FOR
UNCB 90779

(concluded)

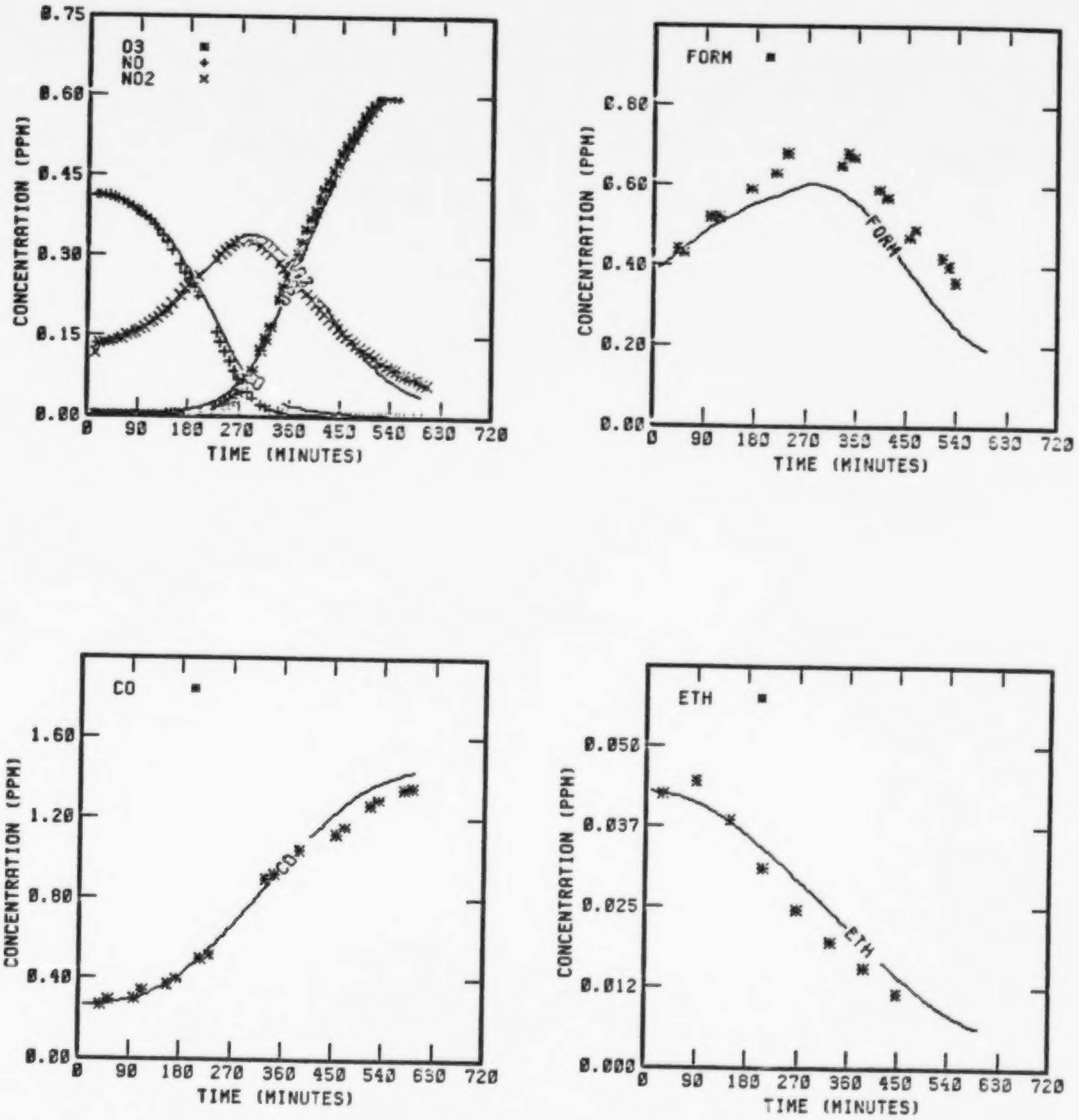

FIGURE 1t. SIMULATION RESULTS FOR UNCR 90773

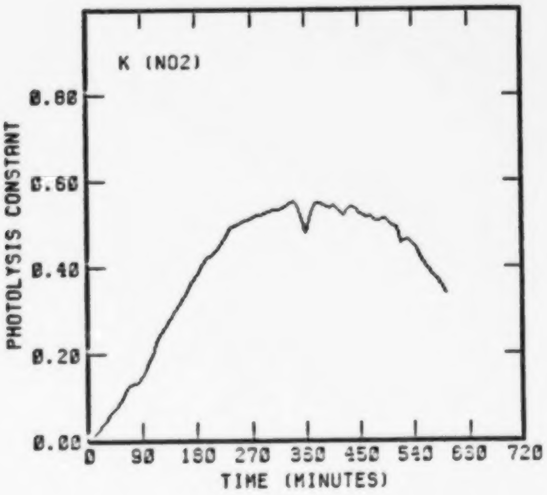

FIGURE 1t. SIMULATION RESULTS FOR UNCR 90779

(concluded)

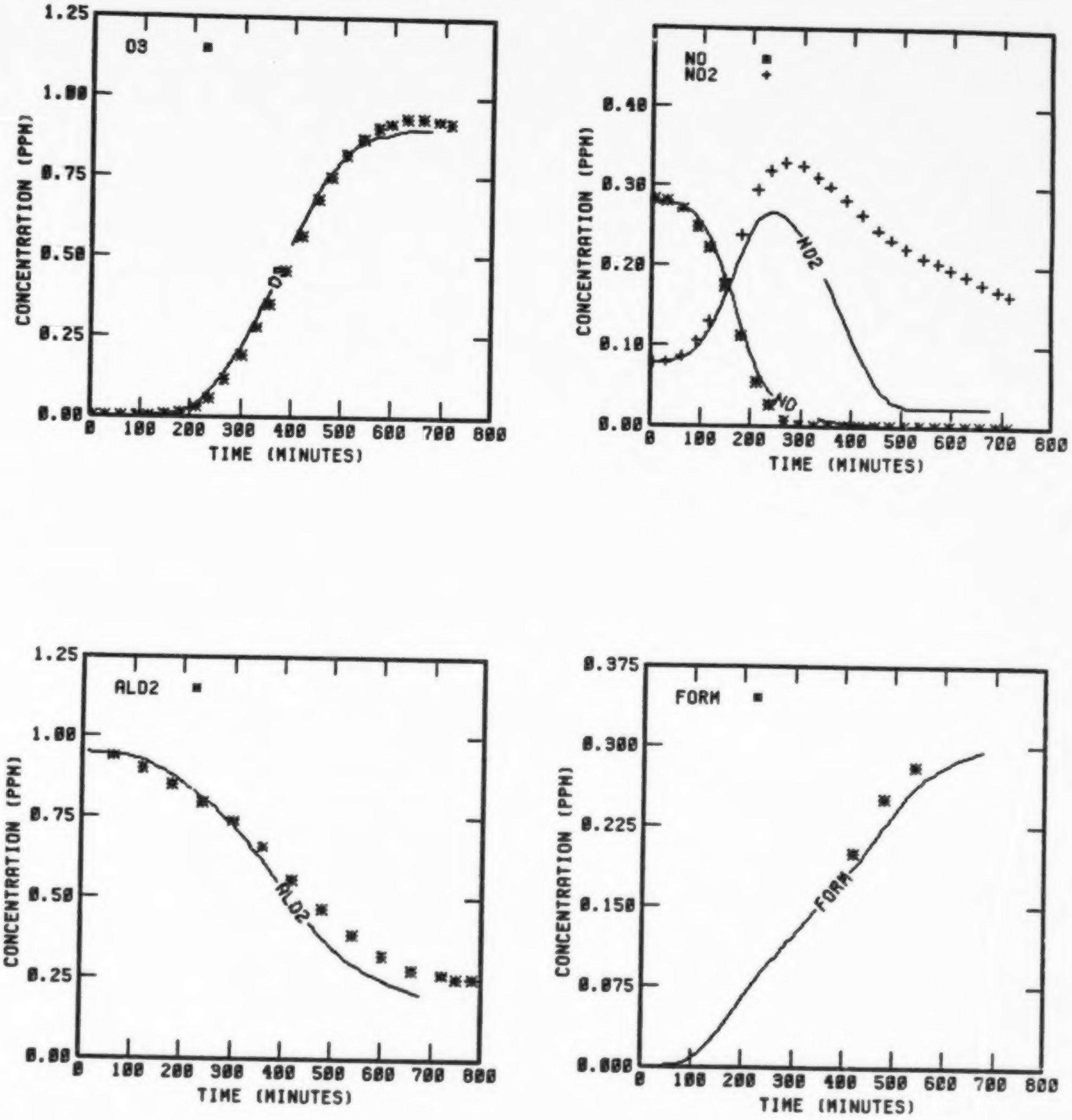

FIGURE 2a. SIMULATION RESULTS FOR UNCR 51877

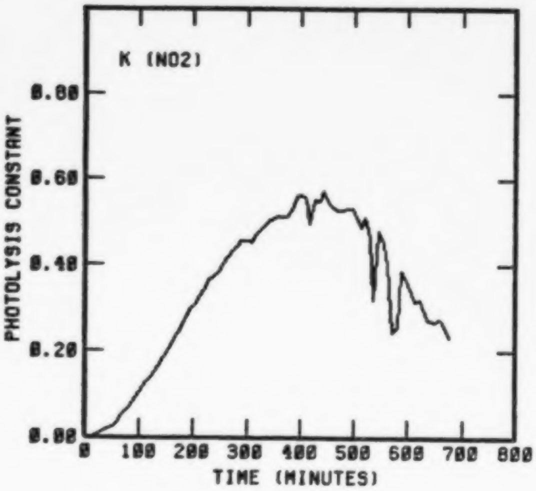

FIGURE 2a. SIMULATION RESULTS FOR
UNCR 51877

(concluded)

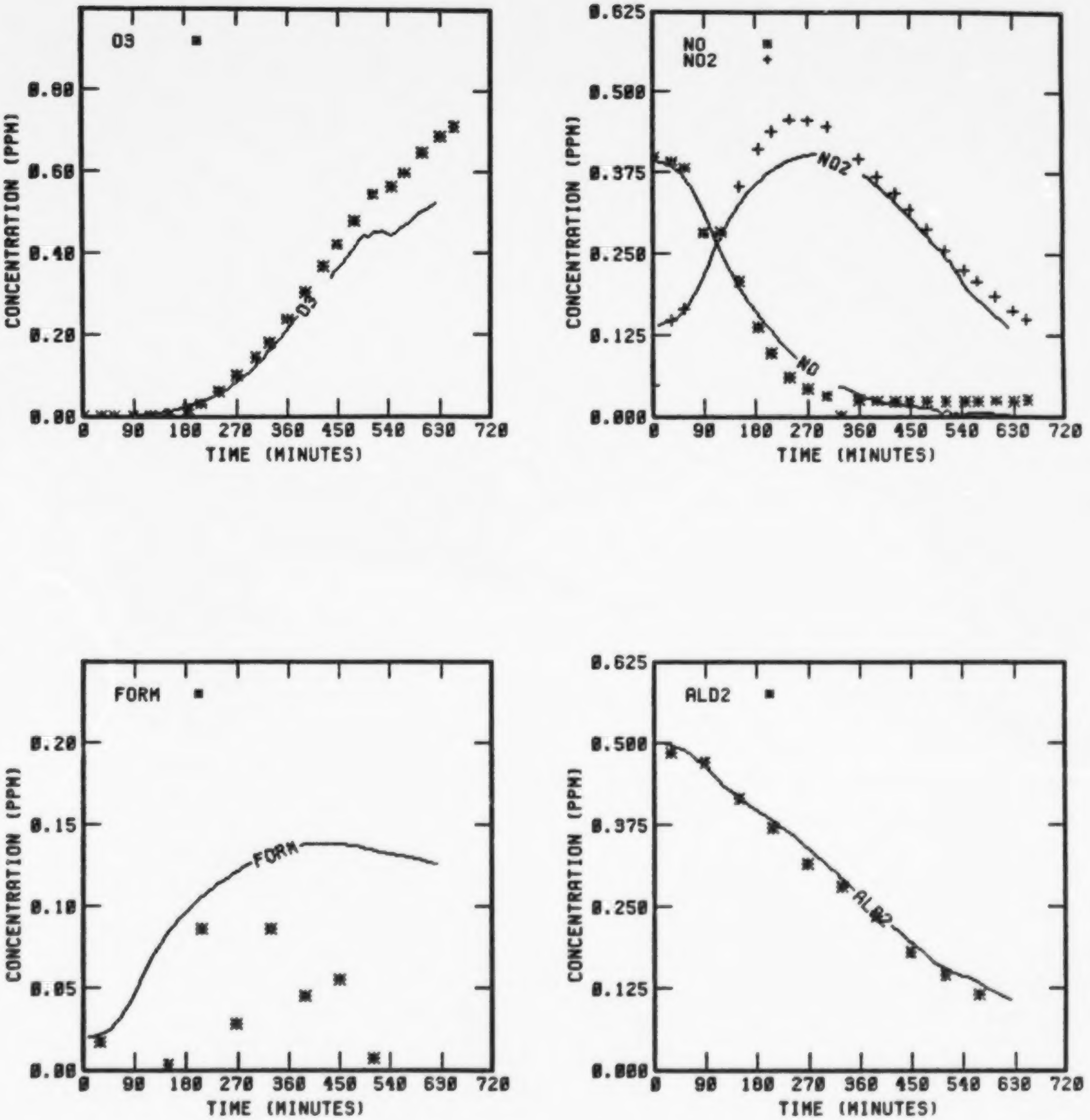

FIGURE 2b. SIMULATION RESULTS FOR
UNCB 71877

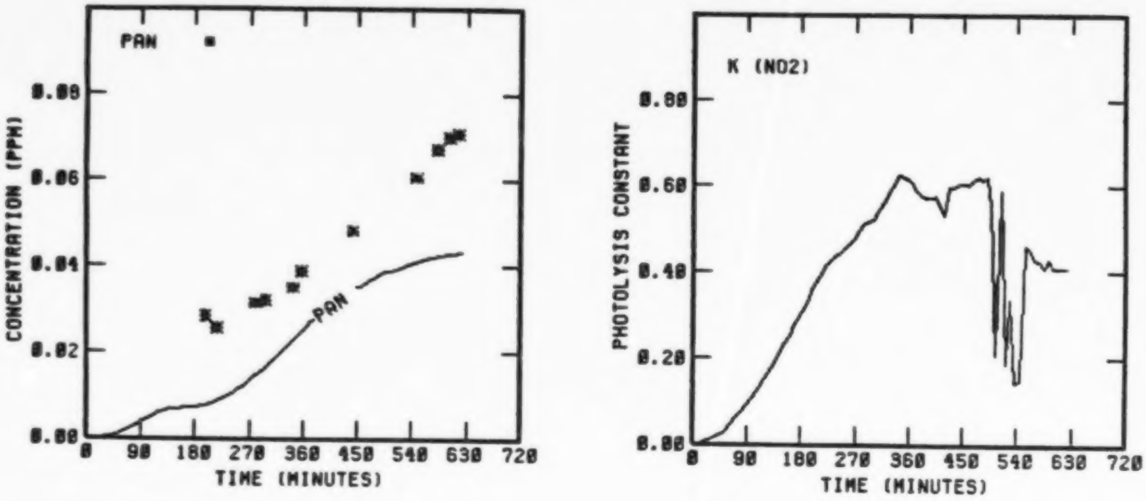

FIGURE 2b. SIMULATION RESULTS FOR
UNCB 71877

(concluded)

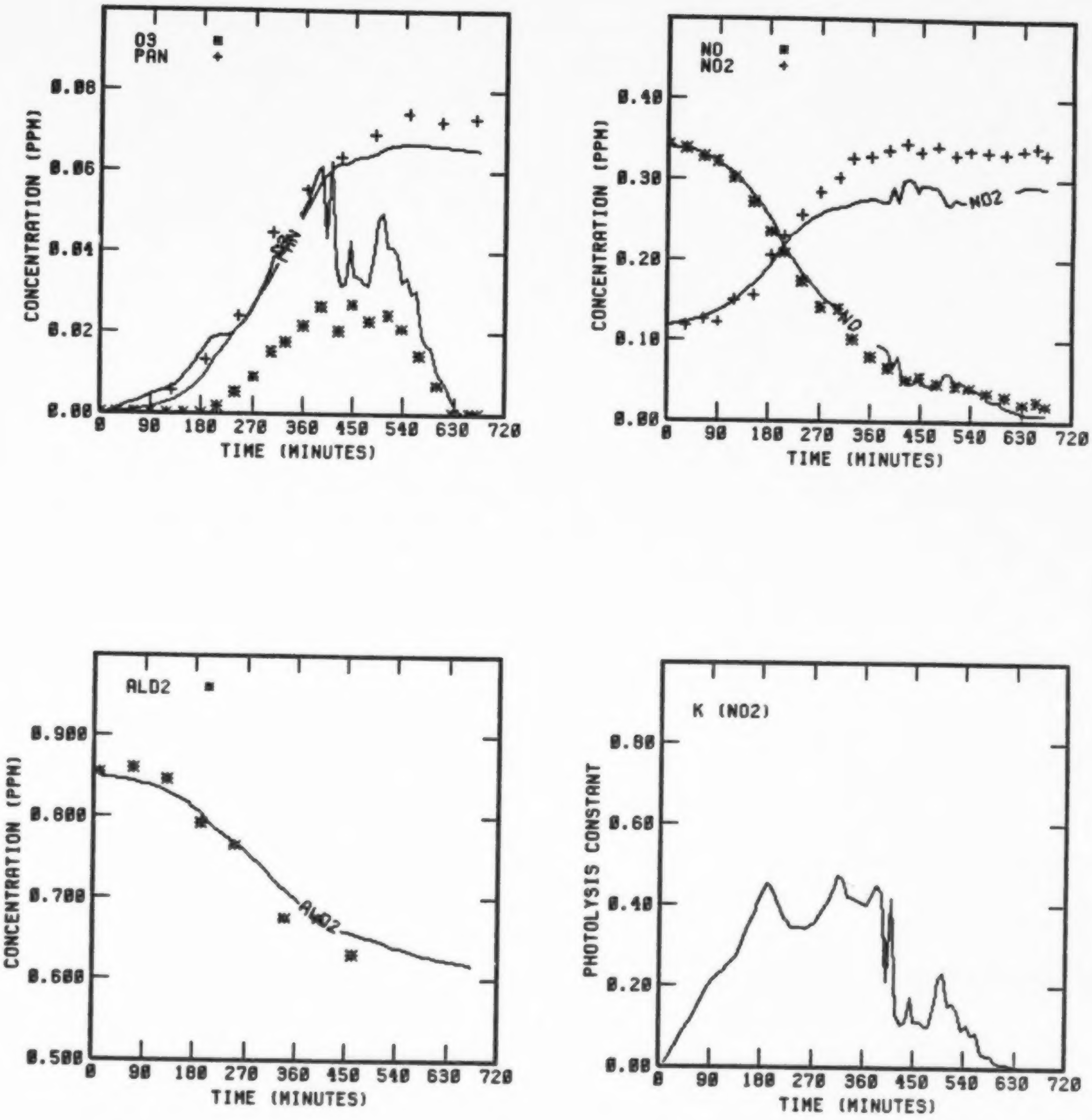

FIGURE 2c. SIMULATION RESULTS FOR
UNCB 111277

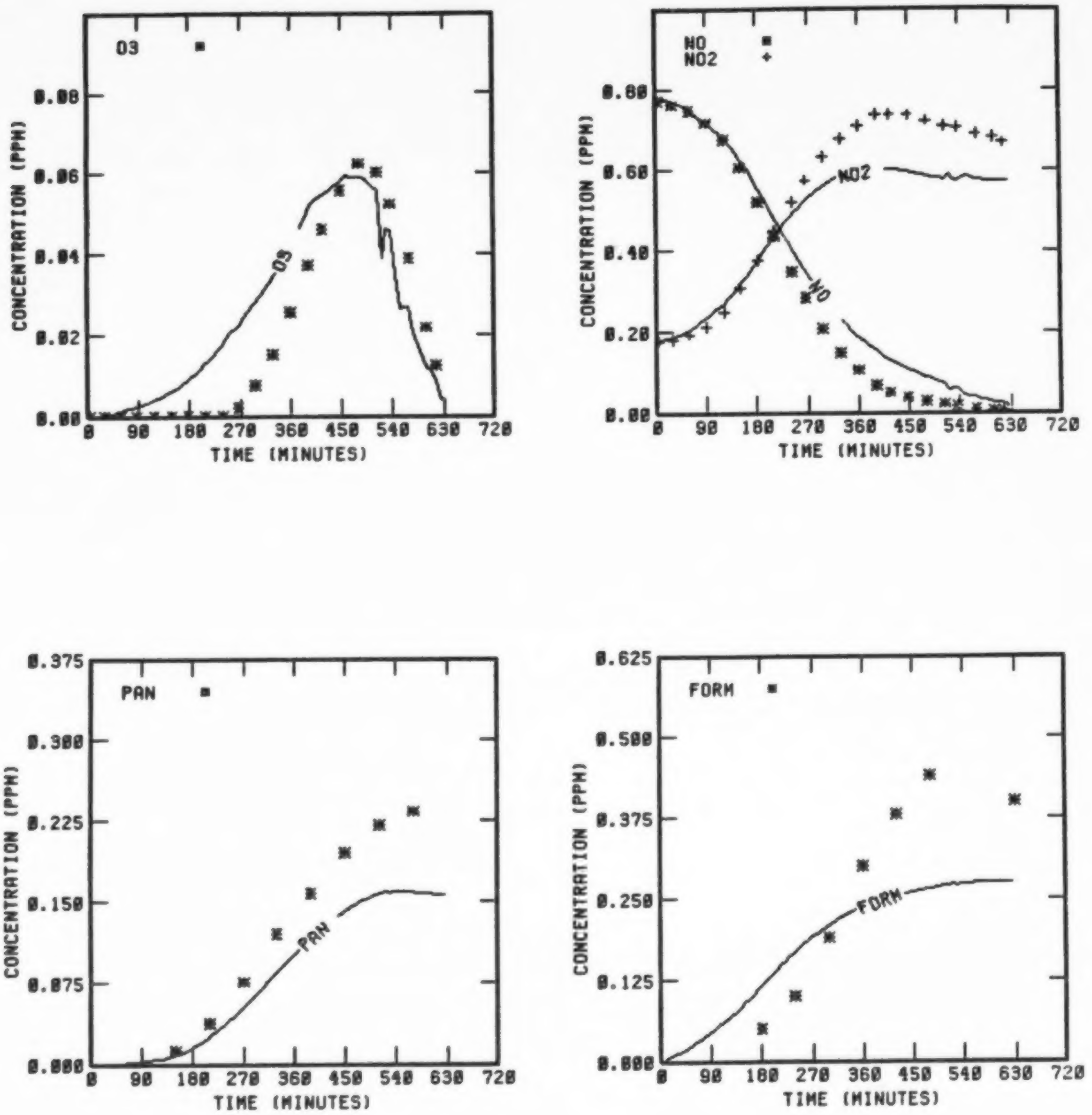

FIGURE 2d. SIMULATION RESULTS FOR UNCB 112077

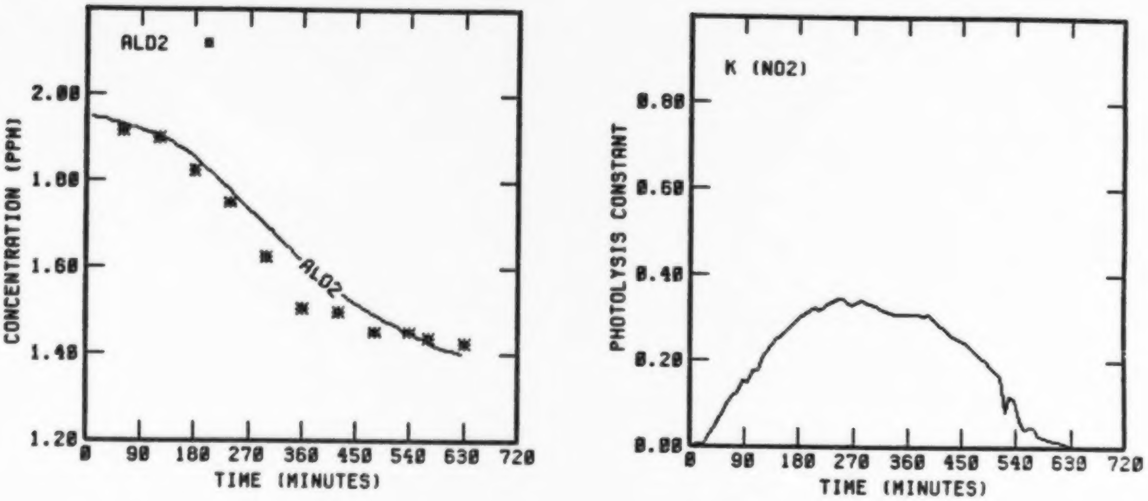

FIGURE 2d. SIMULATION RESULTS FOR
UNCB 112077

(concluded)

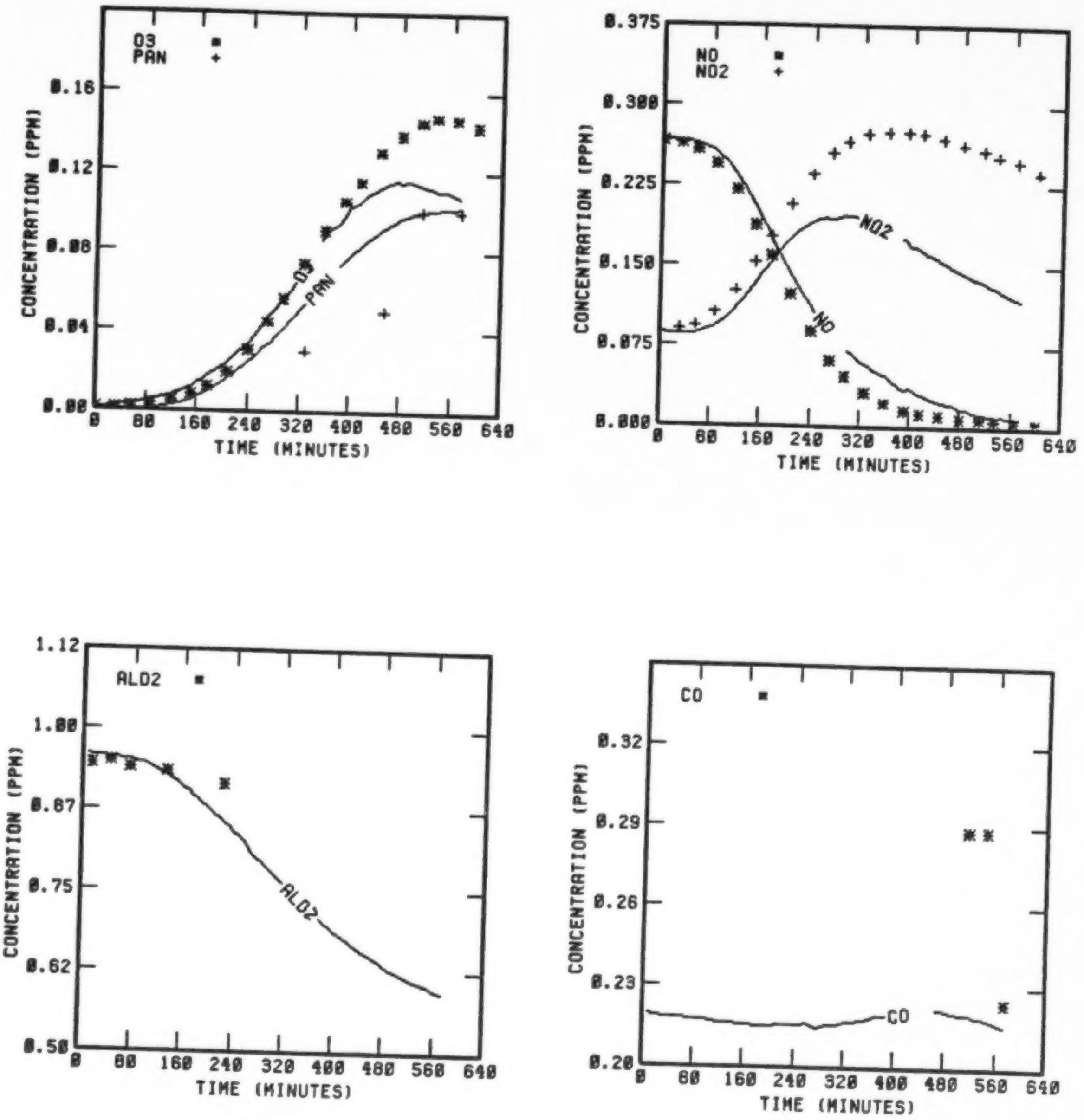

FIGURE 2e. SIMULATION RESULTS FOR
UNCB 2277B

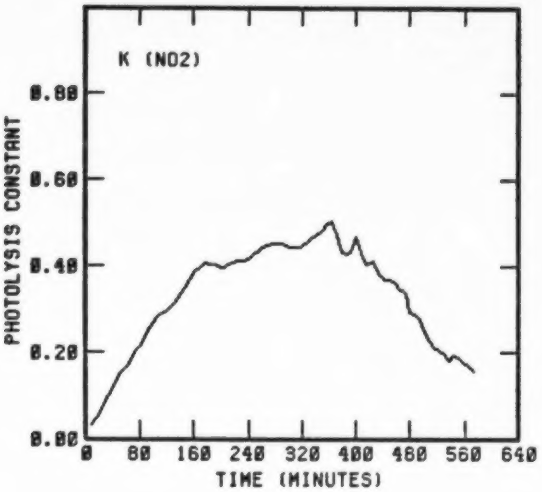

FIGURE 2e. SIMULATION RESULTS FOR
UNCB 22778

(concluded)

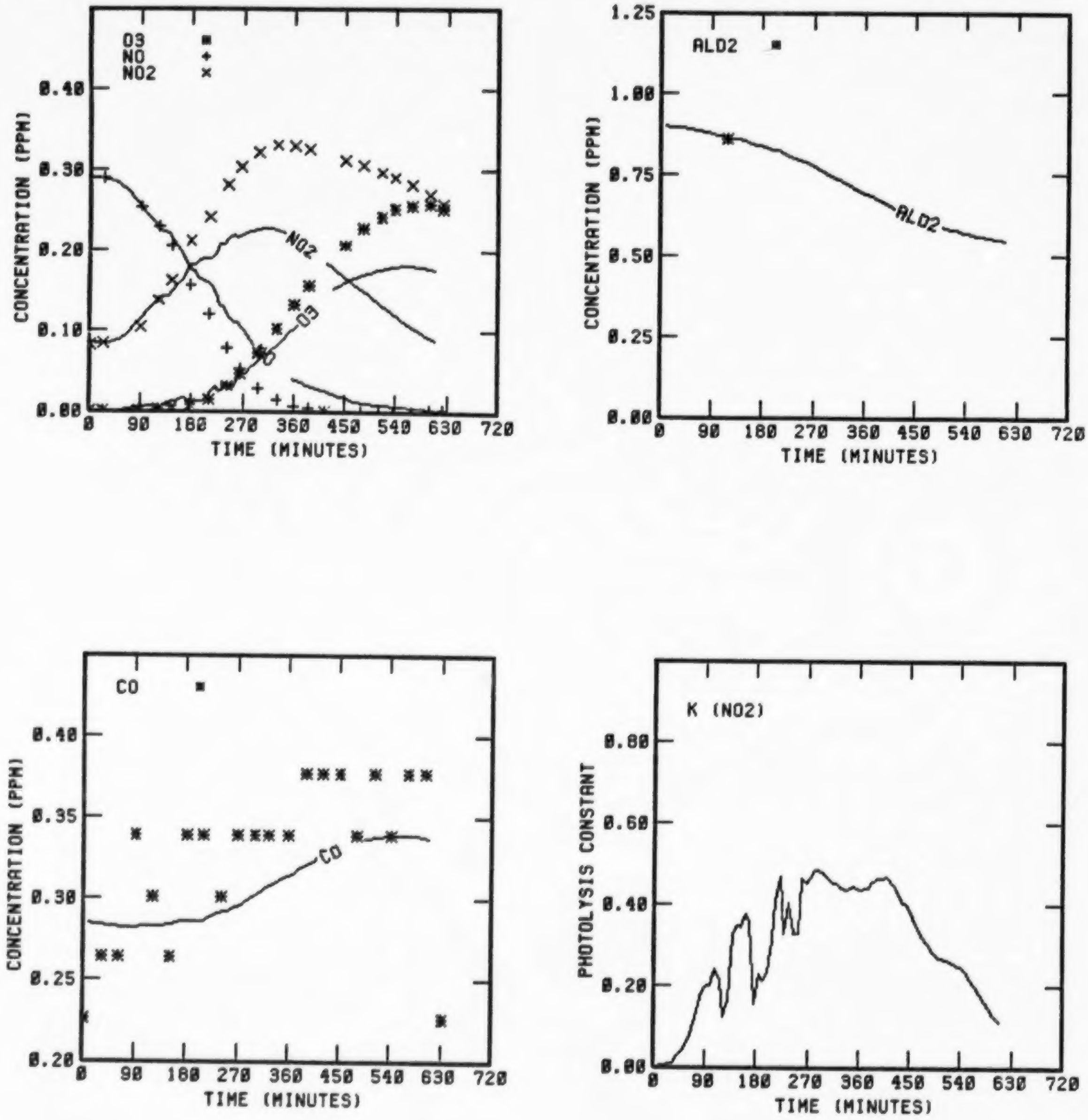

FIGURE 2f. SIMULATION RESULTS FOR
UNCB 30678

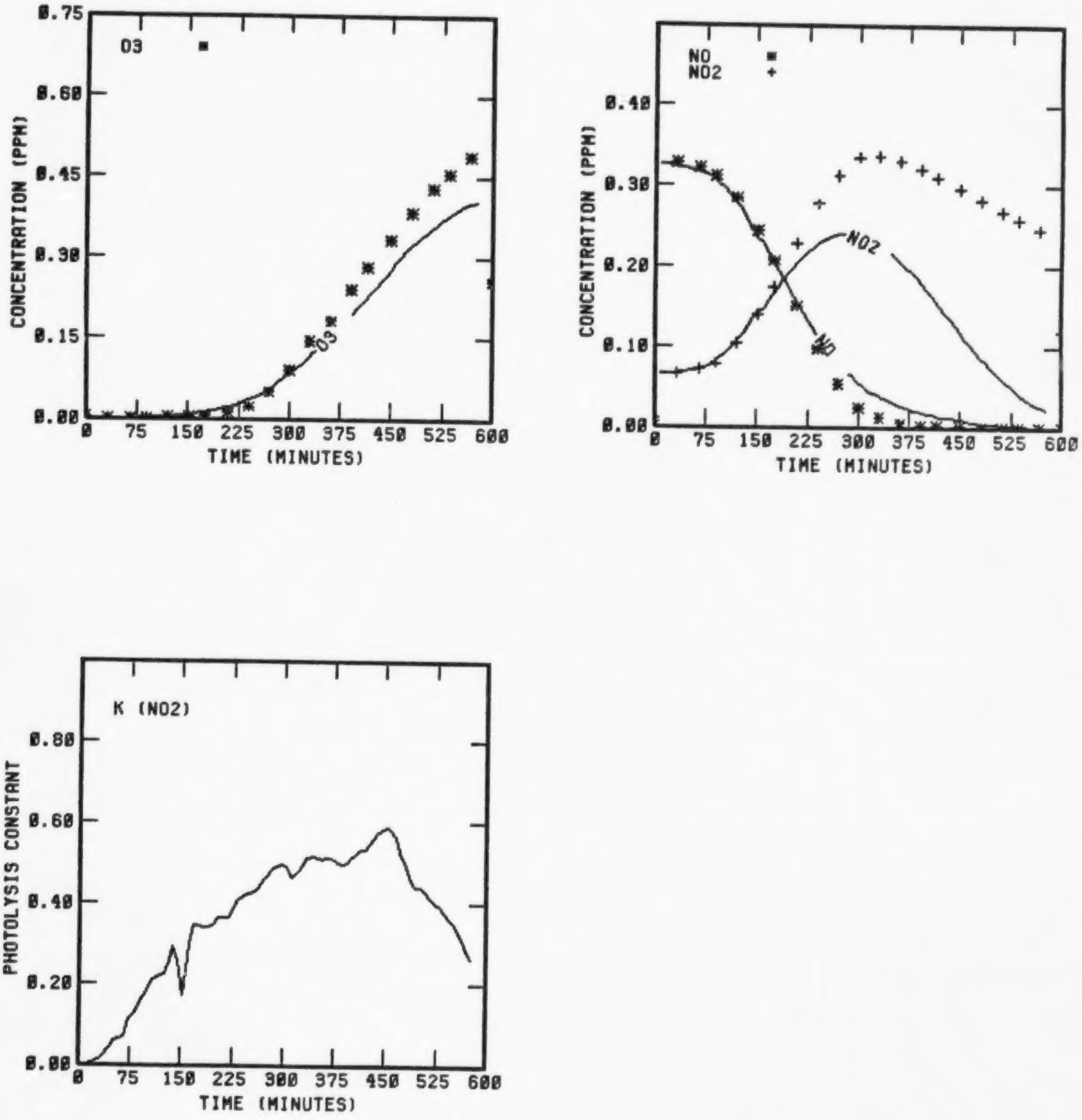

FIGURE 2g. SIMULATION RESULTS FOR UNCB 33178

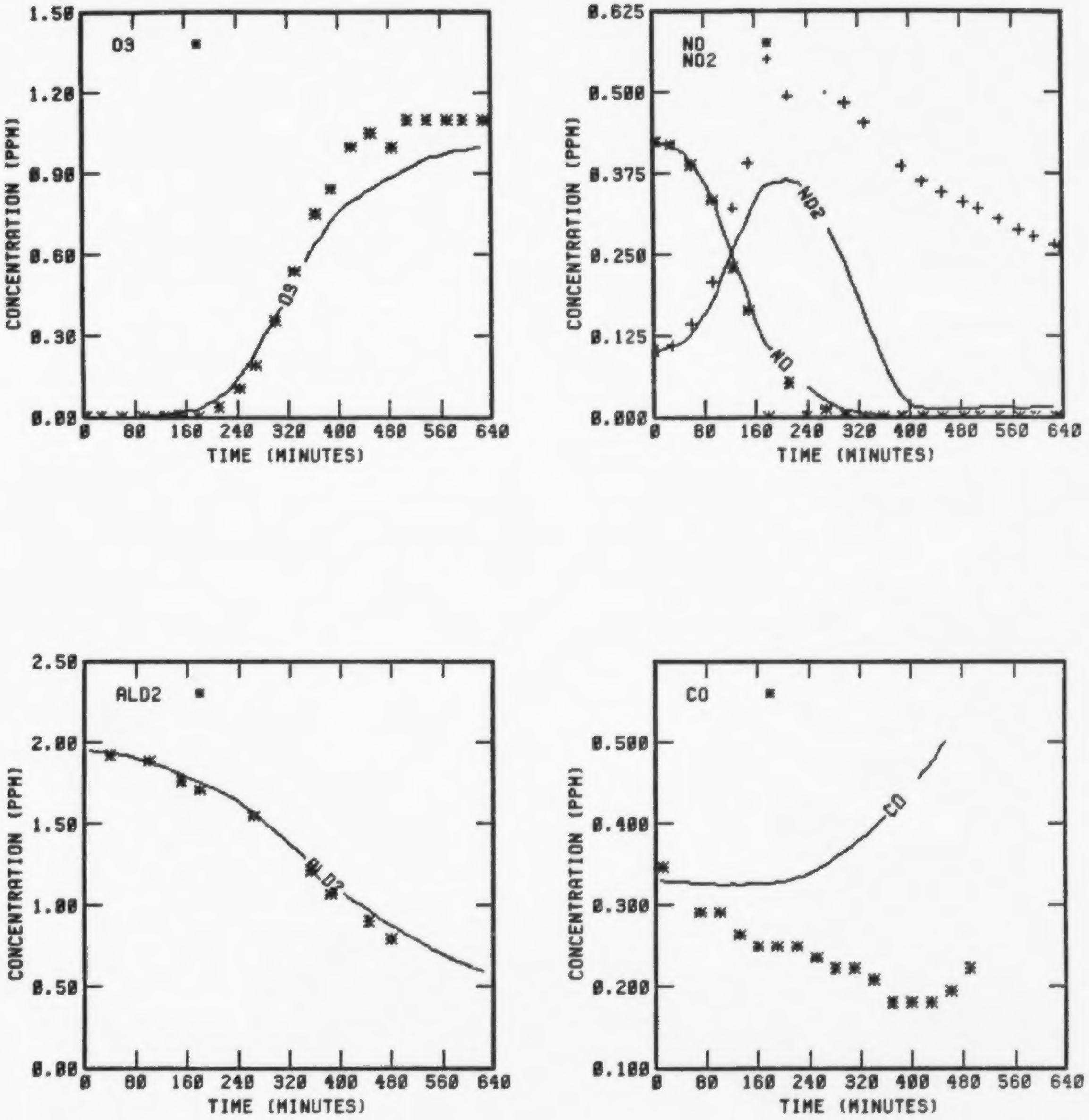

FIGURE 2h. SIMULATION RESULTS FOR
UNCB 80878

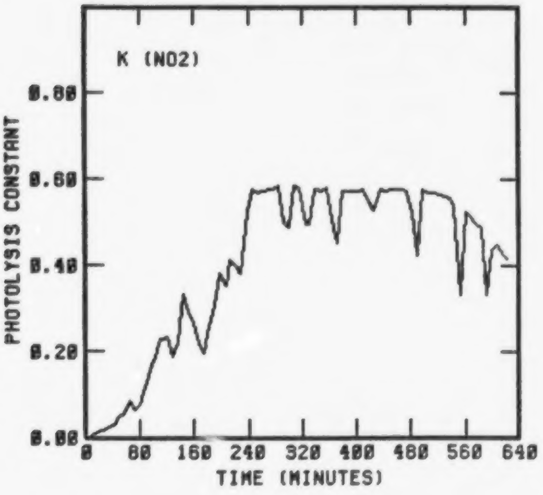

FIGURE 2h. . SIMULATION RESULTS FOR
UNCB 80678

(concluded)

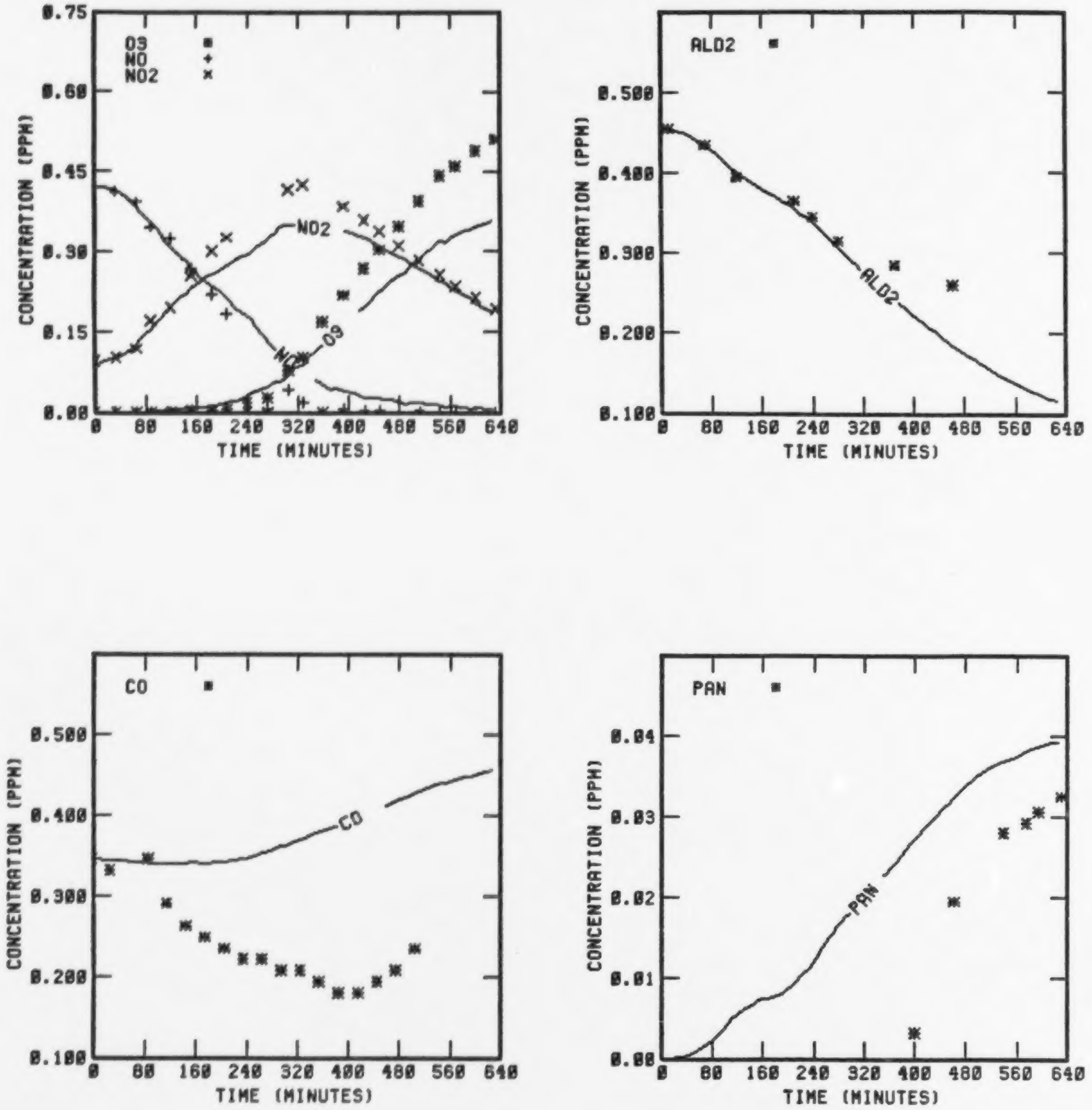

FIGURE 2i. SIMULATION RESULTS FOR
UNCR 80878

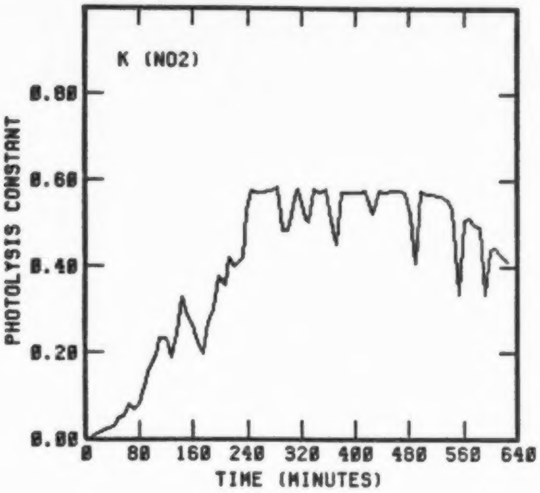

FIGURE 2i. SIMULATION RESULTS FOR
UNCR 80878

(concluded)

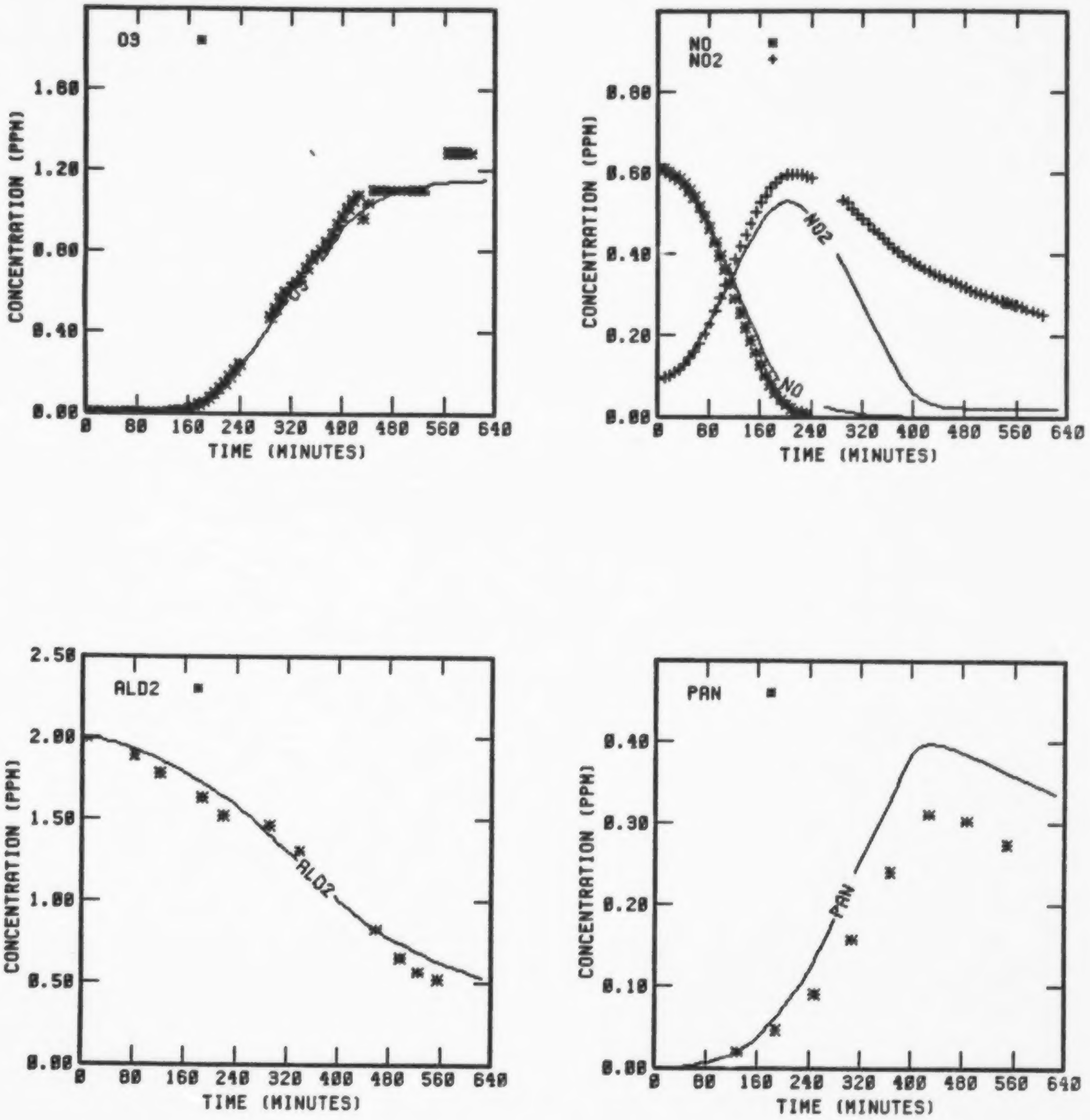

FIGURE 2j. SIMULATION RESULTS FOR UNCB 81778

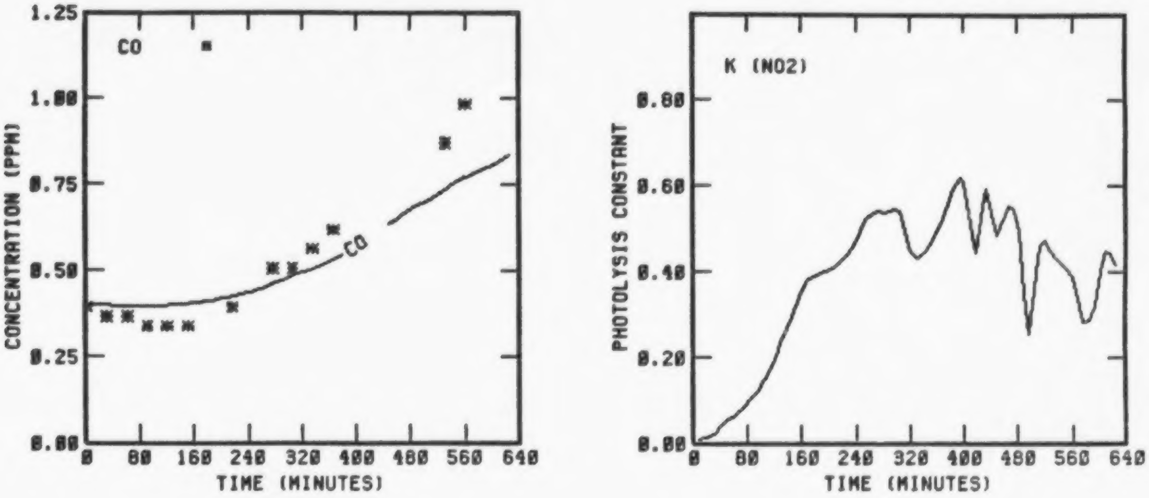

FIGURE 2j. SIMULATION RESULTS FOR
UNCB 81778

(concluded)

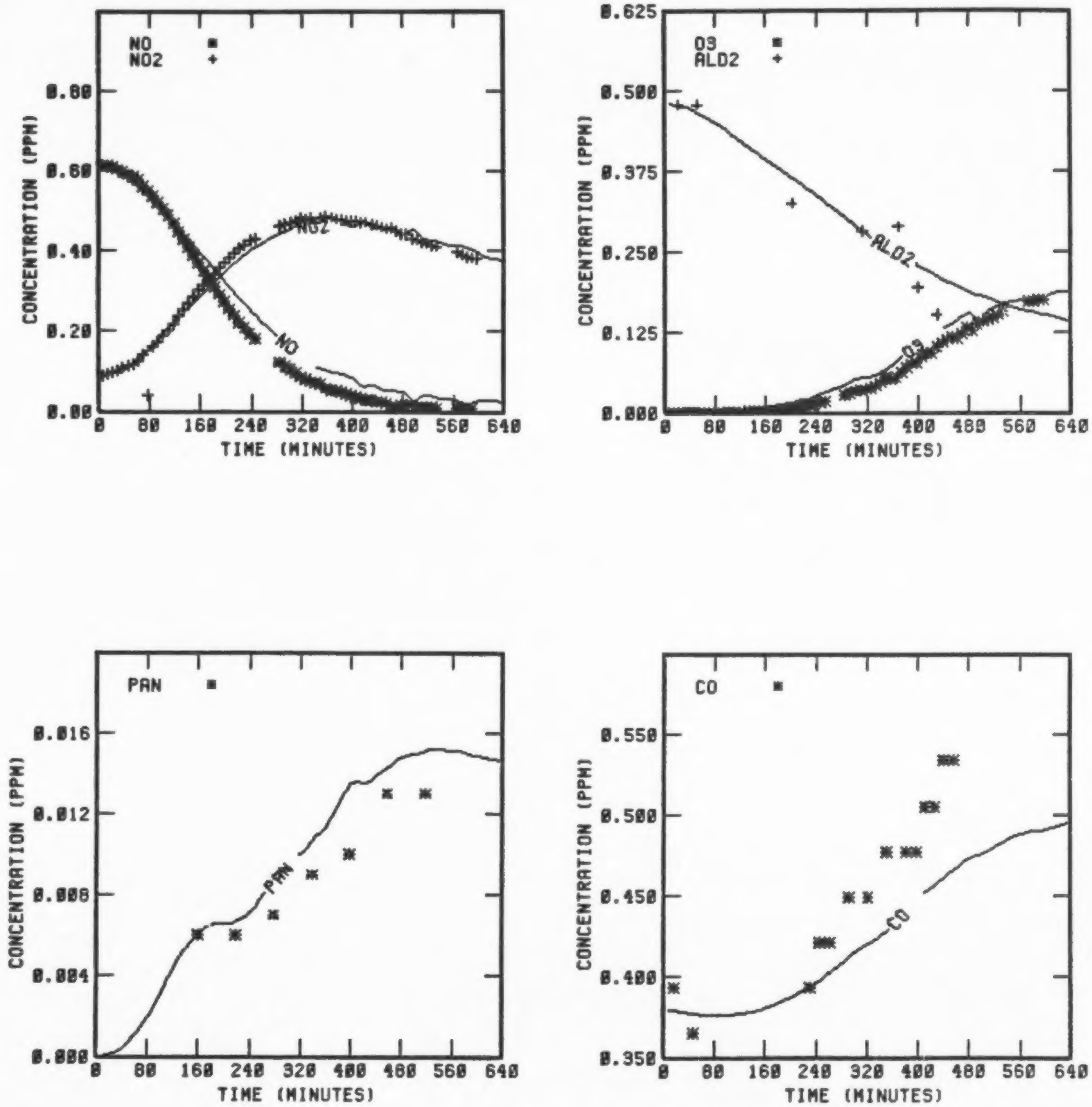

FIGURE 2k. SIMULATION RESULTS FOR
UNCR 81778

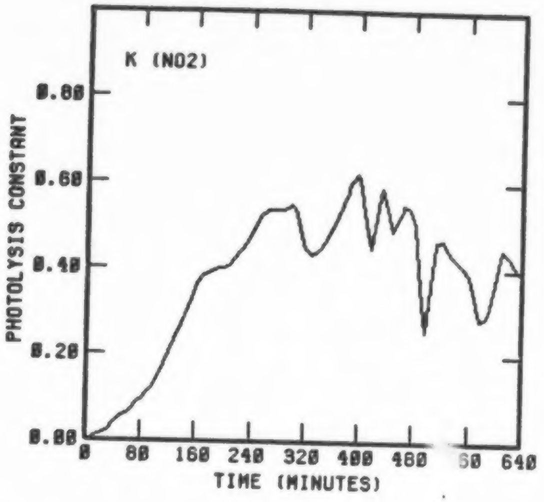

FIGURE 2k. SIMULATION RESULTS FOR UNCR 61778

(concluded)

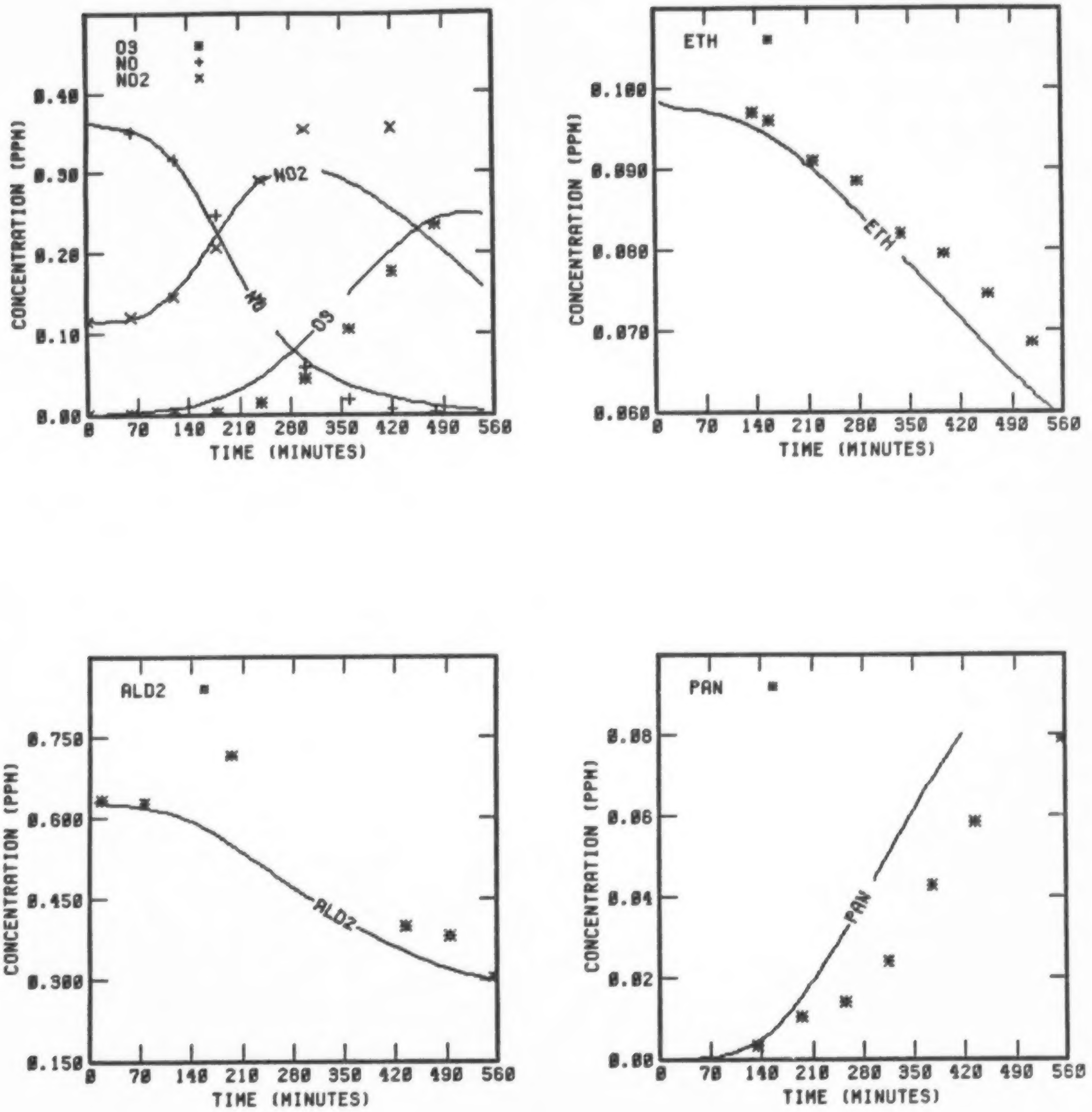

FIGURE 21. SIMULATION RESULTS FOR
UNCR 101278

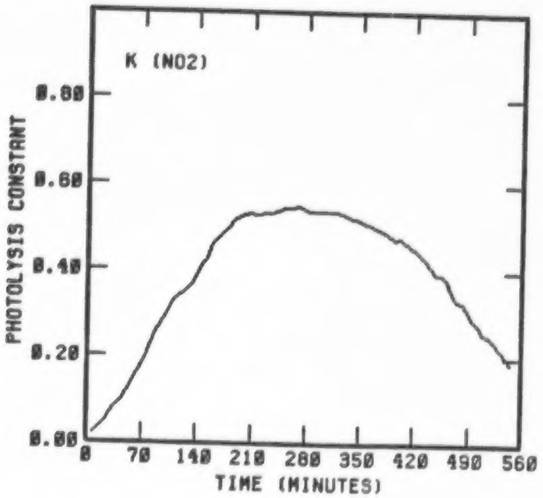

FIGURE 21. SIMULATION RESULTS FOR
UNCR 10127B

(concluded)

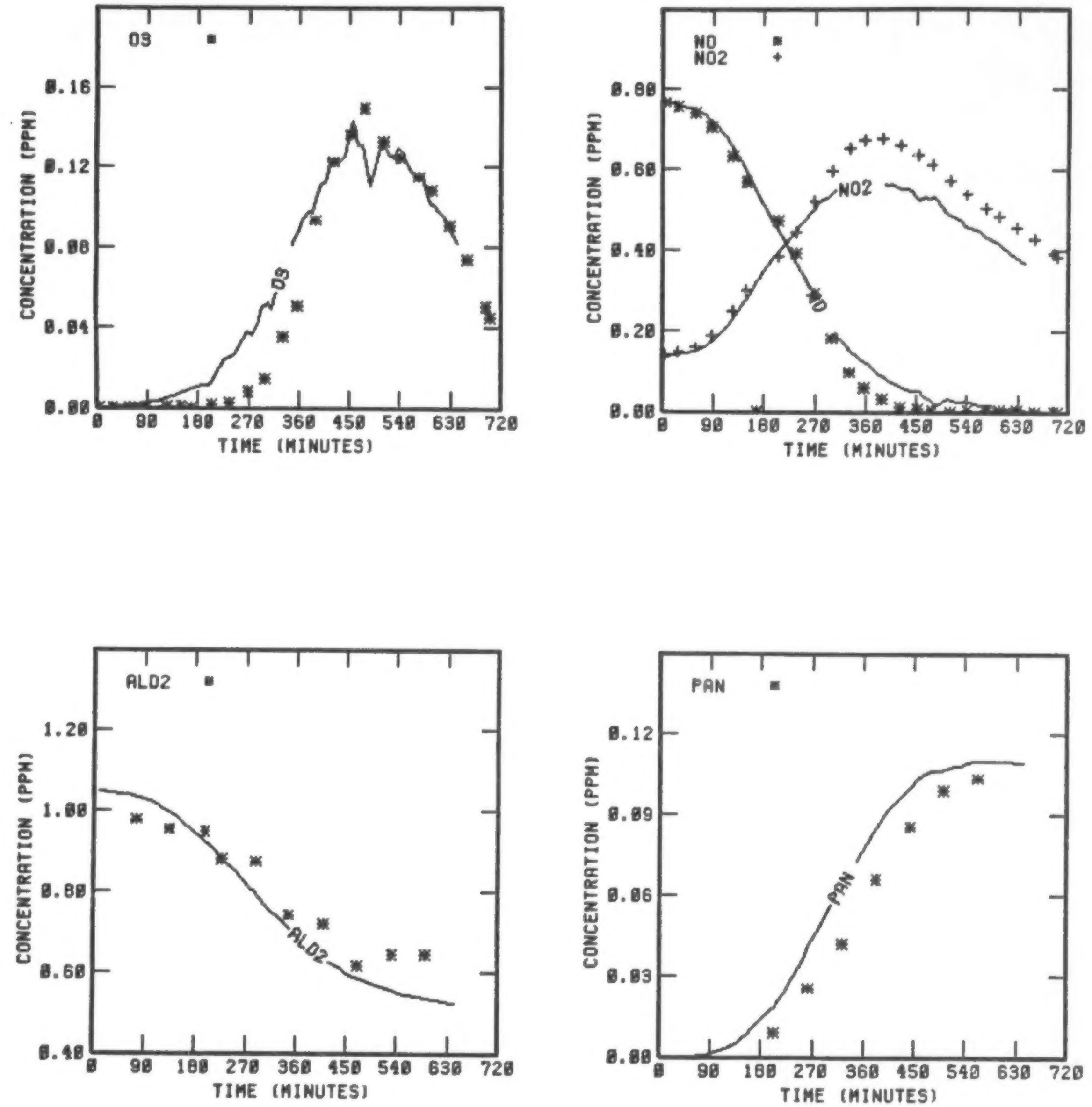

FIGURE 2m. SIMULATION RESULTS FOR UNCB 101378

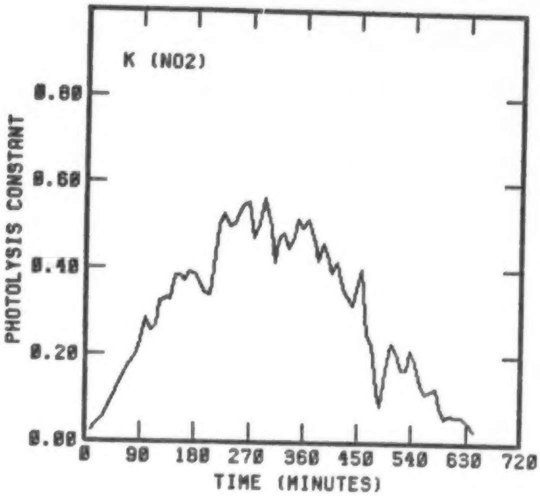

FIGURE 2m. SIMULATION RESULTS FOR UNCB 101378

(concluded)

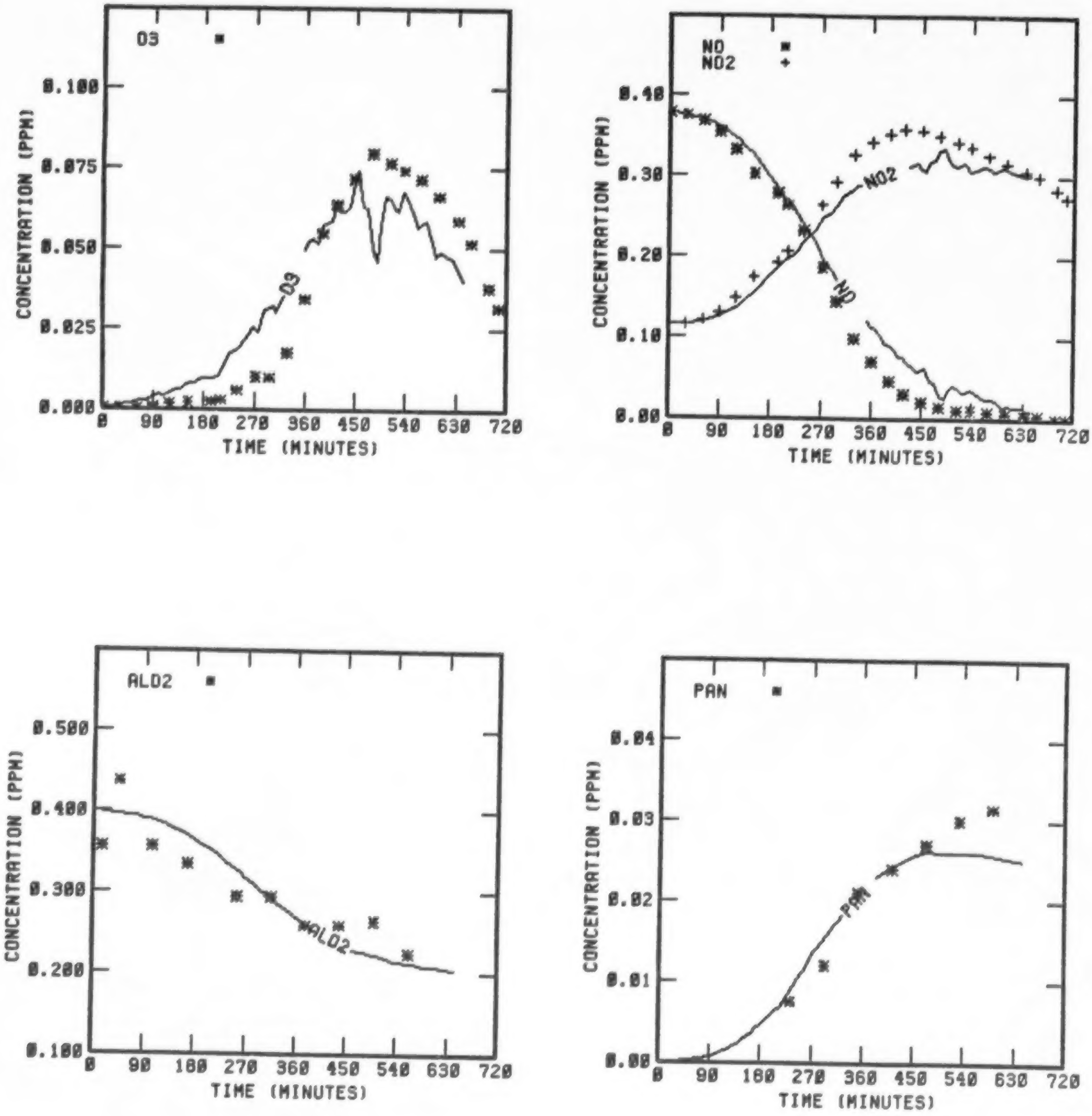

FIGURE 2n. SIMULATION RESULTS FOR
UNCR 101378

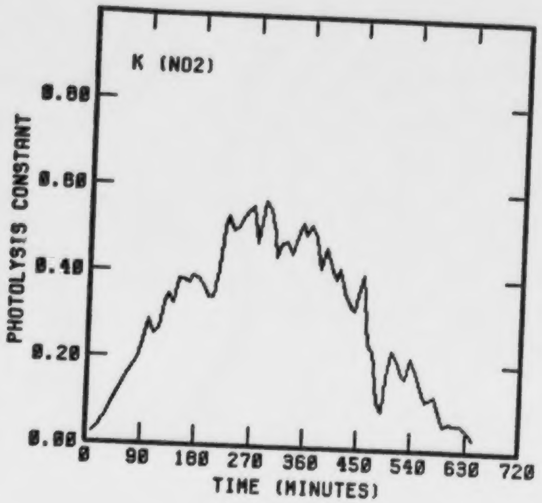

FIGURE 2n. SIMULATION RESULTS FOR UNCR 101378

(concluded)

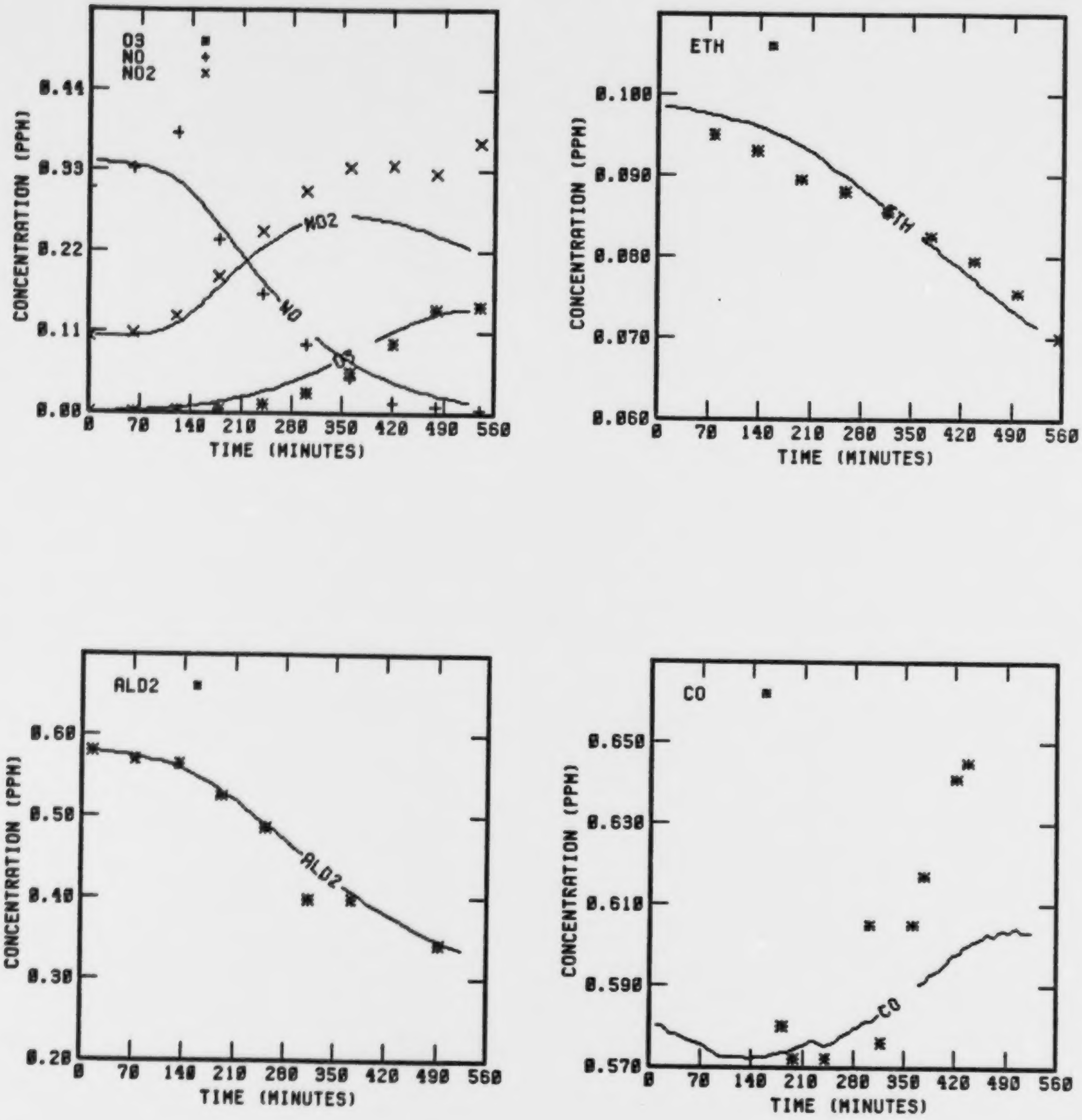

FIGURE 2o. SIMULATION RESULTS FOR UNCR 102578

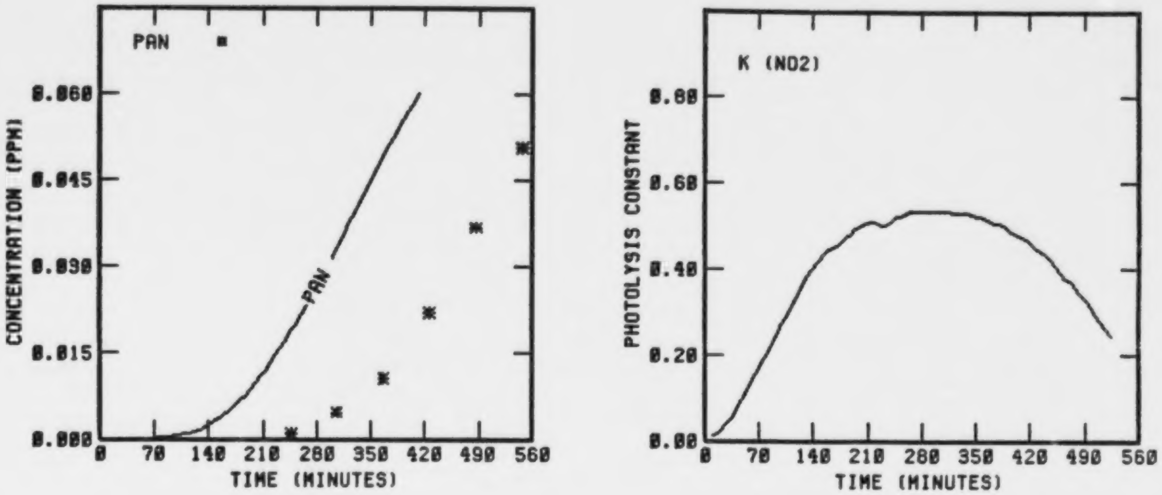

FIGURE 2o. SIMULATION RESULTS FOR
UNCR 102578

(concluded)

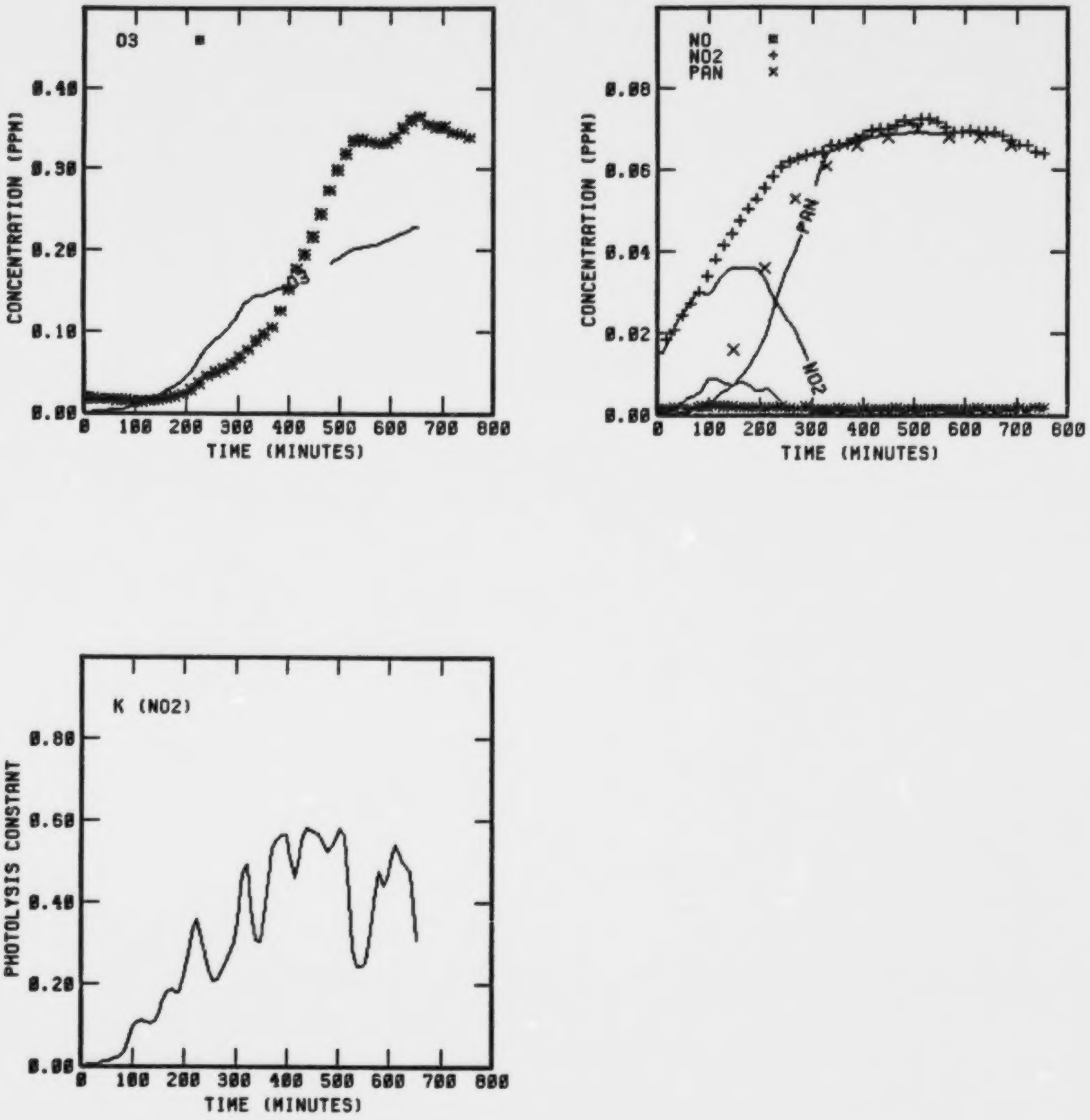

FIGURE 2p. SIMULATION RESULTS FOR
UNCR 72179

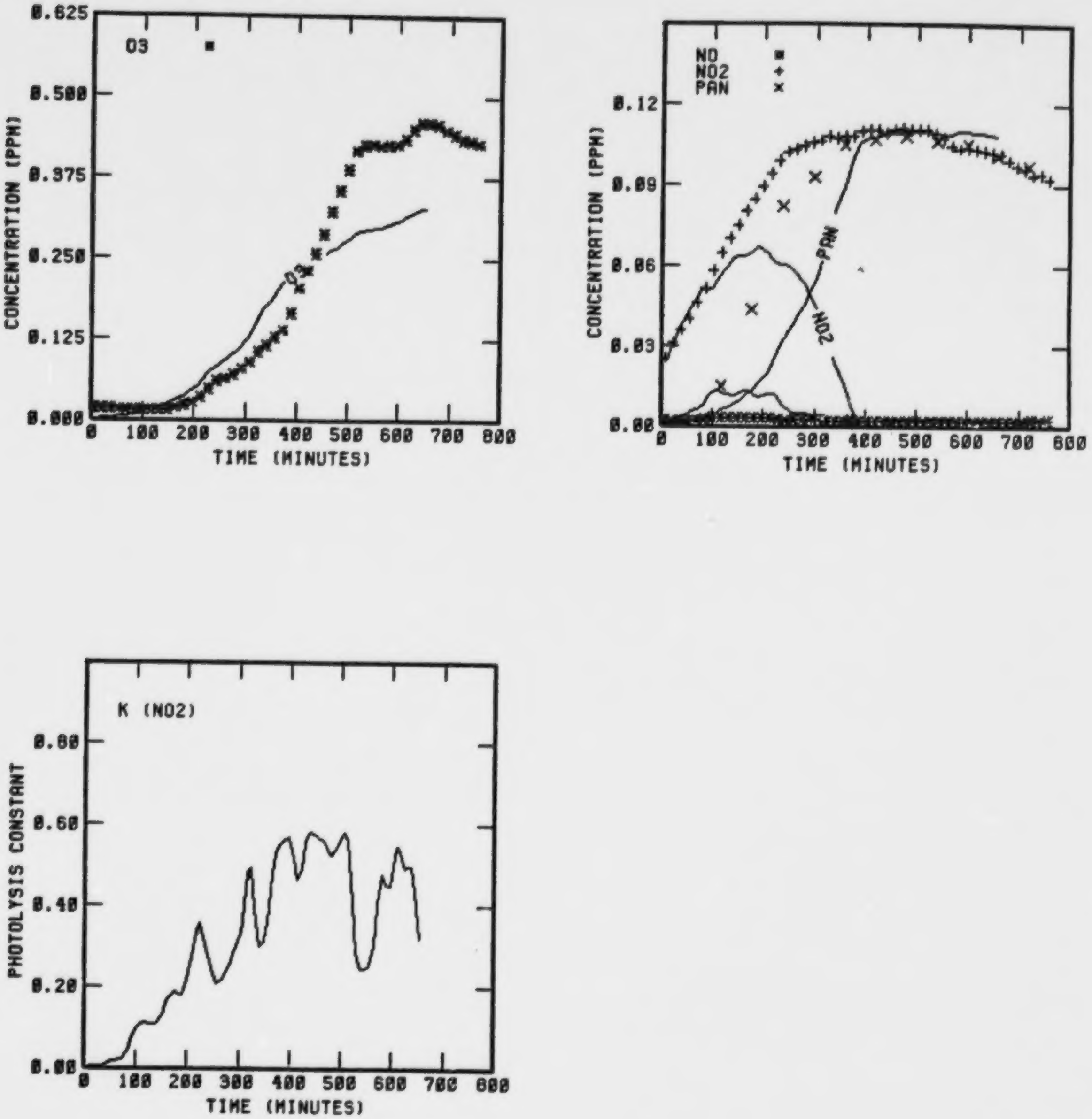

FIGURE 2p. SIMULATION RESULTS FOR
UNCB 72179

(concluded)

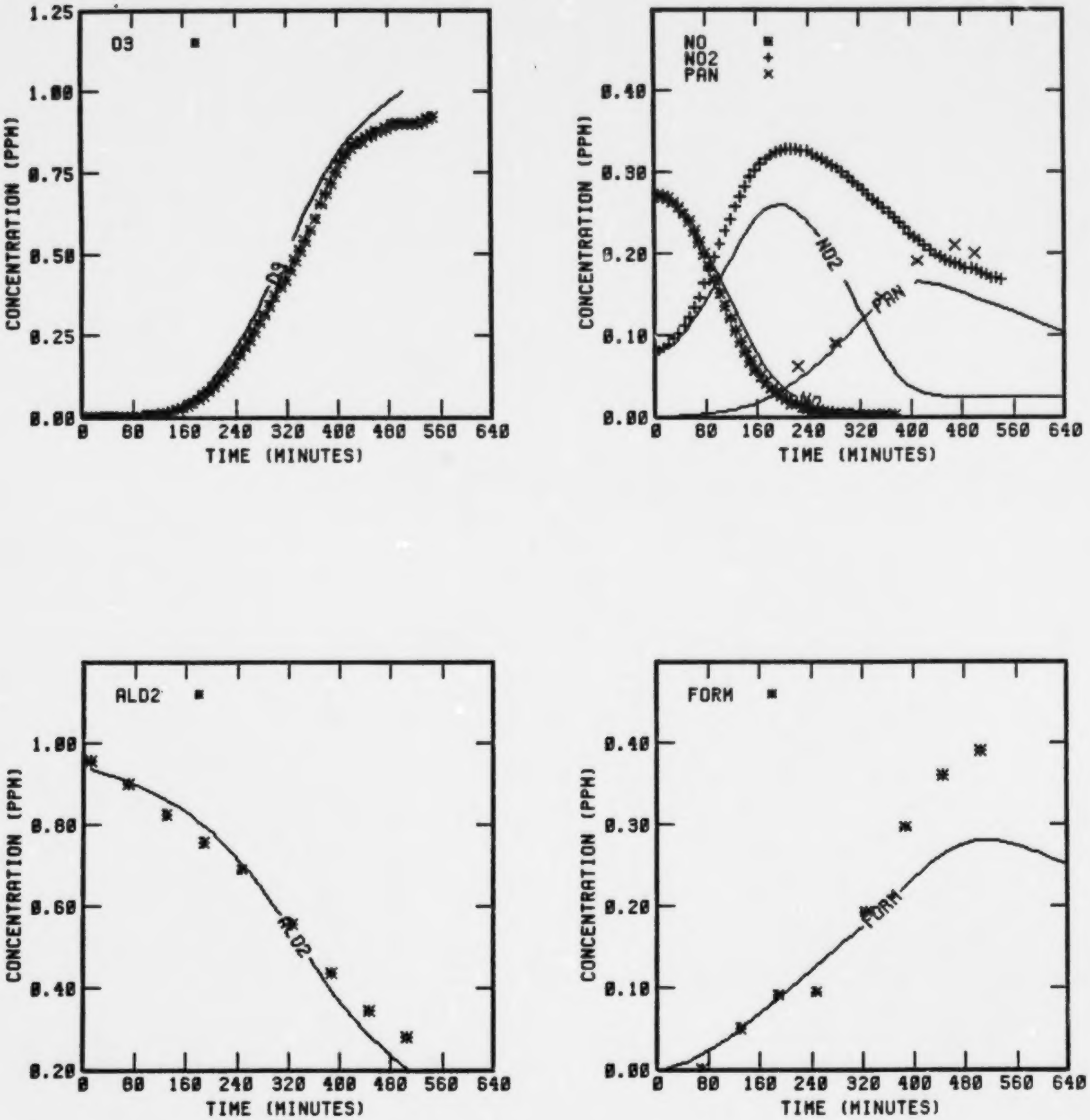

FIGURE 2q. SIMULATION RESULTS FOR UNCR 80179

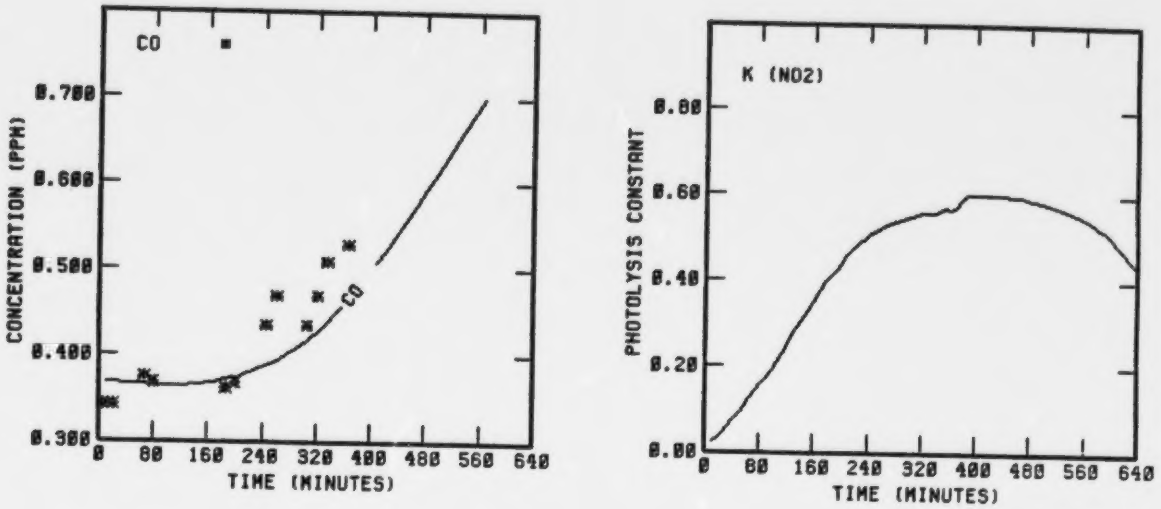

FIGURE 2q. SIMULATION RESULTS FOR
UNCR 80179

(concluded)

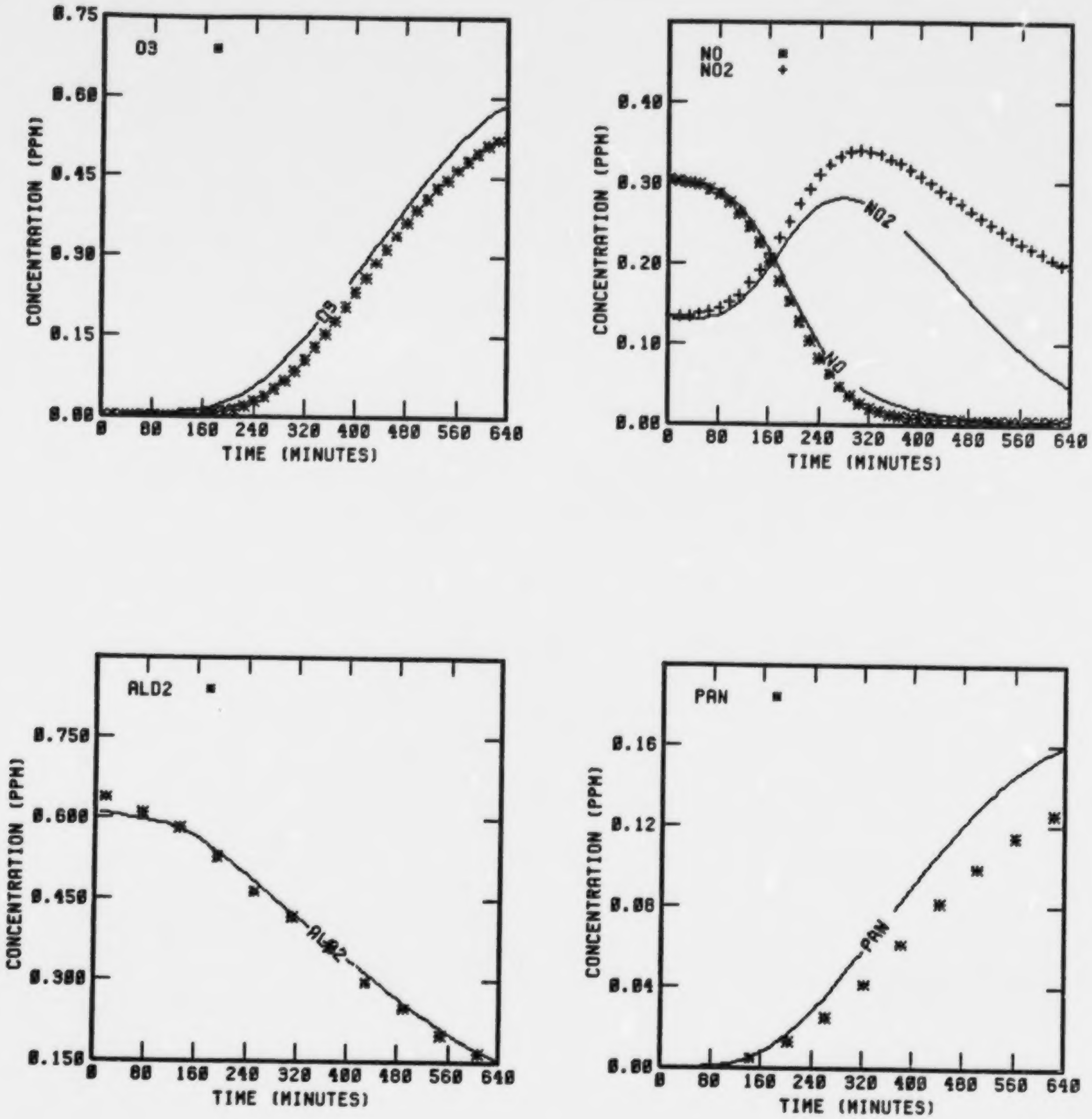

FIGURE 2r. SIMULATION RESULTS FOR
UNCB 81679

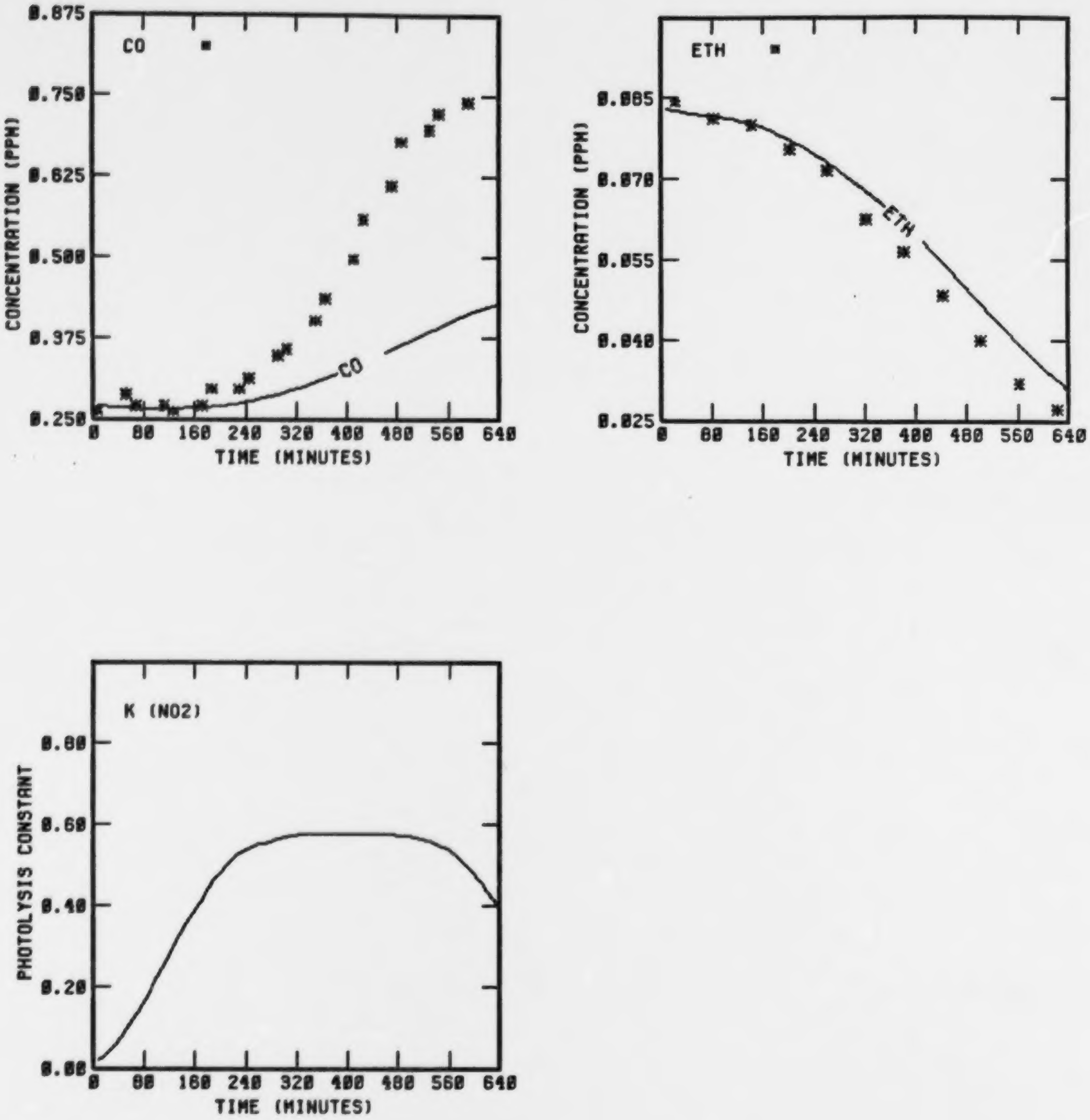

FIGURE 2r. SIMULATION RESULTS FOR
UNCB 81679

(concluded)

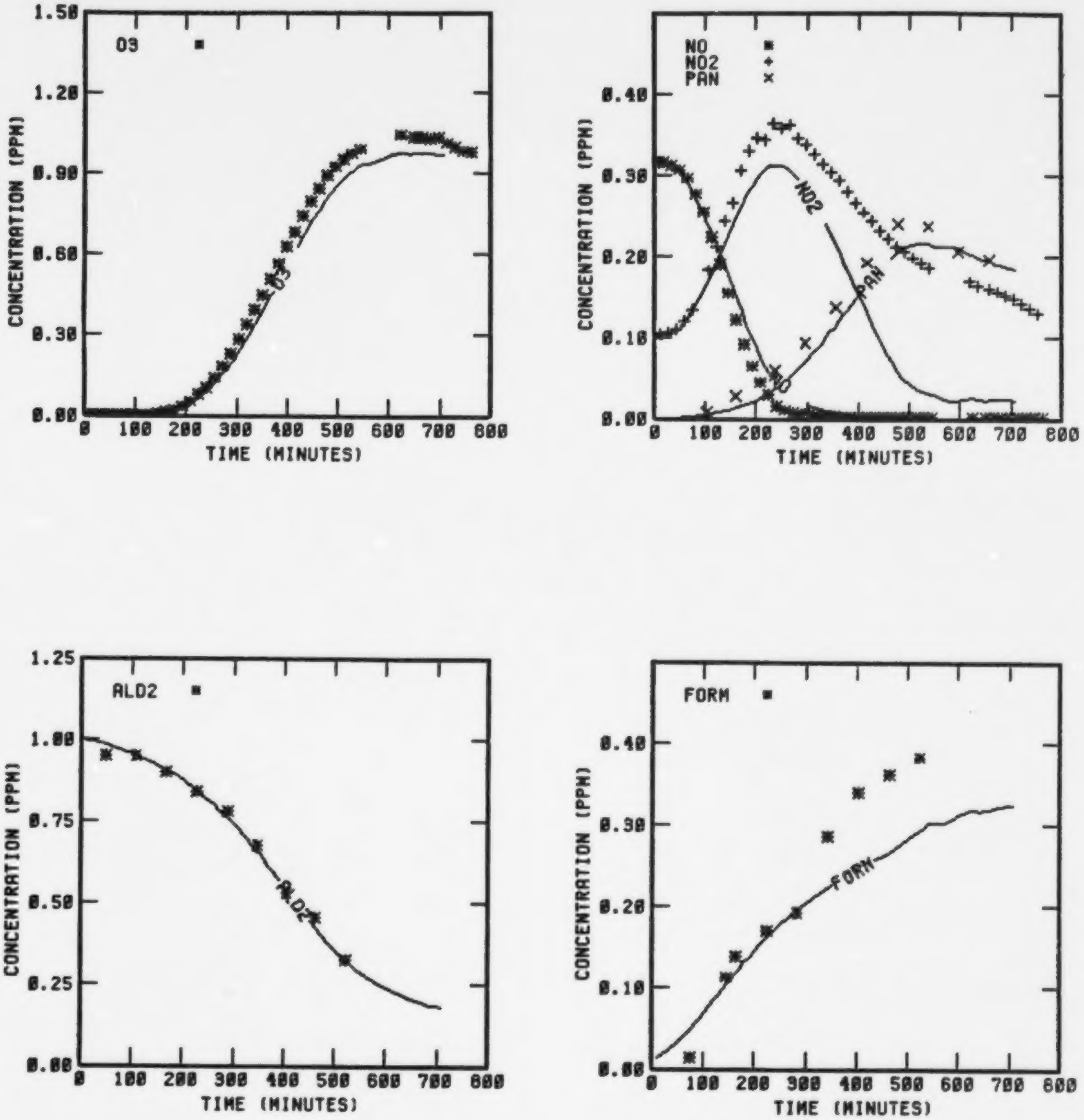

FIGURE 2s. SIMULATION RESULTS FOR UNCR 80880

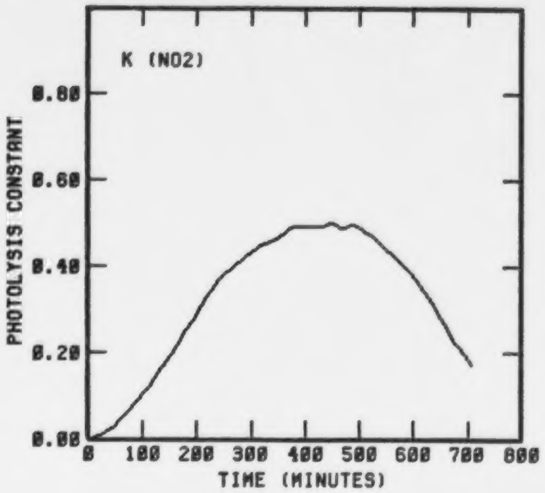

FIGURE 2s. SIMULATION RESULTS FOR UNCR 80880

(concluded)

SECTION 4

THE EXPLICIT MECHANISMS FOR INDIVIDUAL COMPOUNDS

4.1 INTRODUCTION

In Section 3 we described a standard kinetic mechanism consisting of inorganic reactions and the chemistries of formaldehyde, acetaldehyde, and PAN, which are common to almost all hydrocarbon/NO_x photooxidation systems. The reactions in the standard mechanism are the foundation of the kinetic modeling process. To these reactions, reactions that are specific to a particular compound may also be added, thus yielding the complete, explicit mechanism for that compound.

Aside from formaldehyde, acetaldehyde, and PAN, a number of secondary product compounds are common to several hydrocarbon/NO_x photooxidation systems. Oxidation product chemistry is a principle feature of the work accomplished in this study; secondary oxidation products include ketones (found in alkane systems) and dicarbonyls (found in aromatic systems). We describe the modeling of ketone and dicarbonyl chemistry in the final portion of this chapter.

Some revisions have been made to our explicit mechanism for propene; the most important of these revisions has been to include the chemistry of propylene glycol dinitrate. Other minor revisions have been made in the reactions of O_3 and O^3p with propene. We have also revised the mechanism for ethene chemistry. The validation set for ethene chemistry at UNC now includes 28 experiments, made under a wide variety of light, temperature, and humidity conditions.

We have not examined or revised the kinetic mechanism for n-butane per se during this contract. However, we have made major modifications to the mechanism for methylethylketone, a principle product of n-butane oxidation. The chemistry of n-butane is sensitive to trace radical initiation processes, including chamber background sources. For this reason, we have made a study of background reactivity phenomena in both the UNC and UCR smog chambers (Section 5). A resolution of the chamber background issue will allow a reexamination of n-butane kinetics.

We have also extended our description of aromatics chemistry to include m-xylene. Certain features of the ring opening process for m-xylene have implications for the explicit chemistry of toluene as well.

4.2 OLEFIN CHEMISTRY

Olefins represent an interesting and important class of organics in smog chemistry. At present, no less than four species--OH, O_3, O(3P), and NO_3 react with olefins. These reactions can be important under certain conditions.

4.2.1 OH-Olefin Chemistry

In general, the OH radical appears to add to the double bond to create, after oxygen addition, an α-hydroxy peroxy radical:

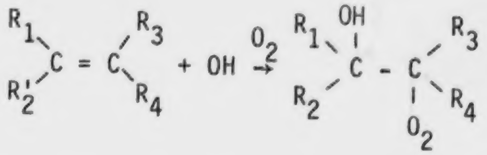

In smog chemistry, peroxy radicals usually convert NO to NO_2, creating the oxyl radical; the olefin-derived α-hydroxy radicals have not been studied extensively. However, the olefins studied to date are normally believed to yield two carbonyl compounds per original OH addition. This would be consistent with abstraction of the hydroxy hydrogen by oxygen and rupture of the original olefin bond. Note that such a pathway to the two carbonyl compounds yields the same carbonyls independent of the carbon atom on which the original OH attack occurred.

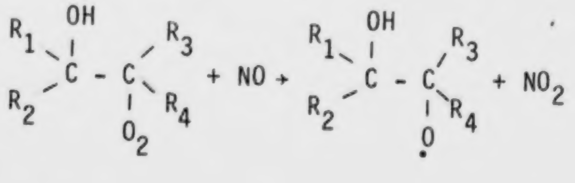

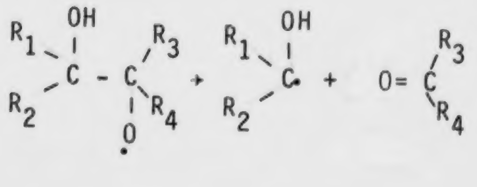

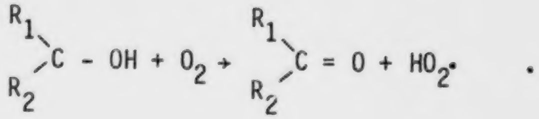

$$R_1R_2C{-}OH + O_2 \rightarrow R_1R_2C{=}O + HO_2\cdot \quad .$$

A recent development has modified this picture somewhat. Using a highly sophisticated long-path Fourier Transform Infrared spectrometer (FTIR), Niki et al. (1981a) identified an α-hydroxy carbonyl, glycolaldehyde, $CH_2(OH)CHO$, in ethene chemistry. Thus, the oxyl radical decomposition appears to be competitive with hydrogen abstraction by O_2 if one or more of the R groups is hydrogen:

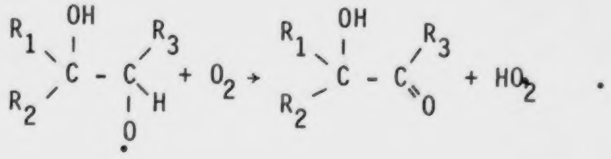

$$R_1R_2C(OH){-}C(O\cdot)(H)R_3 + O_2 \rightarrow R_1R_2C(OH){-}C({=}O)R_3 + HO_2 \quad .$$

However, ethene has all four R groups as hydrogen and Niki et al. (1981a) saw only 21 percent of the ethene react to the glycolaldehyde. The higher olefins would have fewer hydrogens available and the decomposition of the larger oxyl radicals would be expected to be faster than the one derived from ethene. Thus, hydroxy-substituted compounds are unlikely to be important in the chemistry of the higher olefins.

4.2.2 O_3-Olefin Chemistry

The olefins are unique in their atmospheric reactivity to ozone since other common organics do not react with ozone at significant rates. The chemistry following the ozone-olefin reactions has recently been reviewed by Hernon, Martinez, and Huie (1982). The reaction channels that are important in smog chemistry involve species called Criegee intermediates, in addition to the carbonyls formed in the initial reaction:

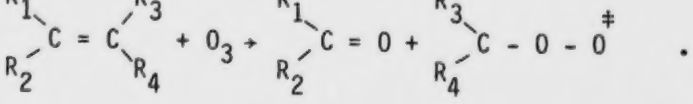

$$R_1R_2C{=}CR_3R_4 + O_3 \rightarrow R_1R_2C{=}O + R_3R_4C{-}O{-}O^{\ddagger} \quad .$$

Criegee Intermediates

These special intermediates are known to have several competing channels for reaction under atmospheric conditions. The excess energy available from the initial reaction promotes decomposition; however, even the stabilized Criegee intermediates appear to have a significant channel to decomposition, in addition to isomerization and bimolecular interactions. Although radical products are possible from the decomposition channels, the overall yield of radicals from the ozone-olefin chemistry is now thought to be small. On the other hand, the bimolecular reactions possible are similar in oxidizing capacity to some of the oxidizing radicals so that species such as NO and SO_2 can be oxidized.

A recent development in this complex chemistry involves the hydrogen-substituted Criegee intermediate formed in terminal olefins, $CH_2O_2^{\ddagger}$. Su, Calvert, and Shaw (1980), Niki, et al. (1981b), and Kan, et al. (1981) have all reported that stabilization of the initial intermediate occurs to the extent of about 37 percent, whereas previous investigators such as Whitten et al. (1980) had assumed that only the higher Criegee intermediate had a significant fraction stabilized under atmospheric conditions. The previous assumption of no stabilization of the $CH_2O_2^{\ddagger}$ was based on the work of Hernon and Huie (1977), which was performed at low pressure (0.01 atm). However, a major finding of this earlier work was the low yield (< 10 percent) for the free radical channel. Hence, the new development of 37 percent stabilization at 1 atm pressure implies an even lower yield of free radicals from $CH_2O_2^{\ddagger}$.

Unfortunately, the important reactions of the Criegee intermediates have yet to be elucidated under smog-like conditions. These reactions involve the competitive bimolecular channels between RO_2, O_2, NO, NO_2, SO_2, H_2O, aldehydes, and alkenes.

4.2.3 O(3P)-Olefin Chemistry

These reactions have been studied for over 30 years, yet the important channels under smog-like conditions are still somewhat uncertain. Most reviewers such as Atkinson and Lloyd (1982) suggest several channels to a mixture of stable products such as epoxides and carbonyls, along with some radical products. During this study, an upper limit to radical products was determined for propene. On the basis of a modeling study, Carter et al. (1979) had recommended a 40 percent reaction channel to radical pairs:

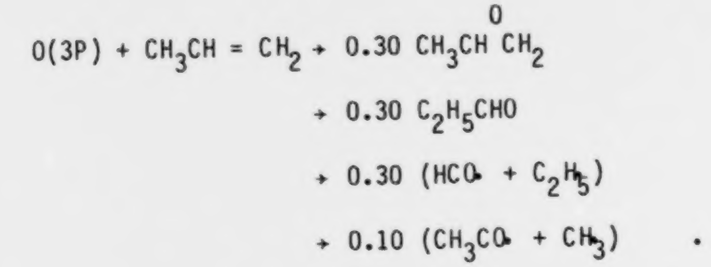

$$\begin{aligned} O(3P) + CH_3CH = CH_2 &\rightarrow 0.30\ CH_3\overset{O}{CH\ CH_2} \\ &\rightarrow 0.30\ C_2H_5CHO \\ &\rightarrow 0.30\ (HCO\cdot + C_2H_5) \\ &\rightarrow 0.10\ (CH_3CO\cdot + CH_3) \quad . \end{aligned}$$

Two experiments performed in the Japanese NIES chamber support these estimates. Simulations of these experiments are shown in Figures 3 and 4.* (The propene reaction mechanism is shown in Table 4.) However, it should be noted that the 40 percent radical pair yield estimate should be taken as an upper limit for these experiments because no initial HONO was assumed and because the chamber walls were assumed to be neutral (neither a source nor sink of radicals).

4.2.4 NO_3-Olefin Chemistry

Although NO_3-olefin reactions have been known for some time, the products formed from these reactions have only recently been identified in the NIES chamber. The toxic compound propene glycol 1,2-dinitrate (PGDN) was identified by Akimoto et al. (1978) in propene smog chamber experiments and Hoshino et al. (1978) demonstrated that NO_3 or N_2O_5 was the necessary precursor. This latter study also identified a minor yield of 1-formylethyl nitrate [$CH_3CH(ONO_2)CHO$], which is consistent with the following scheme.

$$CH_3C = CH_2 + NO_3 \rightarrow CH_3CH(ONO_2)CH_2$$

$$CH_3CH(ONO_2)CH_2 + O_2 \rightarrow CH_3CH(ONO_2)CH_2O_2$$

$$\begin{aligned} CH_3CH(ONO_2)CH_2O_2 + NO &\rightarrow CH_3(ONO_2)CH_2O + NO_2 \\ &\text{or} \\ &\rightarrow PGDN \end{aligned}$$

$$CH_3(ONO_2)CH_2O + O_2 \rightarrow CH_3CH(ONO_2)CHO + HO_2 \quad .$$

---

* Tables and figures are found at the end of the chapter.

Using this chemistry (Table 4) and the conditions used to simulate the NIES experiment shown in Figures 3 and 4, an isopleth of PGDN was constructed using OZIPM (Whitten and Hogo, 1978). The single experiment shown in Figure 3 corresponds to 9 ppmC NMHC and 1.5 ppm NO_x on the isopleth diagram shown in Figure 5. Note that since one molecule of PGDN contains two units of NO_x, the PGDN formed at this base case point corresponds to a sink of about 13 percent for NO_x. At 20 ppmC propene, the predicted yield is over 40 percent of total NO_x. Hence the NO_3 chemistry becomes a major NO_x loss at high concentrations. More experiments with PGDN measurements at high concentrations will be necessary to confirm this prediction.

4.3 ETHENE SIMULATIONS

The standard mechanism described in Section 3 was coupled with the latest versions of the reactions specific to ethene and shown in Table 5. Simulations of the UNC set of ethene experiments using this mechanism are shown in Figures 6 through 36. The initial conditions used are given in Table 6.

Noteworthy experiments are those performed on 10 January 1978 (Figure 11), 1 July 1978 (Figure 15), and for both sides of the chamber on 31 October 1979 (Figures 31 and 32). The first two represent extremes in temperature (260 K to 315 K) and the second pair represent extremes in humidity at equal temperatures (14,000 ppm H_2O versus 6,000 ppm H_2O). Ethene is an important alternate compound with which to study the effects of temperature and humidity. Of the known radical and NO_x sinks, PAN exhibits a large temperature dependence. Hence ethene offers perhaps a minimal estimate of non-PAN-related temperature effects.

The exclusive use of propene to study the effects of temperature gives rise to several confounding chemical propene species: ozone-olefin species, acetaldehyde, formaldehyde, PAN, general inorganic species, and the olefin-hydroyl adduct. The reactions associated with each of these species can have separate temperature effects; hence the propene system would be a complex combination of all. The best approach would seem to involve temperature studies that isolate each type of effect, starting with the general inorganic species and progressing to the system involving formaldehyde and the inorganics only, and so on. Data from similar studies are at least partially available. Ethene fits into this series because it includes some of the propene type reactions, though it circumvents others. Ozone-olefin chemistry is also included; however, the reactions are slower than those of propene and therefore less important, and methyl-substituted intermediates are not formed. Therefore the ethene system is simpler than the propene system.

The olefin-hydroxyl adduct chemistry, the inorganic chemistry, and formaldehyde chemistry are included in both the ethene and propene systems. However, the strong temperature effects associated with PAN chemistry and the possible effects associated with acetaldehyde are seen only in propene experiments. Hence the successful simulation of temperature effects in ethene experiments, in addition to formaldehyde, acetaldehyde, and propene experiments, serves as an important overall validation of the complex and interrelated temperature effects. In the same way, the minor humidity effect seen in the ethene experiments and simulations demonstrate that similar results using more complex molecules probably do not result from large but compensating effects in the complex molecule experiments.

The temperature, light, and humidity effects come into play all at once through the effect seen in outdoor smog chambers. The pair of ethene experiments of 10 January 1978 and 1 July 1978 demonstrate an interesting contrast because the overall diurnal development of these two experiments is close to the point where small changes in radical source and sink behavior in the model are most severely tested. The January experiment has low temperatures (260-270 k), low light (maximum $k_1 < 0.4 \text{ min}^{-1}$), and low water content (~ 1300 ppm); whereas the July experiment has high temperatures (293-307 k), strong light (maximum k, $> 0.6 \text{ min}^{-1}$), and fairly high water content (~ 10,000 ppm). However, neither experiment is accurately simulated by the present ethene mechanism and known experimental conditions.

As demonstrated in Figure 11, the simulated ozone for the January experiment is far too high, even though the observed NO-to-NO_2 behavior appears to be followed by the model. Hence something may be suppressing the amount of ozone normally generated from a given ratio of NO_2/NO at these conditions, up to about 300 minutes of the experiment. Most of the discrepancy between the simulated and observed ozone values can be explained by the measurement delay caused by the length of the sample line. The high levels of NO present react in the dark line to destroy ozone. The two curves (simulated versus observed) should converge as NO is reduced. Another problem with the current simulation of this experiment is the inadequate hydrocarbon decay in the model results. If the observed decay were simulated correctly, the NO-to-NO_2 conversions would be more than the observed amount, and the simulated ozone would be even greater than the observed amount.

Problems in the July experiment seem to stem from a lack of radicals. Extra amounts of background contamination by formaldehyde were added to help bring up the simulated CO and radical concentrations. However, the observed decay of ethene was still not matched by the model and so the necessary NO-to-NO_2 conversions and final ozone level were not simulated. Note that a sample-line delay problem probably exists in this experiment up to about 450 minutes, since high levels of NO are present until this time.

4.4 m-XYLENE

In our previous studies of the toluene-NO_x photochemical system (Killus and Whitten, 1982a), we observed several features that distinguished it from olefinic (e.g., propylene) photooxidation systems. These special features included

(1) A powerful NO_x sink (ascribed to the formation of nitrophenols from the reaction of cresols with NO_3, and from secondary reactions of benzaldehyde.

(2) A high production rate of radicals (ascribed to methyl glyoxal formation and photolysis).

(3) Inefficient ozone formation due, in part, to the features described in (1) and (2).

In the extension of our aromatics mechanism to include m-xylene (Table 7) [simulations of two experiments performed at the University of California, Riverside (UCR), smog chamber are shown in Figures 34 and 35], we have found several important mechanistic differences when m-xylene is compared with the toluene system that go beyond the factor-of-three differences in OH rate constants. Notably, the radical source strength is higher for m-xylene than for toluene, as might be expected from the existence of two methyl substituent groups that produce two methyl glyoxal molecules per xylene molecule.

The NO_x sink strength for m-xylene is, by contrast, somewhat less than for toluene; this suggests a lower yield of phenolic compounds in the m-xylene system, whereas the yield of PAN is higher for m-xylene than for toluene. There is also evidence of a reaction of the aromatic OH adduct radical with NO_2. This latter feature may also exist in the toluene system, as we will discuss later.

4.4.1 Ring Opening in m-Xylene

Radical initiation in the m-xylene NO_x system is prompt; the best simulation results are obtained if one assumes immediate ring opening and the full yield of two methyl glyoxal molecules per molecule of m-xylene. This indicates a reaction scheme that fully oxygenates the aromatic ring (see Figure 36).

Hendry (1979) concluded that the reaction of NO_2 with the toluene OH adduct radical was negligable at NO_2 concentrations of less than 1 ppm. However, the experimental procedures used by Hendry precluded observations for the thermalized adduct radical; hence significant direct products of nitrotoluene might occur in the toluene-NO_x system. In the m-xylene system, there is evidence for an NO_2-linked radical sink reaction that we have attributed to the reaction of NO_2 with the thermalized OH adduct (Reaction 82). In the future, we intend to examine the possible effects of such reactions on our toluene mechanism in cases for which nitrotoluene is the expected product.

By analogy with toluene chemistry, phenolic hydrocarbons are also assumed to be produced in m-xylene oxidation, and subsequent reactions of methylcresol with OH and NO_3 are set at rates similar to those for cresol.

4.4.2 Hydrogen Abstraction OH

The yield of m-tolualdehyde in the m-xylene oxidation is low; thus the NO_x sink created by aromatic aldehyde oxidation to nitrophenols (Niki et al., 1979) is largely absent from the m-xylene system. In the toluene system, 15 percent of the toluene-OH reaction leads to benzaldehyde, which reacts with OH to ultimately produce a phenoxy radical:

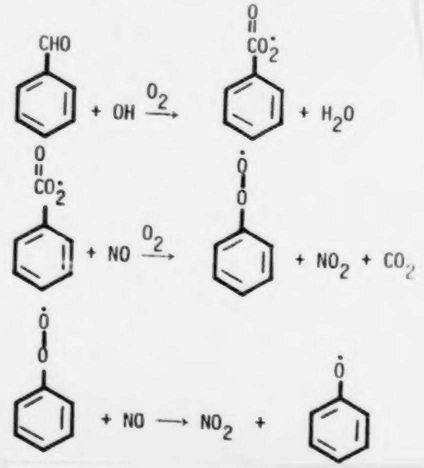

The phenoxy radical is an NO_x scavenger, forming nitrophenol as a product:

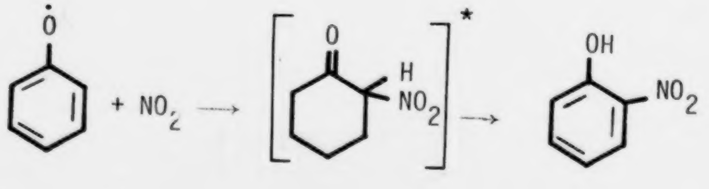

The formation of para-nitrophenol has also been observed by Niki et al., and must proceed by intermolecular reaction.

Subsequent NO_x sink reactions of the nitrophenols are possible, e.g.:

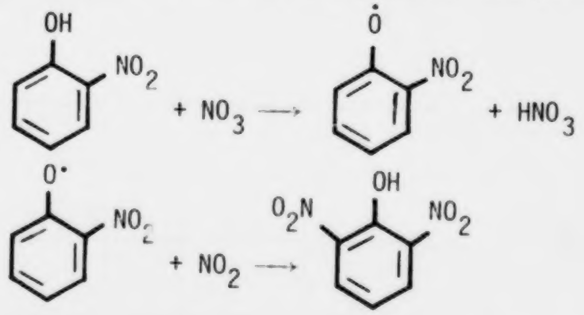

Thus, formation (and subsequent reactions) of benzaldehyde is a strong NO_x sink in the toluene system.

In the xylene system, the yield of tolualdehyde is less than 4 percent; thus, the NO_x sink created by aromatic aldehyde oxidation to nitrophenols is largely absent.

4.4.3 Ozone Generated Per NO_x Loss ($\Delta\ O_3/\Delta\ NO_x$)

One effect of NO_x sink processes in photochemical systems is to reduce the quantity of ozone generated for a given quantity of NO_x precursor. Sakamaki, Akimoto, and Okuda (1981) have developed a methodology to quantify the $\Delta\ O_3/\Delta\ NO_x$ for any specific hydrocarbon. They note that for a given initial concentration of NO_2 at a particular NO_2 photolysis rate (k_1) there exists a photostationary concentration of ozone, $[O_3]_{ps}$. For any given hydrocarbon, under conditions of hydrocarbon excess, maximum O_3 is proportional to $[O_3]_{ps}$. Since $[O_3]_{ps} \cong k_1/k_3\ [NO_2]^{1/2}$ (where k_3 = rate of reaction between O_3 and NO), $[O_3]_{max}$ is approximately proportional to the square root of initial $[NO_2]$.

The proportionality constants (k_p) derived by Sakamaki, Akimoto, and Okuda (1981) are

k_p		Hydrocarbon
9.93	for	C_2H_4
9.21	for	C_3H_6
8.45	for	1-C_4H_8
8.24	for	1-C_5H_{10}

We have extended this analysis to some of the data from the University of California, Riverside smog chamber (Pitts et al., 1979). Although the UCR experiments typically use a mixture of NO and NO_2 as the initial NO_x, the measured NO_2 peak can be used to calculate $[O_3]_{ps}$.

The UCR experiments show greater variability than those of Sakamaki, Akimoto, and Okuda (1981). Some of the variance in the k_p for each hydrocarbon may be due to reaction products formed prior to the NO_2 peak. Also, changes in chamber conditions and analytical procedures might be responsible. Our analysis indicates that the ratio of aldehyde photolysis to k_1 may influence $[O_3]_{max}$ since the photolysis ratio has a strong effect on radical formation rate and NO_x loss rate. Chamber-related emissions of NO_x may also have an effect on k_p .

Our calculations of k_p for various hydrocarbons in the UCR chamber yield the following results:

Hydrocarbon	Average k_p	Range of k_p
Ethene	13.5	10.4 → 16.2
Propene	7.9	6.76 → 9.42
Butane	12.1	11.5 → 13.6
2,3 dimethylbutane (2 experiments)	14.2	12.8 → 15.6
Formaldehyde (2 experiment)	9.35	9.35
Toluene	6.63	6.25 → 7.5
m-xylene (2 experiments)	7.3	7.06 → 7.53

Note that toluene appears to be the least efficient ozone producer, whereas m-xylene is similar to propene in Δ ozone/Δ NO_x.

4.5. DICARBONYLS

4.5.1 Biacetyl

The reaction mechanism for biacetyl (a secondary product of o-xylene oxidation; see Darnall, Atkinson, and Pitts, 1979) is very simple. Hydrogen abstraction from the methyl groups is slow and can be ignored; however, photolysis is very rapid:

$$CH_3C(O)C(O)CH_3 \xrightarrow[+\ 2O_2]{h\nu} CH_3CO_3 + CH_3CO_3\cdot \quad .$$

We have simulated two biacetyl (BIAC) experiments for UNCR experiment 70980 and UNCB experiment 80880 shown in Figures 37 and 38. We use a biacetyl photolysis rate of 3.6 percent of k_1, which gives good agreement with measured BIAC decay and is similar to the rate reported by Darnall, Atkinson, and Pitts (1979) for the SAPRC chamber. All observed species are simulated except for formaldehyde, which is underpredicted. PAN decay is underpredicted because these simulations used a lower rate for the radical-radical reactions than that now used in our standard mechanism.

4.5.2 Methyl Glyoxal

Only one experiment has been performed for methyl glyoxal (MG); unfortunately the sunlight on this day was very uneven and no data for MG decay are available. Therefore, we cannot, as yet, properly estimate the rate of MG reaction with hydroxyl. We can, however, draw some conclusions from modeling this experiment. Atkinson et al. (1980) estimate a photolysis rate of approximately 15 percent k_1. As seen in Figure 39, this appears to be too high.

Figure 40 shows the results for MG photolysis at 4.0 percent of K_1, and the OH - MG reaction set to 7000 ppm^{-1} min, which is the value used in our toluene mechanism. We have modified the yield of MG to 100 percent peroxy acetyl (eliminating a 35 percent pathway to MEO_2, 2 CO, and HO_2 as presently used in the toluene mechanism) because of the high observed yield of PAN.

Results for NO_x may be improved slightly (at the expense of ozone and PAN) by lowering MG photolysis still further (to 2 percent of K_1) and by eliminating the reaction of hydroxyl with MG entirely. The photolysis estimates should be interpreted with caution, however, because of the choppiness of the light on this day. Tentatively, we suggest that the photolysis rate of MG is similar to or slightly less than that of biacetyl. However, there may have been some exchange of MG with the chamber wall (Kamens 1982, private communication) and this would complicate the analysis. As with UNCR experiment 70980 (Figure 36) run for biacetyl, formaldehyde is greatly underpredicted in the MG simulations. We have experimented with the possibility of an HO_2 reaction with MG; however, increased formaldehyde production tends to produce excess CO in the simulations. We suspect contamination in the MG source. It is also possible that the formaldehyde measurements may receive a positive interference from PAN, or methyl glyoxal.

4.6 ACETONE AND METHYL ETHYL KETONE

Cox, Patrick, and Chant (1981) studied the OH-induced oxidation of butane, MEK, and methyl isobutyl ketone (MIK). In this study, the OH radicals were generated by photolysis of ppm concentrations of HONO, at atmospheric pressure and ~ 295 K. This system provides an excellent method for studying alkoxy radical decomposition since both oxygen and nitric oxide (formed in HONO photolysis) were at concentrations sufficient to maintain the realistic photooxidation of these compounds.

Biacetyl and methylglyoxal were not observed in either the MEK or MIK experiments. This finding suggests that alkoxy radical decomposition is the primary reaction pathway for MEK:

$$CH_3CH_2C(O)CH_3 + OH \xrightarrow{+O_2} H_2O + CH_3CH(\dot{O}_2)C(O)CH_3 \quad ,$$

$$CH_3CH(\dot{O}_2)C(O)CH_3 + NO \longrightarrow NO_2 + CH_3CH(\dot{O})C(O)CH_3 \quad ,$$

$$CH_3CH(\dot{O})C(O)CH_3 \xrightarrow{+O_2} CH_3C\dot{O}_3 + CH_3CHO \quad .$$

Methyl Isobutyl ketone also shows radical decomposition to be the dominant pathway:

$$OH + (CH_3)_2CHCH_2COCH_3 \xrightarrow{+O_2} H_2O + (CH_3)_2\ C(\dot{O}_2)CH_2COCH_3 \quad ,$$

$$(CH_3)_2C(\dot{O}_2)CH_2COCH_3 + NO \longrightarrow NO_2 + (CH_3)_2C(\dot{O})CH_2COCH_3 \quad ,$$

$$(CH_3)_2C(\dot{O})CH_2COCH_3 \xrightarrow{+O_2} \underset{\text{(acetone)}}{(CH_3)_2CO} + CH_2(\dot{O}_2)COCH_3 \quad ,$$

$$CH_2(\dot{O}_2)COCH_3 + NO \longrightarrow NO_2 + CH_2(\dot{O})COCH_3 \quad ,$$

$$CH_2(\dot{O})COCH_3 \xrightarrow{+O_2} CH_3C\dot{O}_3 + HCHO \quad .$$

The last two steps in this sequence are identical to the oxidation sequence for acetone. Thus alkoxy radical decomposition (rather than methyl gloxyal formation) would be expected to dominate in acetone oxidation.

4.6.1 Results

Results for MEK and acetone in the UNC chamber are given in Figures 41 through 48. The mechanisms used for these compounds (Table 8) are quite simple; only photolysis and reaction with hydroxyl are included. Decomposition of the alkoxycarbonyl radicals are as just given.

Photolysis for acetone is taken to be 6 percent of the rate of formaldehyde photolysis to radicals. Photolysis for MEK is 12 percent of formaldehyde photolysis to radicals. For acetone especially, the error bounds on photolysis are large because the photolysis of acetone is similar to the photolysis of the acetone oxidation products (e.g., formaldehyde). In UNCR experiment 60480, the reactivity of acetone loading is similar to the background reactivity of the UNC chamber.

The rate constant for reaction of OH with MEK given by Cox, Patrick, and Chant (1981) appears to be too low. We use a rate constant of 5100 $\mathrm{ppm}^{-1}\mathrm{min}^{4}$, which is consistent with other investigators (Atkinson et al. 1979). This is greater by a factor of four than that measured by Cox, Patrick, and Chant (1981).

TABLE 4. PROPENE REACTIONS

```
THE REACTIONS                                                            RATE CONSTANT  ACT. ENERGY (K)
 71     O     +   PROP       =   MEO2  +   C203                            6.000E 02     3.240E 02
 72     O     +   PROP       =   PRXD                                      1.780E 03     3.240E 02
 73     O     +   PROP       =   ALD3                                      1.780E 03     3.240E 02
 74     O     +   PROP       =   HO2   +   CO    +    C202                 1.760E 03     3.240E 02
 75     OH    +   PROP       =   RAO2                                      4.200E 04    -5.370E 02
 76     NO3   +   PROP       =   PNO2                                      1.140E 01     0.
 77     O3    +   PROP       =   ALD2  +   CRIG                            5.400E-03     1.897E 03
 78     O3    +   PROP       =   FORM  +   MCRG                            5.400E-03     1.897E 03
 79     O3    +   PROP       =   ALD2  +   HOTA                            3.600E-03     1.097E 03
 80     O3    +   PROP       =   FORM  +   HTMA                            3.600E-03     1.897E 03
 81     HOTA                 =                                             2.500E 01     0.
 82     HOTA                 =   CO                                        5.000E 01     0.
 83     HOTA                 =   HO2   +   HO2                             1.000E 01     0.
 84     HOTA                 =   FACD                                      7.000E 00     0.
 86     CRIG  +   NO         =   FORM  +   NO2                             1.000E 04     0.
 87     CRIG  +   NO2        =   FORM  +   NO3                             1.000E 03     0.
 88     CRIG  +   H2O        =   FACD                                      6.000E-03     0.
 89     CRIG  +   FORM       =   OZD                                       3.000E 01     0.
 90     CRIG  +   ALD2       =   OZD                                       3.000E 01     0.
 91     HTMA                 =                                             2.000E 02     0.
 92     HTMA                 =   MEO2  +   CO    +    OH                   4.000E 02     0.
 93     HTMA                 =   MEO2  +   HO2                             3.200E 02     0.
```

TABLE 4. (concluded)

94	HTMA		=	HO2 +	CO +	FORM +	HO2	8.000E 01	0.
95	MCRG +	NO	=	ALD2 +	NO2			1.000E 04	0.
96	MCRG +	NO2	=	ALD2 +	NO3			1.000E 03	0.
97	MCRG +	H2O	=	ACAC				6.000E-03	0.
98	MCRG +	FORM	=	OZD				3.000E 01	0.
99	MCRG +	ALD2	=	OZD				3.000E 01	0.
100	RAO2 +	NO	=	NO2 +	ALD2 +	FORM +	HO2	1.000E 04	-2.500E 02
101	RAO2 +	NO	=	RNIT				4.160E 02	-2.500E 02
102	RAO2 +	HO2	=					9.000E 03	0.
103	RAO2 +	RAO2	=					5.000E 02	0.
104	PNO2 +	NO	=	PGDN				5.000E 03	0.
105	PNO2 +	NO	=	ACTN +	HO2 +	NO2		5.000E 03	0.
106	C2O2 +	NO	=	NO2 +	ALD2 +	HO2		1.000E 04	0.

TABLE 5. ETHENE REACTIONS

THE REACTIONS											RATE CONSTANT	ACT. ENERGY (K)
99	ETH	+	O	=	MEO2	+	HO2	+	CO		1.060E 03	7.920E 02
101	ETH	+	OH	=	REO2						1.200E 04	-3.820E 02
71	ETH	+	O3	=	FORM	+	CRIG				1.000E-03	2.840E 03
72	ETH	+	O3	=	FORM	+	HOTA				1.700E-03	2.840E 03
73	ETH	+	NO3	=	ENO2						2.100E 00	0.
74	HOTA			=							2.500E 01	0.
75	HOTA			=	CO						5.800E 01	0.
76	HOTA			=	HO2	+	HO2				1.000E 01	0.
77	HOTA			=	FACD						7.000E 00	0.
78	CRIG	+	NO	=	FORM	+	NO2				1.000E 04	0.
79	CRIG	+	NO2	=	FORM	+	NO3				1.000E 03	0.
80	CRIG	+	H2O	=	FACD						6.000E-03	0.
81	CRIG	+	FORM	=	OZD						3.000E 01	0.
82	ENO2	+	NO	=	EDNT						1.000E 04	0.
83	REO2	+	NO	=	NO2	+	REO				1.000E 04	0.
84	REO			=	FORM	+	REM2				6.600E 05	4.000E 03
102	REM2	+	NO	=	NO2	+	FORM	+	OH		1.000E 04	0.
85	REO			=	GLYA	+	HO2				1.820E 05	0.
86	REO2	+	REO2	=	REO	+	REO				5.000E 02	0.
87	REO2	+	HO2	=	REO	+	OH				1.000E 04	0.
89	GLYA			=	HXPX	+	HO2				2.000E-03	0.
90	GLYA	+	OH	=	HXPX						2.000E 04	0.
91	HXPX	+	NO	=	FORM	+	NO2	+	HO2		1.600E 04	0.
92	HXPX	+	NO2	=	HPAN						8.000E 03	0.
93	HPAN			=	HXPX	+	NO2				2.000E-02	1.400E 04
94	HXPX	+	HO2	=	FORM	+	HO2	+	OH		1.000E 04	0.

TABLE 6. INITIAL CONDITIONS FOR OLEFIN EXPERIMENTS[*]

EXPERIMENT	NO	NO_2	Olefin	HONO[x]	CO	H_2O	Form	Wall[§]
NIES-05	1.48	0.02	3.04	0.0	0.0	1.0	---	---
NIES-07	1.36	0.04	3.04	0.0	0.0	16700	---	---
R-101877	0.38	0.11	1.92	2.5	0.30	20000	0.0	0.05
B-101877	0.39	0.11	0.94	3.0	0.30	20000	0.05	0.10
R-111277	0.38	0.11	1.00	5.0	0.30	20000	0.0	0.05
R-111977	0.40	0.11	1.89	5.0	0.30	5000	0.02	0.05
R-112077	0.41	0.11	2.19	5.0	0.30	15000	0.05	0.05
B-11078	0.34	0.14	2.19	0.5	0.20	1300	0.0	0.0
R-61678	0.44	0.18	2.00	5.0	0.30	16000	0.03	0.03
B-63078	0.38	0.10	0.76	2.5	0.30	15000	0.06	0.20
R-70178	0.68	0.20	0.72	30	0.37	10000	0.10	0.20
R-73078	0.40	0.07	0.67	12	0.44	28000	0.05	0.0
B-80678	0.42	0.15	1.25	25	0.30	26000	0.20	0.35
R-81078	0.42	0.11	0.52	15	0.30	21000	0.0	0.05
B-81078	0.41	0.11	1.50	10	0.30	21000	0.0	0.25
B-81578	0.43	0.13	0.79	25	0.30	22000	0.15	0.25
R-82378	0.41	0.10	1.48	2	0.35	15000	0.01	0.06
B-82378	0.42	0.09	1.48	2	0.35	14000	0.01	0.06
B-91478	0.23	0.06	0.44	10	0.21	20000	0.10	0.10

TABLE 6. (CONCLUDED)

EXPERIMENT	NO	NO_2	Olefin	HONO[x]	CO	H_2O	Form	Wall[§]
R-91578	0.41	0.12	1.49	3	0.43	15000	0.03	0.03
R-91878	0.41	0.10	1.49	25	0.33	22000	0.25	0.35
R-91978	0.57	0.12	0.94	25	0.26	23000	0.10	0.30
R-92178	0.19	0.07	0.97	7	0.41	21000	0.15	0.10
B-100278	0.38	0.10	1.49	4	0.36	18000	0.0	0.05
R-100378	0.36	0.14	0.49	4	0.43	15000	0.0	0.10
R-101278	0.36	0.14	0.49	13	0.46	15000	0.0	0.25
R-80479	0.17	0.06	0.44	10	0.34	34000	0.05	0.25
R-80579	0.50	0.14	2.06	7	0.34	29000	0.0	0.0
R-103179	0.40	0.10	1.87	1.5	0.34	14000	0.0	0.0
B-103179	0.40	0.10	1.85	0.0	0.34	5600	0.0	0.0
R-70880	0.36	0.37	1.02	5	0.35	10000	0.03	0.06

---

[*] Concentrations in ppm except for HONO
NIES experiments are propene, remainder are UNC ethene.

[x] Concentrations in ppb

[§] Wall → Formaldehyde with k = 0.002 min

TABLE 7. M-XYLENE MECHANISM

THE REACTIONS											RATE CONSTANT	ACT. ENERGY (K)
43	O3			=							1.600E-03	0.
46				=	NO						1.000E-04	0.
1	NO2			=	NO	+	O				4.000E-01	0.
8	O3			=	O						1.000E-02	0.
7	O3			=	O1D						4.000E-04	0.
19	HNO2			=	OH	+	NO				6.000E-02	0.
15	N2O5	+	H2O	=	HNO3	+	HNO3				1.500E-05	0.
24	H2O2			=	OH	+	OH				6.400E-04	0.
27	NO3			=	NO2	+	O				3.600E 00	0.
28	NO3			=	NO						5.280E-01	0.
60	MNIT			=	MEO	+	NO				1.200E-01	0.
37	FORM			=	CO						2.500E-04	0.
36	FORM			=	CO	+	HO2	+	HO2		2.500E-04	0.
47	C2O3	+	NO	=	MEO2	+	NO2				1.040E 04	0.
53	C2O3	+	NO2	=	PAN						6.000E 03	0.
61	PAN			=	C2O3	+	NO2				2.200E-02	1.400E 04
64	C2O3	+	HO2	=							8.000E 03	0.
65	GLY			=	FORM	+	CO				1.000E-03	0.
49	ALD2			=	C2O3	+	HO2				1.200E-04	0.

TABLE 7 (Concluded)

78	XYL	+	OH	=	XYLO							1.500E 03	0.
79	XYLO	+	NO	=	NO2	+	HO2	+	TLA			1.200E 04	0.
77	TLA	+	OH	=	TLO2							2.000E 04	0.
76	TLO2	+	NO	=	NO2	+	PHO					4.000E 03	0.
75	PHEN	+	OH	=	PHO							1.000E 04	0.
82	OPEN	+	NO2	=	NXYL							3.500E 02	0.
84	XYL	+	OH	=	RARO							9.000E 03	0.
85	XYL	+	OH	=	OPEN							2.600E 04	0.
86	RARO	+	NO	=	NO2	+	PHEN					4.000E 03	0.
87	OPEN	+	NO	=	NO2	+	MGLY	+	HO2	+	APRC	6.000E 03	0.
88	APRC			=	MGLY	+	GLY					2.000E 01	0.
89	PHEN	+	NO3	=	PHO	+	HNO3	+	BNO3			1.000E 04	0.
90	PHO	+	NO2	=	NPHN							4.000E 03	0.
91	NPHN	+	NO3	=	NPHO	+	HNO3					1.000E 03	0.
92	NPHO	+	NO2	=	DNPH							5.000E 03	0.
93	MGLY			=	C2O3	+	HO2	+	CO			1.100E-02	0.
96	MGLY	+	OH	=	C2O3	+	CO					7.000E 03	0.
94	MGLY			=	MEO2	+	HO2	+	CO	+	CO	5.500E-03	0.
95	NPHN			=	WPHN							1.500E-02	0.
97	GLY	+	OH	=	HO2	+	CO	+	CO			1.500E 04	0.
98	PHEN	+	OH	=	OPN2	+	CO	+	CO			1.000E 05	0.
99	OPN2	+	NO	=	NO2	+	HO2	+	APRC	+	PVAC	1.200E 04	0.

TABLE 8. **MECHANISM FOR ACETONE AND MEK**

	Rate Constant (ppm^{-1} min^{-1})
AONE + OH → AONR	5000.
AONR + NO → NO_2 + C2O3 + HCHO	9000.
AONR → MeO_2 + C2O3	($0.06 \times K_{36}$)
MEK + OH → MKO2	5100.
MKO2 + NO → NO_2 + C2O3 + ALD2	9000.
MEK → C2O3 + C2O2	($0.12 \times K_{36}$)

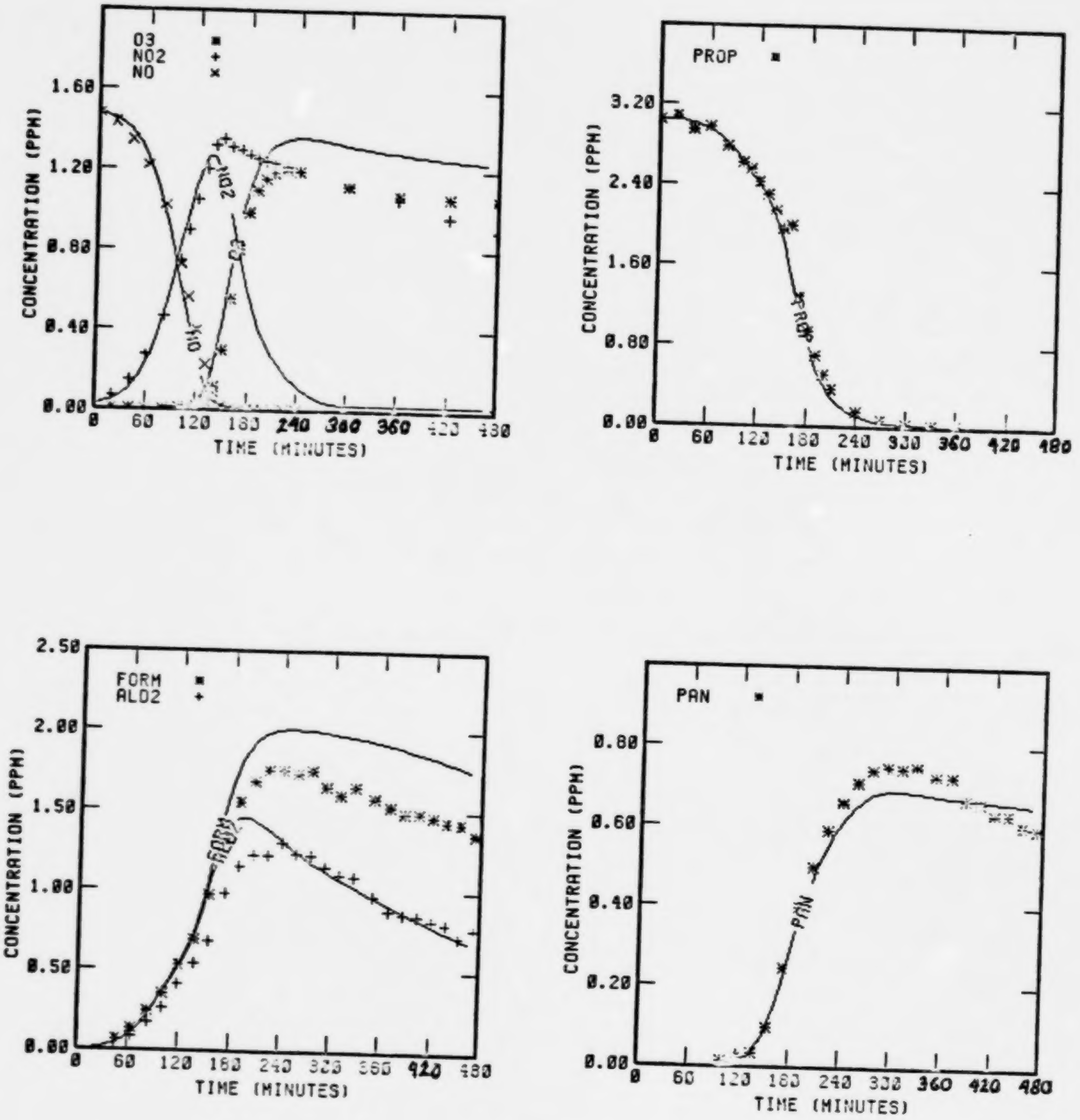

FIGURE 3. SIMULATION RESULTS FOR NIES-780705

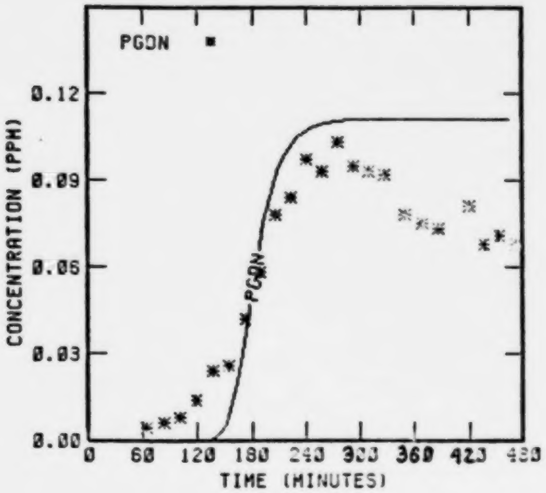

FIGURE 3. SIMULATION RESULTS FOR
NIES-780725
(Concluded)

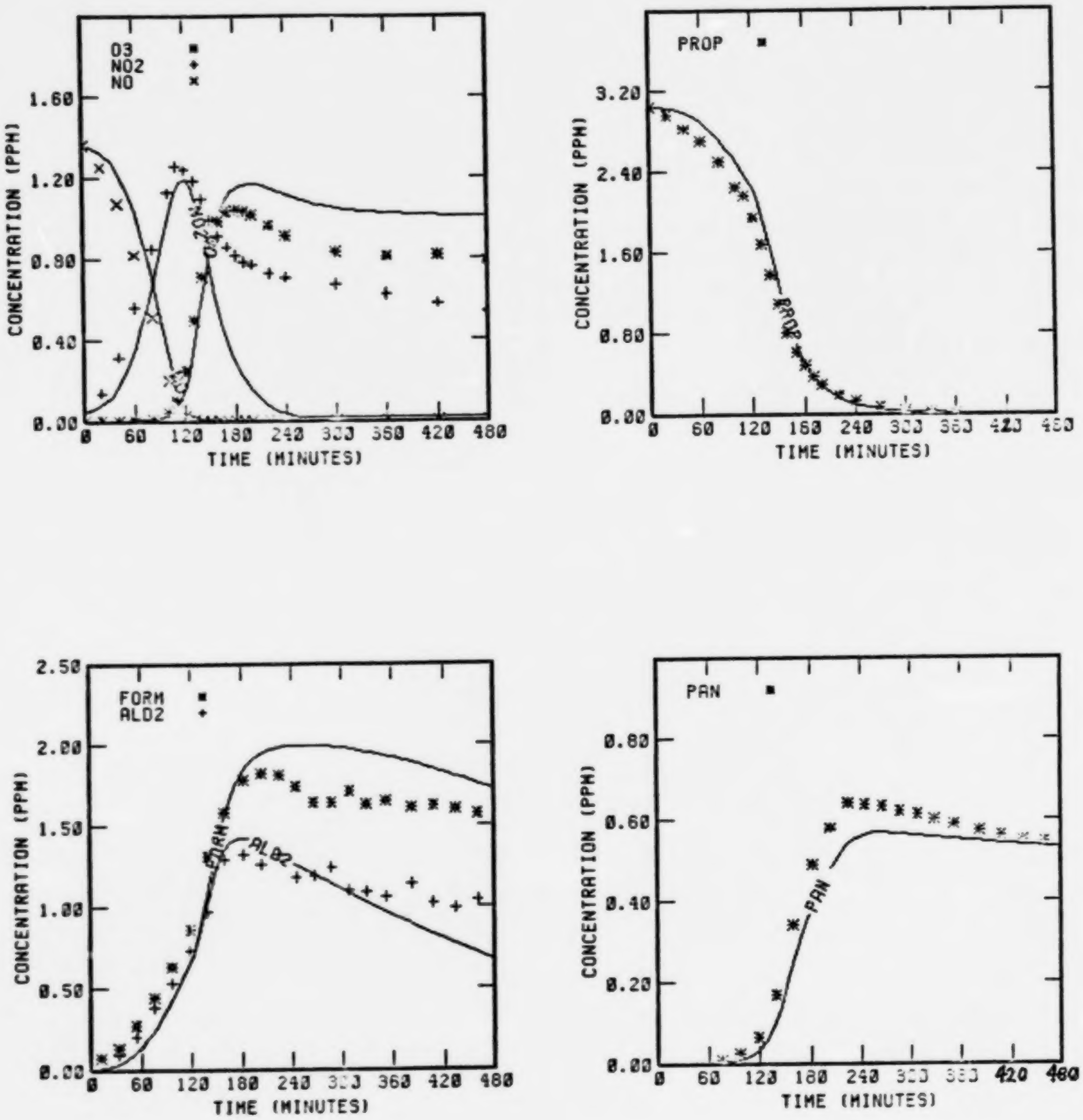

FIGURE 4. SIMULATION RESULTS FOR NIES-780707

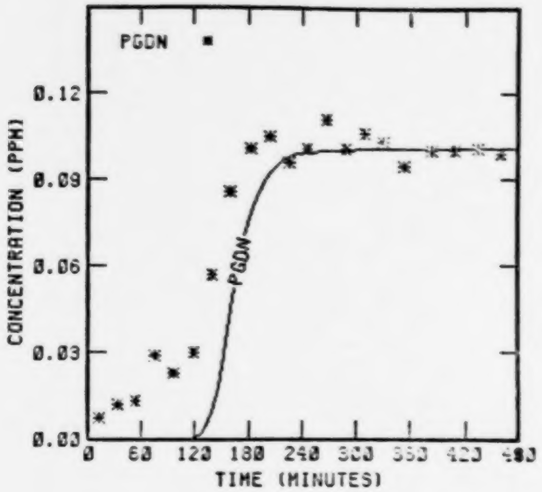

FIGURE 4. SIMULATION RESULTS FOR NIES-780707 (Concluded)

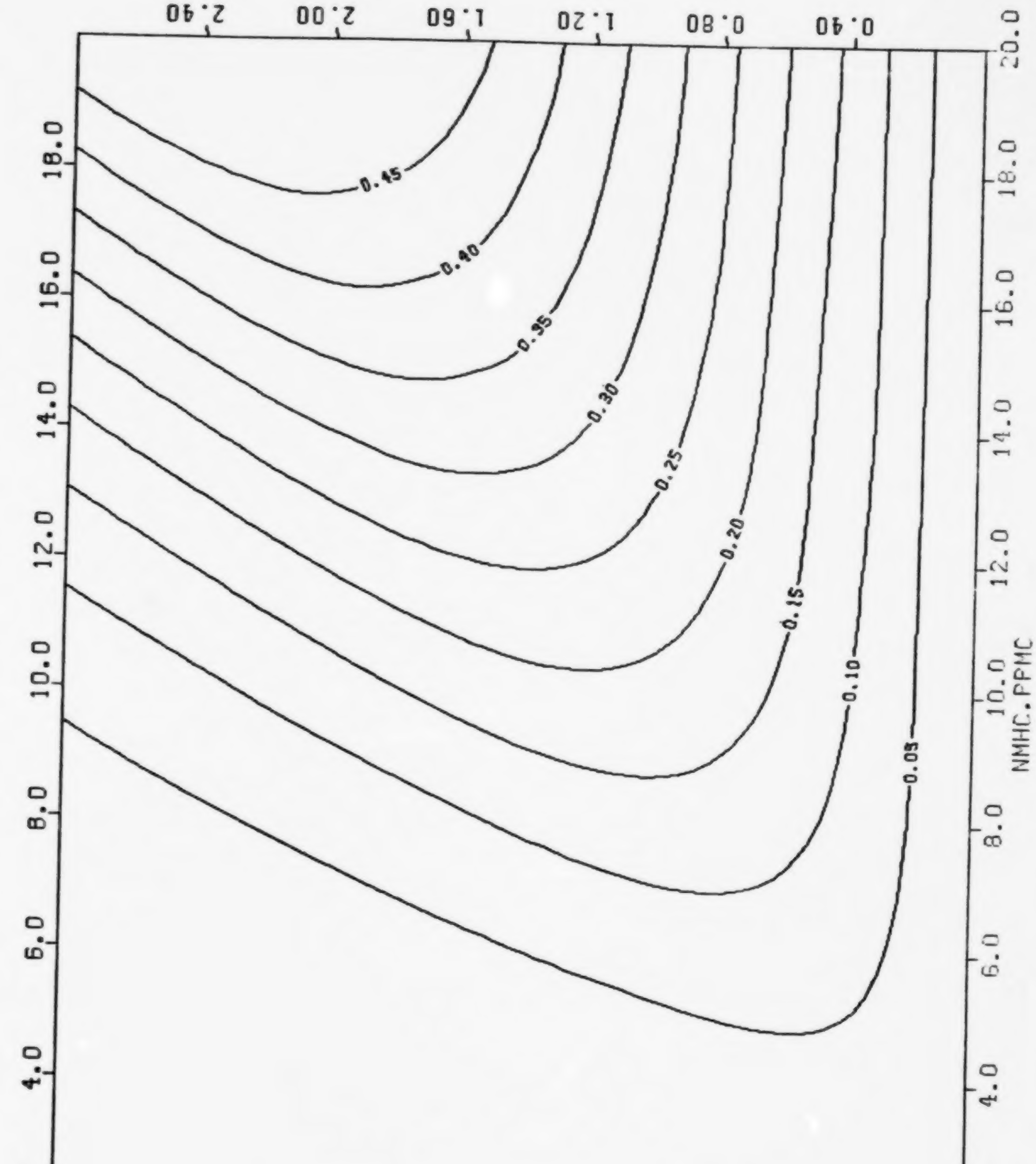

FIGURE 5. PRØPYLENE GLYCØL DINITRATE ISØPLETH

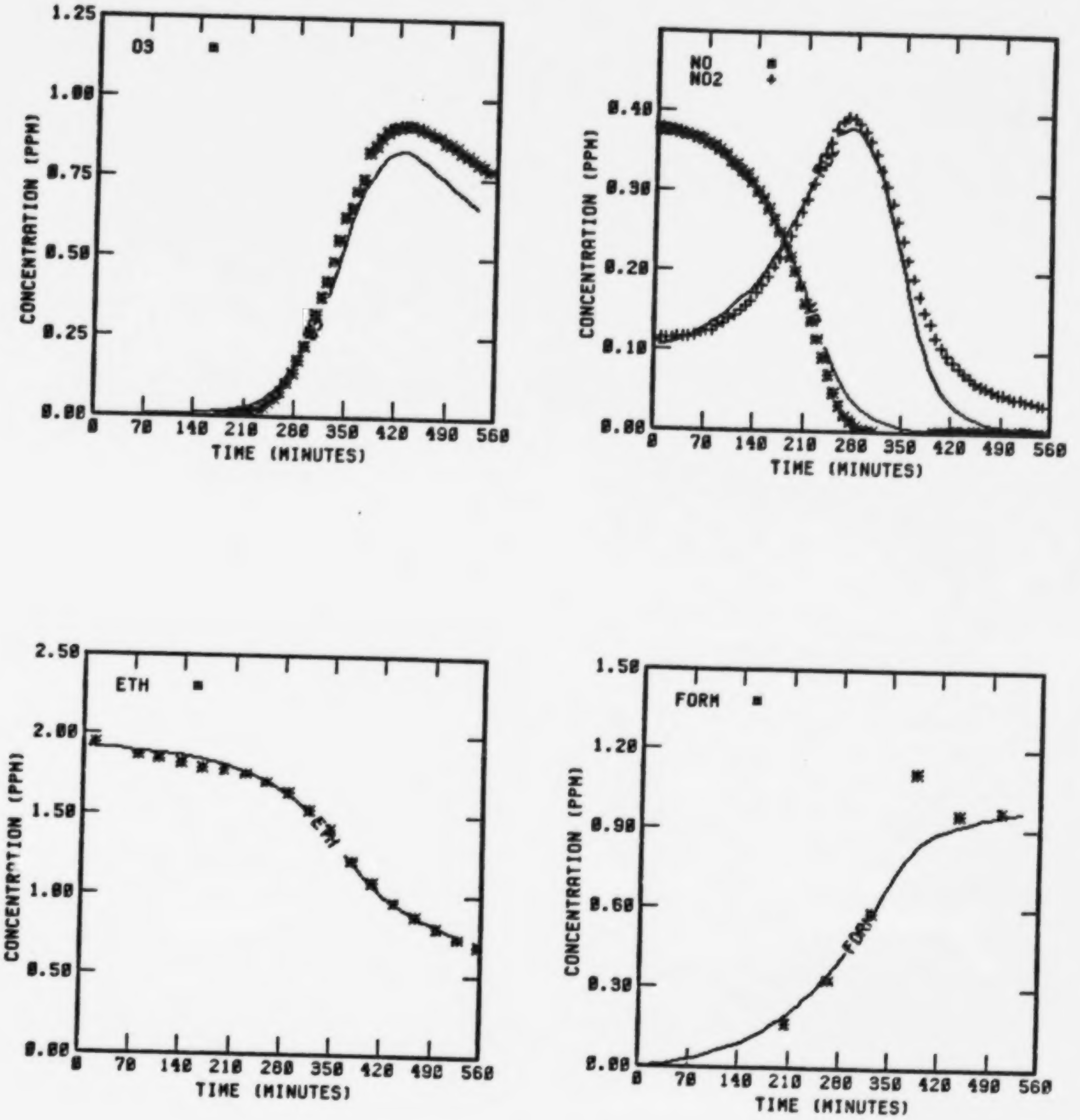

FIGURE 6. SIMULATION RESULTS FOR UNCR 101877

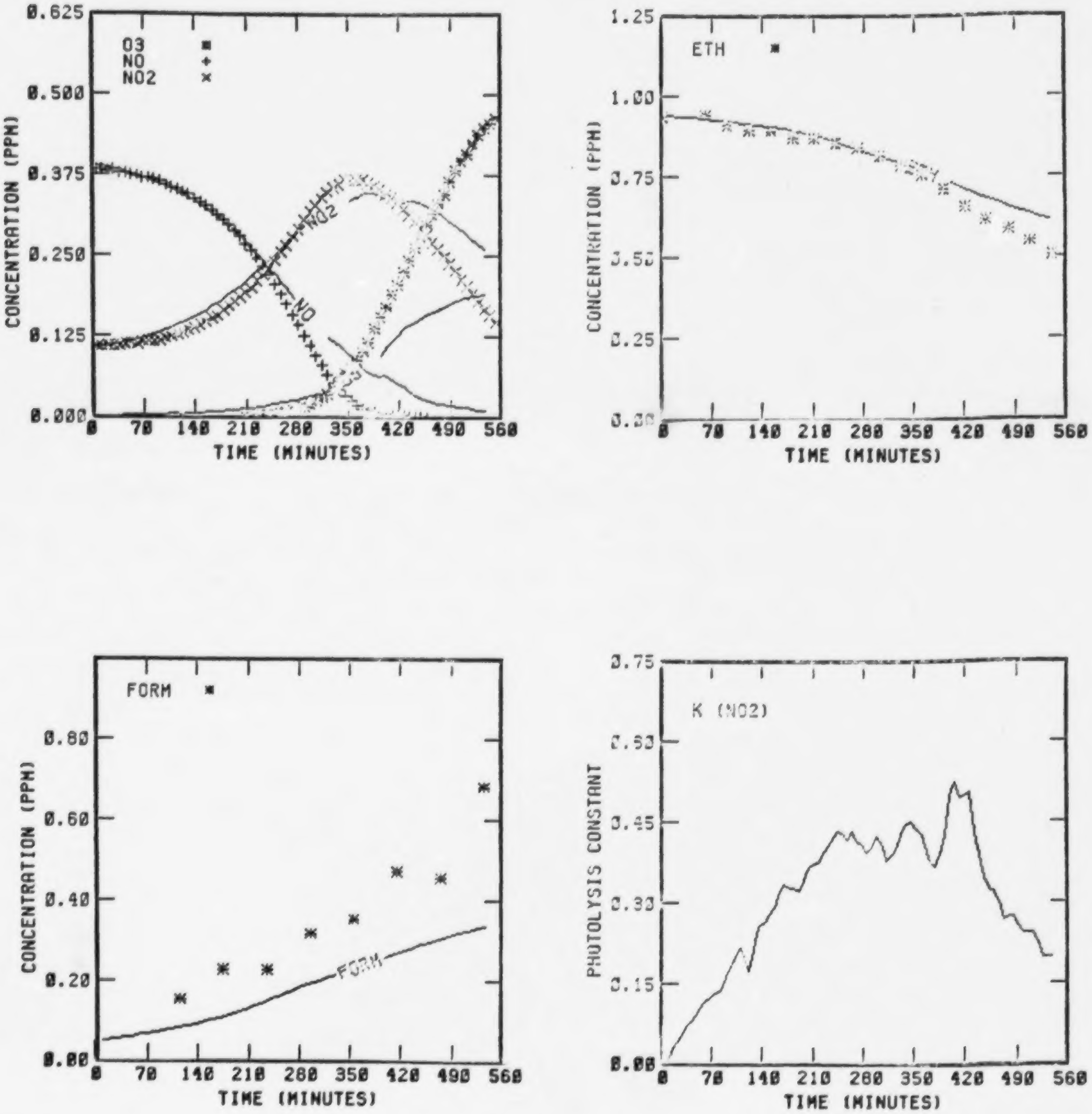

FIGURE 7. SIMULATION RESULTS FOR UNCB 101377

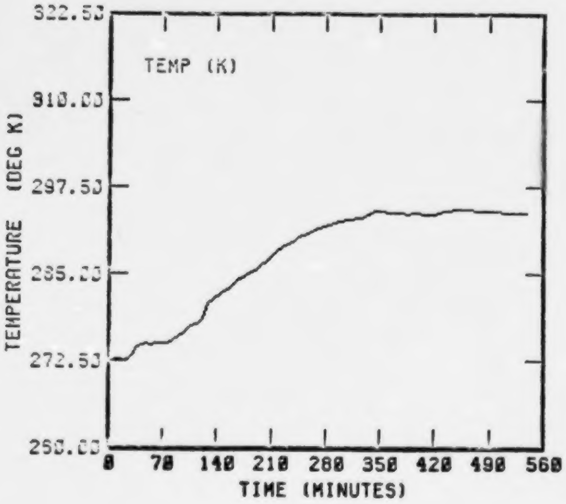

FIGURE 7. . SIMULATION RESULTS FOR
UNCB 101377
(Concluded)

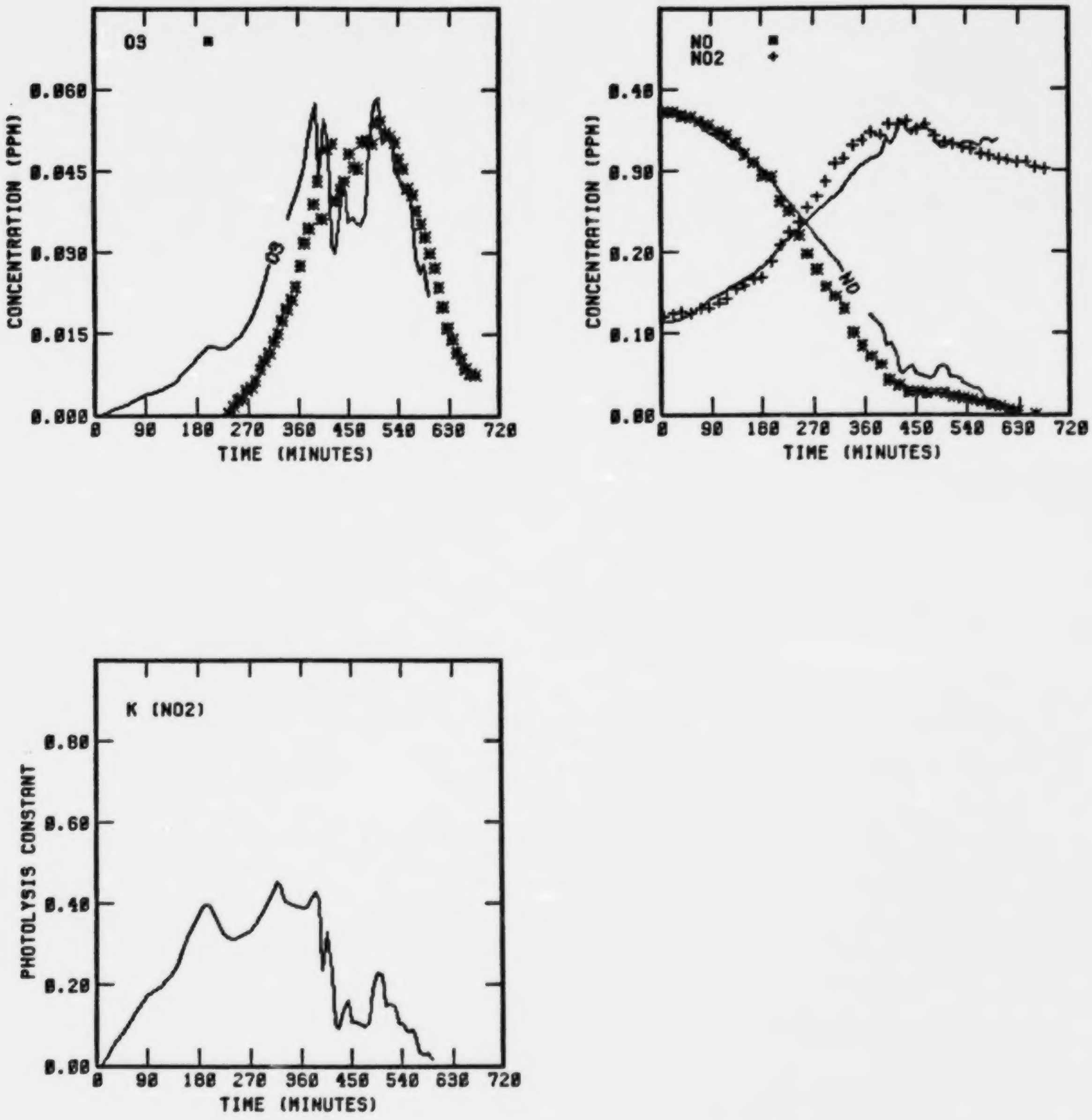

FIGURE 8. SIMULATION RESULTS FOR UNCR 111277

Reproduced from
best available copy.

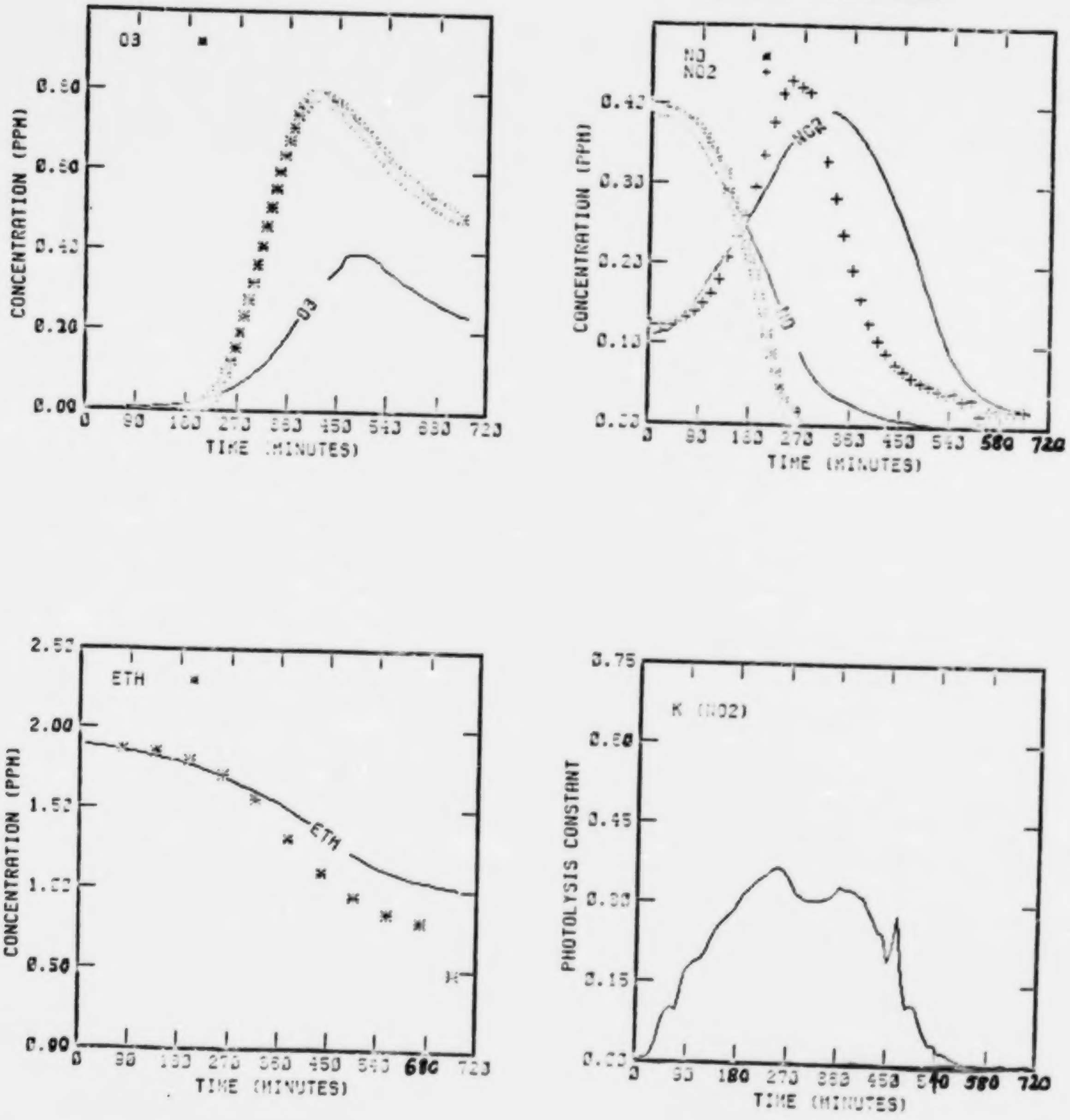

FIGURE 9. SIMULATION RESULTS FOR
UNCR 111377

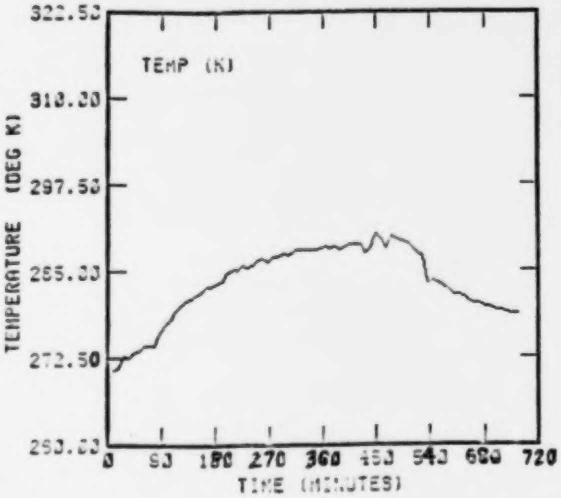

FIGURE 9. SIMULATION RESULTS FOR
UNCR 111977
(Concluded)

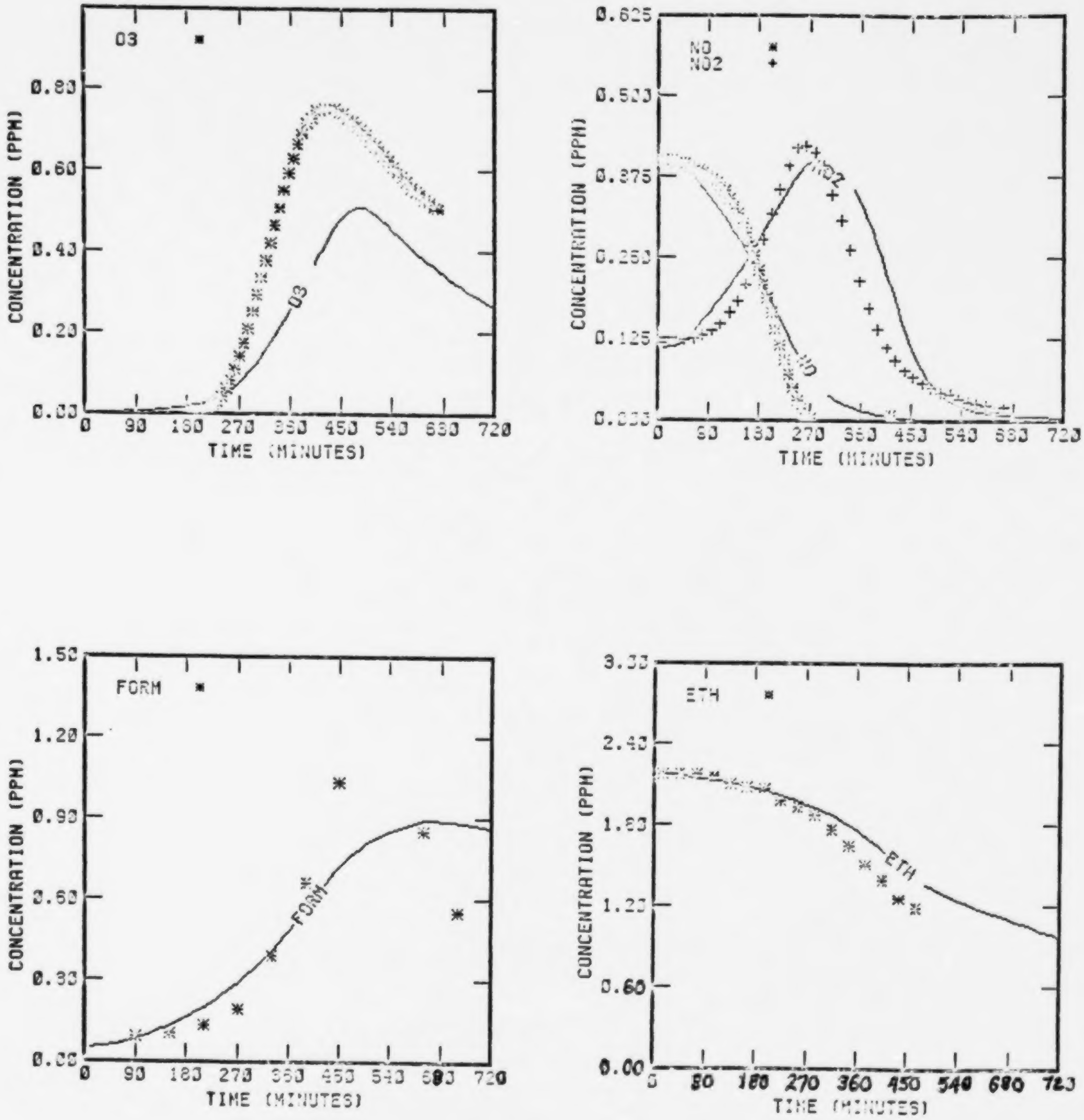

FIGURE 10. SIMULATION RESULTS FOR UNCR 112077

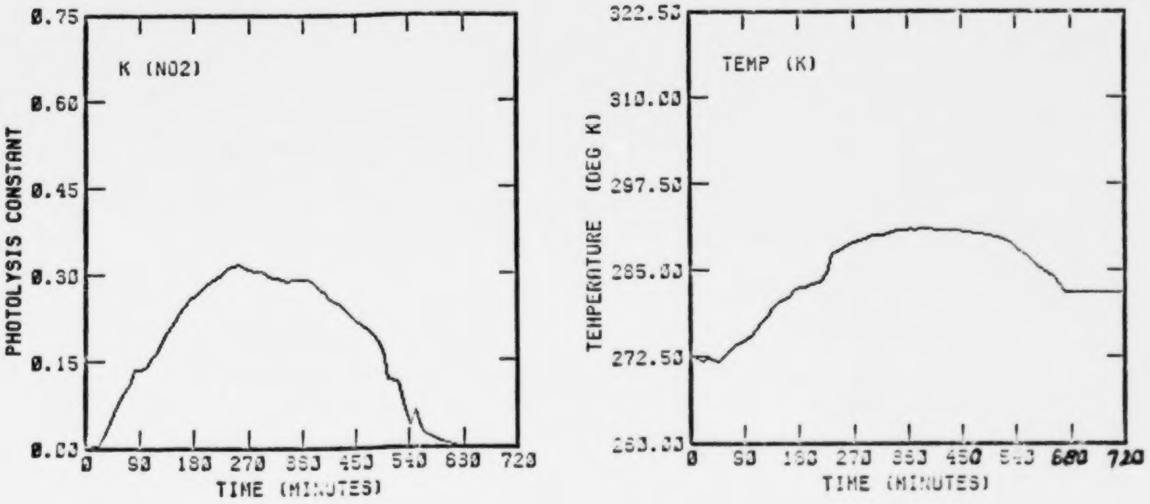

FIGURE 10. SIMULATION RESULTS FOR
UNCR 112077
(Concluded)

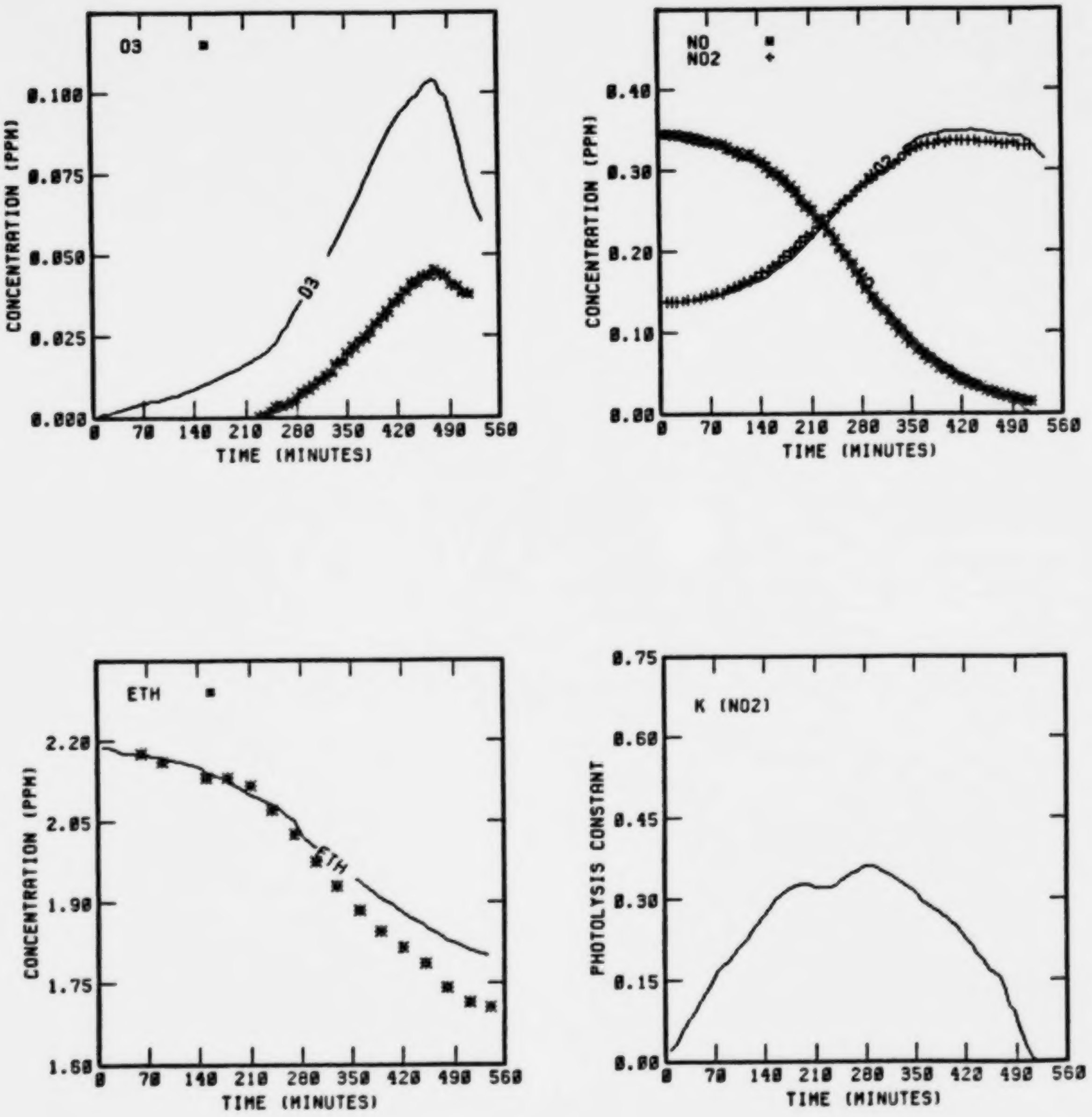

FIGURE 11. SIMULATION RESULTS FOR
UNCB 11078

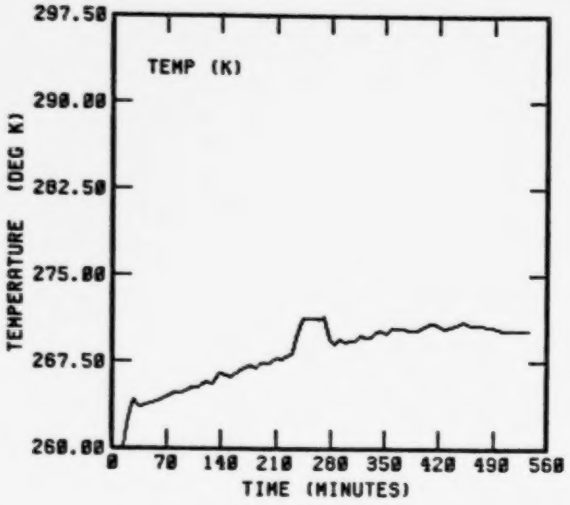

FIGURE 11. SIMULATION RESULTS FOR
UNCB 11078
(Concluded)

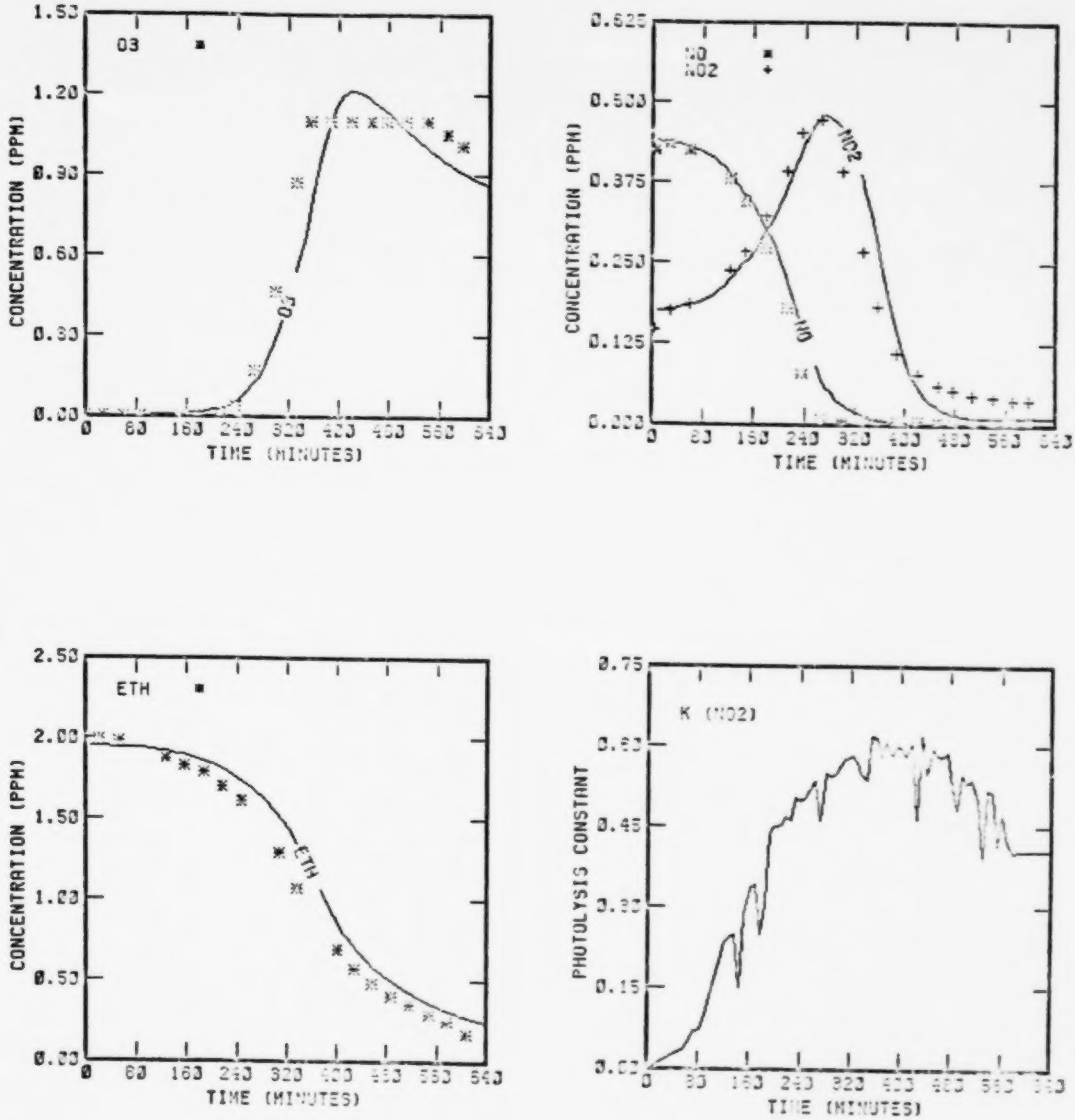

FIGURE 12. SIMULATION RESULTS FOR
UNCR 61673

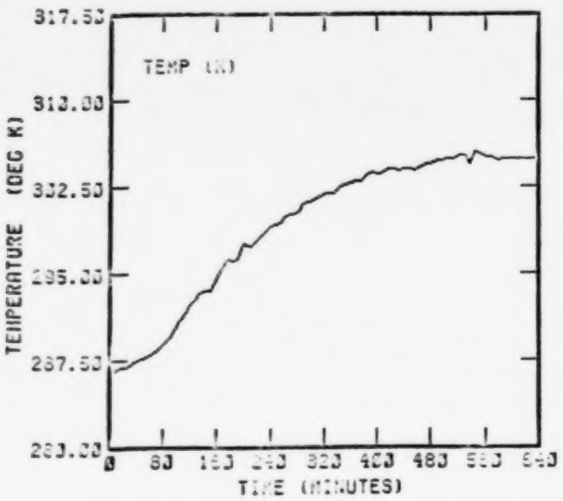

FIGURE 12. SIMULATION RESULTS FOR
UMCR 61678
(Concluded)

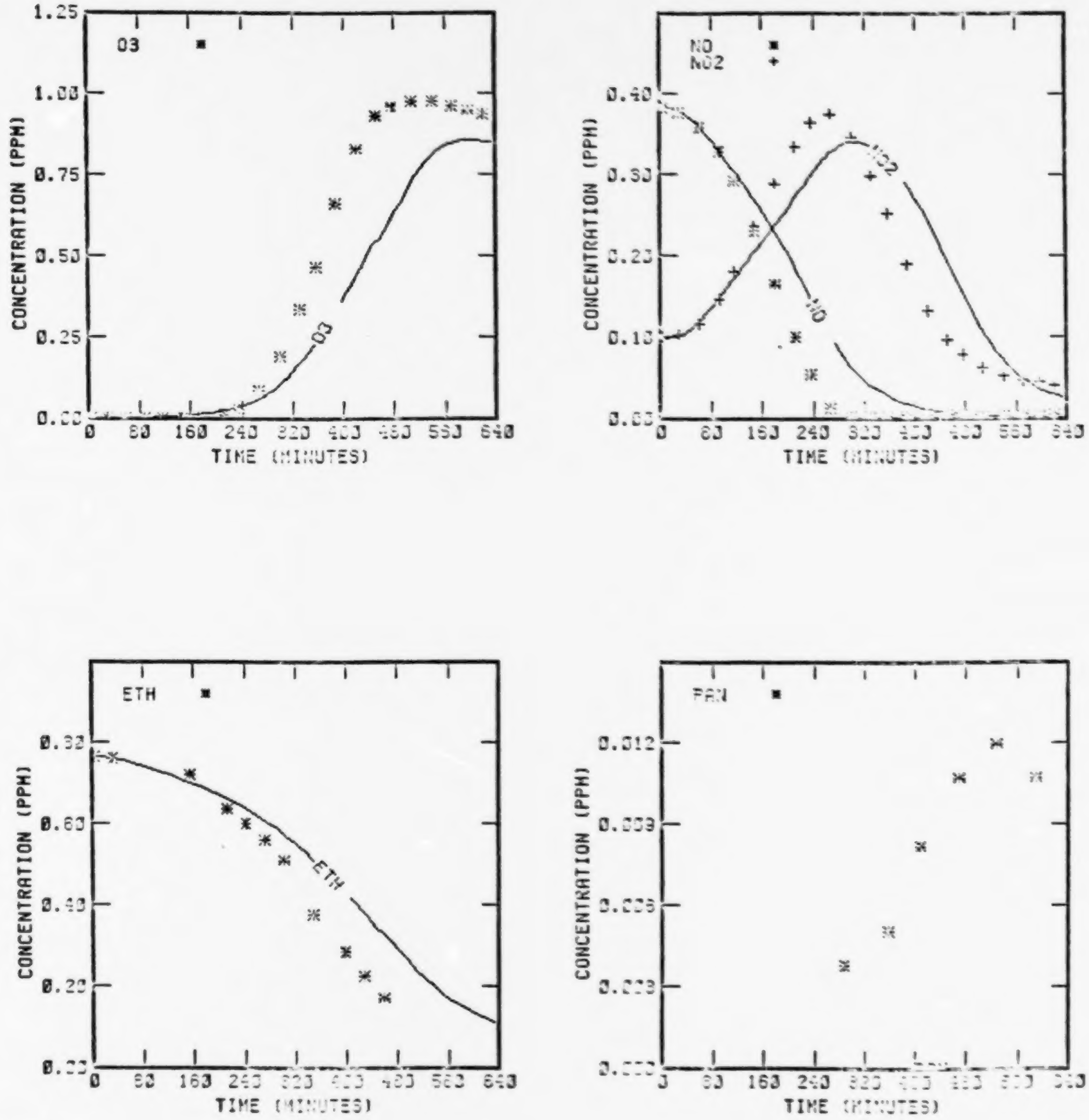

FIGURE 13. SIMULATION RESULTS FOR
UNCB E3073

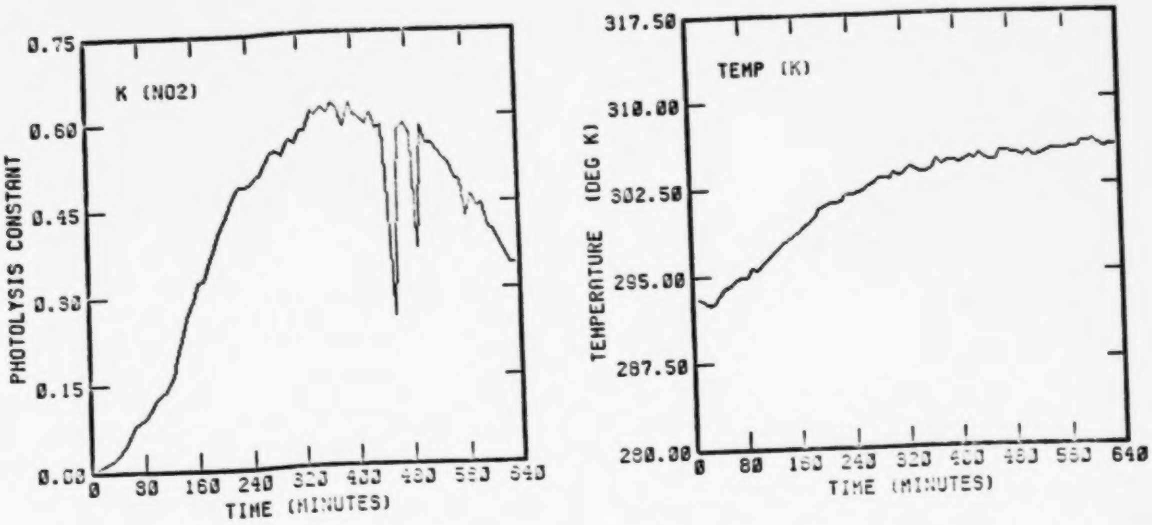

FIGURE 13. SIMULATION RESULTS FOR
UNCB 63078
(Concluded)

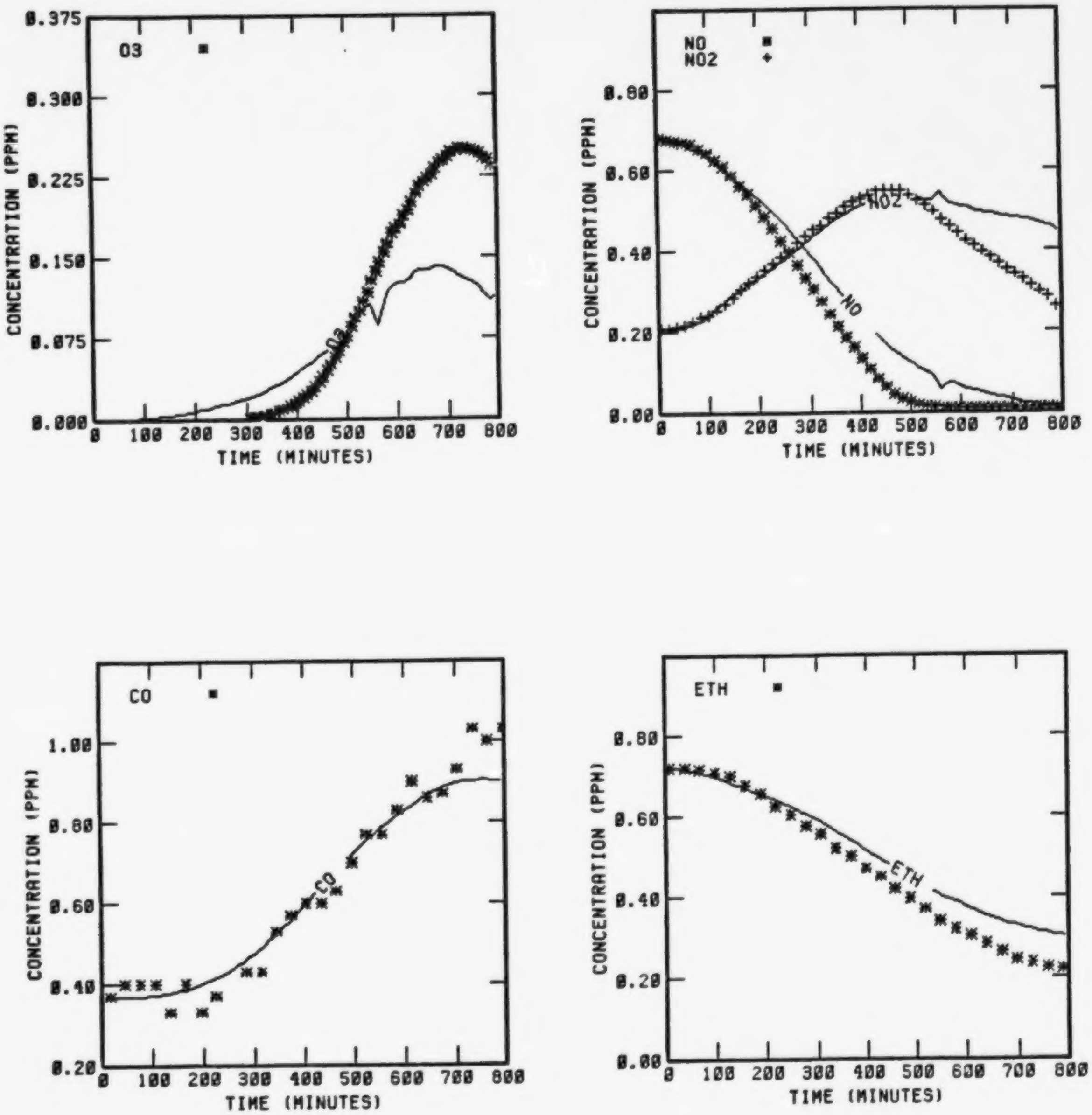

FIGURE 14. SIMULATION RESULTS FOR UNCR 70178

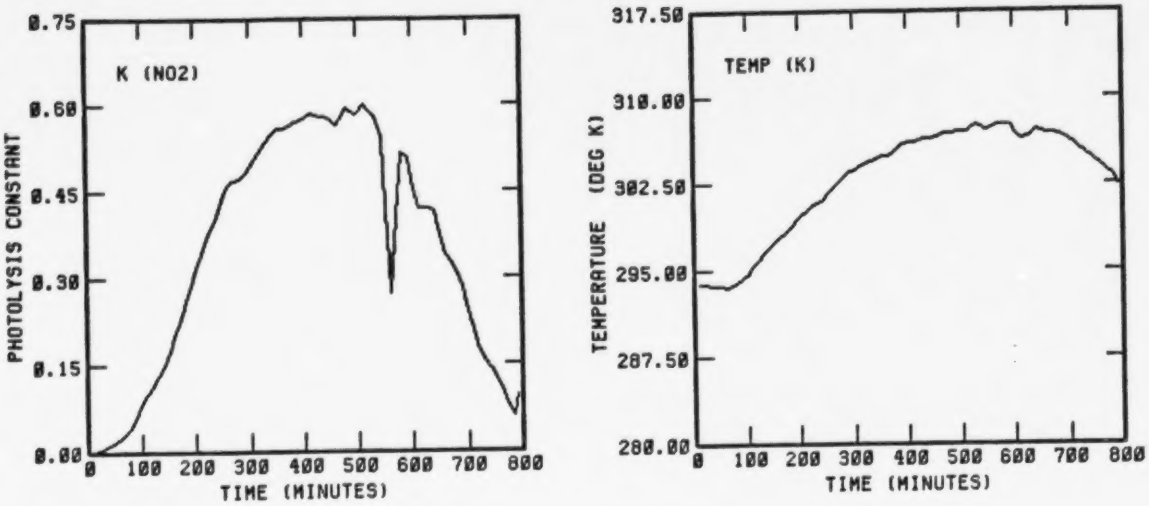

FIGURE 14. SIMULATION RESULTS FOR
UNCR 70178
(Concluded)

Reproduced from
best available copy.

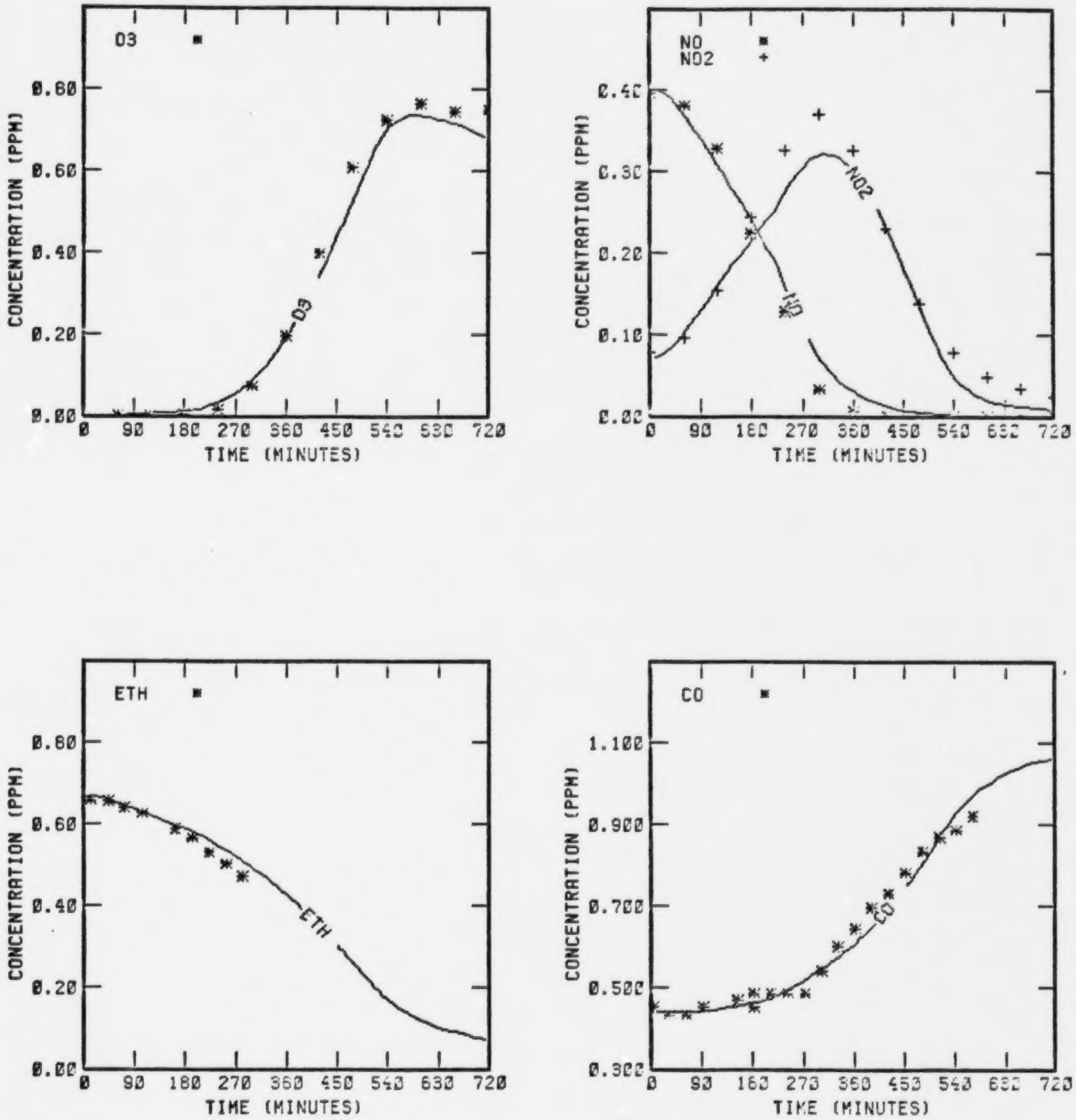

FIGURE 15. SIMULATION RESULTS FOR
UNCR 73078

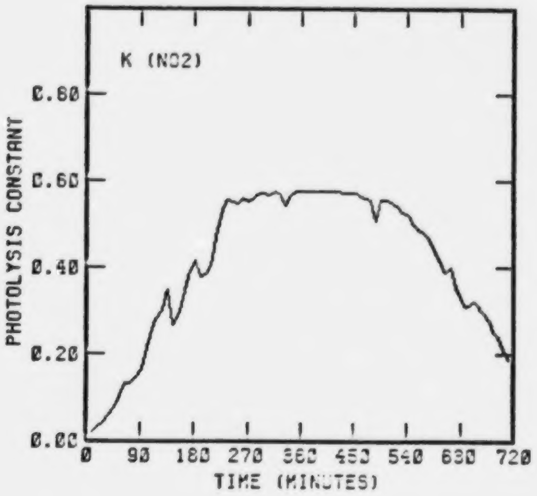

FIGURE 15. SIMULATION RESULTS FOR
UNCR 73078
(Concluded)

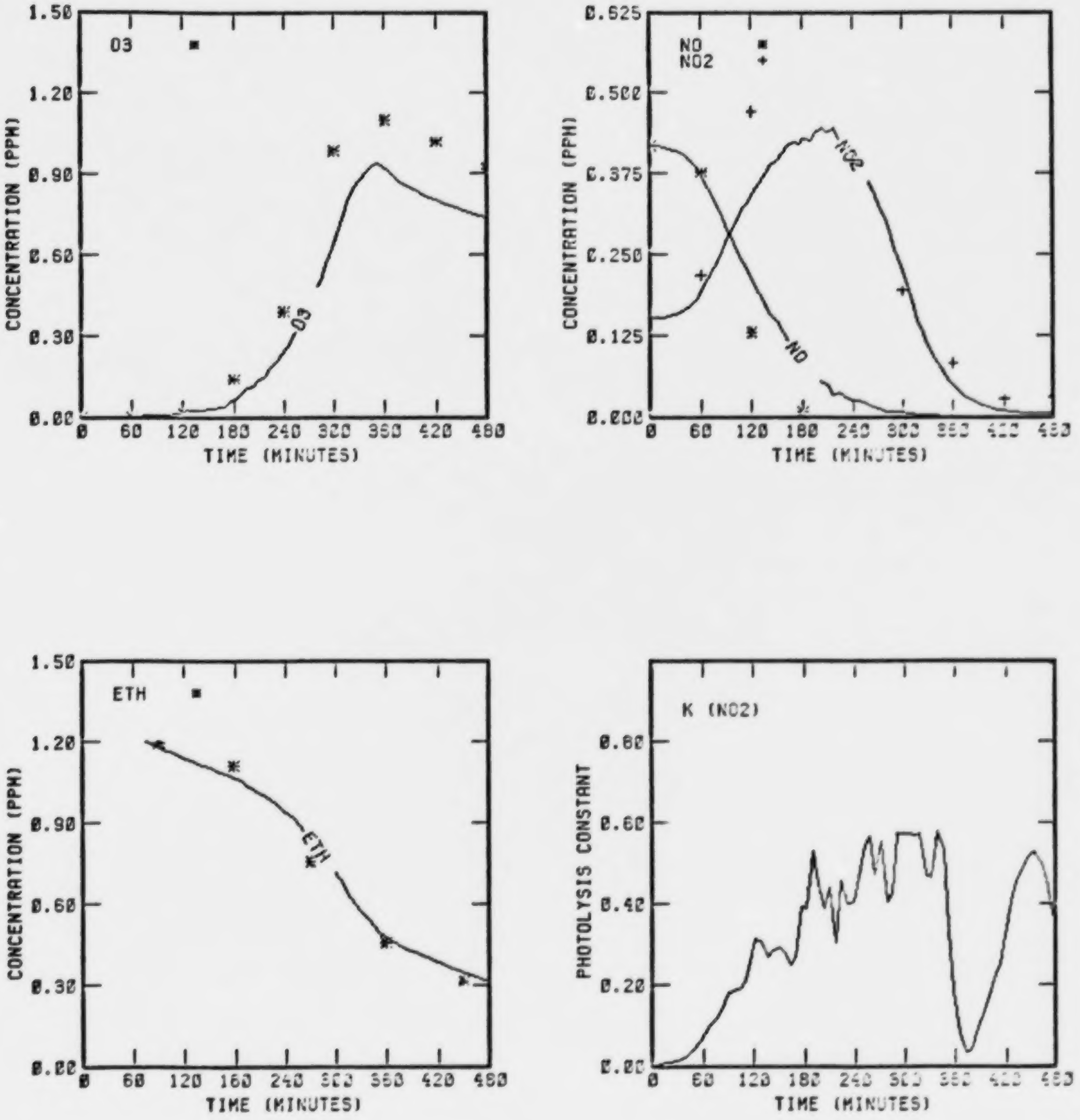

FIGURE 16. SIMULATION RESULTS FOR
UNCB 80678

Reproduced from
best available copy.

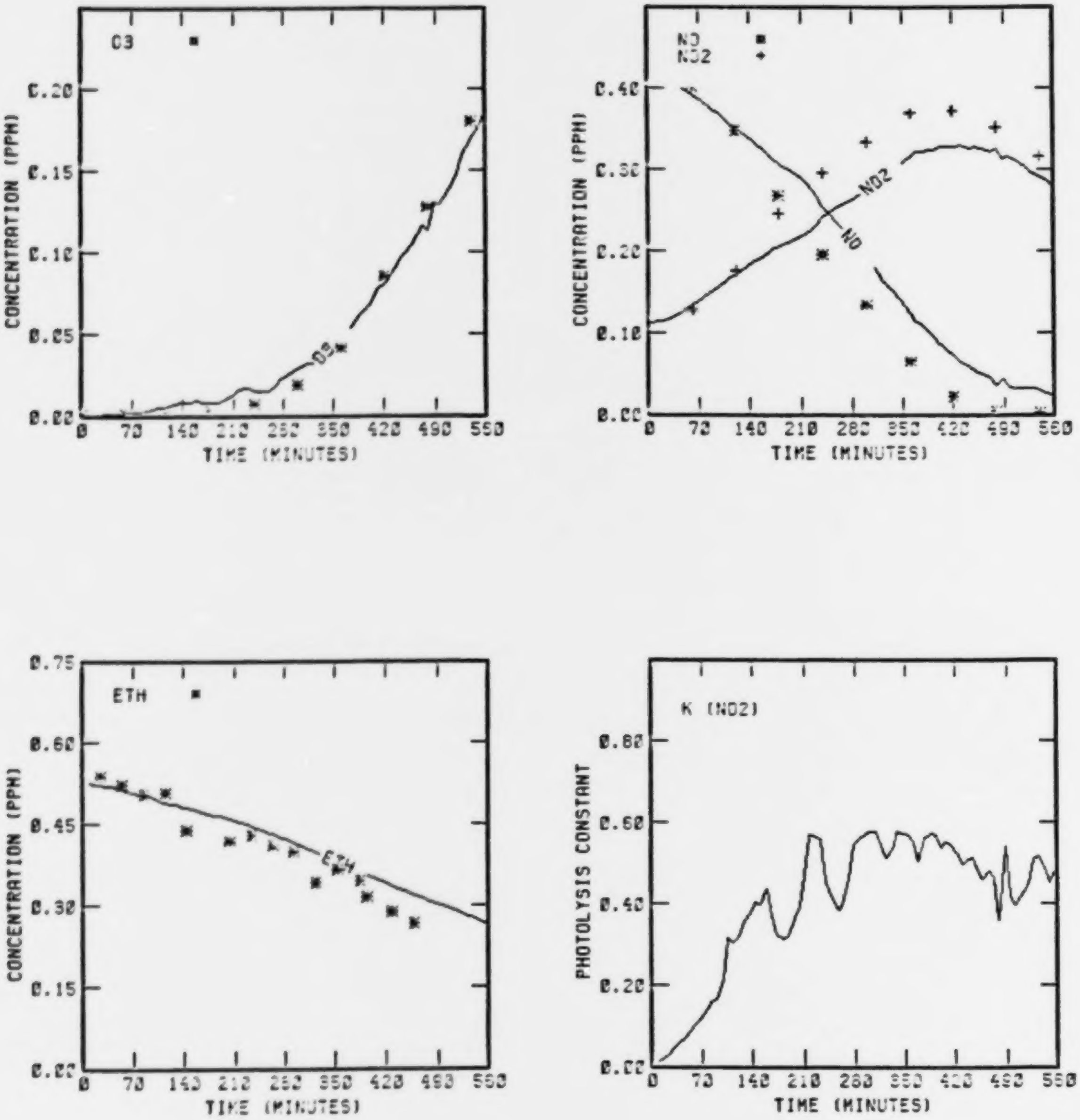

FIGURE 17. SIMULATION RESULTS FOR
UNCR 81078

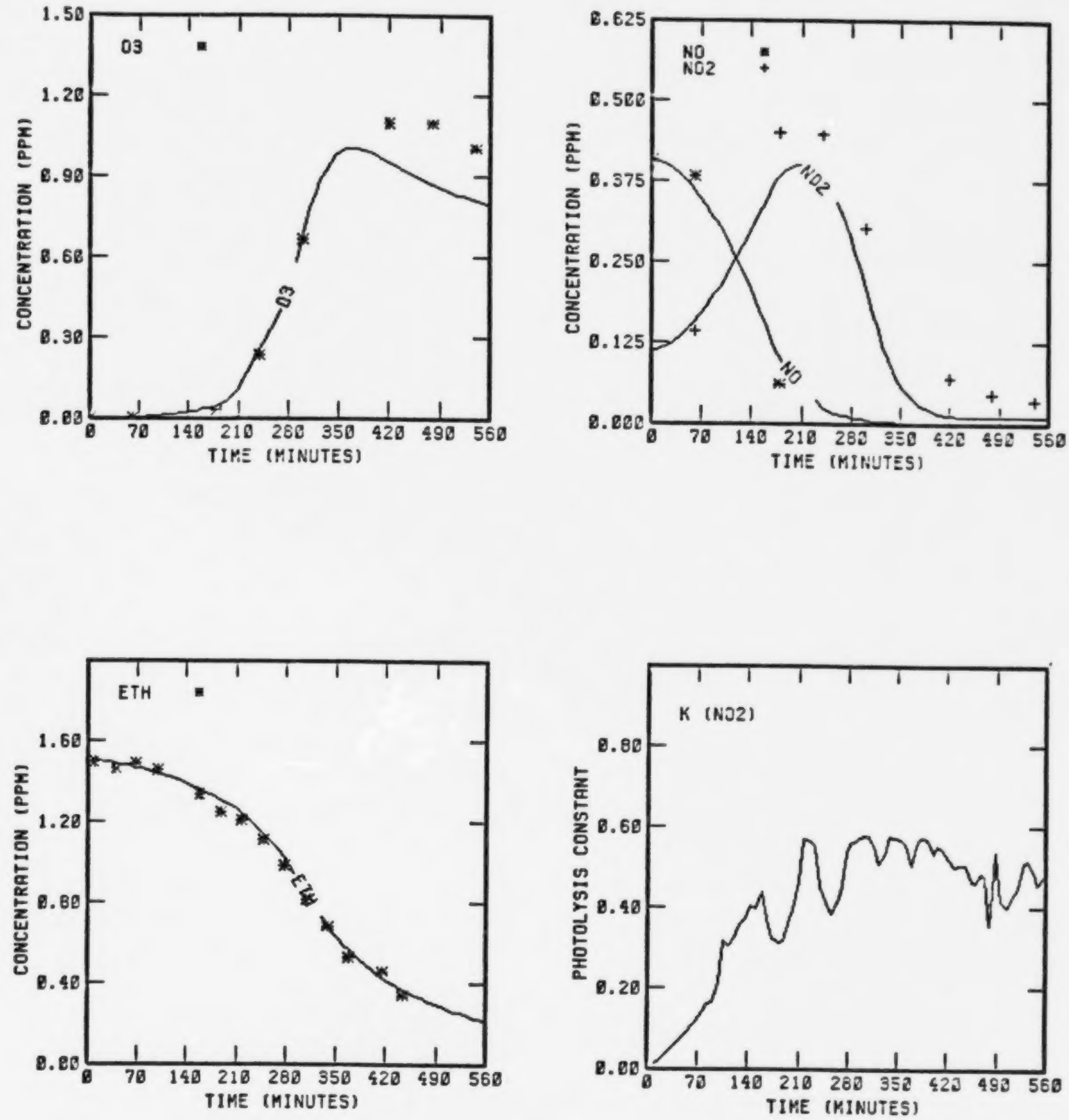

FIGURE 18. SIMULATION RESULTS FOR
UNCB 81078

Reproduced from best available copy.

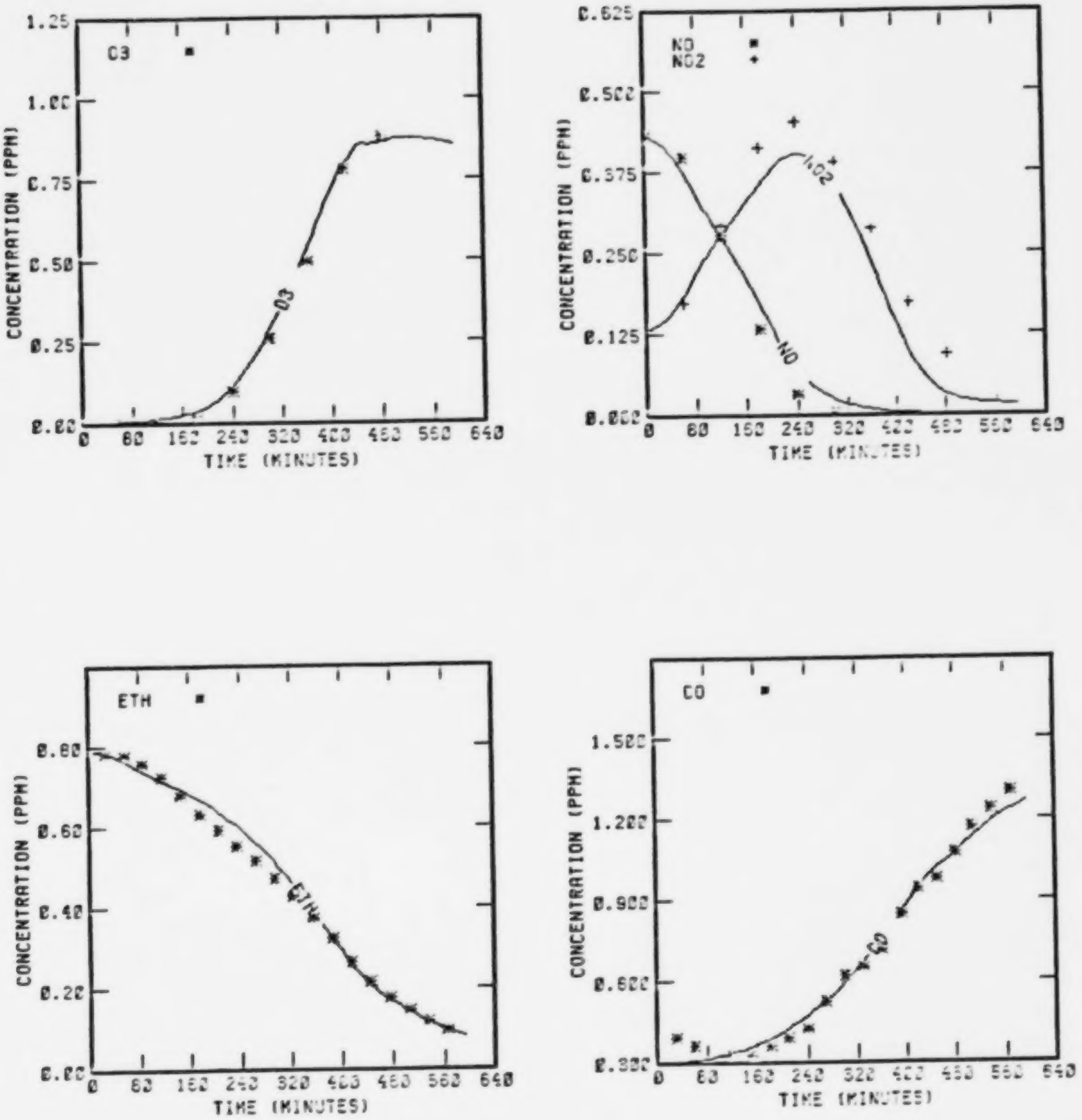

FIGURE 19. SIMULATION RESULTS FOR UNCB 81578

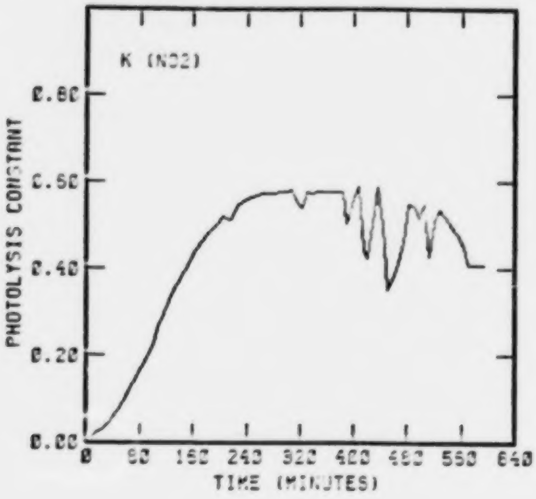

FIGURE 19. SIMULATION RESULTS FOR
UNCB 81578
(Concluded)

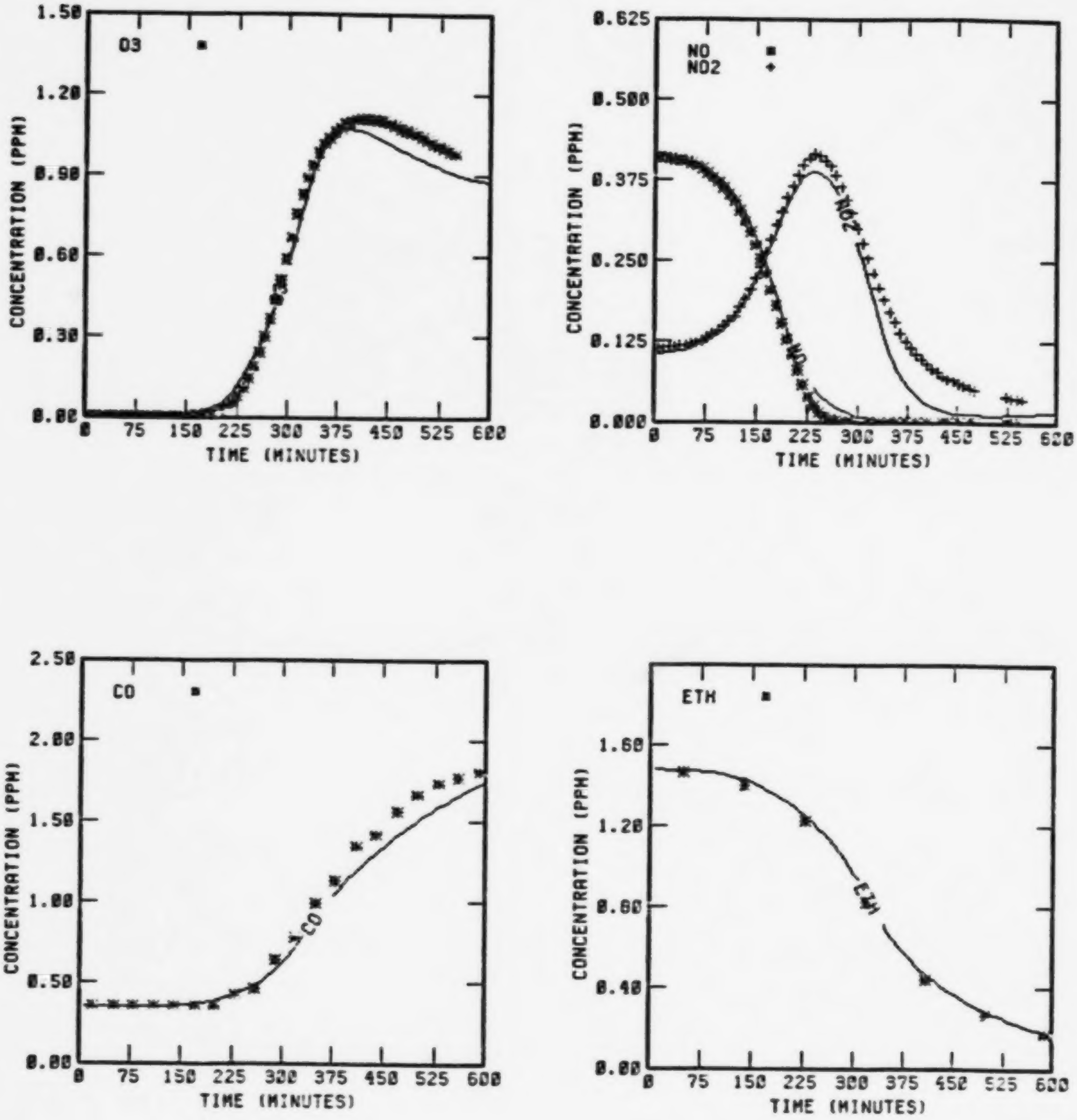

FIGURE 20. SIMULATION RESULTS FOR
UNCR 82870

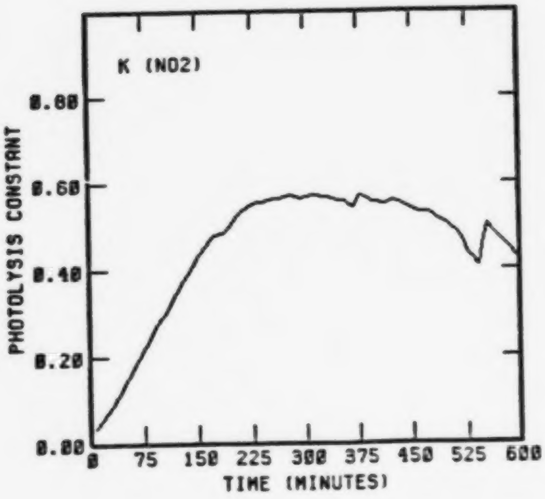

FIGURE 20. SIMULATION RESULTS FOR
UNCR 82378
(Concluded)

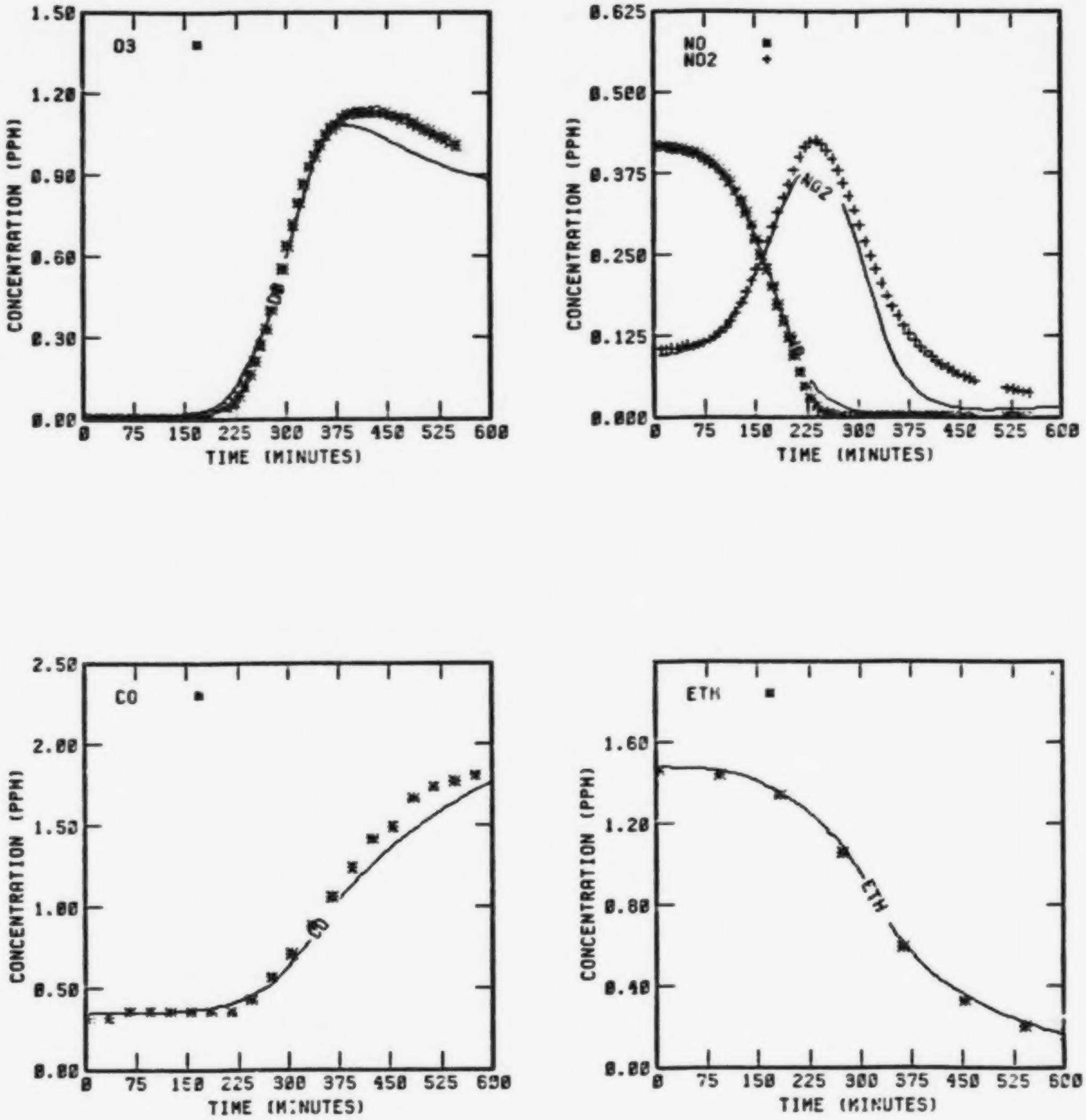

FIGURE 21. SIMULATION RESULTS FOR
UNCB 82378

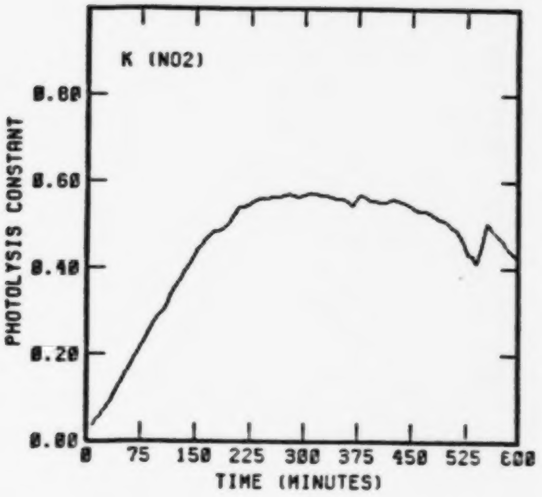

FIGURE 21. SIMULATION RESULTS FOR
UNCB 82378
(Concluded)

Reproduced from
best available copy.

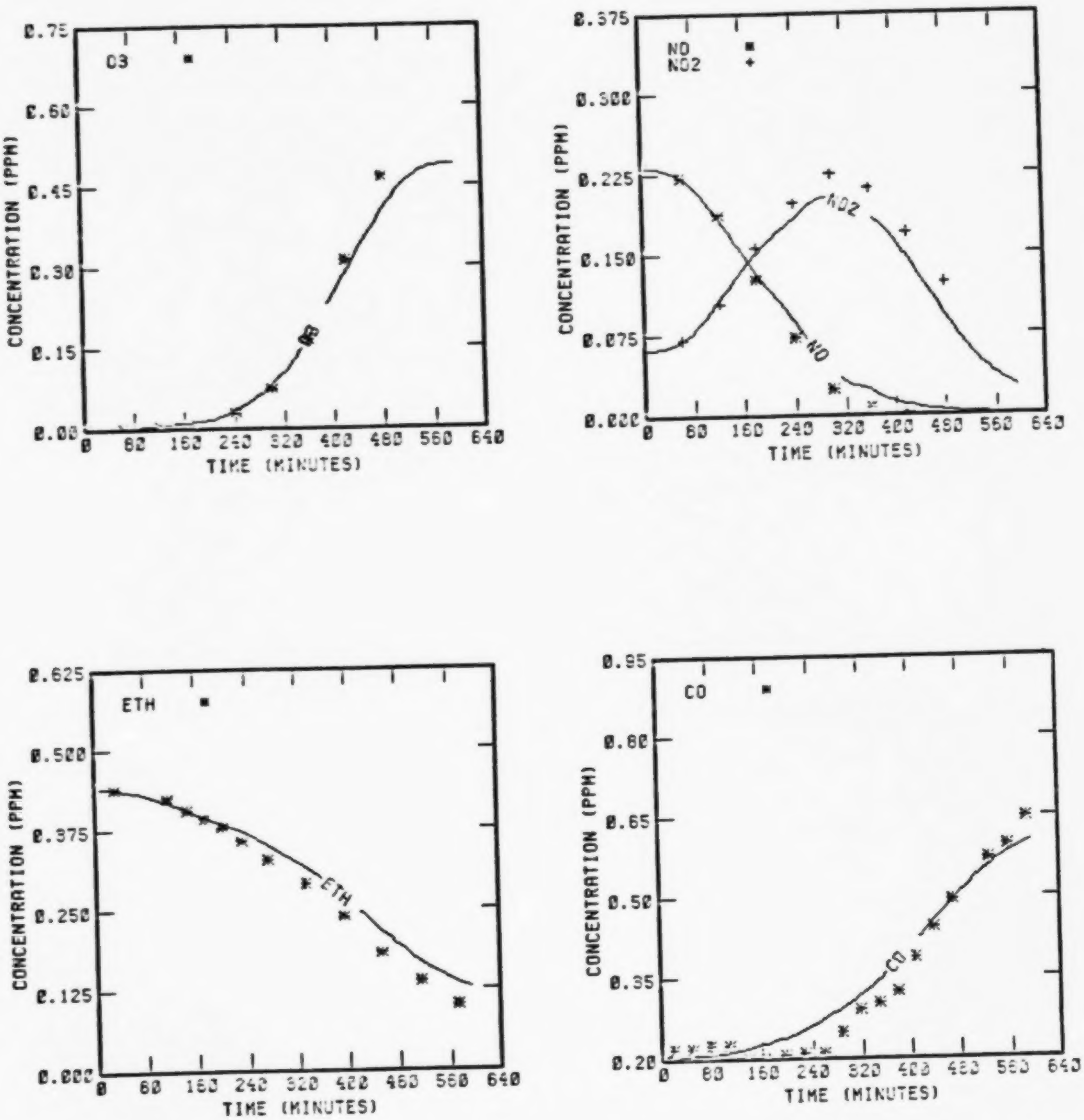

FIGURE 22. SIMULATION RESULTS FOR
UNCB 9147B

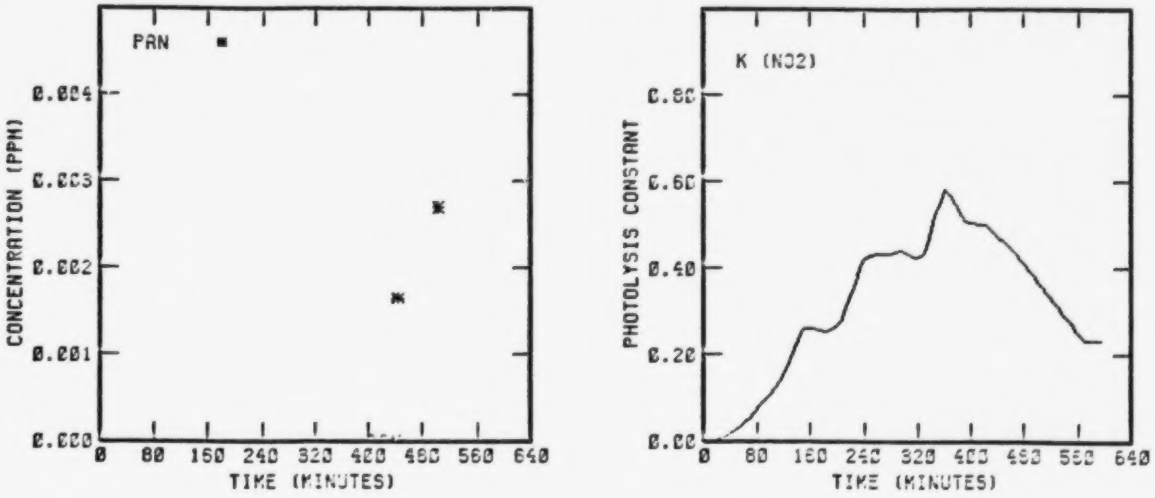

FIGURE 22. SIMULATION RESULTS FOR
UNCB 91478
(Concluded)

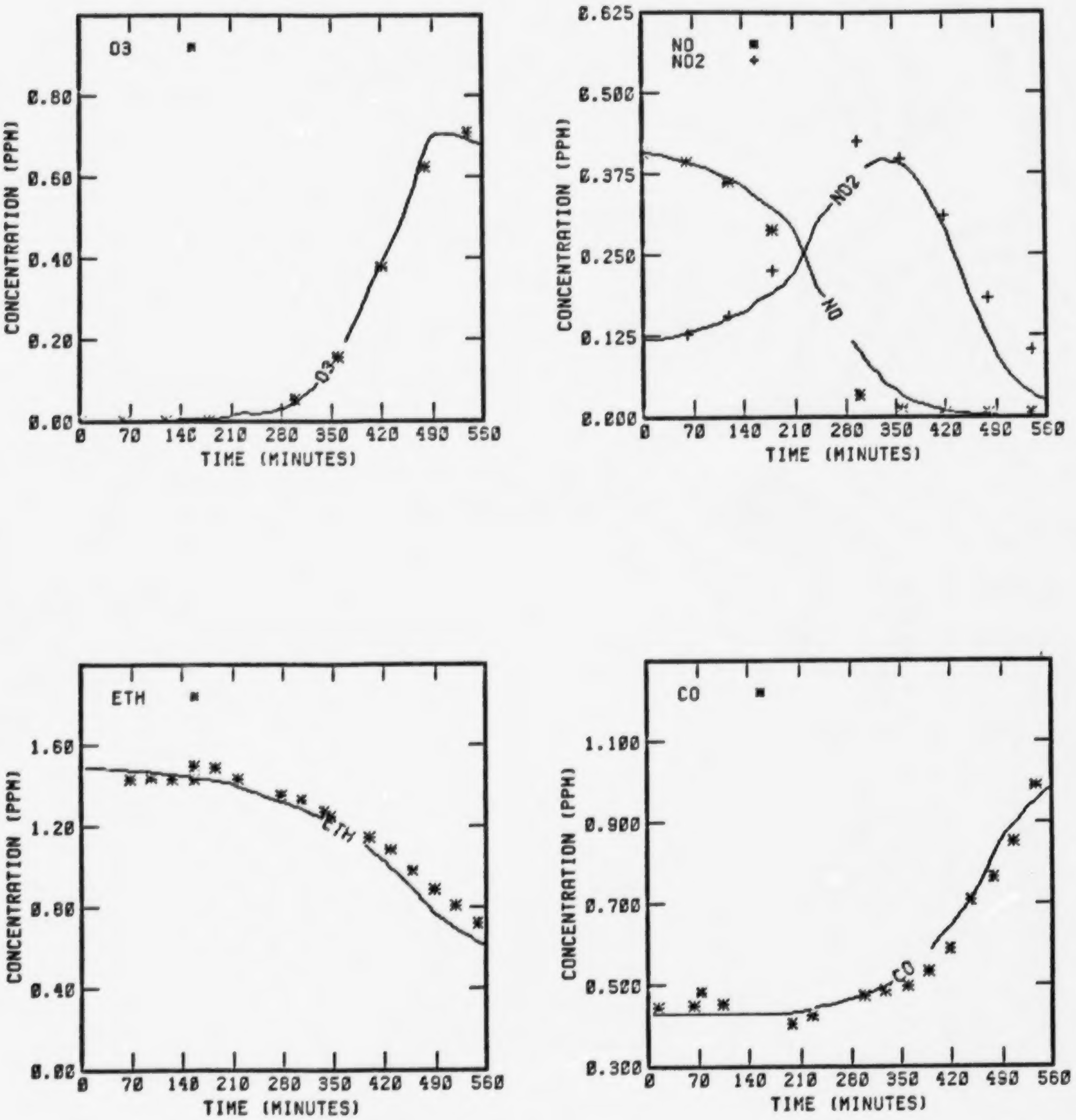

FIGURE 23. SIMULATION RESULTS FOR
UNCR 91578

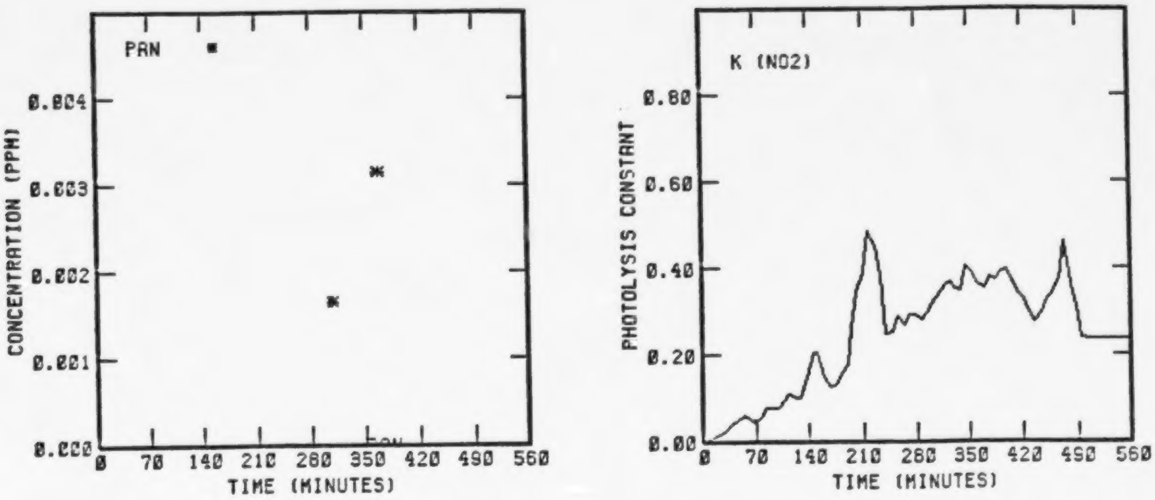

FIGURE 23. SIMULATION RESULTS FOR
UNCR 91578
(Concluded)

Reproduced from
best available copy.

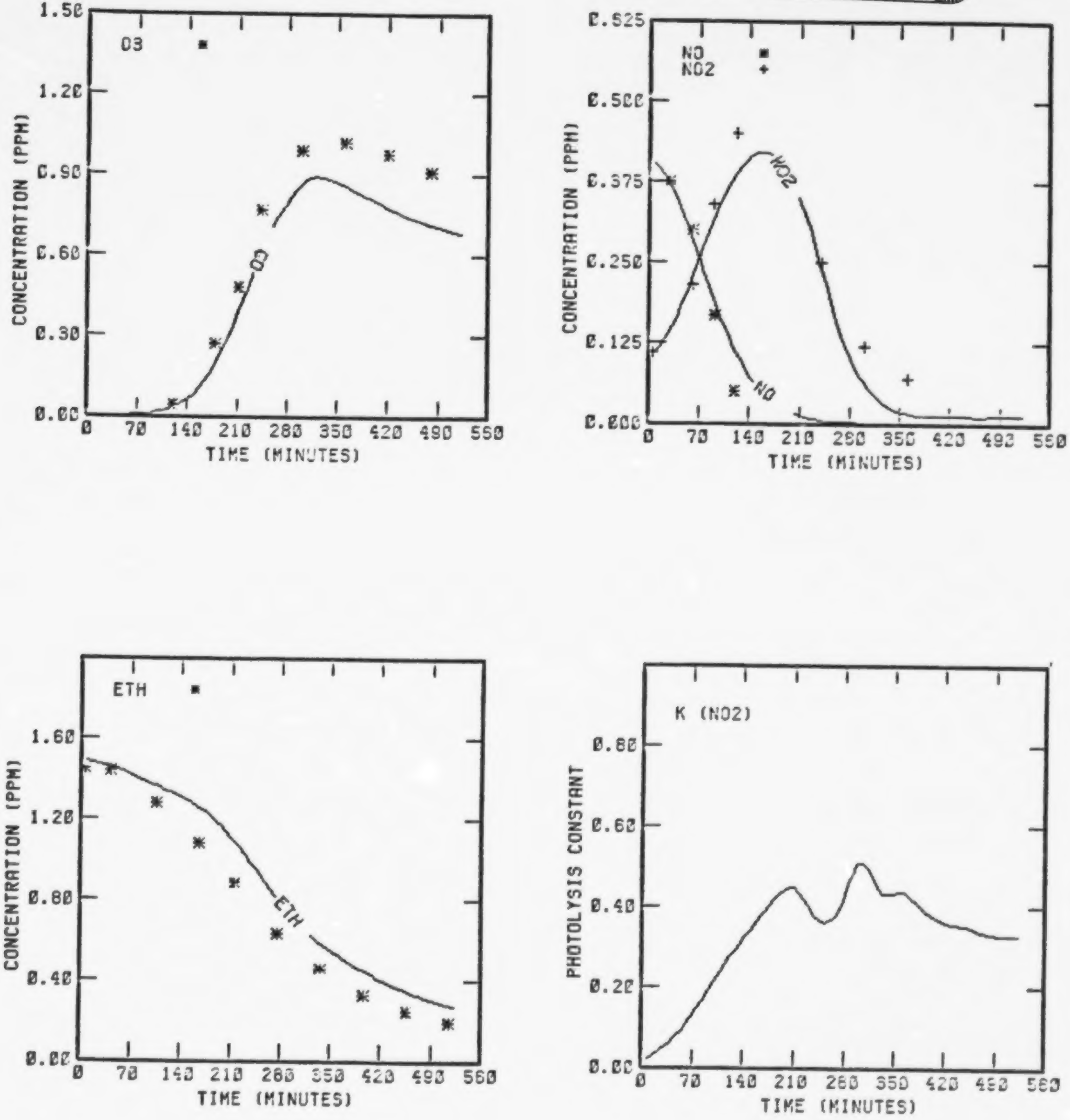

FIGURE 24. SIMULATION RESULTS FOR
UNCR 91678

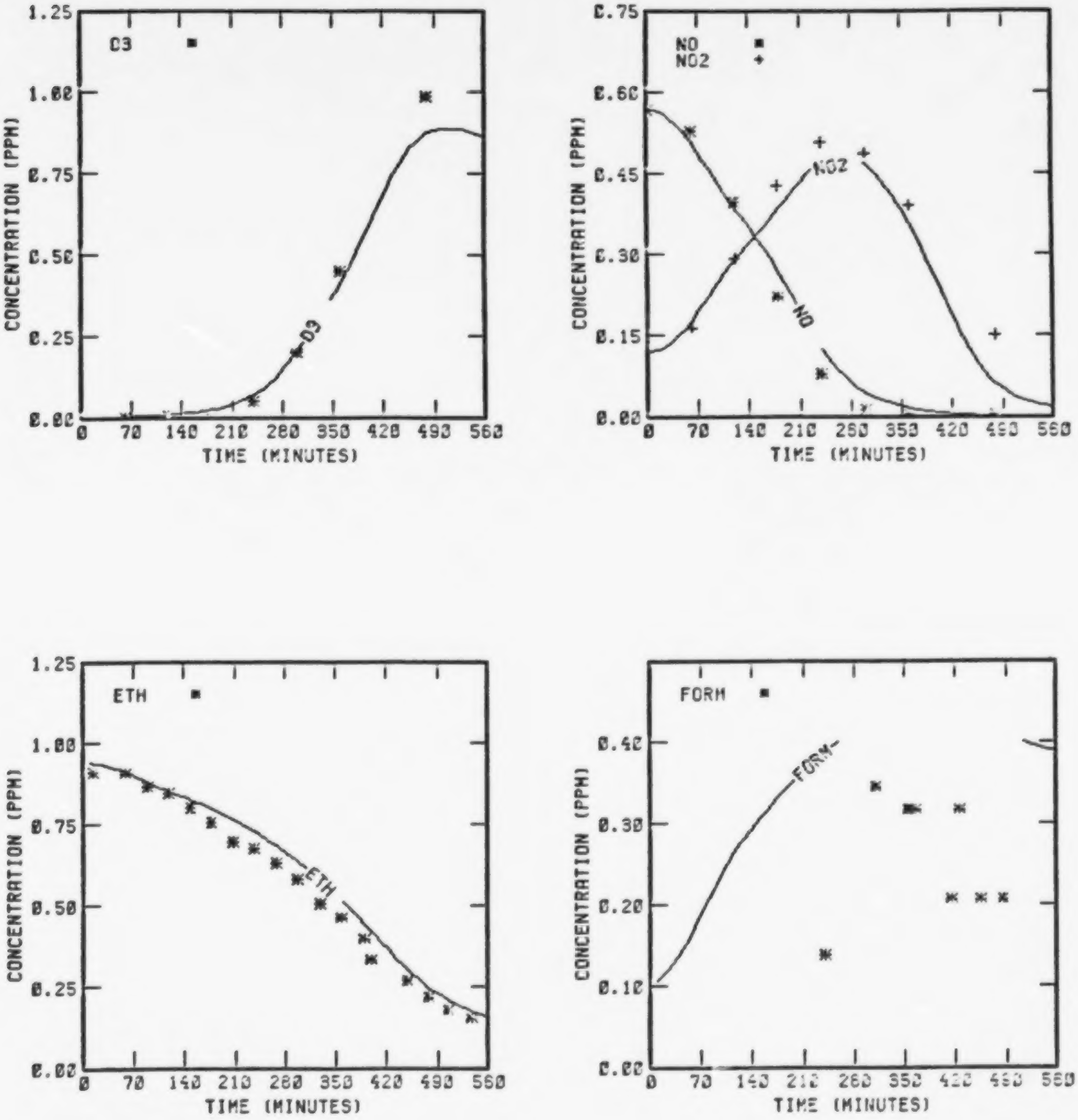

FIGURE 24. SIMULATION RESULTS FOR
UNCR 91978
(Concluded)

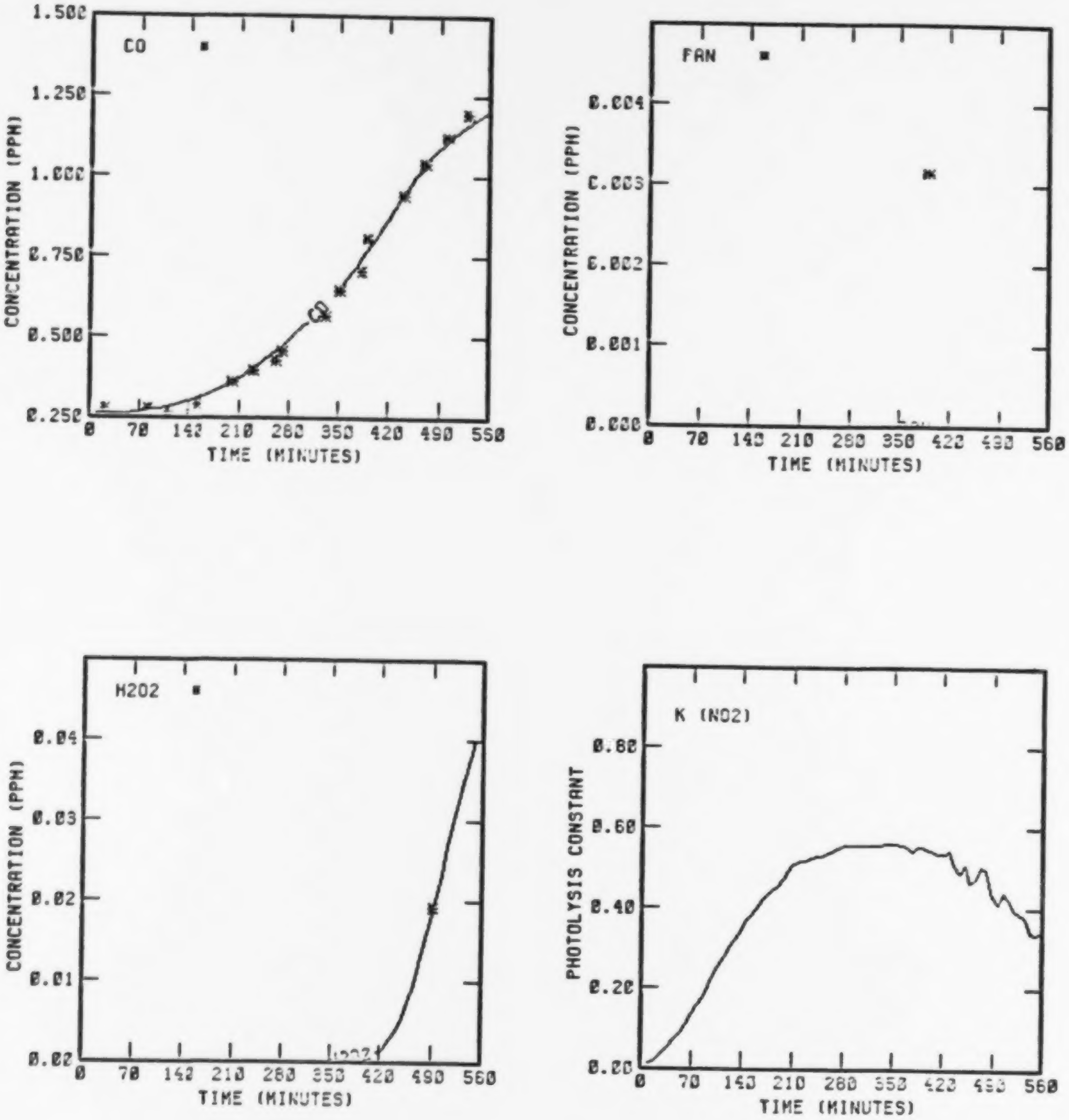

FIGURE 25. SIMULATION RESULTS FOR
UNCR 91978

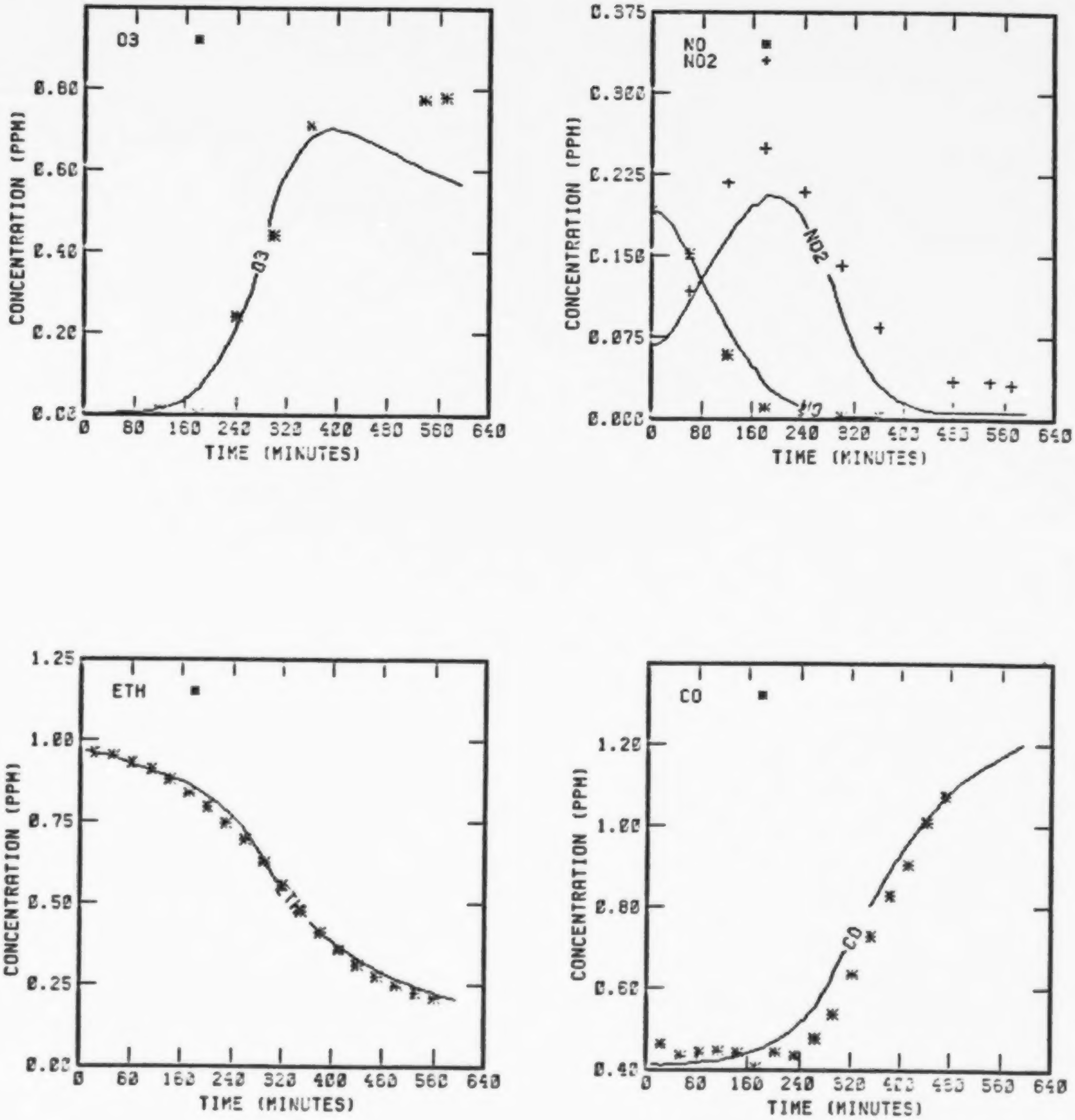

FIGURE 26. SIMULATION RESULTS FOR
UNCR 92178

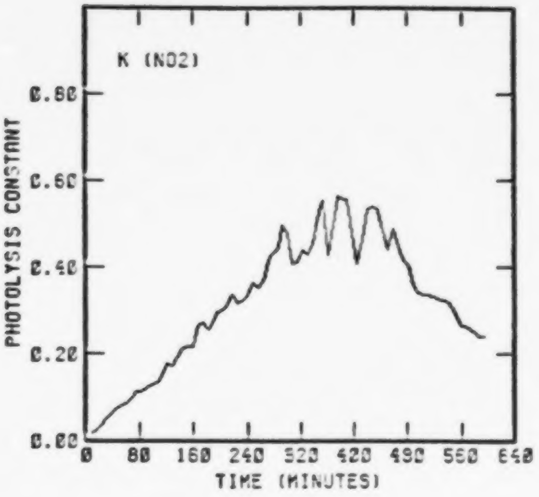

FIGURE 26. SIMULATION RESULTS FOR
UNCR 9217B
(Concluded)

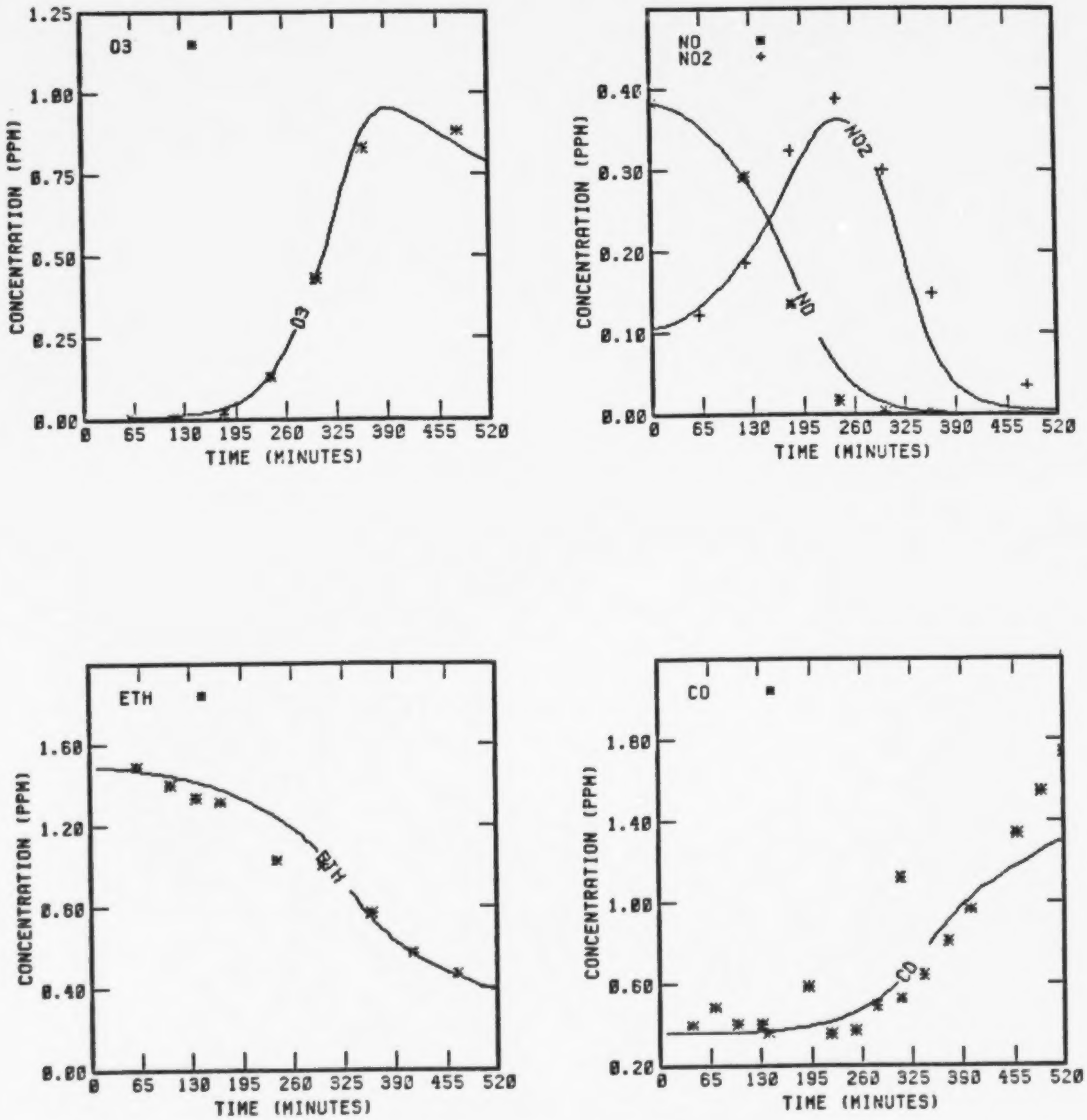

FIGURE 27. SIMULATION RESULTS FOR UNCB 100278

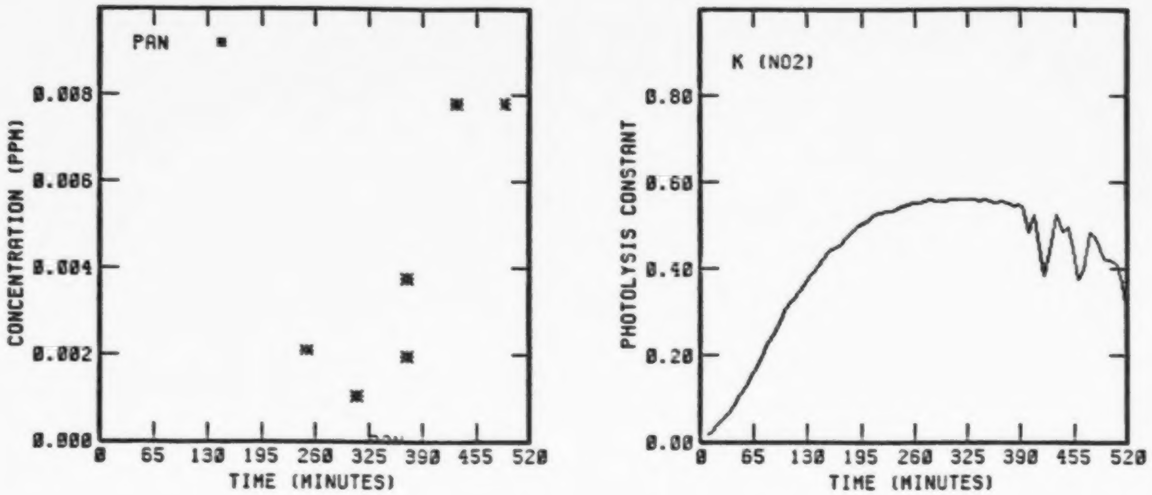

FIGURE 27. SIMULATION RESULTS FOR
UNCB 100278
(Concluded)

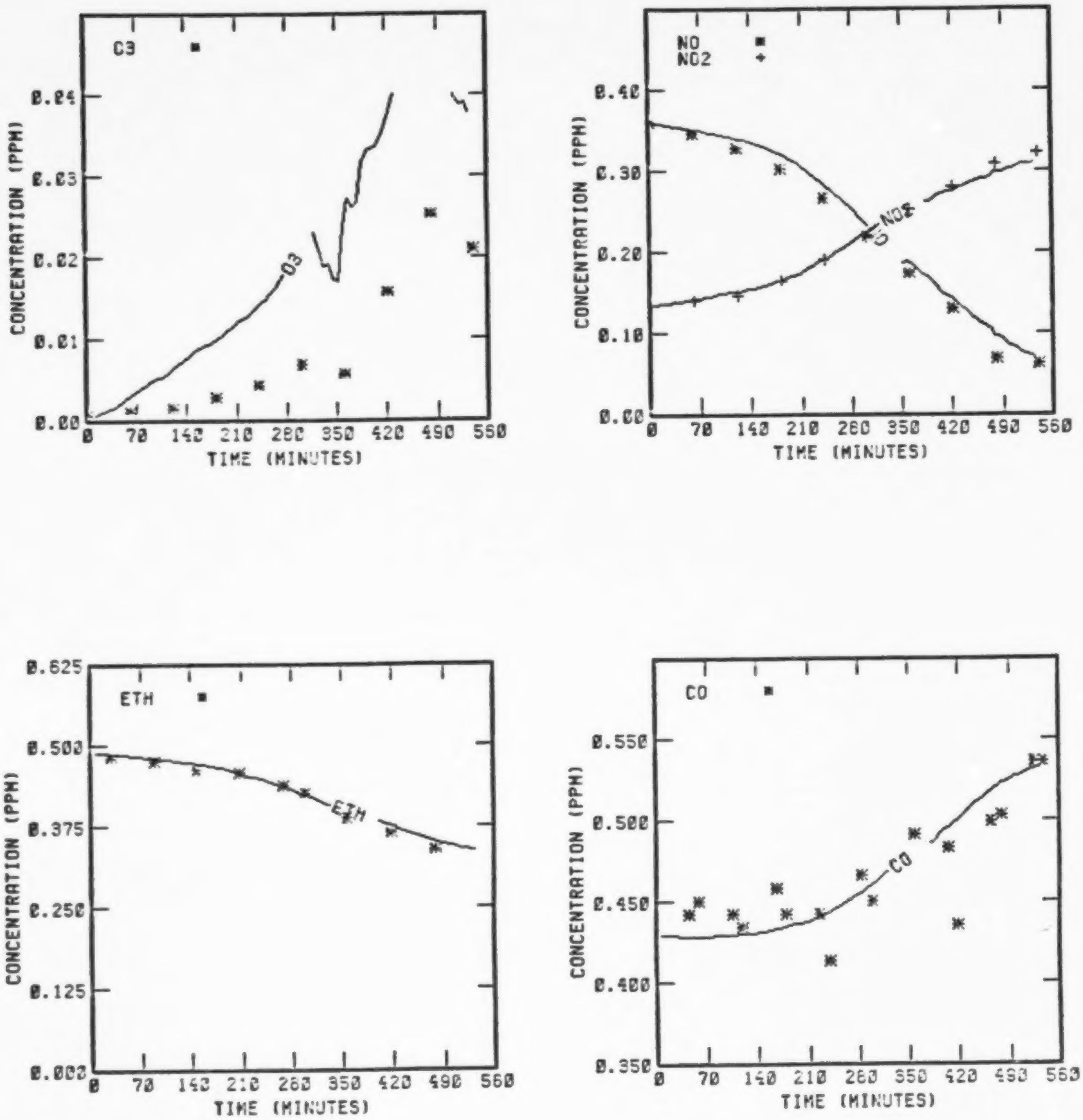

FIGURE 28. SIMULATION RESULTS FOR UNCR 100378

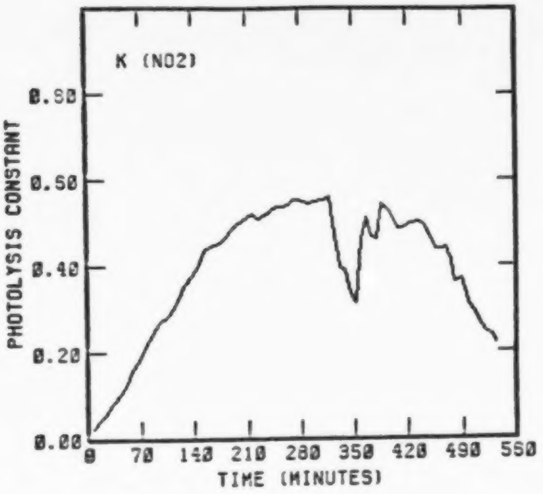

FIGURE 28. SIMULATION RESULTS FOR
UNCR 100378
(Concluded)

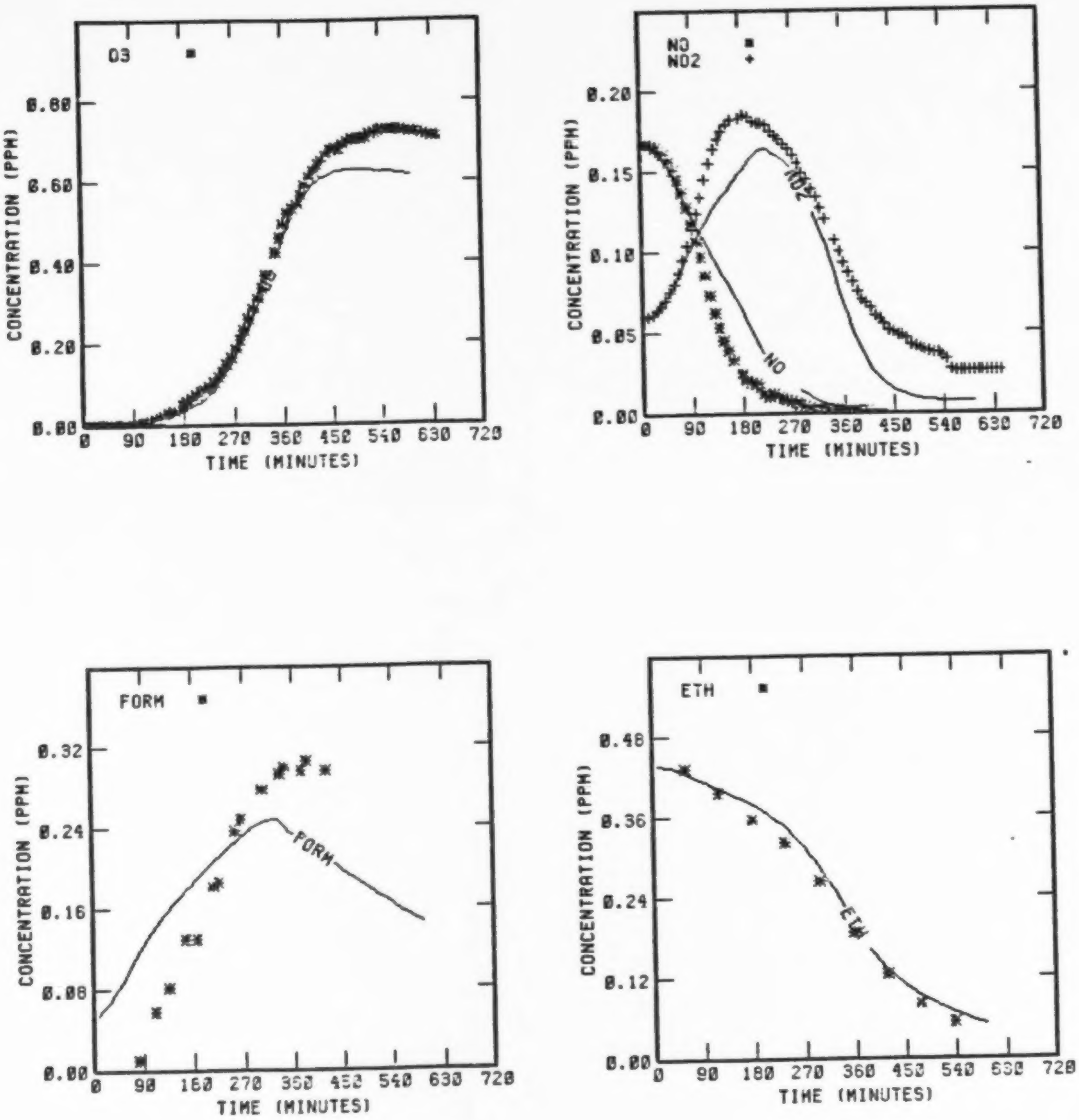

FIGURE 29. SIMULATION RESULTS FOR
UNCR 80479

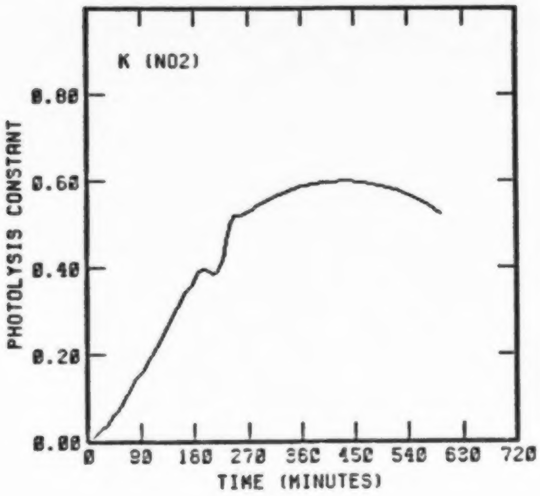

FIGURE 29. SIMULATION RESULTS FOR
UNCR 80479
(Concluded)

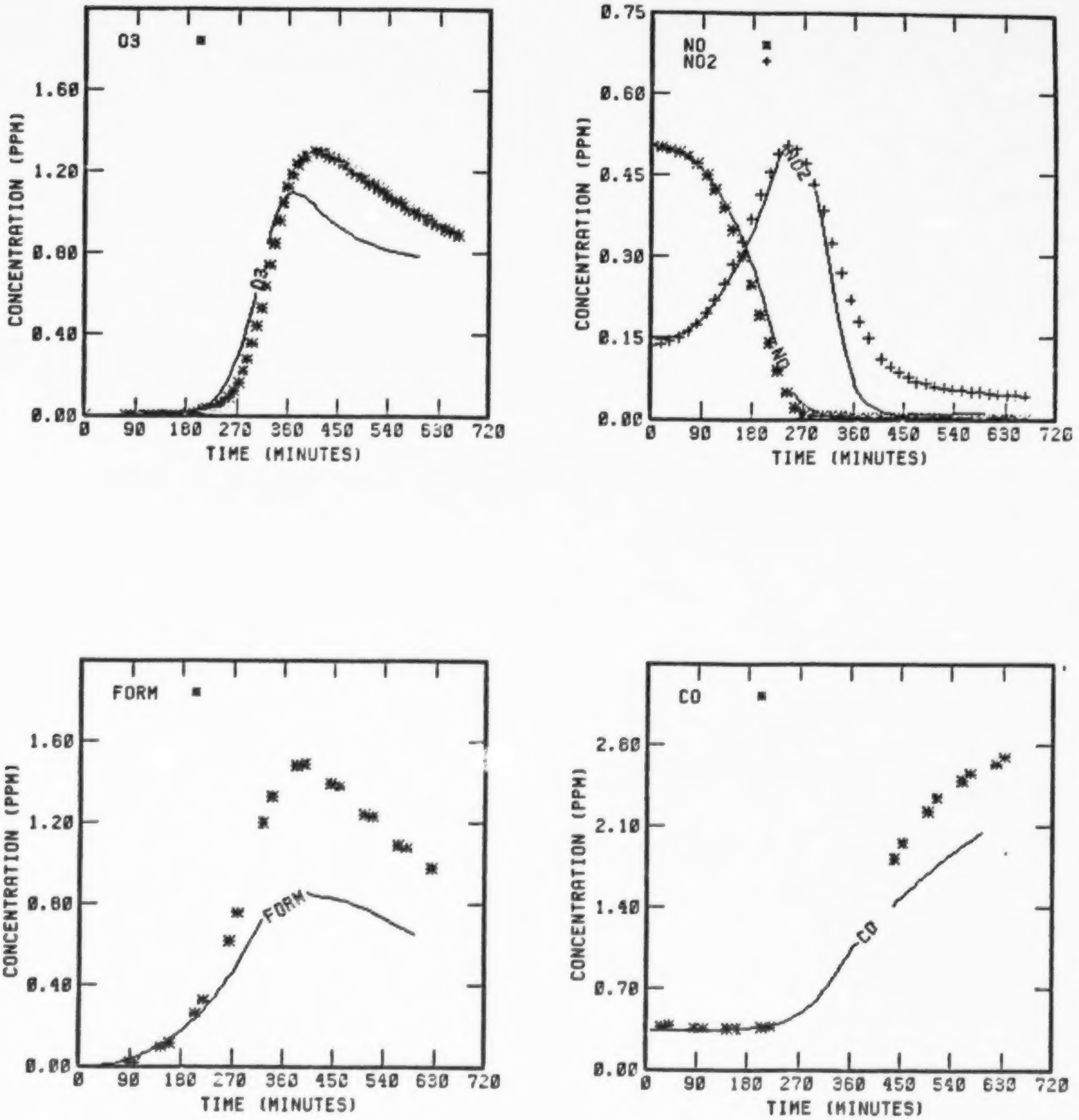

FIGURE 30. SIMULATION RESULTS FOR
UNCR 80579

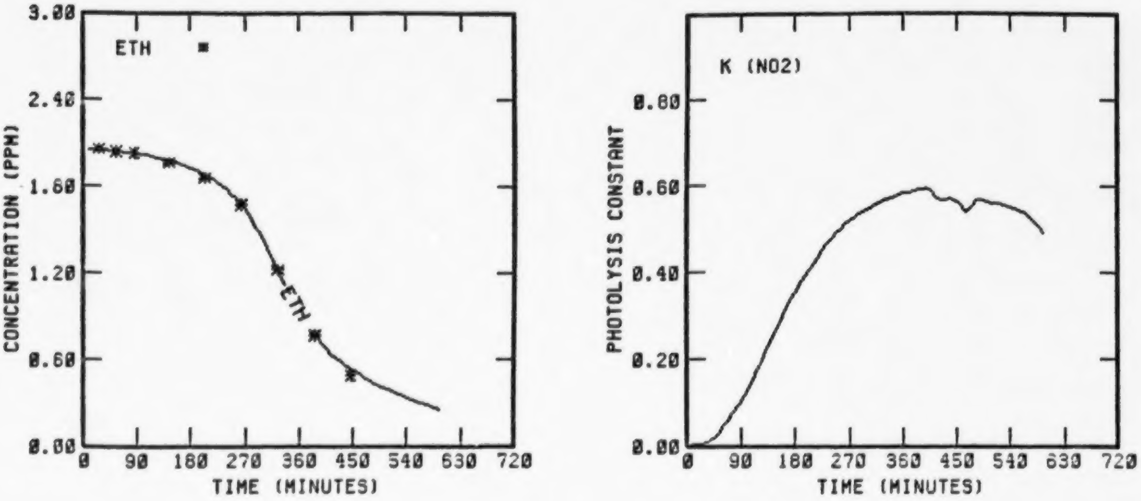

FIGURE 30. SIMULATION RESULTS FOR
UNCR 80579
(Concluded)

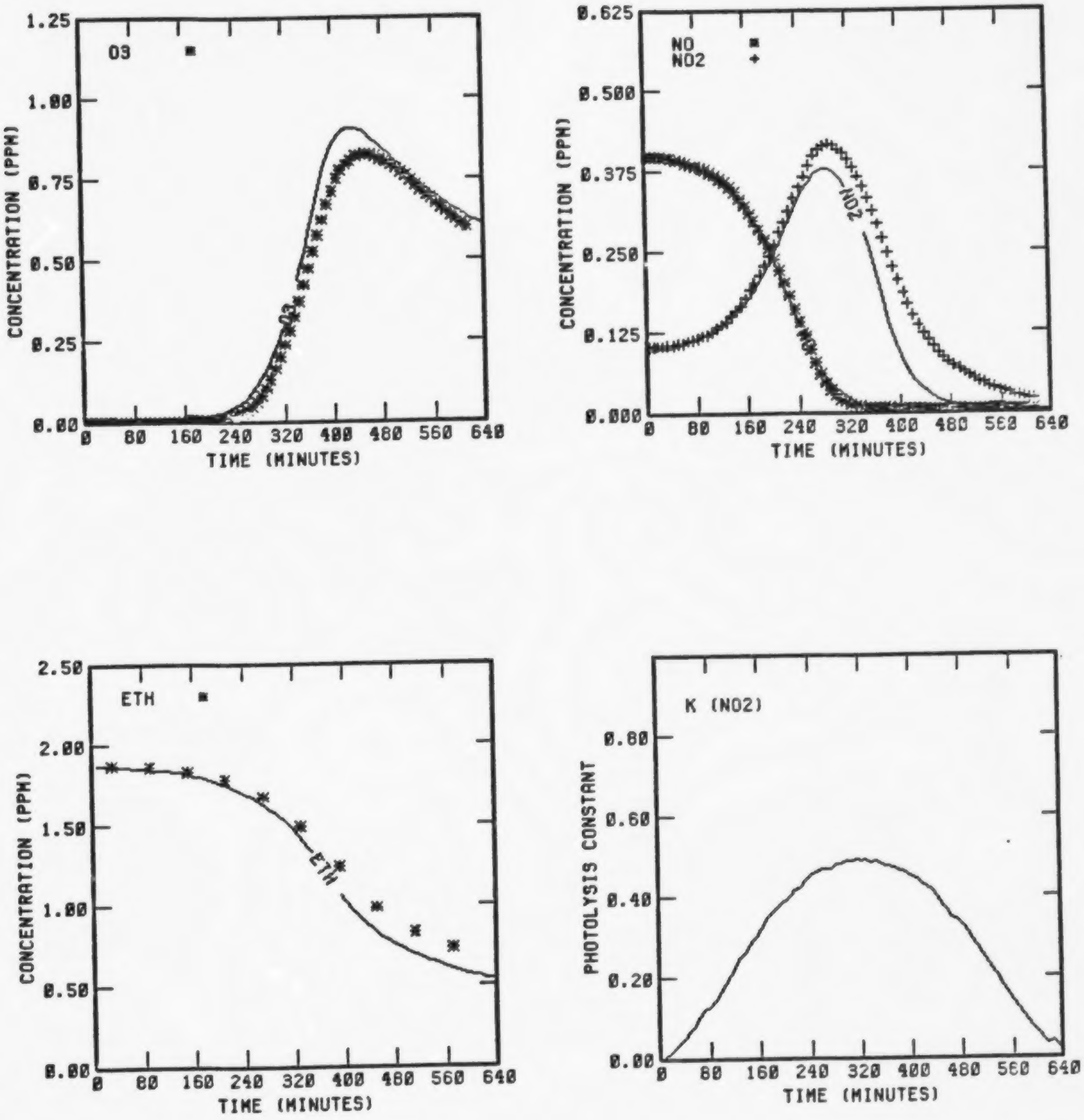

FIGURE 31. SIMULATION RESULTS FOR UNCR 103179

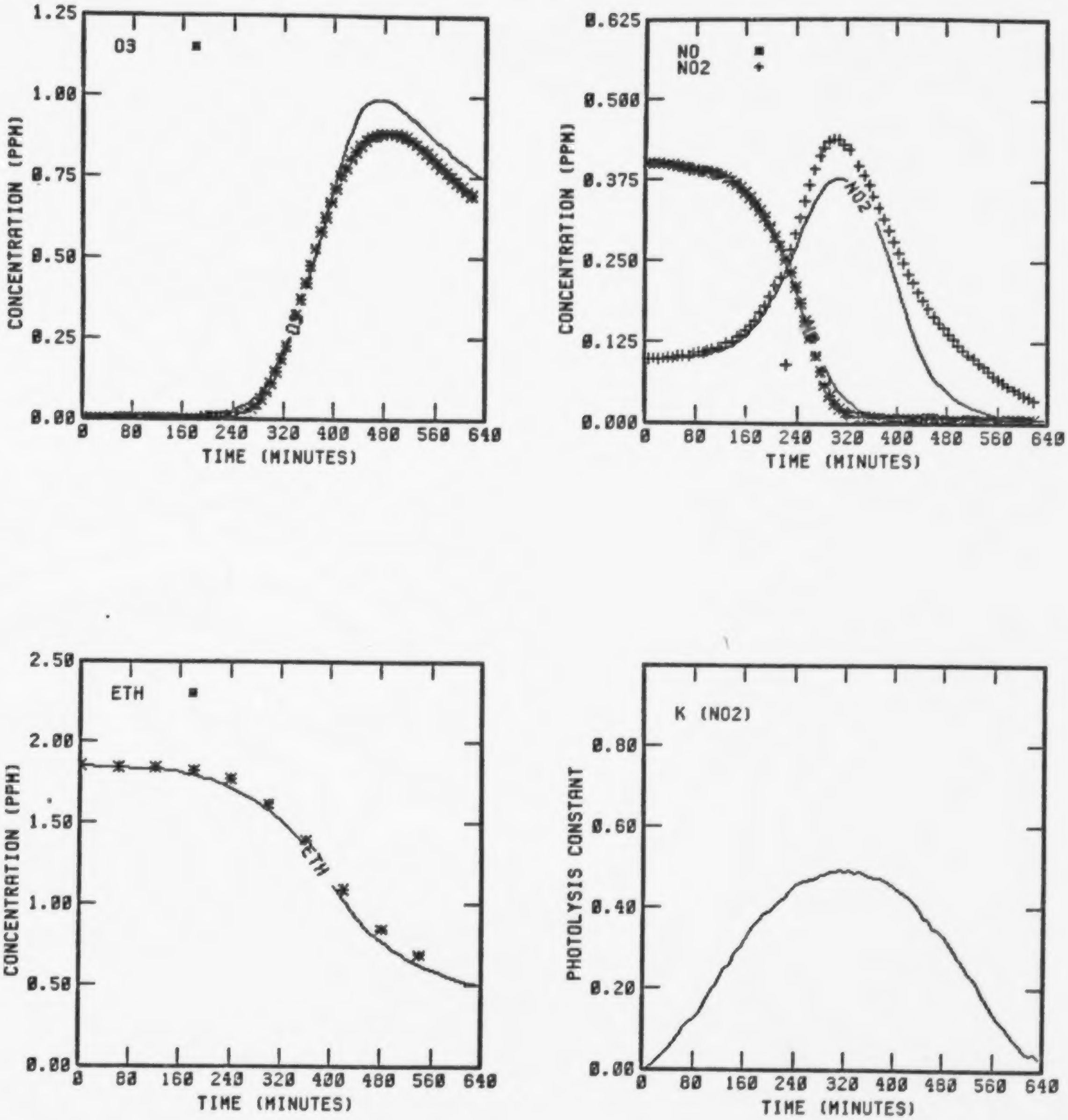

FIGURE 32. SIMULATION RESULTS FOR
UNCB 103179

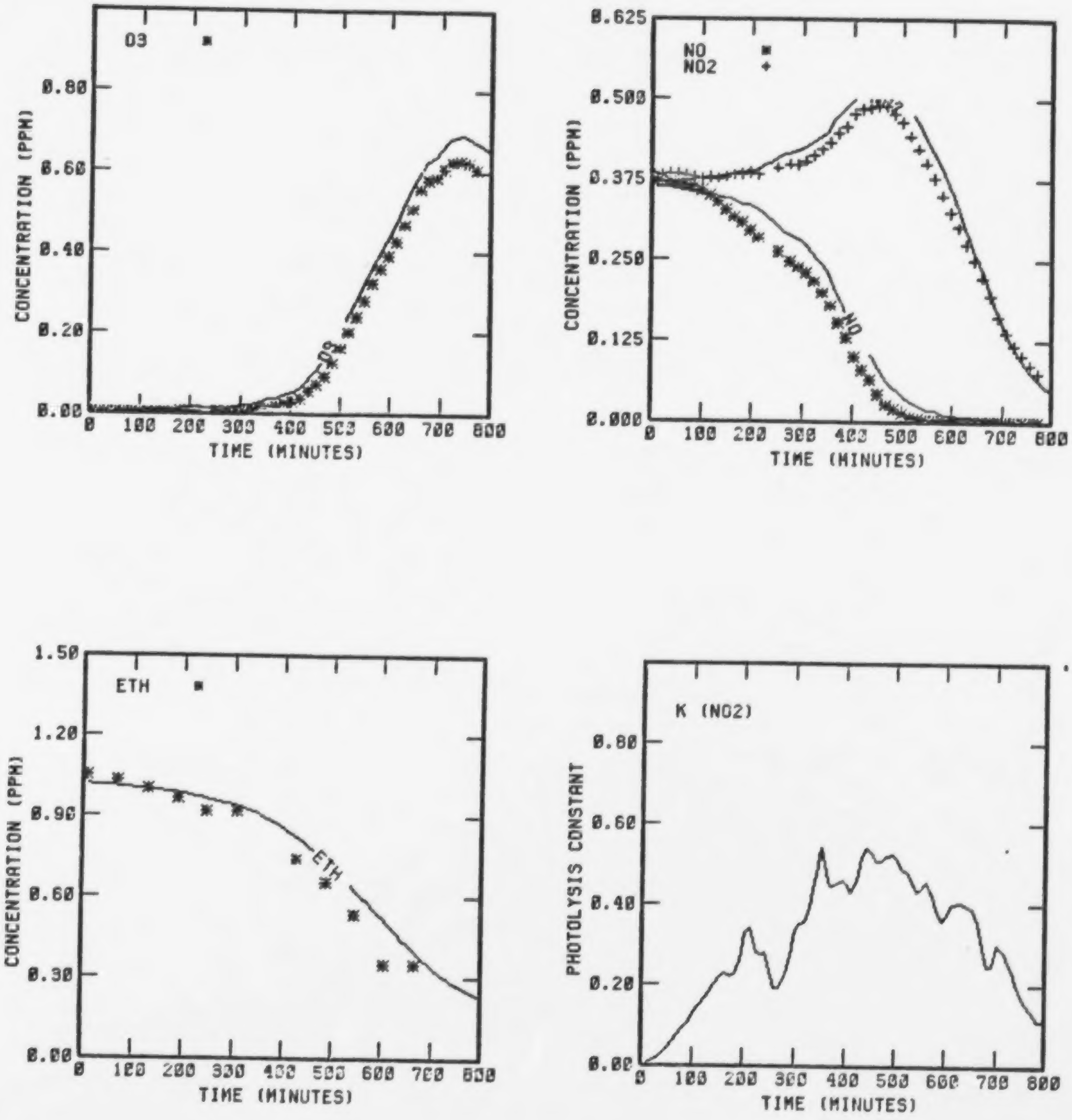

FIGURE 33. SIMULATION RESULTS FOR UNCR 70860

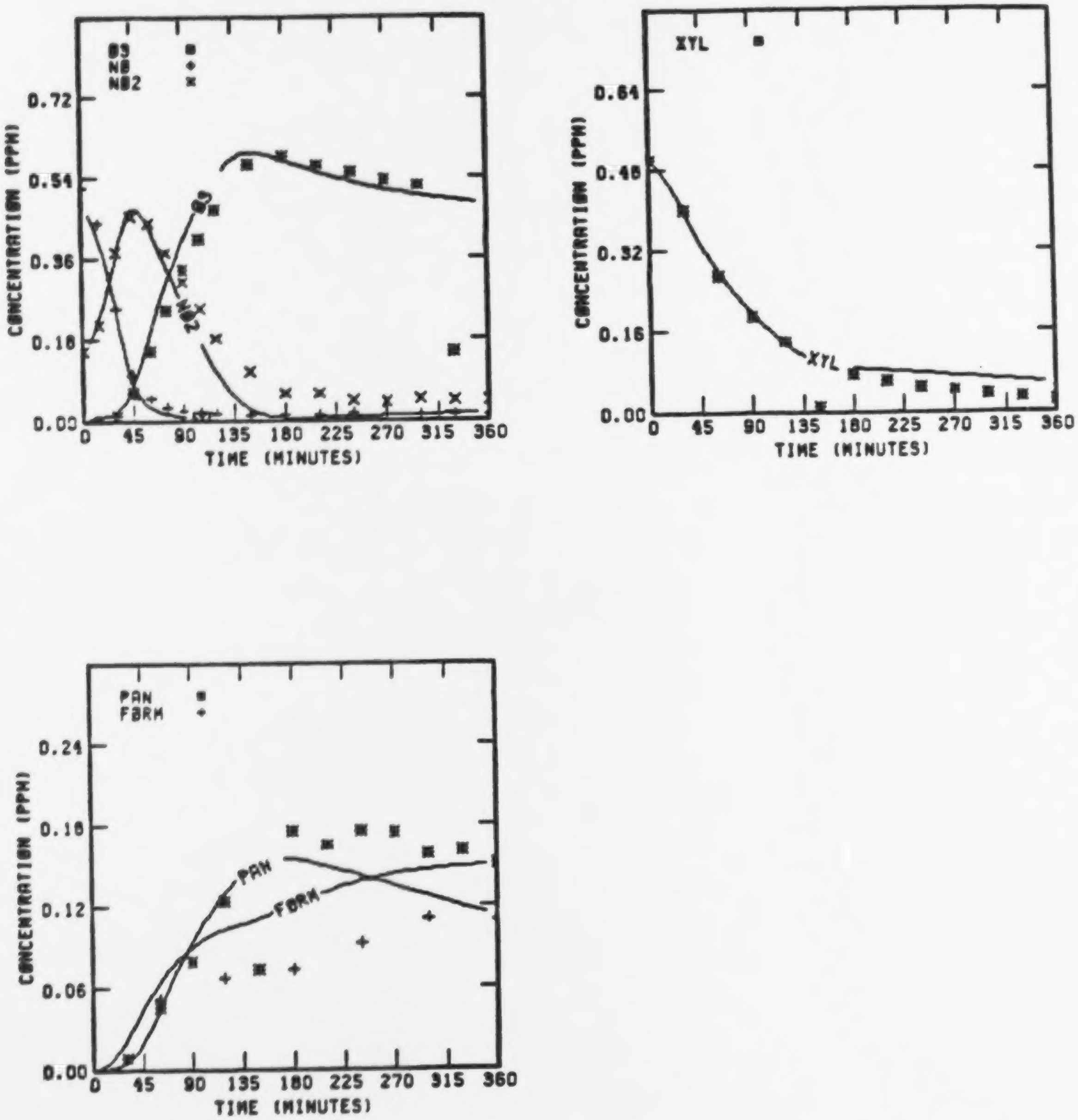

FIGURE 34. SIMULATION RESULTS FOR EC-344

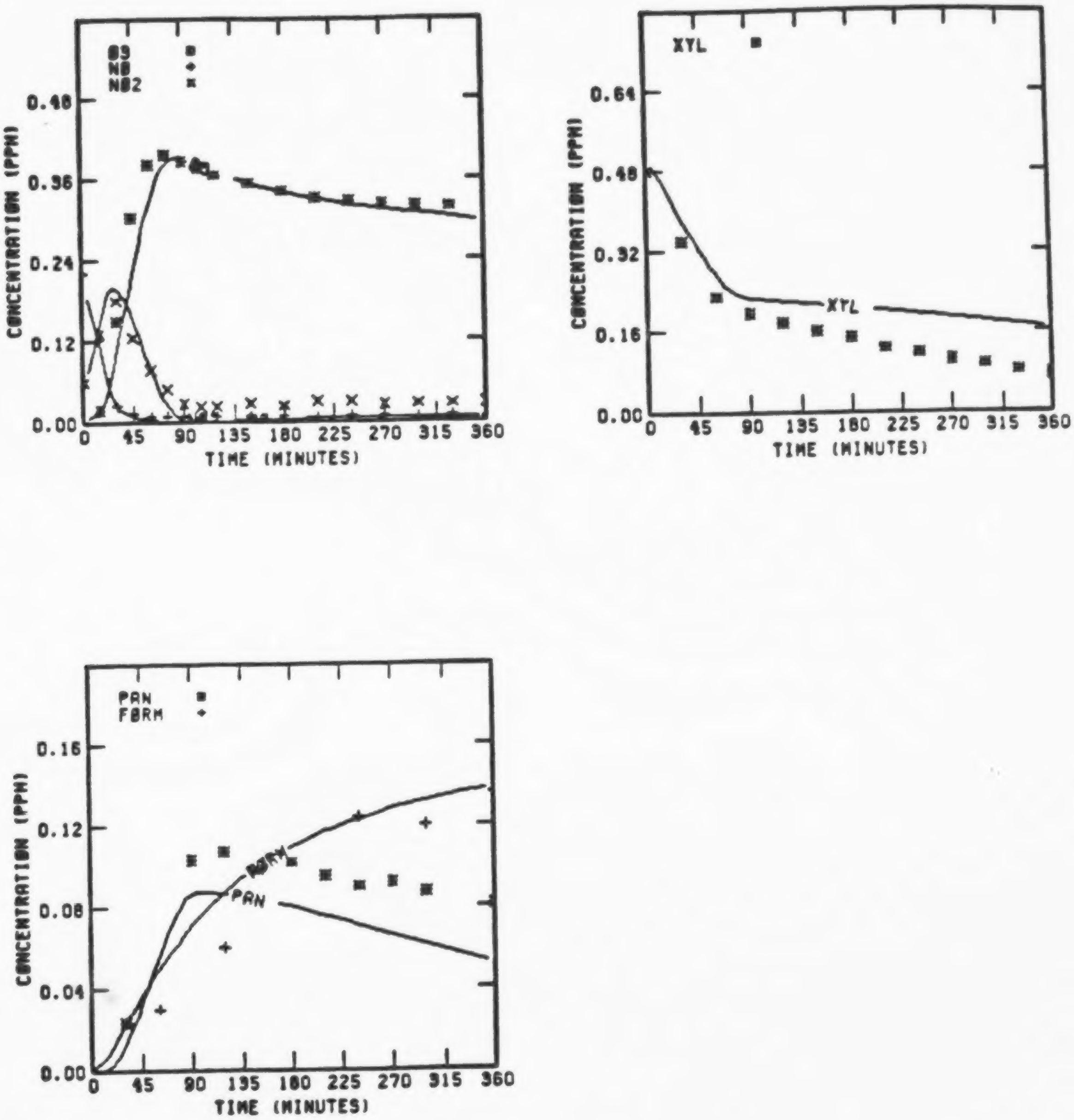

FIGURE 35. SIMULATION RESULTS FOR EC-345

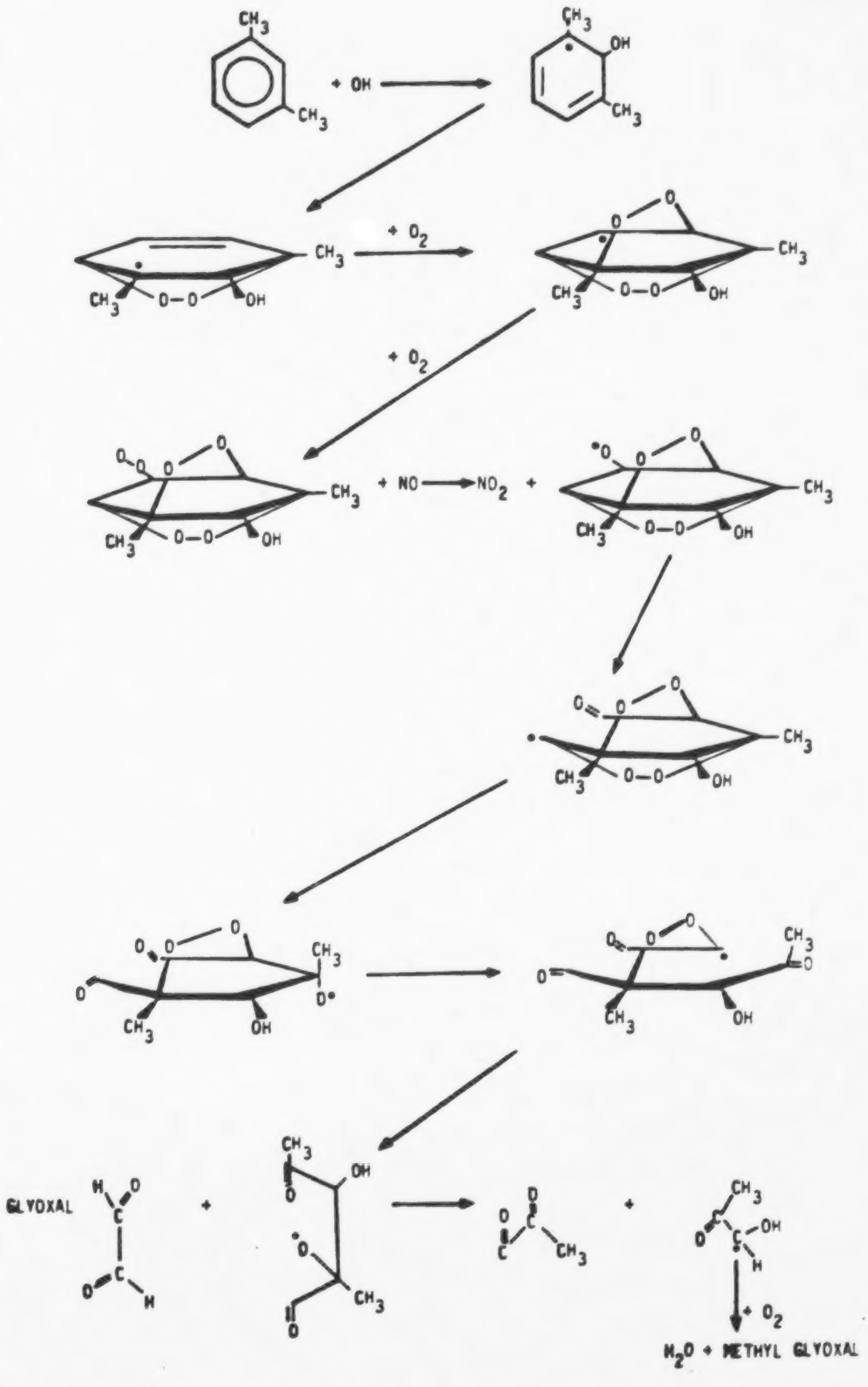

CH3
CH3
+ OH
CH3
OH
CH3
+ O2
CH3
CH3
O—O
OH
+ O2
+ NO → NO2 +
GLYOXAL
+
+
+ O2
H2O + METHYL GLYOXAL

FIGURE 36. RING OPENING OF M-XYLENE

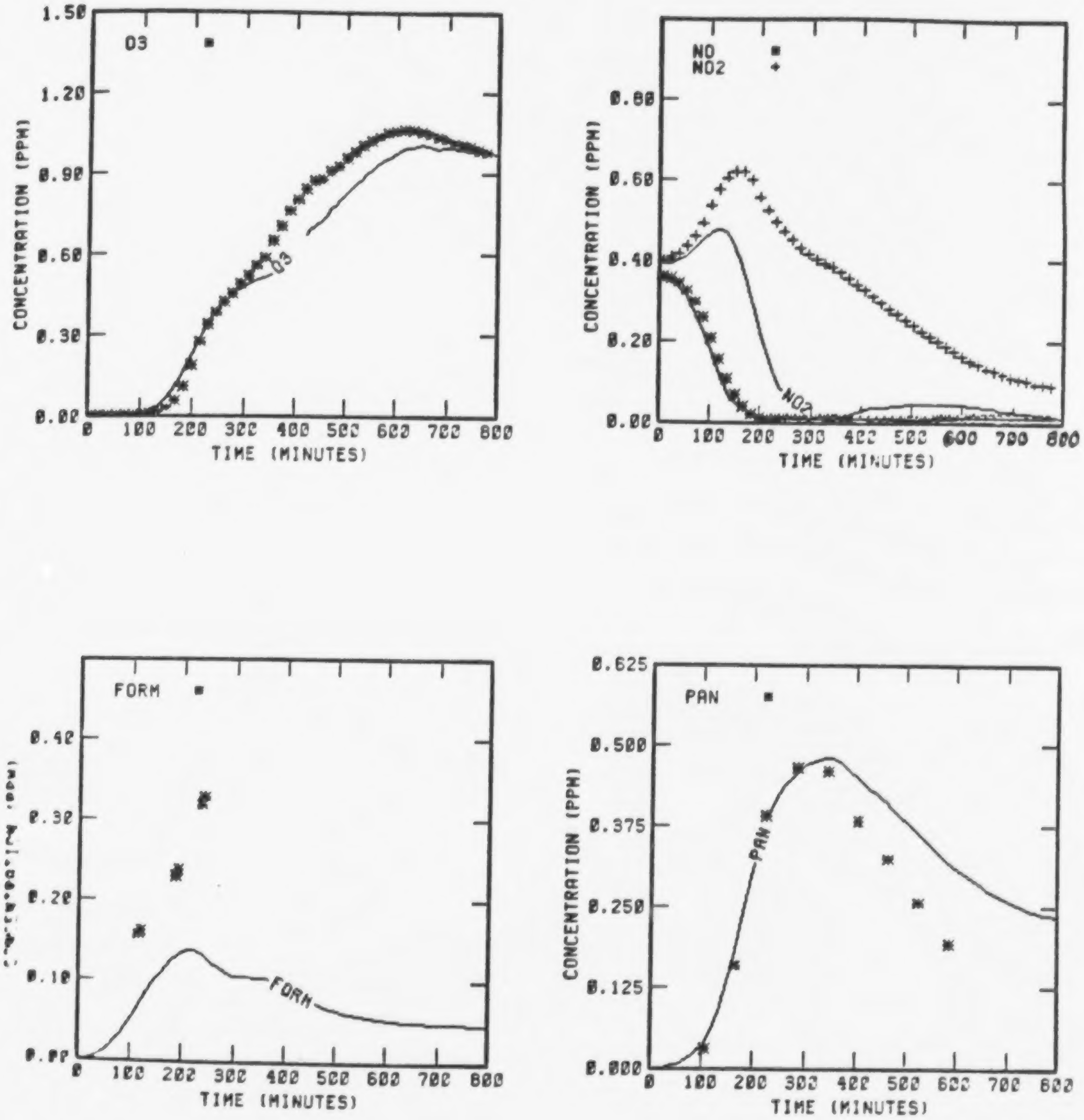

FIGURE 37. SIMULATION RESULTS FOR
UNCR 70980

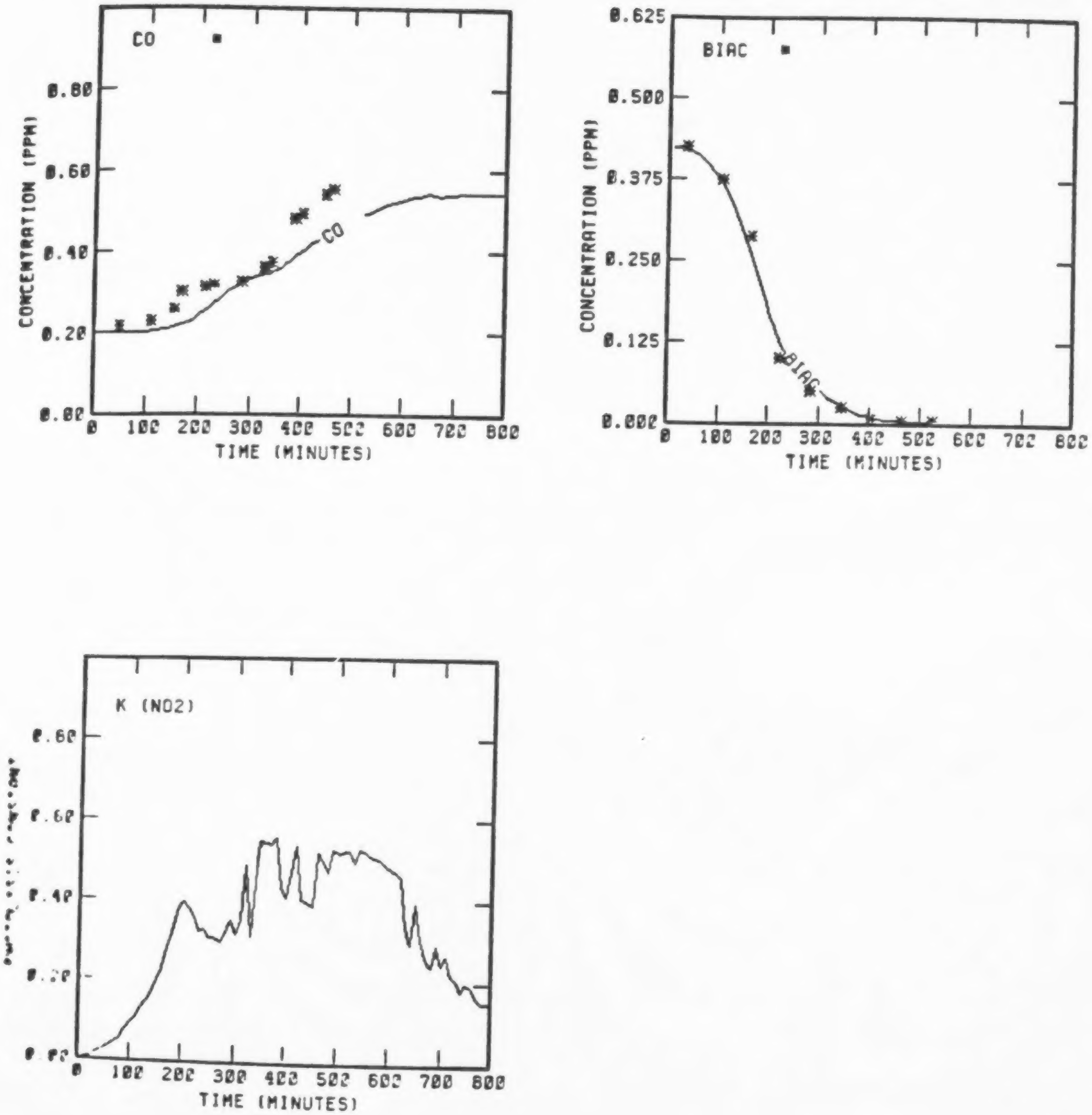

FIGURE 37. (Concluded)

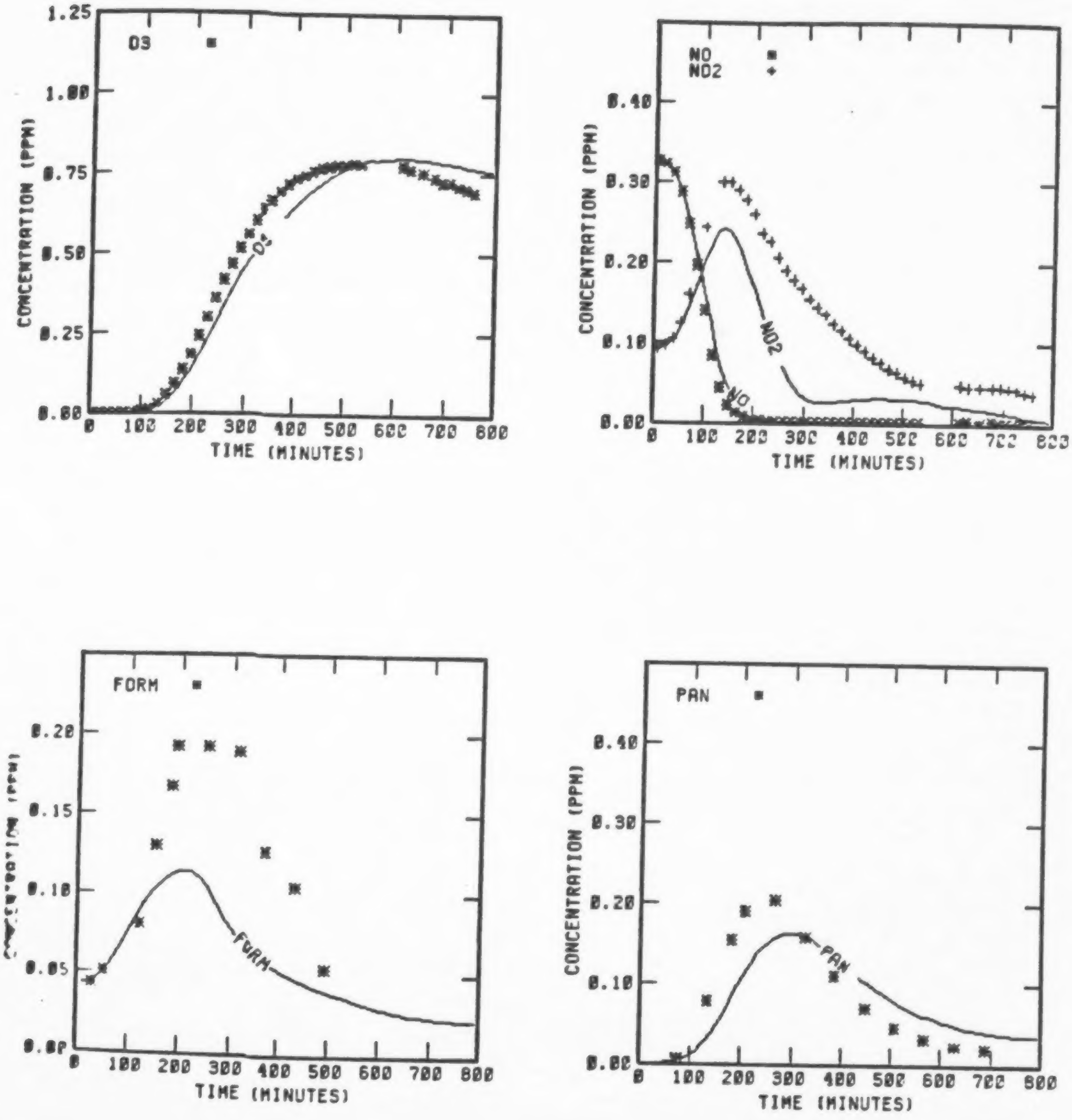

FIGURE 38. SIMULATION RESULTS FOR
UNCB 80880

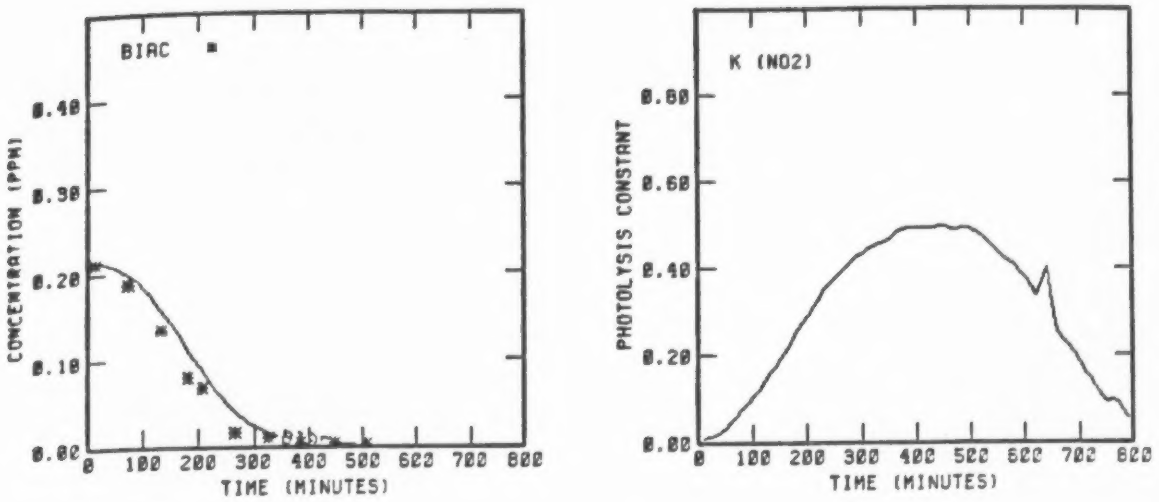

FIGURE 38. (Concluded)

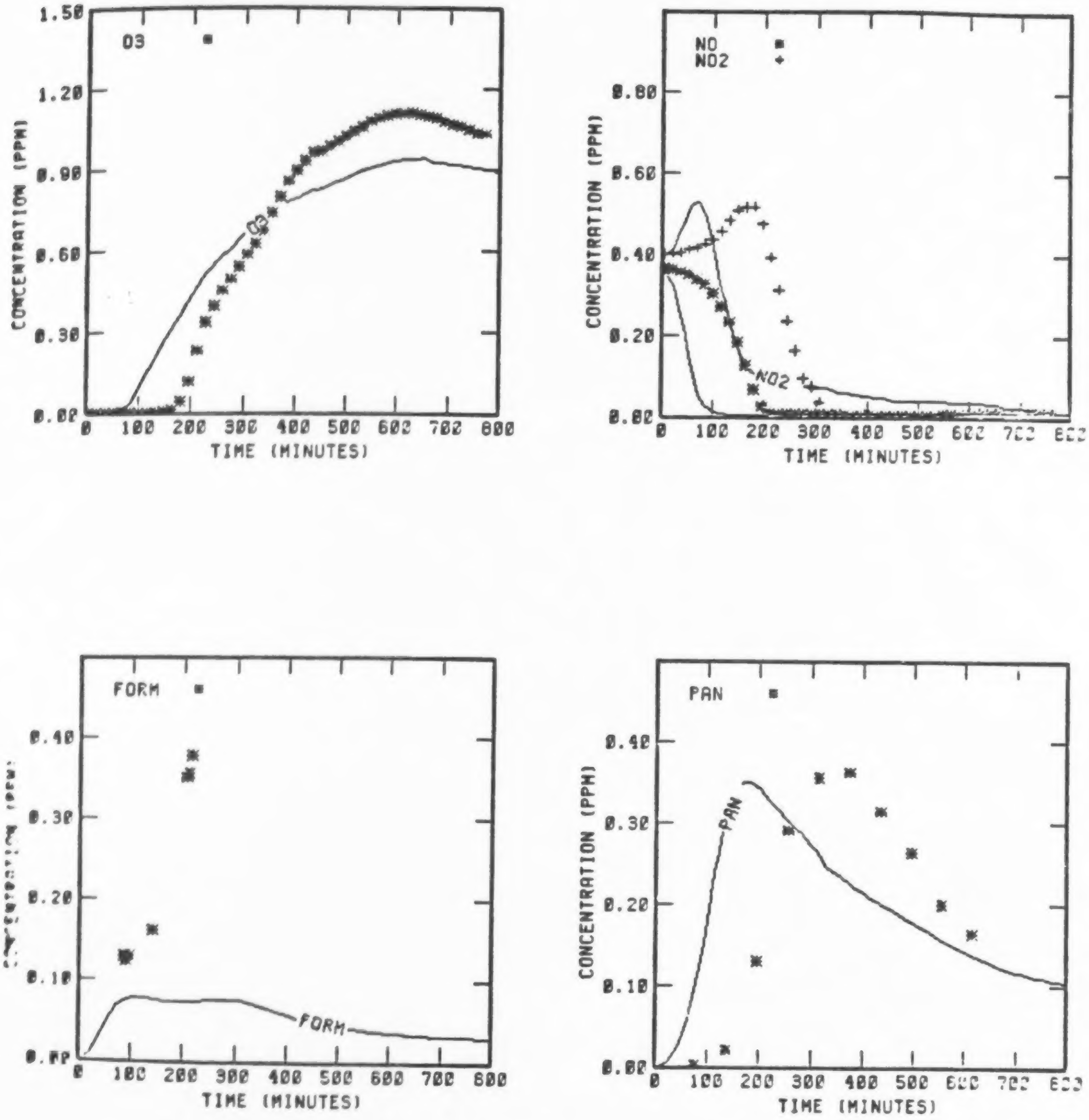

FIGURE 39. SIMULATION RESULTS FOR UNCB 70980 USING METHYLGLYOXAL PHOTOLYSIS EQUAL TO 0.15 k_1.

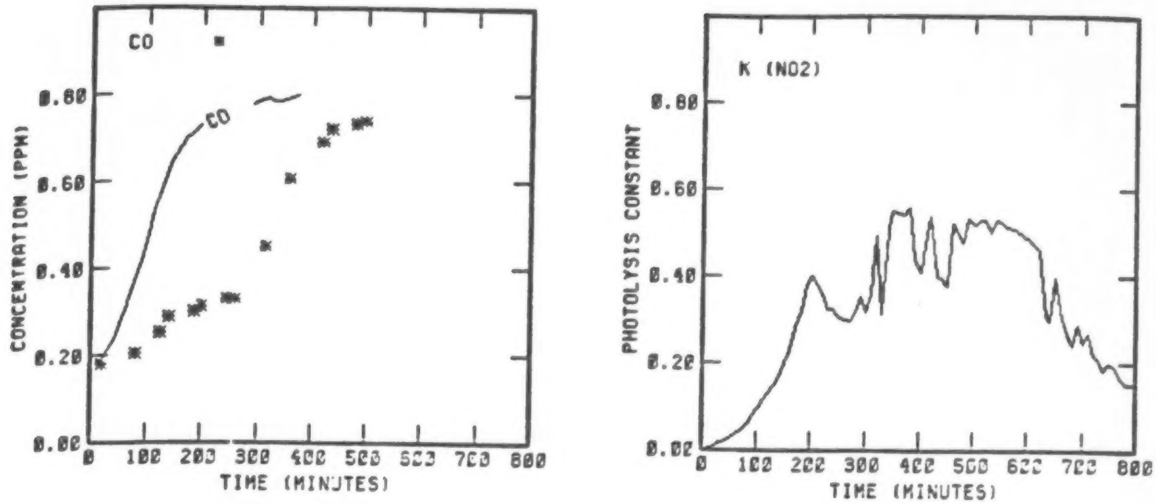

FIGURE 39. (Concluded)

Reproduced from
best available copy.

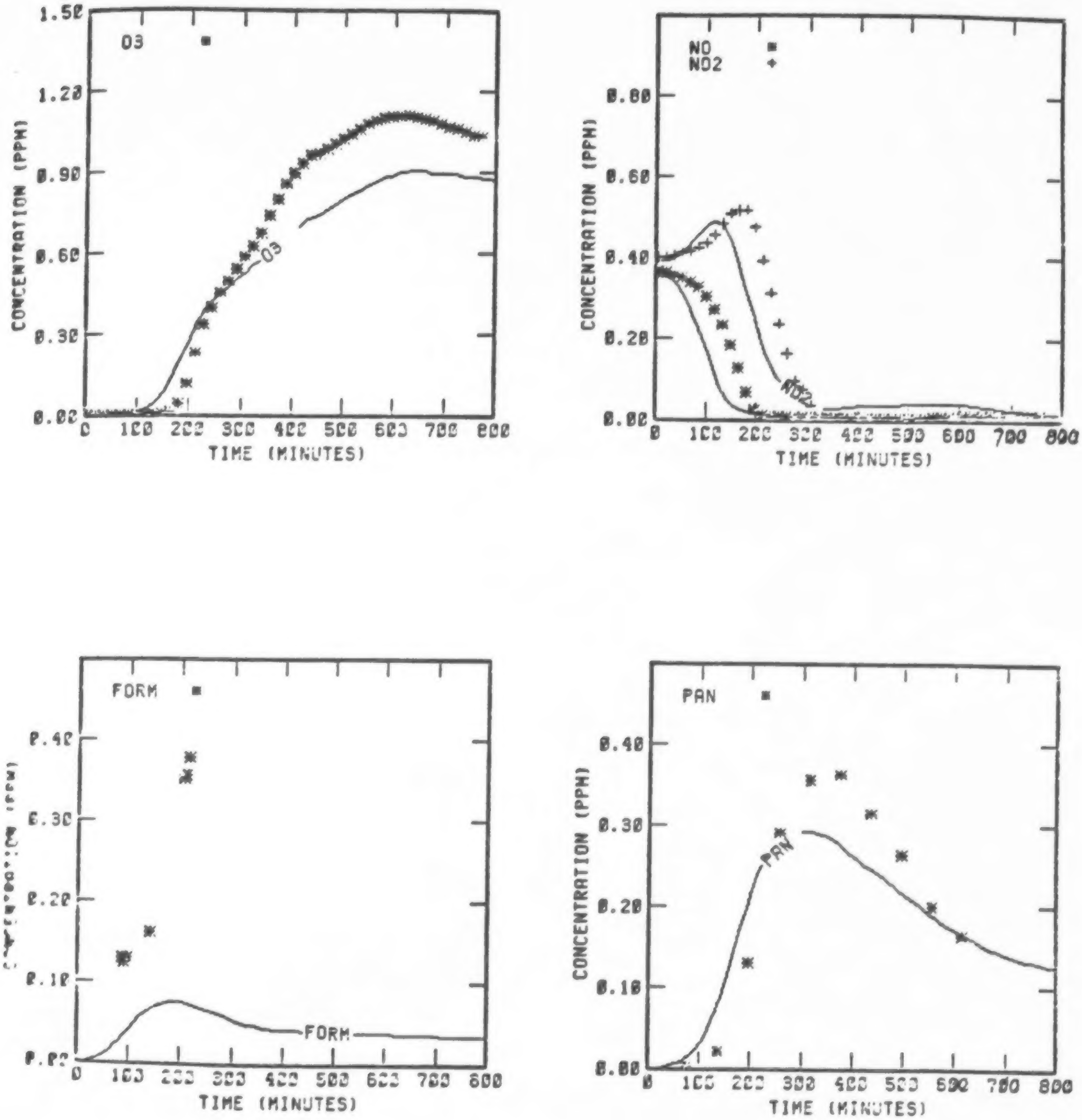

FIGURE 40. SIMULATION RESULTS FOR
UNCB 70960

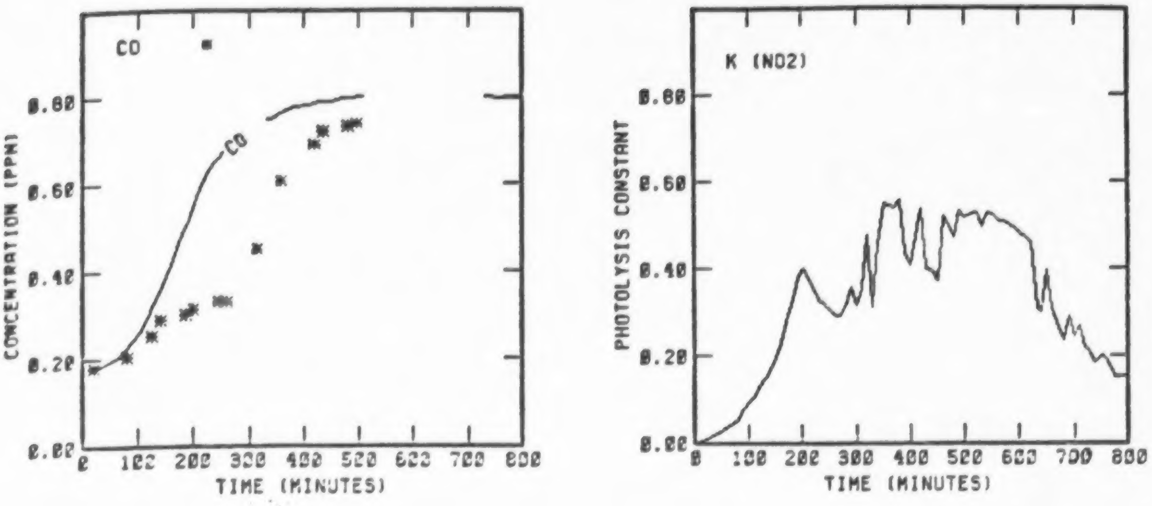

FIGURE 40. (Concluded)

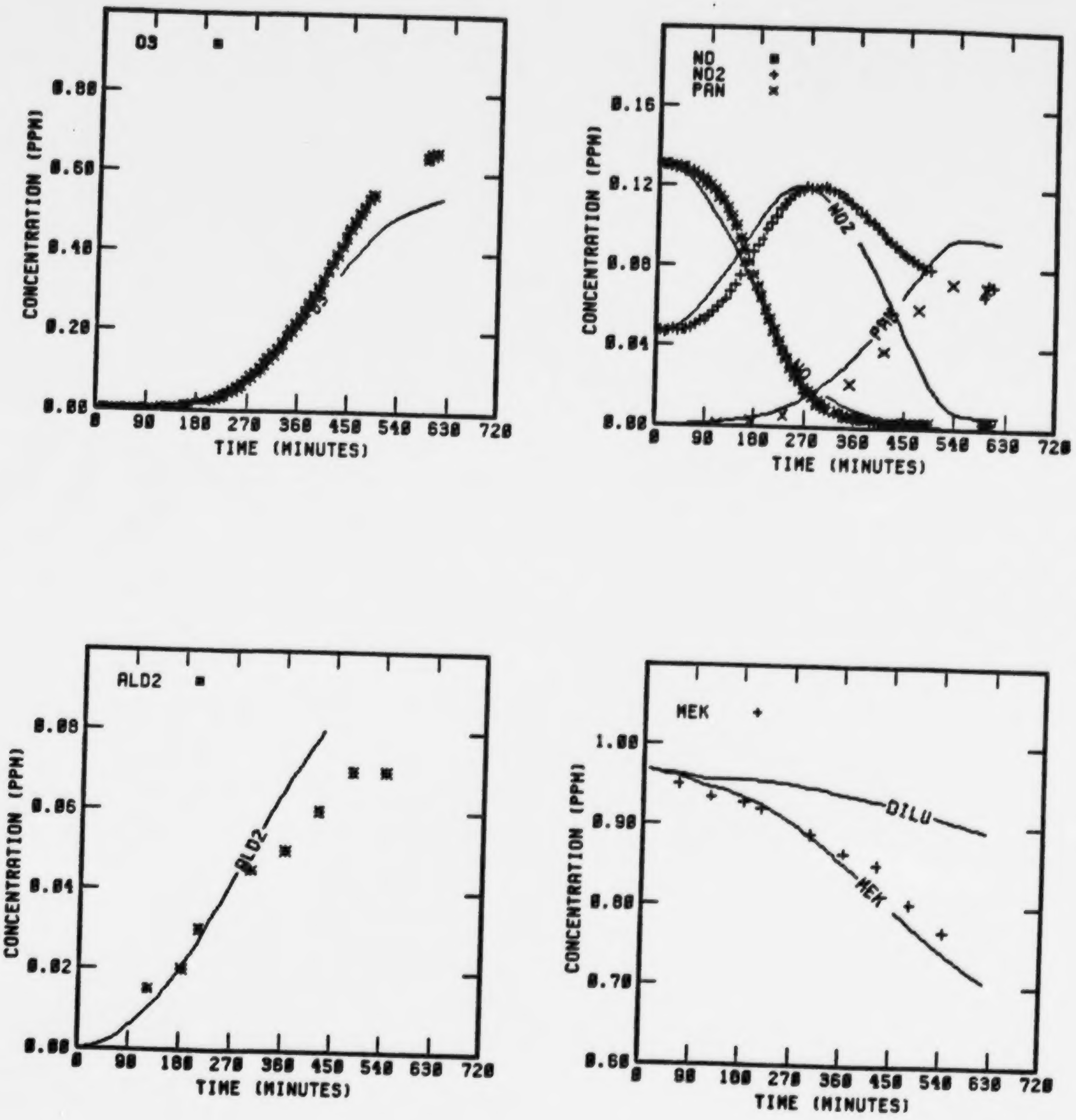

FIGURE 41. SIMULATION RESULTS FOR UNCB 60480

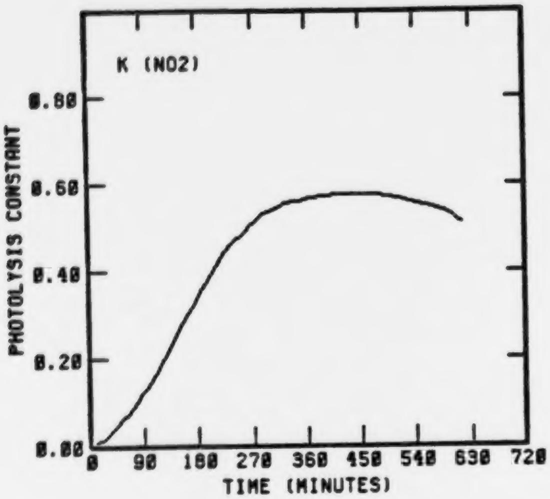

FIGURE 41. (Concluded)

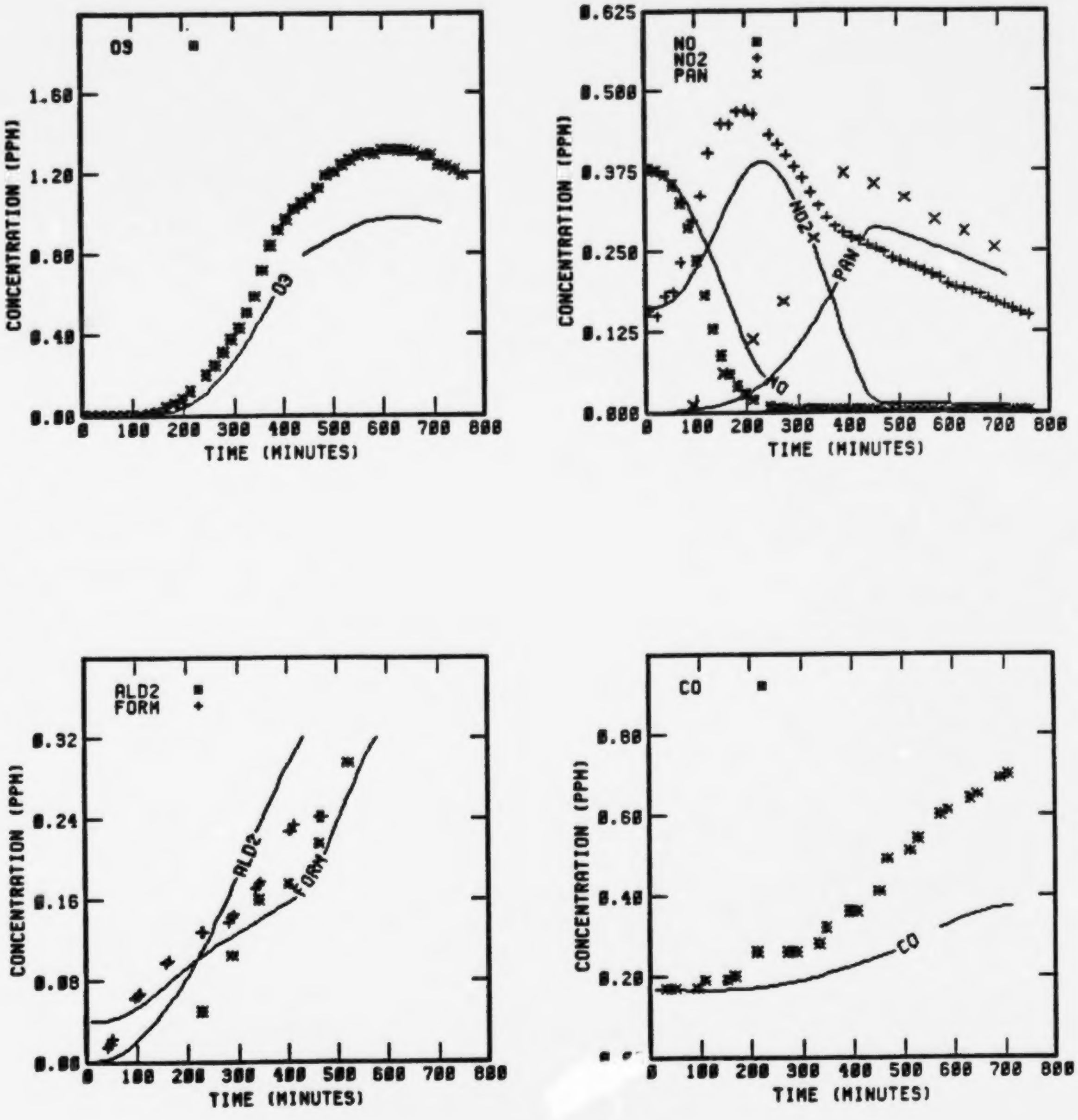

FIGURE 42. SIMULATION RESULTS FOR UNCR 81380

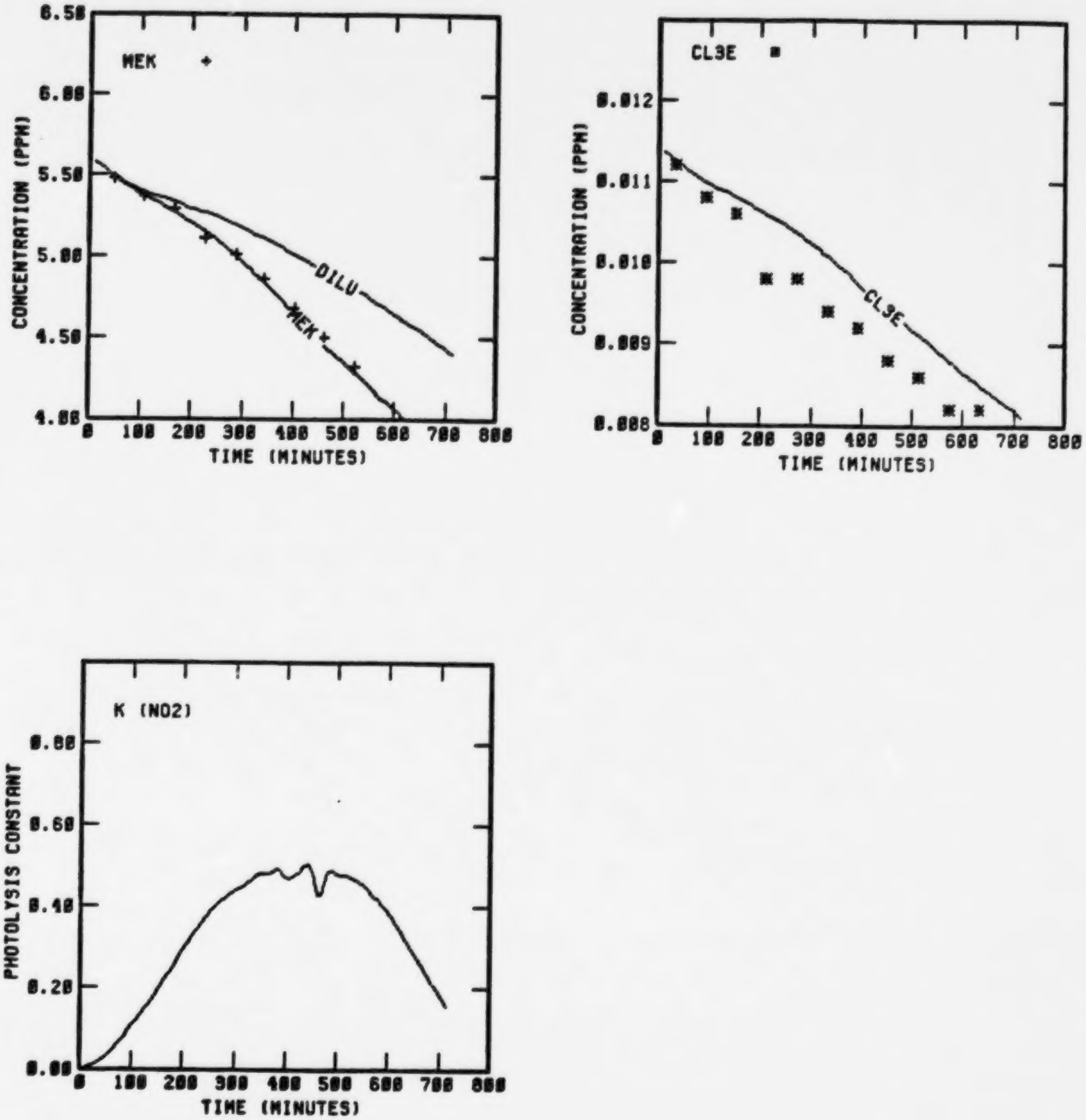

FIGURE 42. (Concluded)

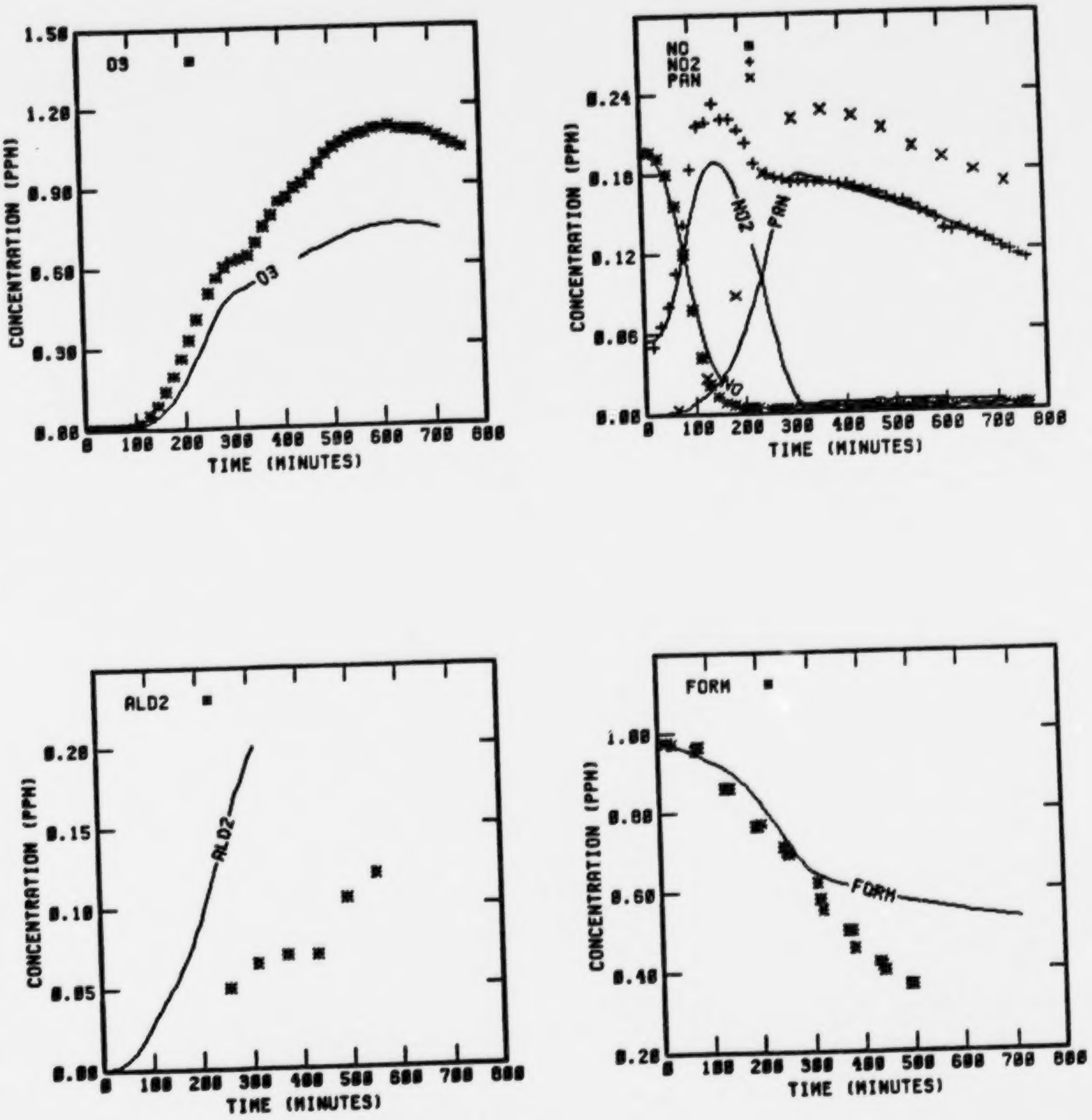

FIGURE 43. SIMULATION RESULTS FOR UNCB 81380

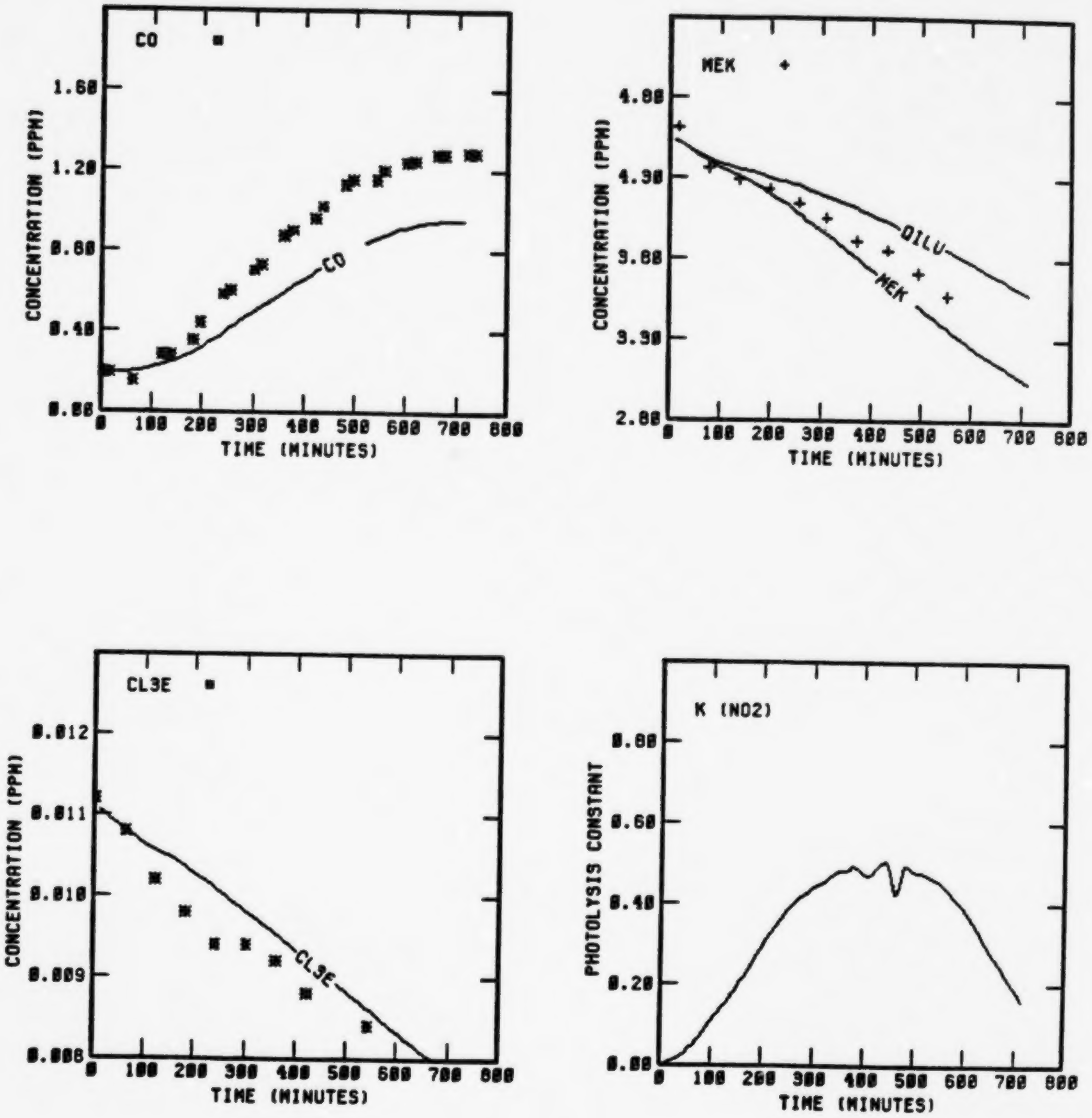

FIGURE 43. (Concluded)

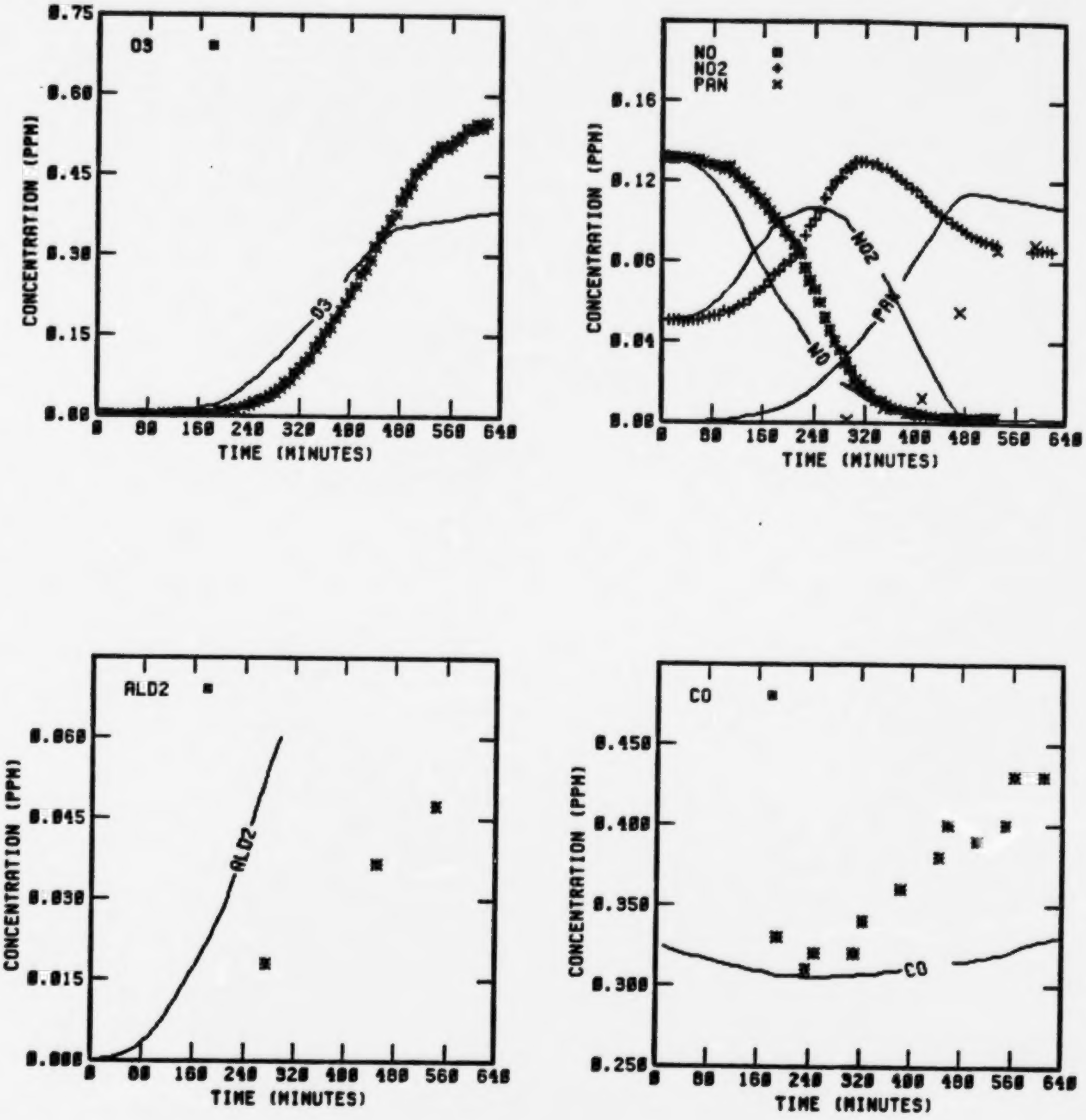

FIGURE 44. SIMULATION RESULTS FOR UNCB 62079

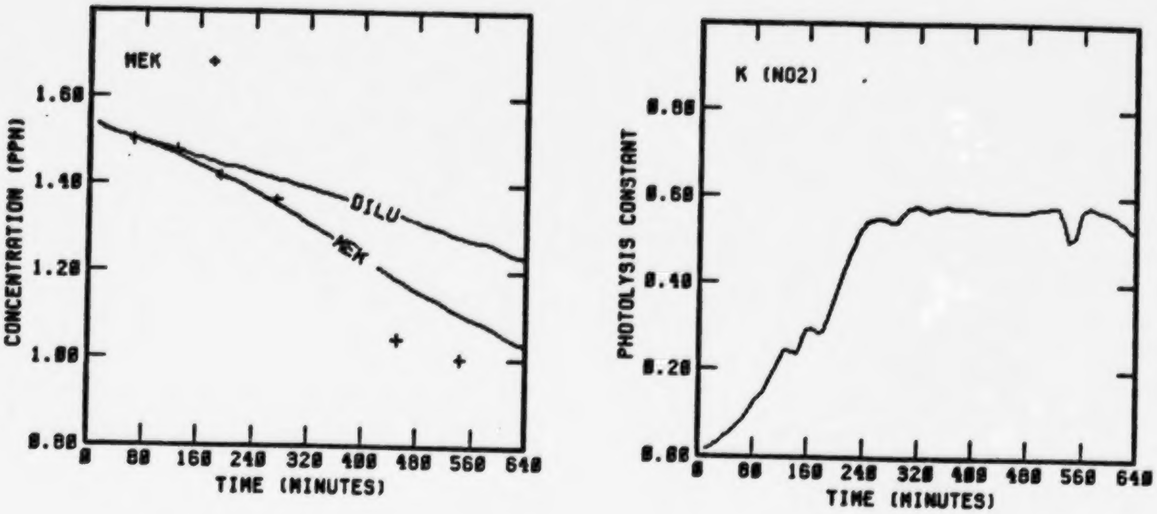

FIGURE 44. (Concluded)

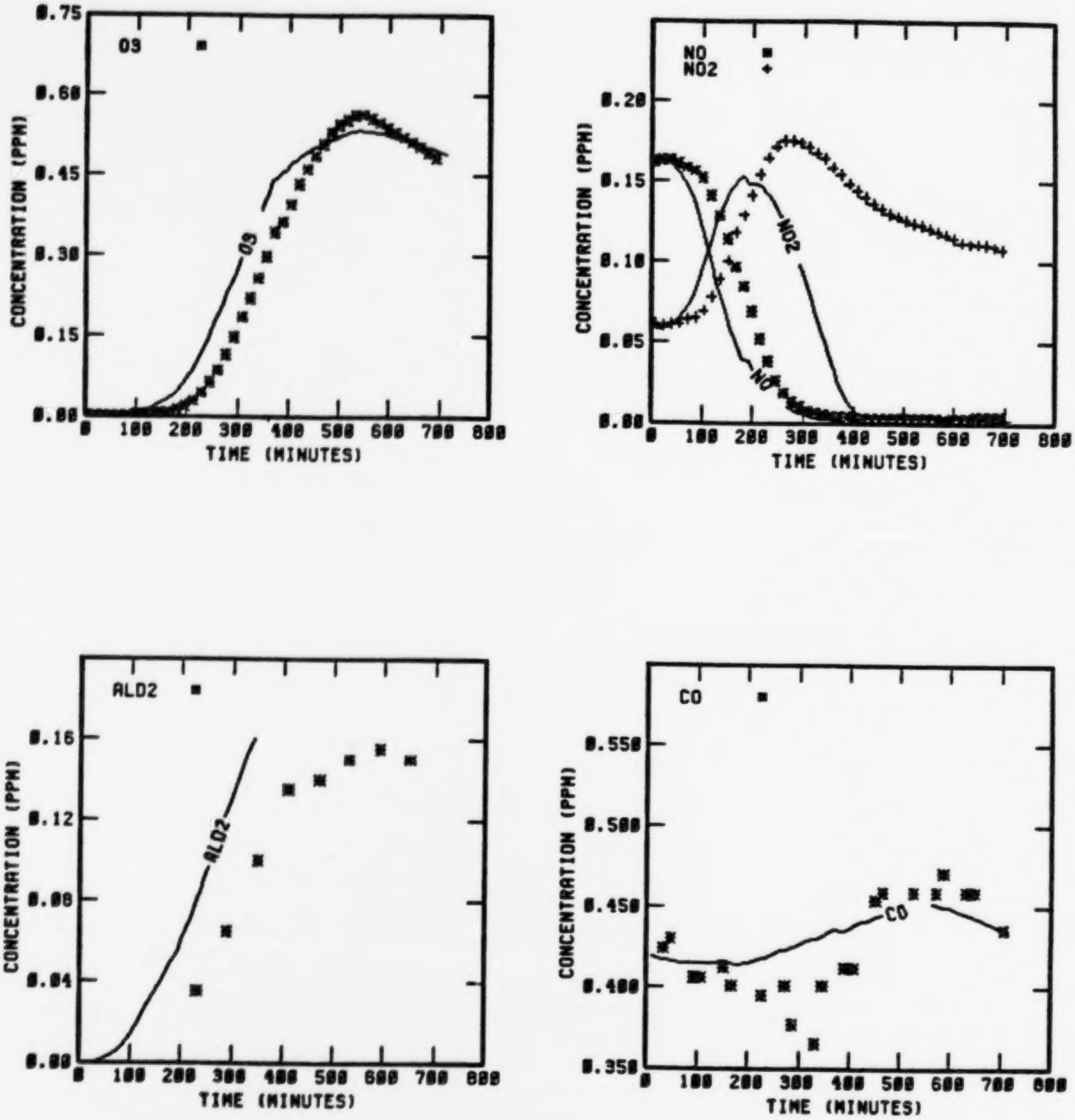

FIGURE 45. SIMULATION RESULTS FOR UNCR 102079

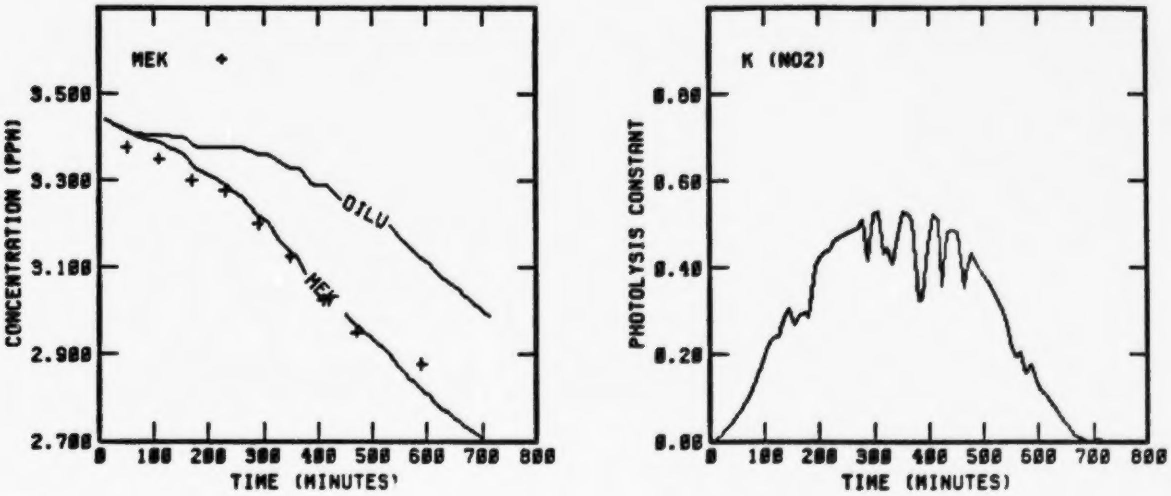

FIGURE 45. (Concluded)

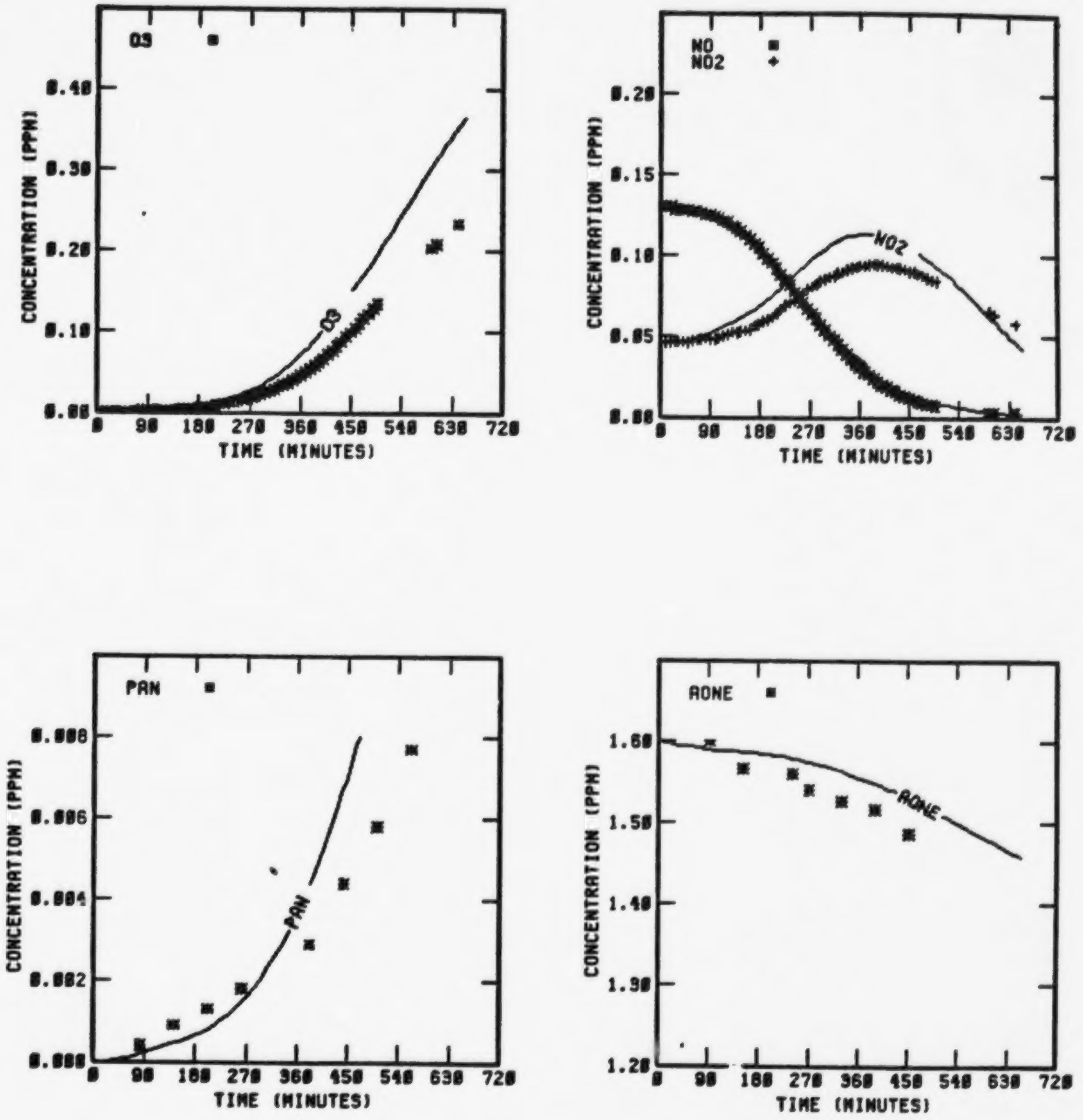

FIGURE 46. SIMULATION RESULTS FOR UNCR 60480

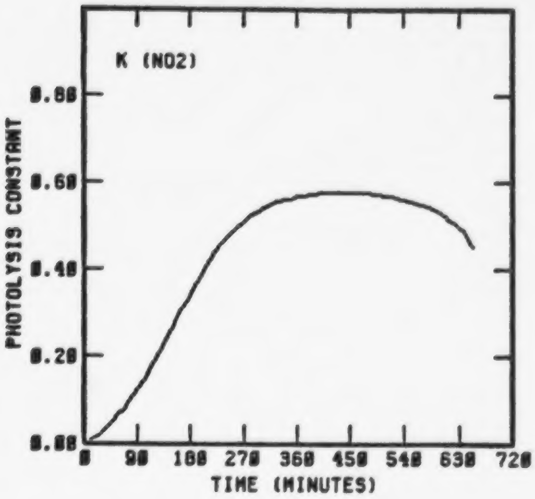

FIGURE 46. (Concluded)

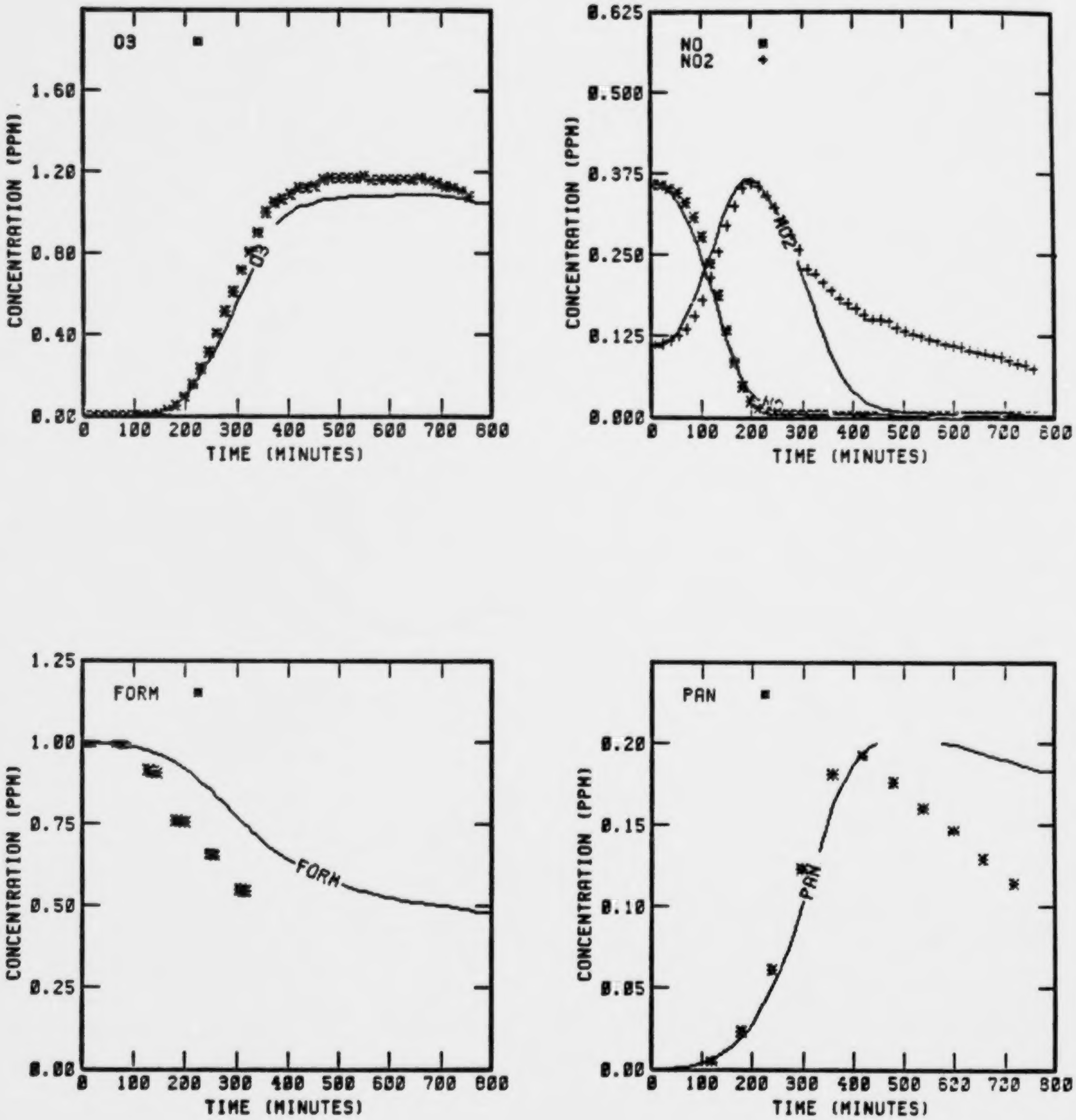

FIGURE 47. SIMULATION RESULTS FOR UNCB 80980

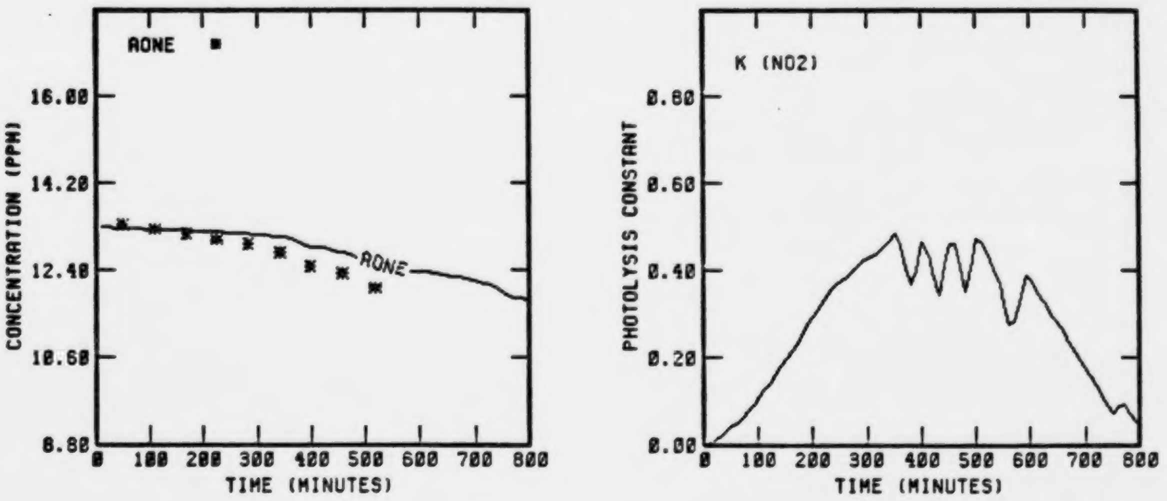

FIGURE 47. (Concluded)

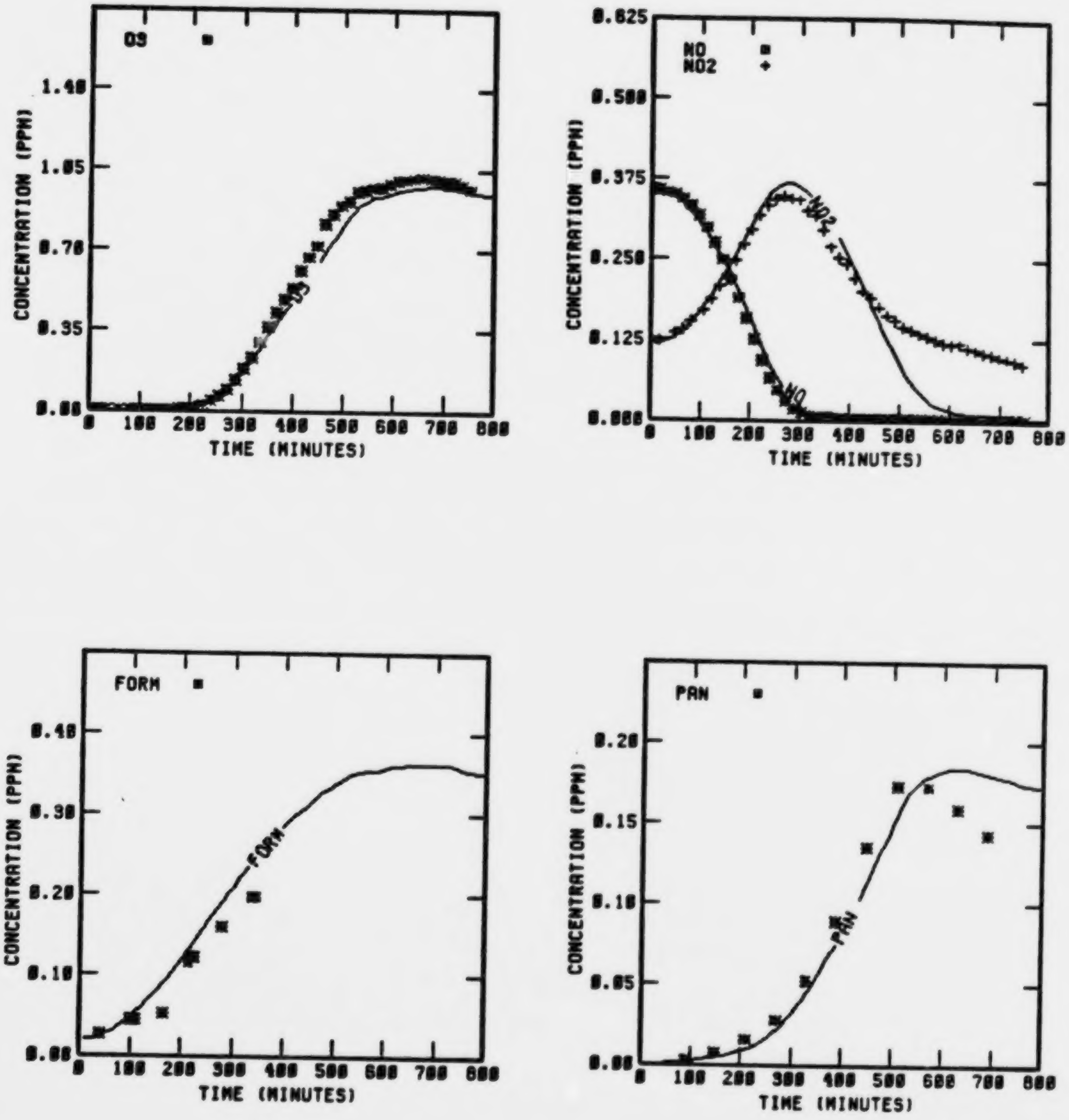

FIGURE 48. SIMULATION RESULTS FOR UNCR 80980

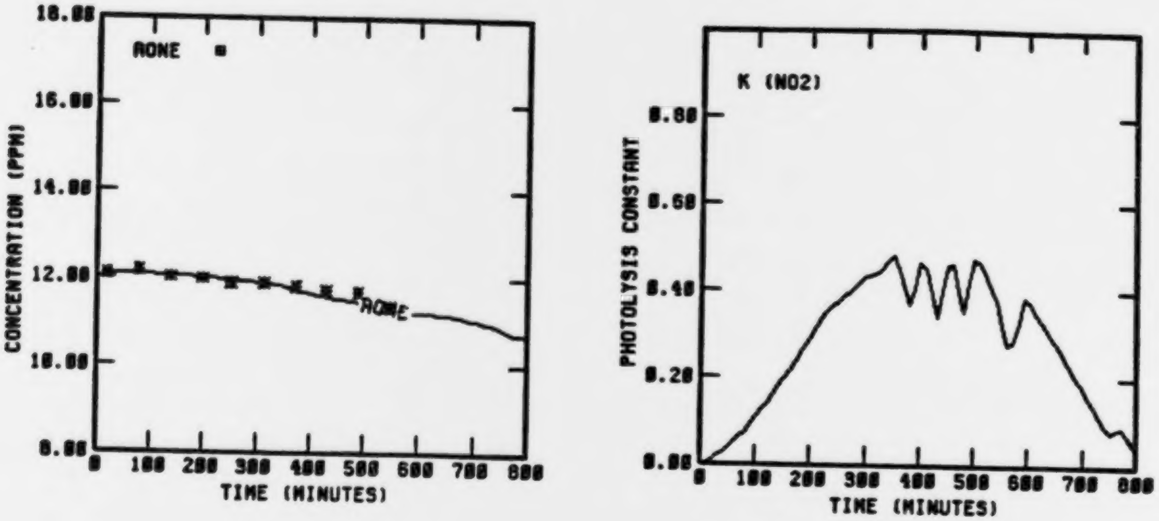

FIGURE 48. (Concluded)

Section 5

BACKGROUND EFFECTS

5.1 BACKGROUND REACTIVITY FOR ATMOSPHERIC MODELING STUDIES

Both smog chambers and the real atmosphere exhibit background reactivity phenomena. Background smog chamber reactivity is caused by the emission of trace contaminants from the chamber walls (NO_x and RHC) as well as by some as yet ill-defined and poorly quantified wall-surface reactions (these phenomena are discussed in Section 5.2). The effects of these background phenomena are to accelerate the oxidation of hydrocarbons and the conversion of NO to NO_2 over and above that which would take place in a zero background environment. Some smog chambers will generate significant concentrations of ozone in the absence of added precursors since the contaminants NO_x and HC are sufficient to yield ozone by themselves. Furthermore, all smog chambers have been shown to emit significant quantities of NO_x, presumably as a result of the reduction of nitric acid on the wall surfaces.

The perturbation due to background reactivity in smog chambers can be reduced by increasing NO_x and RHC precursor concentrations to levels that overwhelm the background phenomena. Unfortunately, this limits the sensitivity of smog chamber methodology; kinetic mechanisms that are validated using smog chamber data obtained at high concentration levels must be extrapolated to lower concentration levels where validation cannot be accomplished. However, most urban smog processes occur at concentration levels that are low compared with those of reproducible smog chamber experiments and the photochemistry of unpolluted atmospheres occurs at concentration levels that are lower still.

The photochemical modeling of polluted atmospheres requires some estimation of what constitutes a "clean atmosphere." Boundary conditions for an urban Airshed Model, for example, should generally be specified as "clean air" concentrations to avoid driving the model with unknown source material. The use of clean air conditions also simplifies the projection of simulation results to future dates for control strategy analysis.

The estimation of background concentrations of ozone and nitrogen oxides can be made fairly easily. Ozone in remote areas has been measured in the range of 20-60 ppb, with occasional exceptions due to photochemical destruction or generation (Routhier, et al. 1980), or from stratospheric intrusion (Singh et al., 1980). Nitrogen oxide data for clean atmospheres ranges from a few ppb to less than a tenth of a ppb (Kelly et al. 1980; Noxon, Norton, and Marovich 1980). Clearly, background concentrations of NO_x are very small when compared with concentrations found in polluted atmospheres. Therefore, background NO_x does not constitute a major perturbation in the urban photochemical system. For example, a concentration of 3 ppb NO_x will generate only about 10 ppb of ozone before conversion to nitric acid.

Background hydrocarbon concentrations constitute a greater problem however. Not only do measured concentrations of background hydrocarbon (and carbon monoxide) constitute a considerable source of reactivity, but there is reason to believe that a considerable amount of background reactivity is due to compounds that are difficult to measure.

It is our purpose here to provide estimates of the background photochemical reactivity that exists in the planetary boundary layer to be used in the calculations of atmospheric photochemical models containing the Carbon-Bond Mechanism (Killus and Whitten, 1982b). Hydrocarbon composition data will be interpreted on a Carbon-Bond basis; however, our estimates of reactivity can be applied to other models and mechanisms as well.

For the purposes of this discussion, the term "reactivity" is best defined in a specific chemical sense as the rate at which hydroxyl radicals react with atmospheric gases to form peroxyl radicals:

$$OH + HC \rightarrow RO_2^{\bullet} \quad .$$

These peroxyl radicals ($HO_2^{\bullet}$, $CH_3O_2^{\bullet}$, $CH_3CO_3^{\bullet}$, etc.) are responsible for conversion of NO to NO_2 in the photochemical process of smog formation that eventually yields ozone. This definition of reactivity is not always suitable for the background effect because it makes no special distinction for variations in concentration levels. A high concentration of slowly reacting species can have the same "reactivity" as a low concentration of quickly reacting species. However, the latter can only be associated with fresh emissions because any true background mixture must be relatively stable in both overall concentration and speciation character.

There are three sources of information concerning the reactivity of background air:

- > Measurement of reaction products, principally carbon monoxide (CO).
- > Direct measurement of the reactive species.
- > Observation of reactivity effects (NO to NO_2 conversion and ozone formation in smog chambers and power plant plumes).

In the following paragraphs, we examine these data sources and attempt to interpret their relevance to the problem of background reactivity. We then present some estimates of plausible background reactivity values and demonstrate the relevance of these estimates to urban smog models.

5.1.1 Background Reactivity of Methane

Methane (CH_4) is usually considered to be an unreactive compound because its atmospheric reaction rate is two or more orders of magnitude less than reactive hydrocarbons. However, methane does react with hydroxyl (though slowly), and since methane exists throughout the troposphere at appreciable concentrations (1-2 ppm), any discussion of background reactivity begins with methane.

The reaction rate constant of methane with hydroxyl is 12 $ppm^{-1}min^{-1}$ at 298 K and atmospheric pressure (Baulch et al. 1980). When combined with the tropospheric background concentration of 1.6 ppm (Heidt et al. 1980), the hydroxyl conversion reactivity of methane alone is 19.2 min^{-1}.

Although the Carbon-Bond Mechanism does not contain methane as an explicit species, in the implementation of the CBM for use in the Urban Airshed Model, we have approximated the effect of methane implicitly. This is done by placing a constraint on the species PAR (rate constant = 1300 $ppm^{-1}min^{-1}$) such that the concentration of PAR must remain above 0.015 ppm. Note that 0.015 ppm PAR x 1300 $ppm^{-1}min$ = 19.5 min^{-1} hydroxyl conversion reactivity.

The oxidation of methane by hydroxyl can be approximated by the following product chain:

$$CH_4 + OH\cdot \xrightarrow{+O_2} CH_3O_2 + H_2O \qquad (1)$$

$$CH_3O_2 + NO \rightarrow NO_2 + CH_3O\cdot \qquad (2)$$

$$CH_3O\cdot + O_2 \rightarrow HO_2 + HCHO \qquad (3)$$

$$HCHO + OH\cdot \xrightarrow{+O_2} HO_2 + CO + H_2O \qquad (4)$$

$$CO + OH\cdot \xrightarrow{+O_2} CO_2 + HO_2 \qquad (5)$$

$$h\nu + HCHO \rightarrow H_2 + CO \qquad (6)$$

$$h\nu + HCHO \xrightarrow[+O_2]{} HO_2 + HO_2 + CO \quad . \qquad (7)$$

If we assume that reaction with hydroxyl is the principal loss mechanism for both CH_4 and CO, then given this sequence and the 1.6 ppm background concentration of methane, the equilibrium concentration of CO can be calculated from the ratio of the reaction rate constant for CO to the reaction rate constant for methane:

$$[CO]_{methane} \cdot K_5 = [CH_4] \cdot K_1$$

$$[CO]_{methane} = \frac{1.6 \text{ ppm} \cdot 12 \text{ ppm}^{-1}\text{min}^{-1}}{450 \text{ ppm}^{-1}\text{min}^{-1}}$$

$$[CO]_{methane} = 0.044 \text{ ppm} \quad .$$

This is equal to the minimum concentration of CO observed in remote areas (Heidt et al. 1980; Seiler 1974).

We can also calculate the upper limit concentration of formaldehyde (HCHO) produced from methane:

$$[\mathrm{HCHO}]_{\mathrm{methane}} \cdot K_4 = [\mathrm{CH_4}] \cdot K_1 \quad ,$$

$$[\mathrm{HCHO}]_{\mathrm{methane}} = \frac{19.2\ \mathrm{min}^{-1}}{14{,}000\ \mathrm{ppm}^{-1}\mathrm{min}^{-1}}$$

$$[\mathrm{HCHO}]_{\mathrm{methane}} = 0.0014\ \mathrm{ppm} \quad .$$

This number is an upper limit because formaldehyde is also lost to photolysis and deposition. There are also alternate chemical product pathways for CH_3O_2 that lead to formic acid rather than formaldehyde; and formaldehyde can also react with $HO_2^{\bullet}$ to give formic acid. The implications of these possibilities are unclear since the photochemistry of formic acid is not well understood (Dawson, Farmer, and Moyers, 1980). In any case, measured values of formaldehyde in remote locations typically range from 0.5 ppb (0.0005 ppm) (Platt and Perner, 1980; Fushimi and Miyaki, 1980; Zafiriou et al., 1980) to several ppb in remote locations. Similar concentrations of formic acid have also been observed (Dawson, Farmer, and Moyers, 1980).

5.1.2 Inference of Reactive Hydrocarbons from CO Observations

The good agreement between the background rectivity of methane and the minimum concentrations of CO observed in remote areas suggests that CO might be used to estimate the reactive hydrocarbon content of background air. Fishman and Crutzen (1978) used a similar procedure in attempting to account for the global tropospheric ozone source and the factor of 4 difference between background CO in the southern and northern hemispheres.

The hydroxyl reactivity associated with the carbon monoxide background at middle latitudes in the northern hemisphere can be calculated from the CO-OH rate constant and background CO. Background CO for the northern hemisphere has been measured at between 0.1 and 0.2 ppm (Heidt et al., 1980; Seiler, 1974; Seiler and Junge, 1970). Over land, especially in the autumn months, the CO concentration appears to be somewhat greater (Jeffries, 1981; private communication).

The previously described oxidation of methane can be simply illustrated:

$$CH_4 \longrightarrow HCHO \longrightarrow CO \longrightarrow CO_2 \quad .$$

That is, in a system where methane is the only hydrocarbon, equilibrium is established when a hydroxyl radical is equally likely to react with CH_4, HCHO, or CO. Thus, the hydroxyl conversion reactivity can be estimated to be three times the reactivity of carbon monoxide.

For more complex hydrocarbons, the situation is complicated somewhat by intermediate reaction pathways that yield CO_2, e.g.:

$$CH_3CHO + OH \xrightarrow{+O_2} CH_3CO_3 + H_2O$$

$$CH_3CO_3 + NO \rightarrow CH_3CO_2 + NO_2$$

$$CH_3CO_2 \xrightarrow{+O_2} CO_2 + CH_3O_2 \quad .$$

If the yield of CO from hydrocarbon oxidation is 50 percent, then the overall hydroxyl reactivity would be six times the reactivity of the CO component alone, i.e., about 500 $ppm^{-1}min^{-1}$ in the boundary layer of the northern hemisphere.

Note that this estimate depends on several factors:

1) The establishment of a photochemical equilibrium for the reacting hydrocarbon and its products; this assumes that hydrocarbons are being replaced in the air mass approximately as rapidly as they are destroyed.

2) An excess of CO over 0.05 ppm (methane-produced background) in the northern hemisphere caused by hydrocarbon oxidation and not by direct emission of CO. This assumption is not critical, however. Anthropogenic activities emit both CO and hydrocarbons at a reactivity ratio of 1:7 [excluding oxygenates (EPA, 1976)]. Thus, the inference of atmospheric reactivity from CO is still reasonable provided assumption 1 applies.

3) The production by hydrocarbon oxidation of a 50 percent yield of CO and, therefore, a ratio of CO rectivity to total reactivity that is ≈ 1:6. This ratio is 1:3 for methane and can be as high as 1:14 for urban air containing fresh anthropogenic emissions (see Killus and Whitten 1982b; Calvert 1976).

Finally, we note that our estimate of hydroxyl conversion reactivity does not, per se, give us concentrations of reactive hydrocarbons. To estimate such concentrations from reactivity estimates alone, we would need a hydrocarbon composition profile. In the next section, we discusss available measurements of atmospheric hydrocarbons.

5.1.3 Direct Measurements of Background RHC

Our picture of the concentration levels and composition of background reactive hydrocarbon derives from several sets of data: Scott Research Laboratories, 1970; Rasmussen, Chatfield, and Holdren, 1977; Altwicker and Dicesare, 1979; and Grosjean, 1980. Two of these data sets include airborne measurements. From comparisons of RHC measurements aloft to measurements in the planetary boundary layer, we observe that RHC in the free troposphere is very low (≈ 1-10 ppbc), whereas boundary layer concentrations are generally an order of magnitude higher. This observation is in keeping with the conceptual model of Fishman and Crutzen (1978), which uses enhanced photochemical activity in the boundary layer.

There are three possible sources of boundary layer RHC: anthropogenic, geogenic, and biogenic (Mayrsohn and Crabtree, 1976; Altwicker and Dicesare, 1979; Rasmussen and Went, 1965). It is not generally possible to make distinctions among these sources from ambient measurements alone because there is considerable overlap in emitted species, and also because the composition of these sources, especially the biogenic component, is not well characterized. However, Rasmussen, Chatfield, and Holdren (1977) did attempt a factor analysis of their data with several interesting results that included the identification of both isoprene and ethylene as biogenic gases (see also Boller and Keude, 1980; and Zimmerman, 1977).

Since high concentrations of reactive hydrocarbons exist in urban areas and extremely low concentrations of RHC exist in the free troposphere, the measured concentration of RHC in the boundary layer can be expected to show great variation. This variation between low and extremely low concentrations makes it difficult to assign a typical background value. It is also difficult to positively identify all hydrocarbon species at low concentration levels. Thus, the hydrocarbon composition of a typical background mix is difficult to specify. Tables 9 through 12

TABLE 9. HYDROCARBON DATA FOR ERT PROJECT A029

Date:	15 August 1979
Site:	Clarksburg
Sampling:	Time 14
Cannister Number:	84

Hydrocarbons	μg/m^{3*}
Ethane	1.35
Ethylene	0.25
Acetylene	0.32
Propane	0.73
Propene	0.28
Isobutane	0.39
n-Butane	0.59
1-Butene	0.11
Isobutene	0.24
trans-2-Butene	0.17
cis-2-Butene	0.00
Isopentane	1.05
n-Pentane	0.69
1-Pentene	0.67
trans-2-Pentene	0.92
cis-2-Pentene	0.00
Cyclopentane	0.00
Isoprene	0.15
2-Methylpentane	0.00
3-Methylpentane	0.80
n-Hexane	1.30
Methylcyclopentane	0.10
2,4-Dimethylpentane	0.00
Benzene	1.01
3-Methylhexane	0.00
Toluene	0.52
Ethylbenzene	0.00
p- and m-Xylene	0.00
o-Xylene	0.18
1,2,4-Trimethylbenzene	1.30
2,2-Dimethylbutane	0.00
Methylcyclohexane	0.00
2-Methylheptane	0.00
2,2,4-Trimethylpentane	0.00
n-Octane	0.00
n-Nonane	0.00

TABLE 9. (Concluded)

2-Ethyltoluene	0.00
4-Ethyltoluene	0.00
1, 2, 3-Trimethylbenzene	0.00
α-Pinene	0.00
Myrcene	0.00

Data Summary	$\mu g/m^3$
Acetylene	0.32
Sum of paraffins	7.00
Sum of olefins	2.79
Sum of aromatics	3.01
Unidentified	3.52
Total NMHC	16.54

Carbon-Bond Splits	
Compound	Value
UR	0.15
ETH	0.015
OLE	0.05
ARO	0.09
PAR	0.48
Unidentified	0.21

---

* $\mu g/m^3$ = Micrograms per cubic meter.

Source: Grosjean, D. (1980).

TABLE 10. HYDROCARBON DATA FOR ERT PROJECT A029

Date 16 August 1979
Site: Wright Tract
Sampling Time: 6
Cannister Number: 113

Hydrocarbon	$\mu g/m^{3*}$
Ethane	1.93
Ethylene	0.92
Acetylene	0.35
Propane	0.81
Propene	0.66
Isobutane	0.19
n-Butane	0.57
1-Butene	0.00
Isobutene	0.24
trans-2-Butene	0.22
cis-2-Butene	0.00
Isolpentane	1.41
n-Pentane	2.52
1-Pentene	0.00
trans-2-Pentene	0.00
cis-2-Pentene	0.00
Cyclopentane	0.00
Isoprene	0.24
2-Methylpentane	0.70
3-Methylpentane	0.48
n-Hexane	0.89
Methylcyclopentane	0.22
2,4-Dimethylpentane	0.00
Benzene	0.69
3-Methylhexane	0.00
Toluene	1.05
Ethylbenzene	0.00
p- and m-Xylene	0.63
o-Xylene	0.18
1,2,4-Trimethylbenzene	0.38
2,2-Dimethylbutane	0.00
Methylcyclohexane	0.00
2-Methylheptane	0.00
2,2,4-Trimethylpentane	0.00
n-Octane	0.00
n-Nonane	0.00

TABLE 10. (Concluded)

2-Ethyltoluene	0.00
4-Ethyltoluene	0.00
1,2,3-Trimethylbenzene	0.00
α-Pinene	0.00
Myrcene	0.00

Data Summary	μg/m³
Acetylene	0.35
Sum of paraffins	9.72
Sum of olefins	2.28
Sum of aromatics	2.93
Unidentified	4.12
Total NMHC	19.40

Carbon-Bond Splits

Compound	Value
UR	0.17
ETH	0.047
OLE	0.04
ARO	0.09
PAR	0.44
Unidentified	0.21

---

* μg/m³ = Micrograms per cubic meter.

Source: Grosjean, D. (1980).

TABLE 11. HYDROCARBON CONCENTRATIONS IN CLEAN AND PERTURBED RURAL AIR

Compound	Clean Situation; 30 August 1975			Urban Plume; 1 September
	8 CST	12 CST	18 CST	5 CST
Ethane	3.1	4.0	4.8	6.2
Ethylene	2.3	1.0	0.8	2.5
Acetylene	0.2	0.4	0.4	2.6
Propane	2.3	3.6	3.7	6.9
Propene	0.0	0.5	0.2	0.6
1-Butane	0.6	0.9	0.8	1.5
n-Butane	1.1	2.1	2.1	4.8
n-Pentane	1.8	1.3	1.1	2.6
Isoprene	0.4	3.7	7.1	4.9
Toluene	1.2	1.0	0.5	2.2
Unknown 1	0.2	0.6	0.6	0.5
Octane	0.2	0.9	0.7	0.7
Unknown 2	1.1	2.0	2.5	2.2
Ethylbenzene	0.0	0.0	0.0	0.5
m-,p-Xylene	0.3	0.2	0.2	1.2
α-Pinene	0.2	0.0	0.0	0.2
Unknown 3	1.7	1.5	2.2	1.8
Others	16.	17.	25.	38.
Total NMHC	33.	42.	53.	79.
CCl_3F	115.	118.	120.	157.

Carbon-Bond Splits

Compound	Value		
	8 CST	12 CST	18 CST
NR	0.14	0.15	0.13
PAR	0.16	0.19	0.15
ETH	0.07	0.085	0.07
OLE	0.001	0.08	0.11
ARO	0.04	0.024	0.01
Unidentified	0.58	0.5	0..57

Note: Concentrations of hydrocarbons are in μg/m^3.
Concentrations of CCl_3f are in ppt v.

Source: Rasmussen, Chatfield, and Holdren. (1977)

TABLE 12. VALUES AND RANGES OF OBSERVED HYDROCARBON CONCENTRATIONS

No.	Constituent	Minimum	Quartile	Median	Quartile	Maximum	Cases
1	Ethane	1.7 8/27 15	2.5	3.0 (2.8,3.1)	3.5	7.3 8/24 10	80
2	Ethylene	0.0 8/27 15	0.7	1.0 (0.9,1.2)	1.5	4.0 8/31 3	80
3	Acetylene	0.0 8/24 7	0.2	0.4 (0.3,0.4)	0.5	0.8 8/29 3	80
4	Propane	0.2 8/25 15	2.0	2.7 (2.5,2.9)	3.4	6.6 8/24 10	80
5	Propene	0.0 8/25 17	0.2	0.4 (0.3,0.4)	0.5	1.0 8/29 1	80
6	I-Butane	0.4 8/31 19	0.7	0.9 (0.8,0.9)	1.1	2.7 8/24 15	80
7	N-Butane	0.6 8/27 15	1.3	1.6 (1.5,1.7)	2.0	5.2 8/31 9	80
8	Sum 1 to 7	5.0 8/27 15	9.0	10.0 (10.0,11.0)	12.0	22.0 8/24 10	82
9	N-Pentane	0.5 8/29 23	1.2	1.4 (1.3,1.4)	1.6	6.4 8/27 21	80
10	Isoprene	0.0 8/31 5	2.0	3.7 (3.3,4.9)	6.0	17.0 8/29 19	80
11	Toluene	0.5 8/25 15	0.9	1.1 (1.0,1.2)	1.6	4.4 8/26 21	69
12	Unknown 1	0.0 8/28 7	0.6	1.0 (0.7,1.2)	2.0	5.2 8/21 11	71
13	Octane	0.0 8/28 7	0.5	0.7 (0.6,0.8)	1.2	4.0 8/21 11	71
14	Unknown 2	0.7 8/29 13	1.4	2.0 (1.8,2.2)	2.7	7.0 8/30 19	70
15	Ethylbenzene	0.0 8/27 13	0.0	0.3 (0.2,0.3)	0.4	1.3 8/26 21	70
16	m & p-Xylene	0.0 8/27 13	0.2	0.4 (0.3,0.4)	0.6	3.3 8/26 21	70
17	Al Pinene	0.0 8/21 11	0.0	0.2 (0.1,0.3)	0.4	1.4 8/26 21	69
18	Unknown 3	0.0 8/27 19	1.2	1.5 (1.5,1.7)	1.8	3.1 8/20 19	68

TABLE 12. (Concluded)

19	Others	9.0 8/28 13	17.0	21.0 (19.0,23.0)	27.0	63.0 8/26 21	71
20	Sum 9 to 19	16.0 8/26 5	29.0	36.0 (33.0,38.0)	43.0	92.0 8/26 21	71
21	NMTHC	27.0 8/26 5	38.0	48.0 (44.0,51.0)	54.0	103.0 8/26 21	71

Notes:

1. The entries directly beneath each minimum and maximum give the date and time of that extremum. For example, the maximum acetylene reading occurred on August 29 at 3 CDT.
2. The figures under the median give a non-parametric measure of the confidence interval for that median. See the text.

present reactive hydrocarbon measurements from the study of Grosjean, 1980; and Rasmussen, Chatfield, and Holdren, 1977. These data are typical of measurements that show low concentrations of RHC and that might be taken as examples of "clean air" in the planetary boundary layer. Note that the proportion of unidentified compounds is fairly high, 21 percent in the California study and over 50 percent for the Missouri site.

The minimum NMHC concentrations observed by Rasmussen, Chatfield, and Holdren (1977) was 27 μgm/m^3 or 38 ppb. Grosjean (1980) reported boundary layer minima NMHC as low as 12 μgm/m^3 (17 ppb), while measured concentrations aloft were from 2 to 4 μgm/m^3 (3 to 6 ppb), with unreactive ethane as the principal constituent. The Scott Research data base is presumably influenced strongly by urban emissions. The minimum ground measurement of 35 ppb is consistent with the other data sets, however. Airborne monitoring by Scott Research (1970) did not exceed 1500 ft. in altitude; however, airborne concentrations were lower than ground values. Minima aloft were as low as 10 to 20 ppb.

On the basis of our examination of these data sets, we suggest that nonmethane hydrocarbon concentrations in the planetary boundary layer (which has a thickness of perhaps 100 to 1000 meters), may be as low as 15 ppbc (0.015 ppmc). Concentrations as low as this are rare, however, occurring only under strong ventilation conditions (e.g., after rainstorms) when the boundary layer air has been mixed with the cleaner air aloft. Concentrations of 30 to 50 ppbc are typically observed, with long-range transport of hydrocarbons allowing concentrations as high as 100 to 200 ppbc (0.1 to 0.2 ppmc) downwind of continental land masses. Such high background concentrations are almost certainly the result of transported anthropogenic emissions.

Available data suggest that "clean air" (i.e., air relatively uncontaminated with anthropogenic emissions) has a higher hydrocarbon loading over land than over water, presumably reflecting biogenic emissions from land plants. Background reactive hydrocarbons ascribable to biogenic emissions are highest in the fall (Jeffries 1981, private communication). Stevens et al. (1972) attributed this fall maximum to chemical degradation of chlorophyll.

Table 13 contains our recommendations for background hydrocarbons for atmospheric modeling within the planetary boundary layer. Our lower limit estimate has a hydroxyl to peroxyl conversion reactivity of 128 min^{-1}, which is only twice that of methane and its products. Paraffinic hydrocarbons, the least reactive species, are specified as the only reacting compound.

TABLE 13. RECOMMENDED BACKGROUND OF REACTIVE HYDROCARBONS

Carbon Fraction		Concentration	CBM Species	
Low	0.91	0.03 ppmC	PAR	0.03 ppmC
	0.09	0.003 ppm	CARB	
		0.1 ppm	CO	OH to RO_2 reactivity = 125
Mid	0.61	0.035 ppmC	PAR	0.043 ppmC (+ 0.015 ppm CARB)
	0.083	0.0008 ppm	ARO	
	0.034	0.001 ppm	ETH	
	0.014	0.0004 ppm	OLE	
	0.26	0.015 ppm	CARB	OH to RO_2 reactivity = 387 min^{-1}
	0.0005	0.00003 ppm	DCRB	
		0.2 ppm	CO	
High	0.57	0.1 ppmC	PAR	0.144 ppmC (+ 0.03 ppm CARB)
	0.07	0.002 ppm	ARO	
	0.12	0.01 ppm	ETH	
	0.07	0.006 ppm	OLE	
	0.17	0.03 ppm	CARB	
	0.0005	0.00008 ppm	DCRB	OH to RO_2 reactivity 1153 min^{-1}
		0.5 ppm	CO	

Note: All estimates include 0.015 ppmC PAR as surrogate for background methane.

The middle reactivity, or our "best" estimate, has a hydrocarbon concentration of 0.043 ppmc in equilibrium with 0.015 ppm carbonyl compounds. The total hydroxyl to peroxyl reactivity is ≈ 400 min^{-1}. This agrees well with our general reactivity estimates based on observed carbon monoxide, and the hydrocarbon concentration is typical of measured background. The fractional hydrocarbon composition reflects compositions of the previously mentioned rural monitoring studies. The suggested hydrocarbon compositions are similar to the composition of typical urban emissions, (Killus and Whitten 1982b), except that the aromatic fraction is less.

Carbonyl concentrations in our mid-range estimate are based on a specific equilibrium situation where hydrocarbons in a reacting mixture are replaced as soon as they are destroyed. Thus the degree of oxidation of the mixture is midway between "fresh" and "spent." This is the point at which carbonyl concentrations are highest as a fraction of total reactive carbon. If emissions into the air mass of background hydrocarbons cease, the carbonyl fraction will drop rapidly, as will the concentrations of the more reactive compounds such as olefins and aromatics. The existence of measurable concentrations of olefins, for example, is evidence of recent emissions of reactive hydrocarbons.

Hydroxyl reactivity is our mid-range estimate can be apportioned as follows: 24 percent CO, 13 percent paraffins, 13 percent fresh reactives (aromatics, olefins, and ethylene), and 50 percent carbonyls. Carbonyl concentrations are about one third the concentration of reactive hydrocarbon. In a "spent" air mass, (e.g., our lower background estimate) the carbonyl component is only 10 percent of the RHC concentration, yet it accounts for one third of the reactivity.

Several points should be made concerning our high estimate. Not only is the hydrocarbon concentration much higher than the mid-range estimate, but the reactivity of the hydrocarbons (excluding carbonyls) is higher as well. However, the carbonyl fraction is lower than the mid-range estimate, indicating a departure from photochemical equilibrium. It is our feeling that hydrocarbon concentrations as high as this upper limit estimate are transitory, reflecting either temporary pulses of biogenic emissions (e.g., autumn emissions) or anthropogenic contamination, or both. Thus, both the carbonyls (CARB) and CO, are less than would shortly develop as this mixture reacts, and therefore less than would be calculated from our equilibrium criteria.

The hydroxyl to peroxyl reactivity of the high background estimate is ≈ 1200 min^{-1} (≈ 1000 min^{-1} excluding CO). Modeling of background reactivity experiments in the University of North Carolina outdoor smog chamber also requires a reactivity of 1000 min^{-1} excluding CO (Killus and Whitten 1982b). Since there is evidence that the UNC smog chamber is a hydrocarbon source under some conditions, we take this reactivity as an upper limit. In a study that modeled the ozone formation in a power plant plume (observed by Miller et al. 1978), Stewart and Liu (1980) specified ambient hydrocarbons equivalent to a reactivity of 900 min^{-1}. In this case, transport from an urban area was estimated to be responsible for about half of the hydrocarbon involved.

5.1.4 Background Hydrocarbon Reactivity Effects on Atmospheric Models

The three estimates of background pollutant composition and concentration levels shown in Table 13 represent the high, best, and low estimates resulting from our study of atmospheric reactivity. These estimates represent typical observations seen throughout the day. They do not represent initial conditions such as the 0600 to 0900 values associated with urban smog studies or methods such as the EKMA. However, the isopleth-generating program sometimes used with the EKMA (OZIPM) was used to generate the isopleths shown in Figures 49 through 52. These diagrams were constructed to supplement the background pollutant reactivity study through practical illustration of the ozone-forming potential of these composition estimates. The model chosen to generate the isopleths is very simple: the chemistry (CBM-II, Stewart and Liu, 1980) was modified so that all hydrocarbon loss reactions exactly compensated for the loss of the hydrocarbon species involved. For example, the olefin reaction with the hydroxyl radical (OH) was modified to include the olefin among the reaction products. An exception to this simple approach involved the carbonyls, which are already generated by several pathways within the mechanism. The only significant sources for the other hydrocarbon species are the initial conditions and emissions. This treatment keeps all precursor concentrations as constant as possible during the single-day simulations.

Although background air, in general, may have diurnal variations in reactivity, these variations are not well documented. Indeed, measurements of background air are often reported without reference to the time of day at which the measurements were taken. Hence, the model was set up to demonstrate the amount of ozone generated by a given average precursor concentration in one day.

The nitrogen oxide concentrations were not as easily kept constant. The main source of NO_x is emitted as NO, but the main sink for NO_x is the loss of NO_2. Two approaches were used to bracket the situation in some way. In one approach, the NO_2 was included in the product list of NO_x

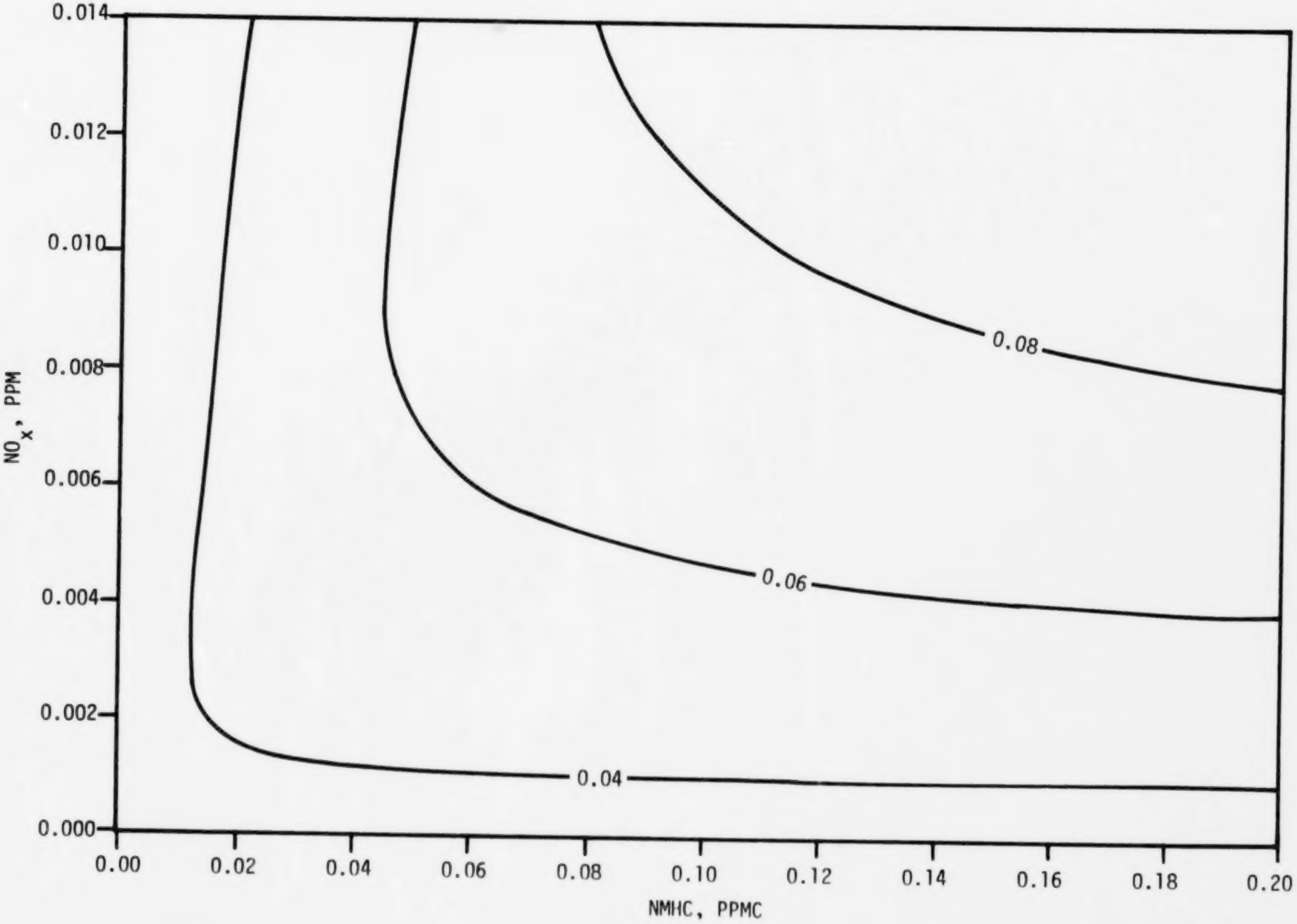

FIGURE 49. SPECIAL CBM-EKMA ISOPLETH WITH LOW-RANGE BACKGROUND LEVELS (NO_x EMISSIONS)

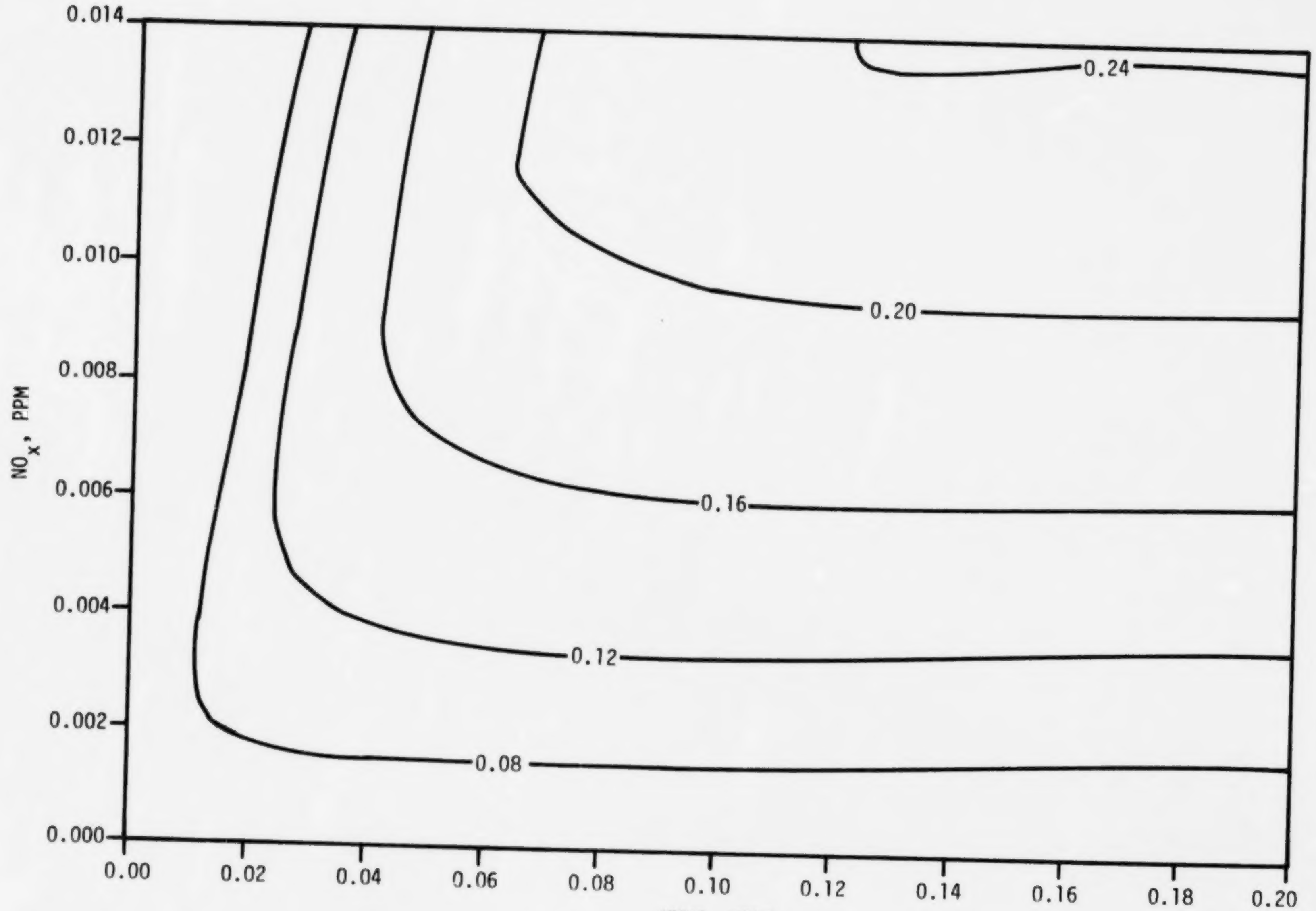

FIGURE 50. SPECIAL CBM-EKMA ISOPLETH WITH MID-RANGE BACKGROUND LEVELS (NO_x EMISSIONS)

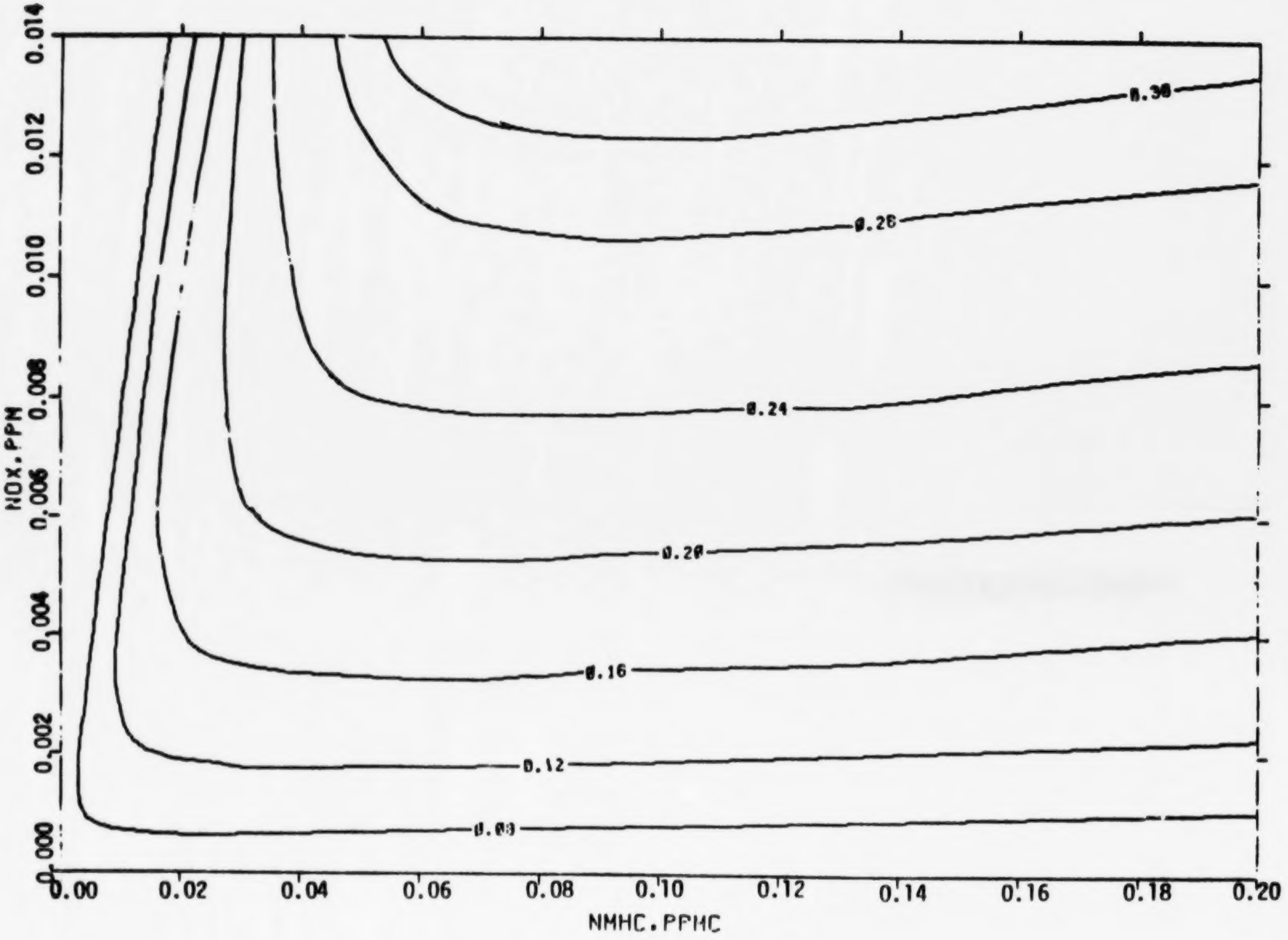

FIGURE 51. SPECIAL CBM-EKMA ISOPLETH WITH HIGH-RANGE BACKGROUND LEVELS (NO_x EMISSIONS)

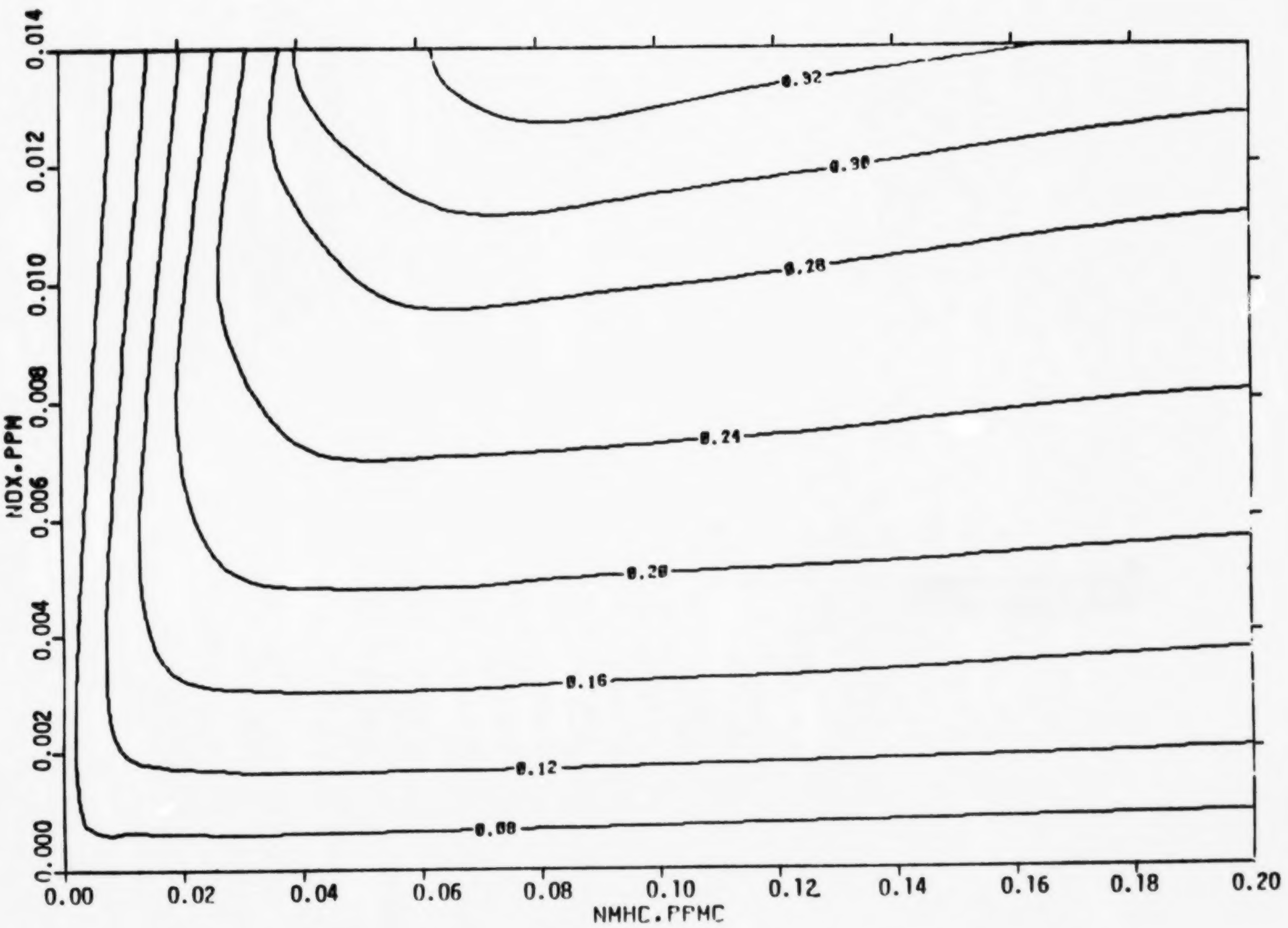

FIGURE 52. SPECIAL CBM-EKMA ISOPLETH WITH HIGH-RANGE BACKGROUND LEVELS

loss reactions. In the other approach, 10 percent of the initial-condition NO_x was emitted into the model during each hour of the simulation. Both approaches tended to generate similar and constant NO_x levels in the simulations and, in turn, generated similar results. When compared with Figure 51, Figure 52 represents the greatest difference between the two approaches. Figure 52 shows the high reactivity mix using NO_2 as a product in the NO_x sink reactions. Figures 49 through 51 were generated using the 10-percent-per-hour emission of NO_x.

At the very lowest HC/NO_x ratios, the two NO_x approaches differed as expected, but even then, the differences were small. The results were expected to differ because the emitted NO_x used in the OZIPP/EKMA type of model is 90 percent NO. Some additional hydrocarbon is, therefore, necessary to convert the NO to NO_2, yet the other approach had the equivalent of pure NO_2 emissions and did not require the HC necessary to handle the extra initial NO-to-NO_2 conversion. In the isopleth diagrams, this extra required amount of hydrocarbon shows up at the low HC/NO_x ratios as angled isopleth lines. If pure NO_2 is emitted, the low NC/NO_x isopleth lines tend to be less angled and almost vertical.

Note that each of the three base-case concentrations of estimated background precursor mixes is NO_x-limited. This is consistent with other models of tropospheric ozone formation (e.g., Fishman and Crutzen 1978). It is unrealistic to consider any single NO_x concentration as representative of the entire free troposphere (Singh et al., 1980; Noxon 1978). The concentration of background O_3 ($\approx$ 0.04 ppm) places an upper limit on the possible NO_x concentrations.

5.2 BACKGROUND REACTIVITY IN SMOG CHAMBERS

The use of smog chambers to experimentally simulate the behavior of urban smog formation introduces the problem of background reactivity associated with the chamber itself. Surface to volume ratios for smog chambers range from 0.01 to 0.2 cm^{-1}. The surface to volume ratio for an urban smog setting with a mixing depth of only 100 meters is 10^{-4} cm^{-1}, two orders of magnitude less than the largest smog chamber.

In addition to the reactivity of the background air, smog chambers affect the experimentally observed photochemistry via adsorption/desorption of trace species by the chamber walls. To the extent that these processes vary, experiments become less reproducible. The greater the influence of the chamber-specific process, the more difficult becomes the task of elucidating the underlying photochemistry.

In our study of seven smog chamber systems (Whitten et al. 1979), we defined four areas of chamber effects: analytical, wall, temperature, and lighting. We confine our discussion to the effects of the chamber walls on reactivity; although temperature and lighting effects (including spectral distribution) can be much larger than any wall contamination problem, these phenomena can be generalized to the atmosphere and are therefore not part of the chamber specific reactivity problem.

5.2.1 Tests for Background Reactivity in Smog Chambers

Dimitriades (1976) noted the following traditional tests for chamber reactivity:

(1) Ozone Formation Test: Background (clean) air is irradiated and O_3 formation is measured and followed.

(2) R_{NO_2}- Test: Background air and added NO are irradiated and rate of NO_2 formation (R_{NO_2}) is measured.

(3) Aerosol Formation Test: Background air is irradiated and aerosol formation is measured and followed.

(4) SO_2 Oxidation Test: Background air and added SO_2 are irradiated and loss of SO_2 (and formation of SO_4^{2-}) is measured and followed.

Other chamber tests discussed by Dimitriades were

(1) Ozone Loss Test: Ozone loss in the chamber is measured in the dark and under irradiation.

(2) NO_2 Loss Test: NO_2 loss in the chamber is measured in the dark and under irradiation.

(3) Propylene Loss Test: Background air and added propylene are irradiated and loss of propylene and formation of products are measured and followed.

More recently we have studied extensions of the R_{NO_2} test and the ozone formation test. In particular, we have studied the R_{NO_2} test with added CO to assess radical generation and hydroxyl-to-peroxy radical conversion separately. We have also studied the ozone formation in chambers having high concentrations of acetaldehyde to more easily estimate (from PAN formation) the emission of NO_x from chamber walls. We will first discuss the R_{NO_2} test experiments.

5.2.2 Background R_{NO_2} Tests in the UNC Chamber

Experiments in the UNC smog chamber are conducted using ambient air from the area surrounding the experimental facility. In addition to the trace contaminants that might exist in the nighttime rural air of the region, smog precursors from previous experiments, such as formaldehyde and NO_x, might be released from the chamber walls during subsequent experiments. On two days in August 1978, routine smog chamber data were taken for four experiments that did not involve any additional organics. On one day, 14 August 1978, a substantial quantity (~ 0.5 ppm) of NO_x was added to each side of the chamber. On one side, 50 ppm of CO was also added. On the other day, 11 August 1978, both sides of the chamber contained only ambient air. This section describes the results of these ambient air modeling experiments.

Experiments using high NO_x, both with and without CO, offer certain advantages to the study of the reactivity of background air. First, the presence of CO on one side tends to amplify the effect of any radical sources:

> The primary radical sink reaction of hydroxyl radical reacting with NO_2 is suppressed by the hydroxyl radical reacting with CO. For the 14 August 1978 experiment, the hydroxyl radical reaction with CO should always be at least four times faster than the hydroxyl radical reaction with NO_2.

> The source of radicals can be either peroxy radicals such as HO_2, which are rapidly converted to hydroxyl via reaction with the high NO concentration, or hydroxyl radicals, which are rapidly converted to peroxy radicals via reaction with CO. Hence, the length of the NO-to-NO_2 conversion chain is extended and the original radical type is not important.

Second, the presence of high NO concentrations enhances the analytical accuracy for this species. The conversion rate of NO to NO_2 is central to the reactivity issue. However, the number of conversions per reacted precursor molecule is ordinarily very difficult to measure when high levels of ozone are generated because the NO concentrations are usually driven to very low levels, suppressing the rapid NO reaction with O_3. A rapid initial NO-to-NO_2 conversion rate followed by a slow, or virtually absent, conversion rate would be indicative of a small quantity of a highly reactive species. Similarly, a more sustained conversion rate would imply higher concentrations of a moderately reactive species. Thus, the time-dependent shapes of the NO and NO_2 concentration curves are important to the evaluation of background reactivity.

Third, the comparison offered by the dual chamber approach tests the balance between radical sources, NO-to-NO_2 conversion, and loss of NO_x. A pure source of radicals would show substantial NO-to-NO_2 conversion on the side with CO, but virtually none on the side with only NO_x. Although both sides might require some source of initial radicals, a pure hydrocarbon contaminant might decay to oxygenated products that provide an increasing source of radicals; however, a carbonyl type contaminant such as formaldehyde might show a diminishing source of radicals. It is most likely that the background reactivity is made up of some combination of pure hydrocarbons and carbonyls, but an overly accurate determination of an optimum blend is not warranted by the limited number of experiments and analytical data studied here.

The high NO_x dual chamber experiments of 14 August 1978 were simulated using only formaldehyde as the contaminant species. The results are presented in Figures 53(a) and 53(b). The simulation used 5 ppb HONO and 0.18 ppm formaldehyde as initial conditions, in addition to the measured NO_x quantities. The HONO, as well as a wall source of formaldehyde (6×10^{-5} ppm min^{-1}), were both used to be consistent with other experiments. The initial HONO was added to maintain consistency with other experiments involving substantial NO_x, and the wall release of formaldehye was added to be consistent with the simulations of the 11 August 1978 experiment discussed next.

The lack of agreement between the observed and calculated ozone levels is not considered important because high levels of NO relative to O_3 were present in the sampling line. As discussed in Whitten, Killus, and Hogo (1980), the value of k_1, the NO_2 photolysis constant, goes to zero in the sampling line, and ozone decays rapidly as a result of the high level of NO present. For NO levels near 0.2 ppm, the ozone lifetime is only about 12 seconds.

The twin experiments of 11 August 1978 using only the background air were also simulated using formaldehyde. The NO_x data for these two experiments show a rapid initial buildup of NO_2 that was simulated very simply using $NXW \rightarrow NO_2$, with a rate constant of 0.01 min^{-1} and an initial condition of NO_x on the wall (NXW) of 0.02 ppm. The NO_2 concentration was maintained by a term intended to simulate slow but continuous release of

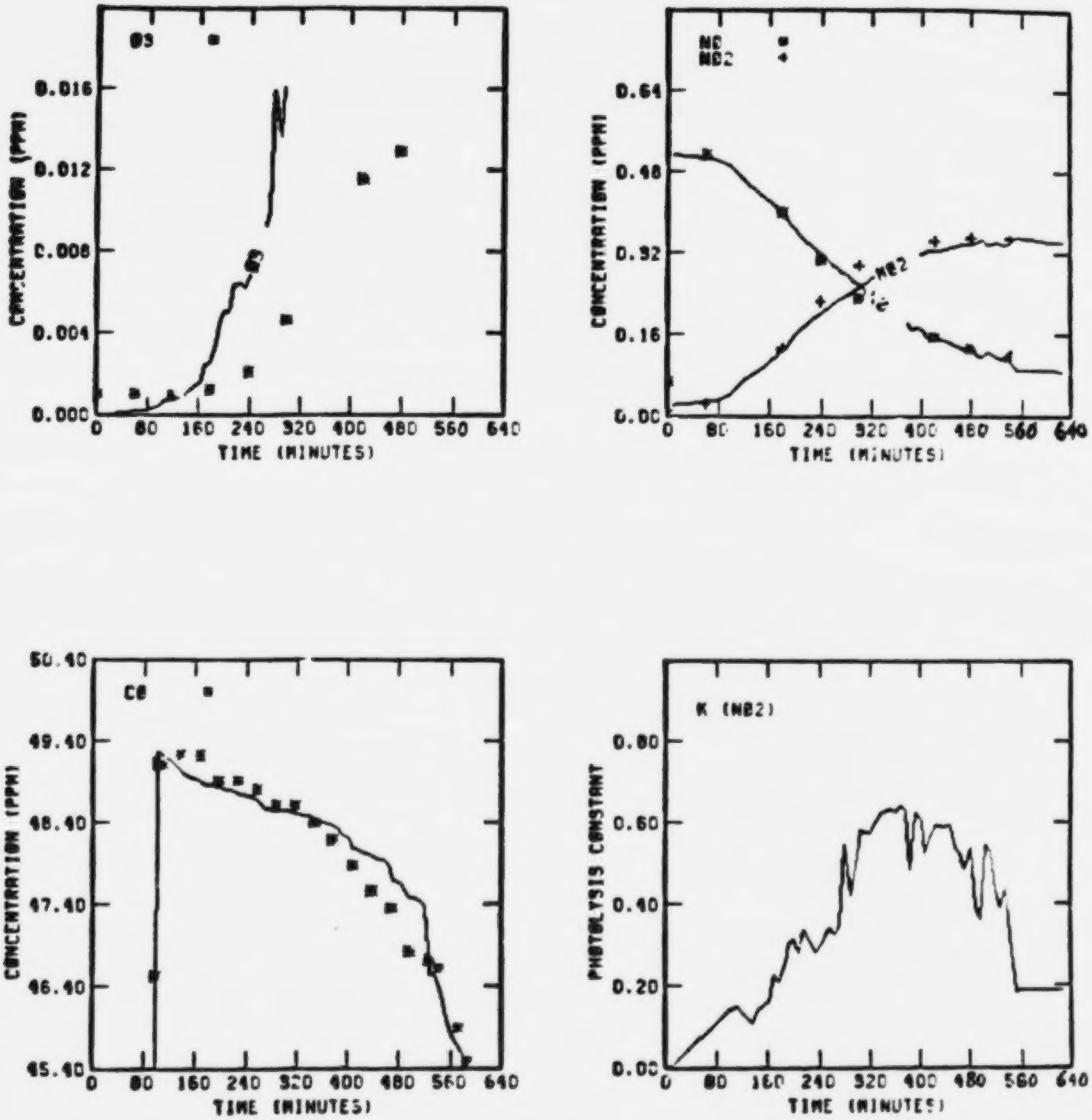

(a) 14 August 1978, UNCB

FIGURE 53. SIMULATION RESULTS FOR UNC EXPERIMENTS

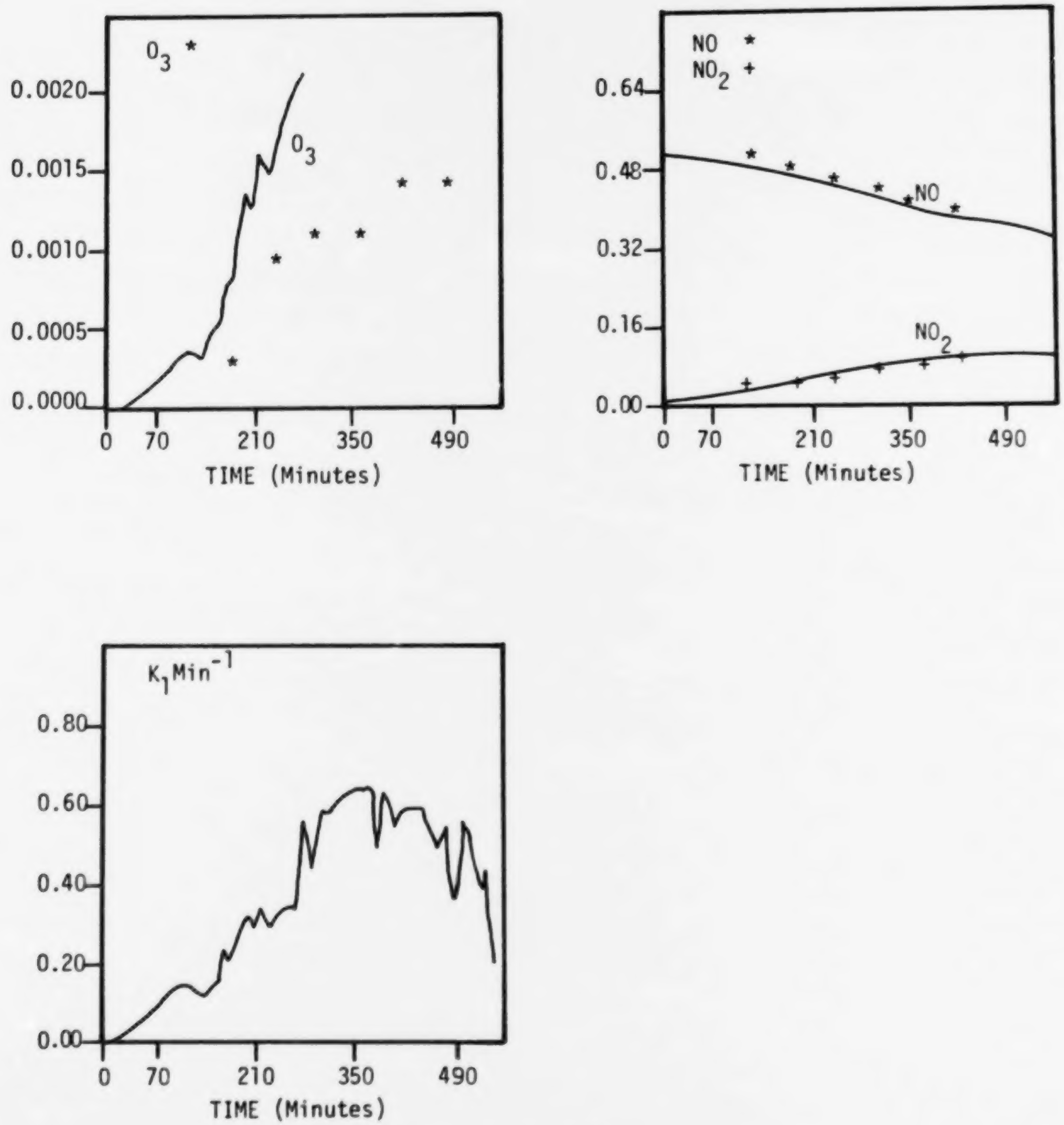

(b) 14 August 1978, UNCR

Figure 53 (Continued)

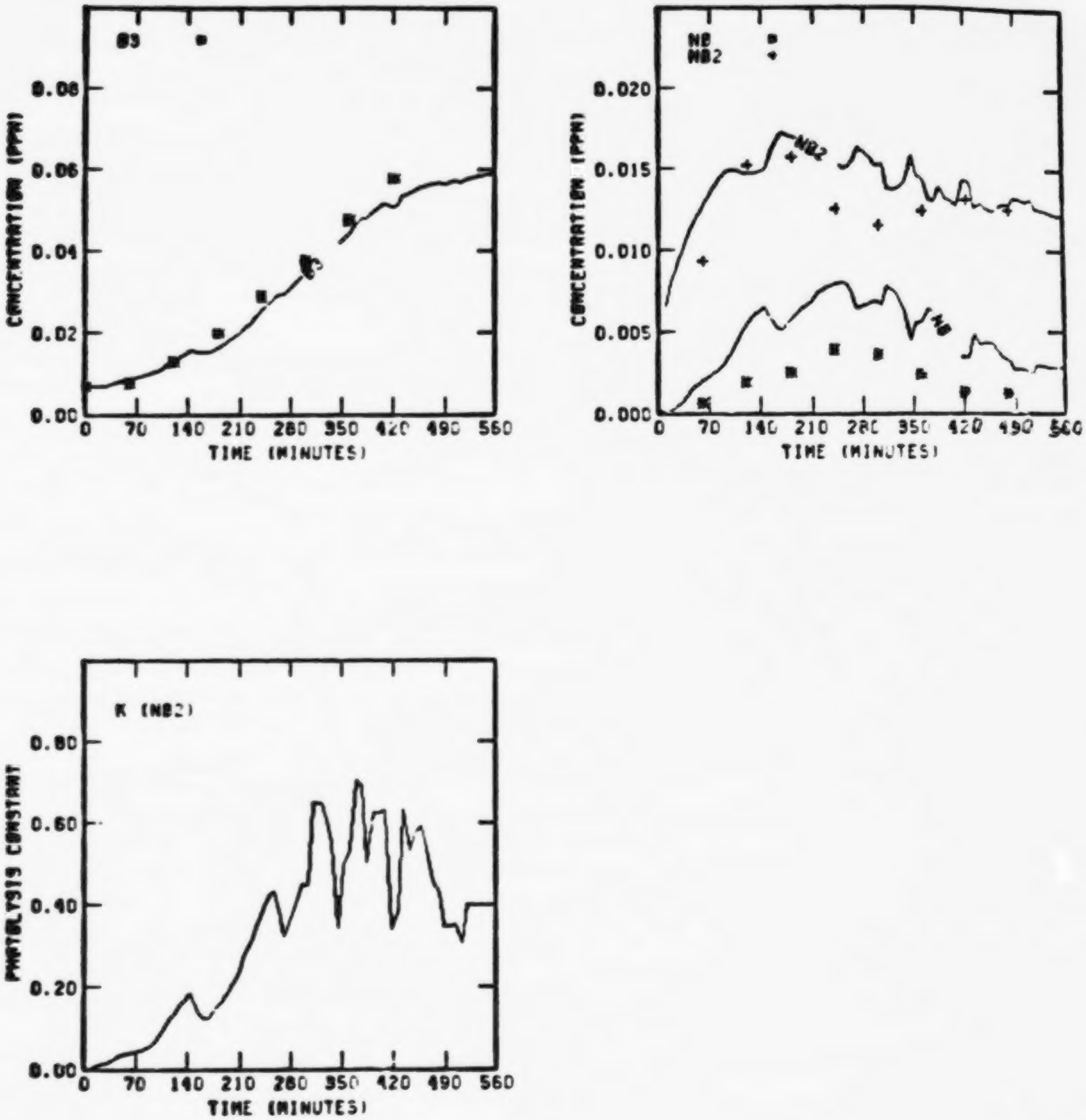

(c) 11 August 1978, UNCR

FIGURE 53. (Continued)

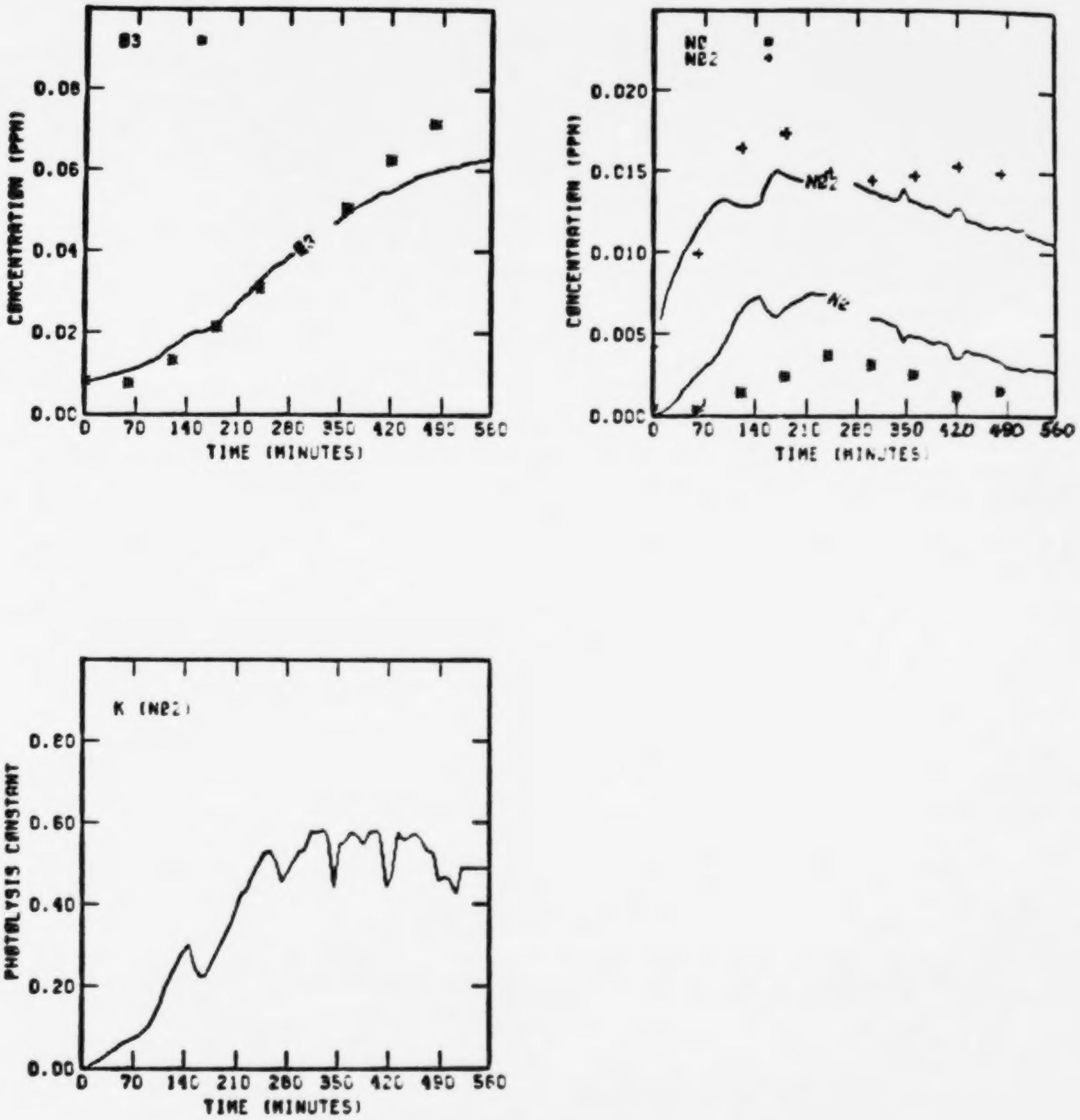

(d) 11 August 1978, UNCB

FIGURE 53. (Concluded)

NO_2 from the walls at 1.5 x 10^{-5} ppm min^{-1}. The formaldehyde initial concentration was set at 0.04 ppm, with a further 0.03 ppm ramped in at 6 x 10^{-5} ppm min^{-1}. The simulation results are illustrated in Figures 53(c) and 53(d).

Although these simulations do not prove that formaldehyde from previous experiments is released from the chamber walls, they do provide a good estimate of the background reactivity found in the UNC experiments, in addition to a measure of variability. The variability seems to be high; the two experiments we have modeled differ by a factor of three.

Recent experiments with the UNC chamber have supported the formaldehyde-release hypothesis. Subsequent blank runs (no added emissions) have been shown to generate 0.065 ppm formaldehyde by the end of the day (Jeffries, private communication). The blank runs also generated 0.2 ppm ozone, owing to the small emission of NO_x from the chamber walls into chamber air. The difference between the 0.2 ppm ozone blank runs and the 0.06 ppm ozone generated in the blank run of 11 August 1978 underscores the variability of the UNC background reactivity. Researches at UNC are currently experimenting with a procedure for removing liquid water from the chamber walls. The "dry down" may also remove formaldehyde and so might reduce background variability in the UNC chamber. Since the chamber background reactivity estimated here is presently 2 to 6 times our estimate of middle background reactivity of the lower troposphere, further cleaning of the chamber might allow direct observation of the reactivity of the rural atmosphere.

5.2.3 NO_x Emission Tests

The generation of significant ozone (~ 0.2 ppm) in smog chambers without the direct addition of precursors can be explained by emission of small amounts of nitrogen oxides from the chamber walls. At low concentrations (~ 1-10 ppb), NO_x generates ozone very efficiently; the stoichiometry of the process can be as high as 5 to 10 moles of ozone per mole of emitted NO_x.

An extension of the blank chamber generation of ozone involves the introduction of high concentrations of acetaldehyde into the chamber. One example of this methodology is experiment EC-253, performed at UCR using a large evacuable chamber. Such an experiment is sensitive to the release of NO_x from the chamber walls. During the experiment, PAN increased up to 40 ppb in six hours, yet NO_2 and NO remained below the detection limit of 10 ppb. Evidently, most NO_x leaving the chamber walls is held in the gas phase as PAN, which can be readily monitored with the PAN analyzer. Without acetaldehyde as the dominant organic species, the NO_x would typically be converted to HNO_3, a species that is not only difficult to measure, but is also subject to absorption by the walls. The NO_x "off gassing" from the walls was modeled for experiment EC-253 by a simple zero-order reaction that produced NO at the rate of 1.0×10^{-4} ppm min^{-1}. The production of PAN and ozone were successfully simulated, as shown in Figure 54.

5.3 RADICAL SOURCES IN THE UCR CHAMBER

In a recent paper, Carter et al. (1981) presented preliminary evidence for a chamber-associated radical source. A more comprehensive analysis of data concerning this phenomenon by these authors is forthcoming (Carter et al., 1982, in press). Most experiments performed by Carter et al. (1981) used a tracer technique that inferred OH radical levels from the decay of small amounts of propene relative to propane. Radical source strength was then calculated on the basis of the source needed to compensate for the loss of OH through reaction with NO_2. The apparent radical source strength was found to depend on the temperature, relative humidity, light intensity, and NO_2 concentration. Data for experiments at 303 K and 50 percent RH were presented in the form of a regression equation:

$$\text{flux (ppb min}^{-1}) = k_1\ [(0.34 \pm 0.06) + (2.7 \pm 0.2)\ [NO_2] \quad .$$

We have demonstrated that this equation is incorrect because of the interference caused by the attack of oxygen atoms and ozone on propene at high NO_2 concentrations (private communication to W.P.L. Carter). Since the calculation for OH flux depends on the NO_2 concentration, and since both O^3p and O_3 increase with NO_2 concentrations, the interference effects are quadratic for NO_2. The apparent OH flux for the propene/propane tracer technique can be estimated as

$$\text{"}O^3p\text{ OH flux" (ppb min}^{-1}) = 0.58\ [NO]_2^{\ 2}\ k_{\ 1} \quad ,$$

$$\text{"}O_3\text{ OH flux" (ppb min}^{-1}) = 0.27\ [NO_2]^2\ k_1/NO \quad .$$

Figure 55 shows a plot of the OH radical flux as originally characterized by the UCR researchers. In addition to the correction curve for O^3P, the ozone curve exceeds that for O^3p at NO concentrations of less than approximately 0.5 ppm.

Correction for oxygen atoms and ozone greatly reduces the "NO_2 effect" (the apparent tendency for OH levels to remain constant with increasing NO_2, associated with a source of OH that is linked to NO_2). We suspect that this

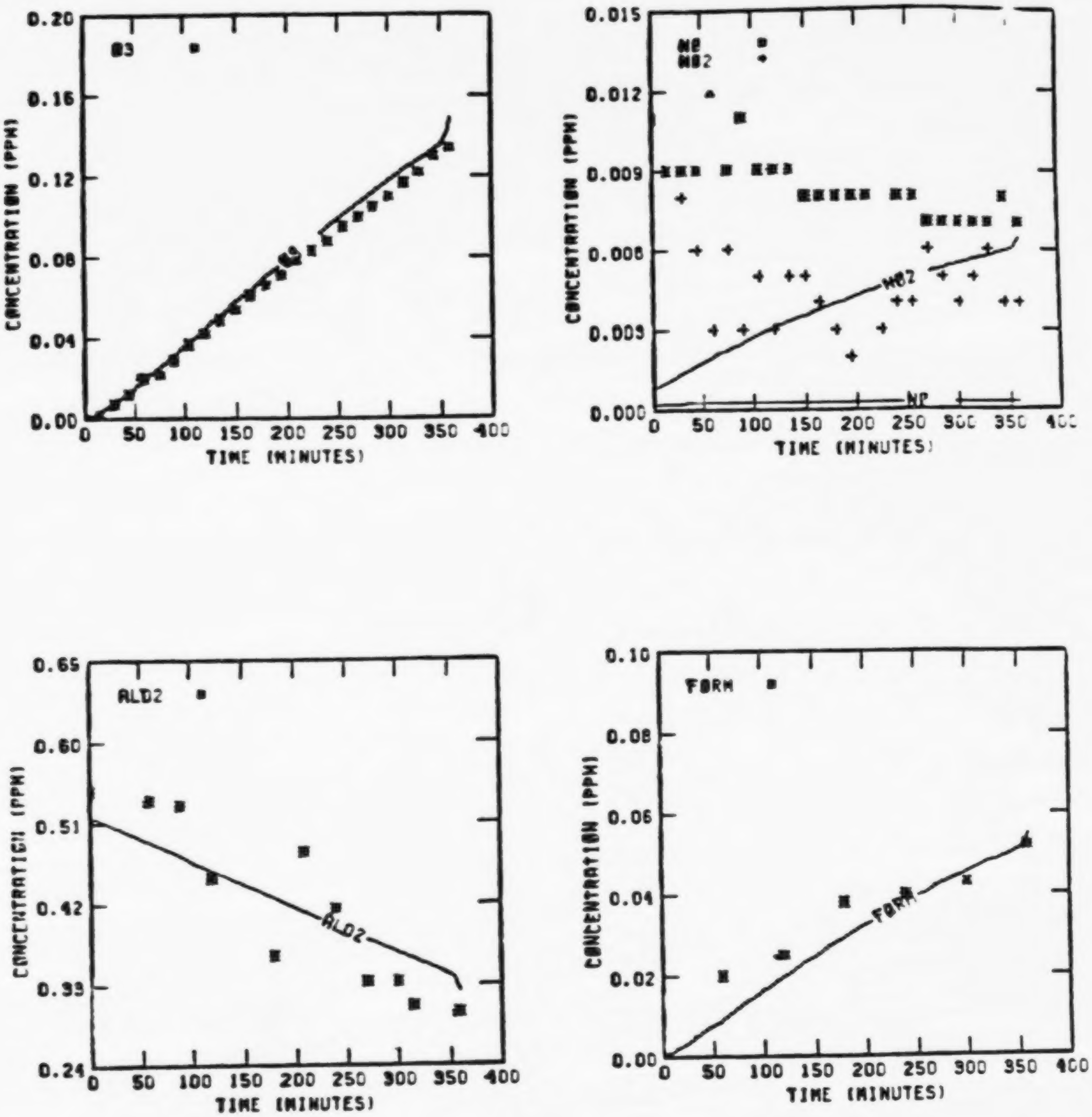

FIGURE 54. SIMULATION RESULTS FOR EXPERIMENT EC-253

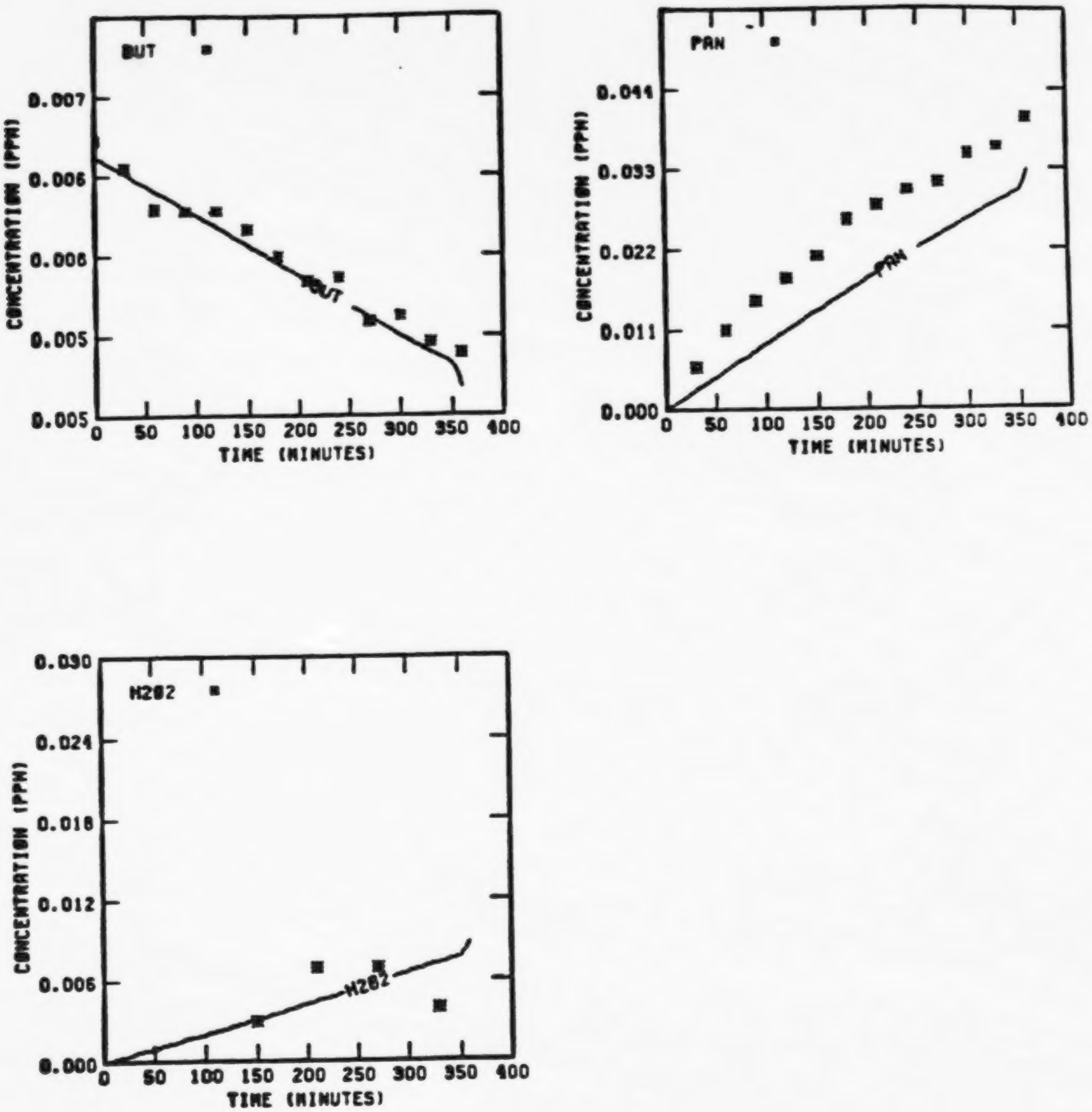

FIGURE 54. (Concluded)

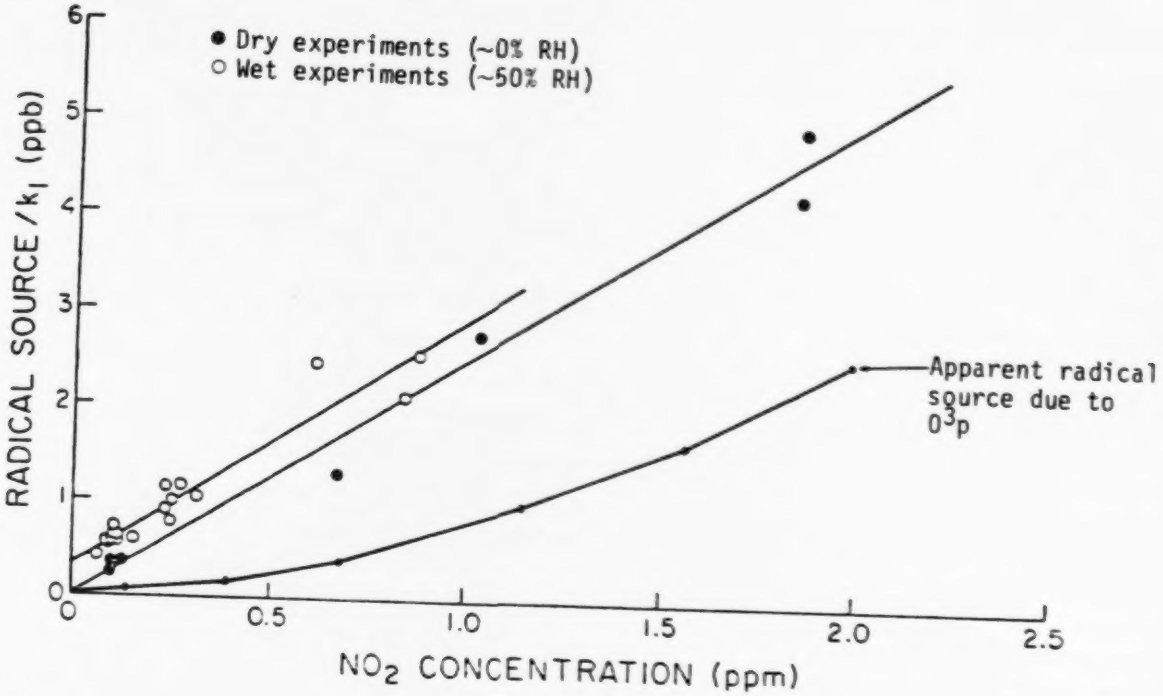

Source: Carter et al. (1982)

FIGURE 55. PLOT OF (RADICAL SOURCE/K_1) AGAINST NO_2 CONCENTRATION AT 303 K.

effect is, in part, an artifact of the tracer methodology and that NO_2-linked sources of OH, if any, are small. This topic is discussed in detail in a subsequent section.

Although we question the precision of the propene/propane tracer methodology, we believe that the UCR researchers have made a significant advance in the experimental characterization of the magnitude of radical production in the UCR chamber. The following section examines that evidence and the possible sources of the background reactivity in the evacuable chamber facility. Currently, the researchers at Riverside have released their data in summary form only; therefore, the following analysis is preliminary and is meant to provide rough estimates only.

5.3.1 The "Dirty Chamber" Effect

The UCR chamber emits a variety of chemical species from its walls. We first consider hydrocarbon species. Table 14 presents experiments for which hydrocarbon contamination can be estimated. In the listed experiments, certain observed species can be ascribed to chamber contamination, either because no hydrocarbons were added to the chamber or because the observed species could not have been formed from the hydrocarbon that was used (e.g., PAN is not a known product of formaldehyde oxidation).

Because of chemical reactions at the end of the experiment, the integrated emissions of oxygenated species are somewhat higher than the observed concentrations. Table 15 presents estimates of typical emissions of various reactive compounds under standard conditions.

TABLE 15. TYPICAL EMISSIONS OF HYDROCARBONS FROM THE UCR EC WALLS

Hydrocarbon	Emission (ppb/min)
HCHO	0.08
Acetaldehyde	0.06
Propionaldehyde	0.04
Buryraldehyde	0.02

It is also significant that an increase in humidity seems to cause an increase in emissions. This effect is to be expected, since polar compounds are more readily desorbed in the presence of water vapor. Elevated temperatures would also be expected to increase the wall emissions of oxygenates.

TABLE 14. EXPERIMENTS FOR WHICH HYDROCARBON CONTAMINATION CAN BE ESTIMATED FROM PITTS ET AL. (1977; 1979)

		Contaminant Concentration (ppb)		
Experiment	Experimental Conditions	Compound	Initial	Maximum
EC-1	Dark	Ald2	4	6
	(RH ~ 30%)	Acetone	11	26
EC-6	Pure Nitrogen (K_1 = 0.24)	O_3	0	22
	(RH ~ 0)	NO_x	6	11
		Aldz	1	2
		Acetone	5	12
EC-9	Pure Air (K_1 = 0.23)	Ald2	6	10
	(RH ~ 50%)	HCHO	3	14
		Propald	1	2
		Acetone	8	30
		NO_x	80	90
		O_3	0	36
EC-38	Pure Air (K_1 = 0.25)	NO_x	19	26
	(RH ~ 40%)	O_3	0	42
		PAN	0	2
		Acetone	2	22
		C4-N	2	8
		Ald2 & MEK	1	1
EC-40	Dark, [High NO_x & N-C4]	Ald2	2	4
	(RH ~ 40%)	Acetone	3	7
		MEK	1	2
EC-250	Formaldehyde only	O_3	0	210
	RH ~ 50	PAN	0	7
	(K_1 = 0.3)	Ald2	1	6
		Propald	0	2
		Acetone	1	38
		Ethene	3	2
EC-251	Formaldehyde + NO_x	O_3	0	271
	(RH ~ 53%)	Ald2	1	5
	(K_1 = 0.3)	PAN	0	9
		MEK	0.5	1.6
		Propald	0.4	2

TABLE 14. (Concluded)

Experiment	Experimental Conditions	Contaminant concentration (ppb)		
		Compound	Initial	Maximum
EC-252	Formaldehdye + NO_x RH ~ 52% $K_1 = 0.3$	O_3	0	24
		Ald2	1	5
		MEK	0	2
		Ethene	3	2
		Propald	0	1
		Butald		0.4
EC-156	Ethene + NO_x RH ~ 60% $K_1 = 0.34$	PPN	0	3
	(EC-153 NAS Multiolefin including Butene-1)	Butald	0	4
		Propald	0	16
EC-143	Ethene + NO_x RH ~ 60% ($K_1 = 0.33$)	PPN	0	9
		Butald	0	4
EC-142	Ethene + NO_x RH ~ 60%	Propald	0	8
		Butald	0	4

The desorption of reactive compounds from the chamber walls thus exhibits some principal characteristics of the radical source seen in the UCR chamber.*

Compounds observed to be emitted in the UCR chamber photolyze too slowly to account for the radical sources indicated in the experiments of Carter et al (1981). We estimate that the measured background of approximately 0.02 ppm aldehydes can account for a radical source of 0.06 ppb/min, at most, under typical conditions, which is perhaps 25 percent of the indicated source strength.

However, it seems plausible that a number of unmeasured oxygenated compounds are emitted by the UCR chamber walls. Dicarbonyl compounds are possible candidates for some of the radical sources. Methyl glyoxal, in particular, has the requisite properties of a high photolysis rate and a strong affinity for water.

One feature of a radical source generated by photolysis of emitted organics is the formation of peroxy radicals. Carter et al. (1981) have argued indirectly that the radicals involved in the chamber source are hydroxyl, rather than peroxy, radicals. The calculated hydroxyl concentration is used to calculate the rate of expected NO loss, given the concentration of reactive compounds (principally CO) that convert OH to $RO_2^{\bullet}$. They suggest that the NO loss is completely explained by these processes, and that the introduction of extra conversions (as would be the case for hydrocarbon photolysis to RO_2) can be ruled out.

This argument is not persuasive for a number of reasons. First, the calculated hydroxyl concentration could be too high; it is possible that as yet unidentified processes are responsible for some of the differential propene loss over propane observed in the UCR chamber.

The argument of Carter et al. (1981) also fails to take into account the confounding effect of sources of NO in the UCR chamber. We have previously shown that the UCR chamber emits ~ 0.10 ppb/min NO_x (Whitten, Killus, and Hogo, 1980). If this emission were composed entirely of NO, then NO oxidation would be underestimated by that amount.

---

[*] Another possible source of chamber contamination is the water used for humidification. Akimoto et al. 1979 reported a "water vapor effect" on reactivity that we calculate as equal to a radical source strength of 0.1 to 0.2 ppb/min. This effect was eliminated when water of an ultrahigh purity was used; Sakamaki, Akimoto, and Okuda (1981) ascribed the earlier effect to reactive impurities in the water.

In addition, the conversion of NO_2 to NO by various processes can be important under certain conditions (e.g., the presence of oxygen atoms). The production of NO from the attack of $O^{3}p$ on NO_2 can be expressed as

$$\frac{dNO}{dt} = [NO_2]^2 k_1 [6.1 \text{ ppb/min}] \quad .$$

This effect becomes appreciable at NO_2 concentrations of as little as 0.1 ppm.

Heterogeneous processes can also be responsible for the conversion of NO_2 to NO. The loss of O_3 to the walls is a net converter of NO_2 to NO, since

$$h\nu + NO_2 \xrightarrow[+O_2]{} NO + O_3 \quad .$$

$$O_3 \xrightarrow{wall}$$

However, this effect is negligible for O_3 concentrations of less than 10 ppb.

Other heterogeneous processes could also convert NO_2 to NO. We describe these in the following section.

5.3.2 Heterogeneous Nitrogen Oxide Transformation Processes

Akimoto et al. (1979) reported dark decay rates for O_3, NO_2, and NO in the NIES chamber, which is a duplicate of the UCR evacuable chamber. The loss rate for NO was small ($\sim 1 \times 10^{-4}$ min^{-1}); however, losses for NO_2 and O_3 were about 0.001 min^{-1} and 0.003 min^{-1}, respectively, for typical humidities. The decay rates for both species showed considerable variation and may not have been linear in concentration.

An experiment reported in Sakamaki, Akimoto, and Okuda (1980) demonstrates that the NO_2 loss is accompanied by some conversion of NO_2 to NO. Figure 56 illustrates data and simulation results for this experiment. For this experiment, only NO_2 was added to the chamber. Irradiation caused the photodissociative production of NO and O_3. NO_2 then declined rapidly, with a slight simultaneous increase in NO and a slight decrease in O_3; toward the end of the experiment, the NO gain and O_3 loss reversed themselves.

The simulation results presented in Figure 56 were obtained using our standard mechanism plus the following chamber-dependent reactions:

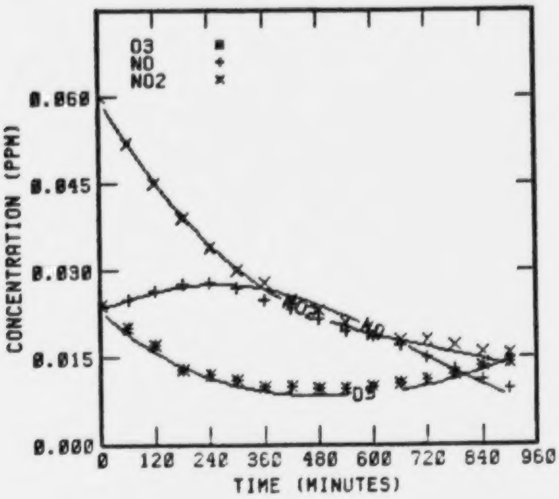

Source: Sakamari, Akimoto, and Okuda (1980)

FIGURE 56. SIMULATION RESULTS FOR NIES.

Reaction	Photolysis Rate
$O_3 \xrightarrow{\text{wall}}$	2.2×10^{-3} min^{-1}
$NO_2 \xrightarrow{\text{wall}}$	1.5×10^{-3} min^{-1}
$NO_2 \xrightarrow{\text{wall}} NO$	8.5×10^{-4} min^{-1}
$\xrightarrow{\text{wall}}$ Form	9.5×10^{-5} ppm min^{-1} .

NO_2 photolysis was 0.26 min^{-1} (a slight increase over the reported value, to account for the observed photostationary equilibrium). Formaldehyde photolysis to radicals was 4.16×10^{-4} min and ozone photolysis to O'd was 10^{-3} min.

The heterogeneous oxidation of NO_2 to nitric acid typically follows either of two stoichiometries:

$$3\ NO_2 + H_2O \rightarrow 2\ HNO_3 + NO$$

$$2\ NO_2 + H_2O \rightarrow HNO_2 + HNO_3 \quad .$$

The simulation results presented in Figure 56 are consistent with the first process. However, we have also simulated the data using the second process. All observed data are matched in the two simulations; OH concentrations differ by as much as a factor of five. Therefore, a question arises concerning the likely yield of HONO relative to NO. Kamens et al. (1981) performed an analysis of the NO_x recycling characteristics of the UNC chamber using the work of Ross (1979) (see Figure 57). In the highly oxidizing region, NO and HONO exist in roughly equal proportions. At lower acidities, NO exceeds HONO by as much as a factor of 10.

To estimate an upper limit for conversion of NO_2 to HONO we take into account the following factors: the loss of NO_2 to the walls is generally less than the loss of ozone. The maximum reported loss of O_3 in the UCR chamber is 1.6×10^{-3} min^{-1}. For an upper limit, we can use NO_2 loss that is equal to O_3 loss. Assuming a 3:1 loss of NO_2 per NO formed, and a ratio of 2:1 for NO_2 loss per HONO emission, equal emissions of NO and HONO would imply a 20 percent yield of HONO. Thus, the upper limit of HONO converted from NO_2 can be stated as

$$NO_2 \xrightarrow{\text{wall}} HONO < 3.2 \times 10^{-4}\ \text{min} \quad .$$

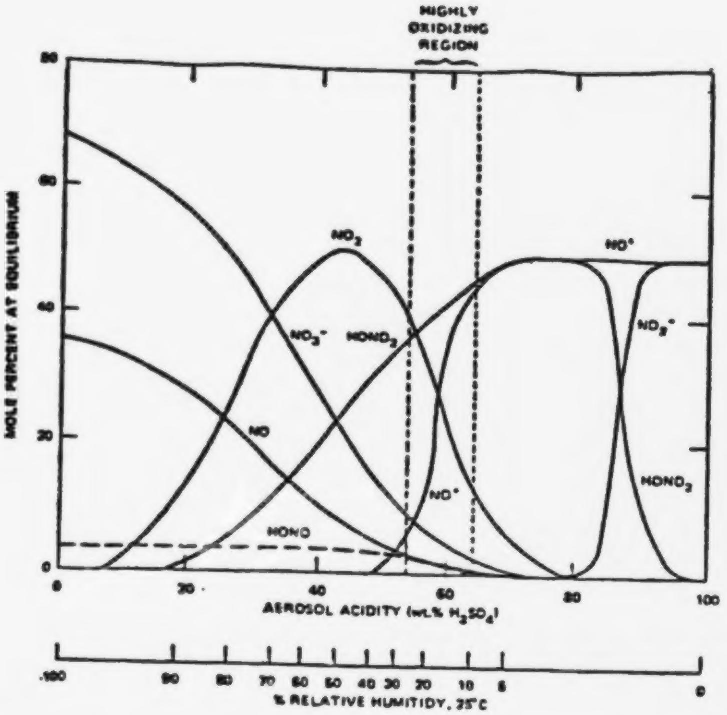

Source: Kamens et al. (1981)

FIGURE 57. ESTIMATED EQUILIBRIUM PROFILES FOR NO_x SPECIES VERSUS AEROSOL ACIDITY (ESTABLISHED FOR AN INITIAL CONDITION OF NO_2 IN EQUILIBRIUM WITH H_2SO_4)

However, since the wall loss of NO_2 is typically one-third the loss of O_3 in the NIES chamber, the same ratio in the UCR chamber gives us a better estimate of 10^{-4} min^{-1}.

This fairly low level of HONO formation is also implied by experiment EC-439 (Carter et al., 1982). In this experiment, the evacuated bakeout of the chamber left the walls in an apparently catalytic state and increased the apparent radical source to 0.23 ppb min^{-1}, from about 0.16 ppb min^{-1} for similar experiments. There was also an indication of a very strong NO_2 loss that we estimate as approximately 7×10^{-3} min^{-1}, using initial and average values of NO_2. Since this NO_2 loss is an order of magnitude greater than that observed in the NIES chamber (and, by analogy, in the UCR chamber as well), a fairly low rate of conversion of NO_2 to HONO is implied.

The fractional contribution of HONO to emitted NO_x is also an important consideration in the assessment of direct HONO emissions from the chamber walls. NO_x has been shown in EC-253 (Figure 54) to be emitted from the evacuable chamber walls at a rate of $\sim$ 0.10 ppb min^{-1}. The maximum ratio of HONO to NO_x in Figure 57 is approximately 10 percent. Assuming a factor of 2 variability in NO_x emissions, we estimate the HONO emission rate to be $<$ 0.03 ppb min^{-1} under standard conditions.

Evidence of HONO storage and release from the chamber walls is provided by EC-460 (Carter et al., 1982). In this experiment, NO was injected into the chamber 27 hours prior to the run. Elevated radical levels were observed that persisted at diminishing levels. Using the increase in radical level and the rate of decrease of the additional radical source, we estimate that the equivalent of 15-20 ppb extra HONO was stored in the walls and was emitted at a rate of 9×10^{-3} min^{-1}, which is a factor of 5-10 times greater than the usual wall emission rate of NO_x and HONO.

5.3.3 Benzaldehyde-Added Experiments

Experiments performed at UCR involving the addition of benzaldehyde to an air/NO_x system offer the strongest corroboration so far of the chamber radical source hypothesis. From the results presented in Table 16, one can see that the addition of benzaldehyde as a radical scavenger does indeed suppress the propene loss in a fashion consistent with the chamber radical hypothesis.

These findings must be cautiously interpreted, however. If propene were being catalytically destroyed by the chamber walls, for example, benzaldehyde would be expected to compete with propene for catalytic sites and would therefore suppress the apparent OH concentration. Similarly, any radical sources from benzaldehyde itself would be a confounding factor.

TABLE 16. UCR EXPERIMENTS INVOLVING THE ADDITION OF BENZALDEHYDE TO AN AIR/NO_x SYSTEM

Experiment	Percent Relative Humidity	Initial Concentration		BZA Added			OH 10^{-8} ppm†		Radical Source (Calculated) (ppb/min)	
		NO	NO_2	Average NO*	Average NO_2	Average BZA	60 Min before BZA	After BZA	Before BZA	After BZA
EC-623	~ 10	0.463	0.099	(0.44)	0.112	~ 0.9	5.65	0.46	0.092	0.083
EC-638	~ 50	0.392	0.068	(0.25)	0.137	1.2	12.1	0.6	0.135	0.157
EC-646	~ 50	0.398	0.095	(0.27)	0.155	0.63	14.7	1.36	0.23	0.21
EC-647a	~ 50	0.797	0.142	(0.7)	0.168	1.09	12.0	1.28	0.28	0.31
EC-647b	(0.2 ppm NO_2 added)			(0.58)	0.44	0.94		1.71		0.44

---

* NO_2 and BZA data were supplied by UCR; NO was estimated.

† Corrected for O_3 and O^3p.

Benzaldehyde does appear to be photolyzing in experiment EC-647 at a rate of approximately 10^{-3} min^{-1}. Although this rate of photolysis is consistent with our previous analysis (Killus and Whitten, 1982), direct photolytic radical production from benzaldehyde does not seem to be the process involved. However, subsequent reaction and photolysis of the (at present unidentified) products of benzaldehyde photolysis might well represent a radical source that increases in magnitude during the course of the experiment. For this reason, EC-647 is at best a weak indication of an NO_2-linked radical source.

5.3.4 Conclusions

Assuming that the propene tracer technique is not confounded by some, as yet unidentified, hydrocarbon loss process, the experiments at UCR indicate a radical source strength at standard conditions (303 K, ~ 50% RH, $K_1 \sim 0.4$, $NO_2 = 0.1$ ppm) of 0.15 to 0.3 ppb min^{-1}. As much as 0.1 ppb min^{-1} of this source can be explained by known contaminants in the UCR chamber that include hydrocarbons and HONO emitted from the chamber walls and the reactions of the propene tracer itself.

Radical source processes linked to NO_2 concentrations are as yet unproven. Our estimate of wet conversion of NO_2 to HONO is 10^{-4} min^{-1}, with an upper limit of three times this figure. Measurements of HONO in the UCR chamber may add to our understanding when these data become available.

The large experiment-to-experiment and chamber-to-chamber variability seen in the UCR study indicates that these phenomena are indeed chamber-related effects rather than the result of unknown gas-phase processes.

As we have shown previously, the UNC chamber background reactivity can easily be described as a reactive hydrocarbon (formaldehyde) background (except in cases for which a NO_x bleed is also observed). The radical background for the UNC chamber seems to be somewhat less than that of the UCR evacuable chamber, which underscores the usefulness of the UNC facility for mechanism validation purposes.

5.4 UNC SOLAR LIGHT STUDIES

As the modeling of outdoor smog chambers improves, the effects of the intensity of diurnally varying light become more apparent. In previous studies (Whitten, Killus, and Hogo, 1980) the photolytic rates of aldehydes and NO_2 may not always have been accurately simulated, but the use of adjustable levels for radical precursors like HONO or of adjustable amounts of formaldehyde attached to the chamber walls could often overshadow the effects of diurnal light. The orientation of the present study is toward the details of smog formation rather than toward seeking a generalized mechanism, as in previous studies. The present report deals with refinements to earlier work. This section discusses the details of our work to date on the solar ultraviolet flux.

5.4.1 NO_2 Photolysis in the UNC Chamber

Data are supplied to us from UNC as total solar radiation (TSR) and as ultraviolet (UV). Occasionally, one or both of these data may be missing or only partially available. Both of these types of data are obtained from Eppley pyranometers. In a previous study, Whitten, Killus, and Hogo (1980) found that the UV data seemed to provide better simulations than the TSR data for similar modeling experiments performed on different days. The ratio of UV to TSR apparently changes as a result of turbidity and cloud reflections, and the photolysis reactions considered most important to smog formation are driven by the UV flux. However, Jeffries* has obtained a more consistent correlation between actual NO_2 photolysis rate measurements and the TSR data. Thus, we have developed a priority scheme for modeling UNC experiments that utilizes UV data first, then TSR data (except 1979 data), and finally the solar function discussed next.

When we first compared the solar function for NO_2 photolysis developed by Demerjian, Schere, and Peterson (1980), we found that the diurnal shape of the TSR data from UNC agreed with the solar function, but the curve derived from UNC UV data that we had been using produced a distinctly different shape. The reason for the discrepancy was explained by the work of Nader and White (1969), Zafonte, Rieger, and Holmes (1976), and Stedman, Harvey, and Dickerson (1977) on the subject of converting flat-plate Eppley-UV data to NO_2 photolysis. Figures 58 and 59 show the type of conversion curves recommended in those studies. Until now we had been using UV data from UNC as a substitute for TSR data, with a constant conversion factor rather than with the variable factor now used for UV data. Figures 58 and 59 show the old and new conversion factors. The next step toward an improved modeling of NO_2 photolysis involved the albedo correction.

The UNC chamber uses a reflective bottom which has been shown by Jeffries, Fox, and Kamens (1975) to enhance the NO_2 photolysis inside the chamber. We had been using a 15 percent enhancement in the photolysis constants at solar noon as recommended by Jeffries.* Between 0900 and 1200,

---

* H. Jeffries, private communication, 1980.

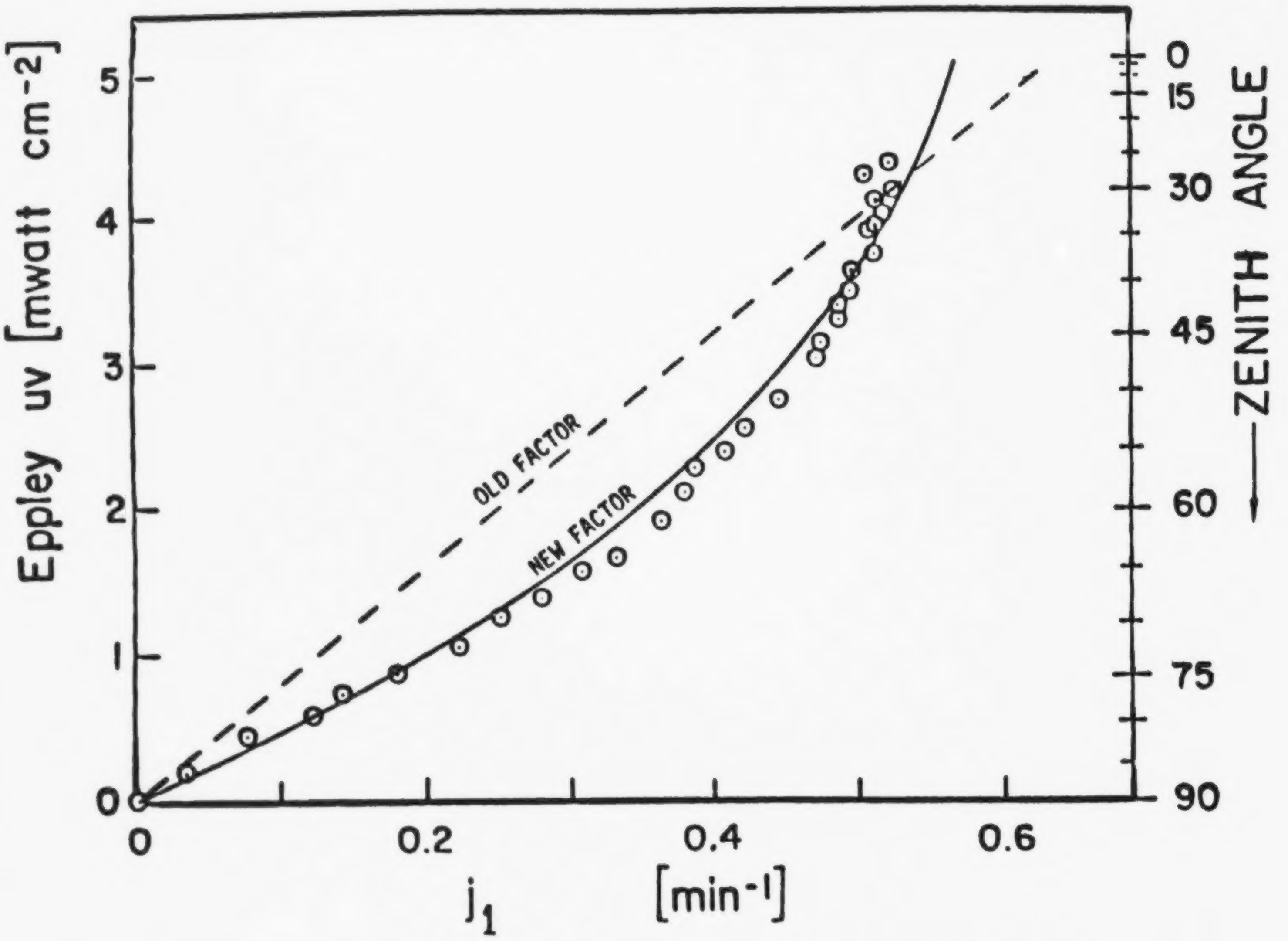

FIGURE 58. DATA POINTS TAKEN FROM STEDMAN, HARVEY, AND DICKERSON (1977)

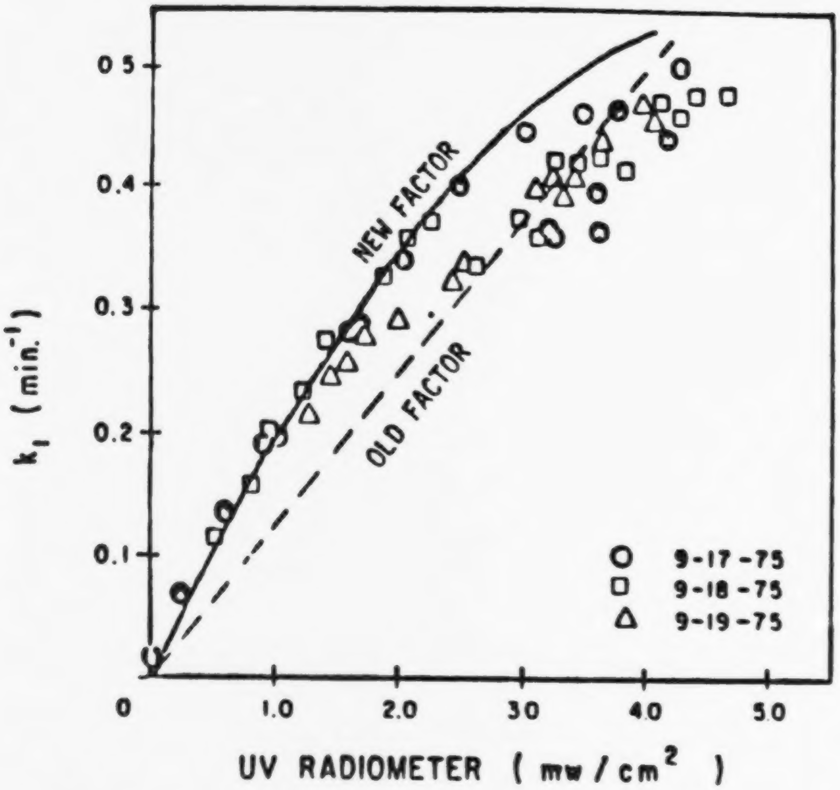

FIGURE 59. DATA POINTS TAKEN FROM ZAFONTE, RIEGER, AND HOLMES (1976)

and between 1300 and 1600, we had linearly increased and decreased the enhancement. Now, we have converted to an enhancement factor that depends on solar zenith angle $\nu\theta$.

On 13 October 1976, several instruments were used to measure k_1 inside and outside the UNC chamber. The 15 percent enhancement had been based on the results taken on 13 October 1976. According to our calculations, the minimum zenith angle that day was 18 degrees. At 0900, the zenith angle was about 60 degrees. The new enhancement factor algorithm, for k_1 in the UNC chamber uses somewhat higher factors for 13 October 1976, but the factors depend on zenith angle rather than time:

$$k_1' = k_1 \ (0.85 + 0.40 \cos \theta)$$

for zenith angles, θ between 44° and 72°,

$$k_1' = k_1 \times 1.2$$

for θ less than 44°, and

$$k_1' = k_1$$

for θ greater than 72°.

This enhancement factor is added to k_1 from any data source.

The solar function now in use is based on the computer algorithm found in the computer program OZIPP, which was deveoped for the Empirical Kinetics Modeling Approach (EKMA) (Whitten and Hogo, 1978). This computer algorithm was equivalent to the one published by Schere and Demerjian (1977). Modifications to the algorithm now include the following:

> A correction for changes in solar intensity resulting primarily from changes in the distance to the sun (Becker et al., 1966). The maximum flux in January is almost 7 percent greater than the minimum in July.

> A correction for turbidity based on the work of Peterson et al. (1980). However, the curve they suggested was flattened for July and August to provide closer agreement with the measured annual variation of NO_2 photolysis found in the UNC data.

---

* H. Jeffries, private communication, 1978.

> Use of the curve shown in Figure 60 in the solar function for the turbidity correction. In the computer algorithm, monthly average values are interpolated linearly for the day of the month. The NO_2 photolysis is then reduced by the factor f_τ where

$$f_\tau = \exp(-0.36\tau)$$
$$\tau = 2.303 \times \text{turbidity in Figure 60.}$$

The constant 0.36 was determined to provide a good fit with the observed seasonal variance at UNC.

> Multiplication of an arbitrary enhancement factor of 1.2 into the solar function to provide the final seasonal agreement shown in Figure 61. The original solar function, as found in OZIPP, provided quite close agreement with observed NO_2 photolysis rates for the July and August period. However, the predicted NO_2 photolysis rates for January and December were noticeably low (almost 30 percent in some cases). Since the original solar function was not attenuated for the turbidity nor corrected for the distance to the sun, the addition of these corrections resulted in a solar function that was about 20 percent low for the entire year. The reasons for the 20 percent discrepancy are under investigation.

The results using the corrected solar function are plotted for the 13 October 1976 day in Figure 62, along with the original solar function as used in OZIPP and the data taken at the UNC facility.

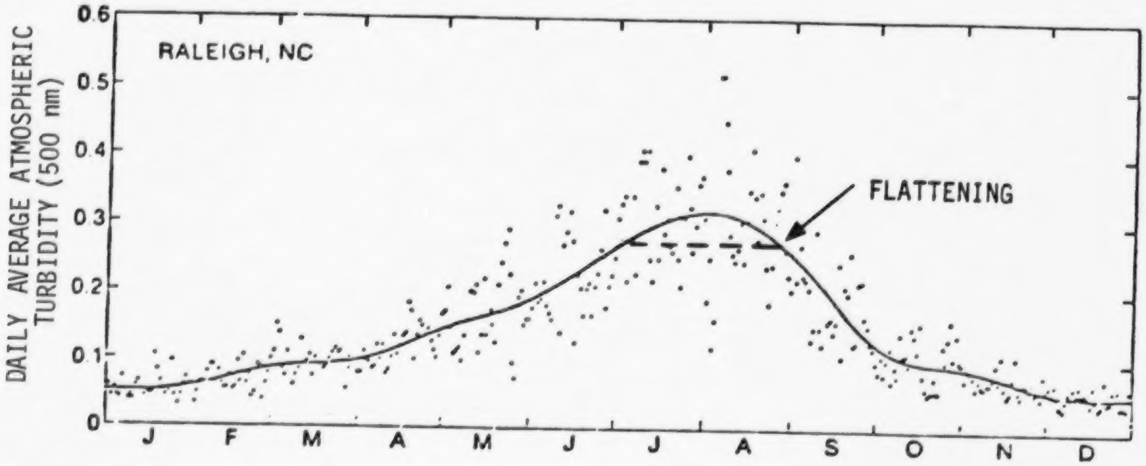

Source: Peterson et al. (1980)

FIGURE 60. DAILY AVERAGE ATMOSPHERIC TURBIDITY (500nm)

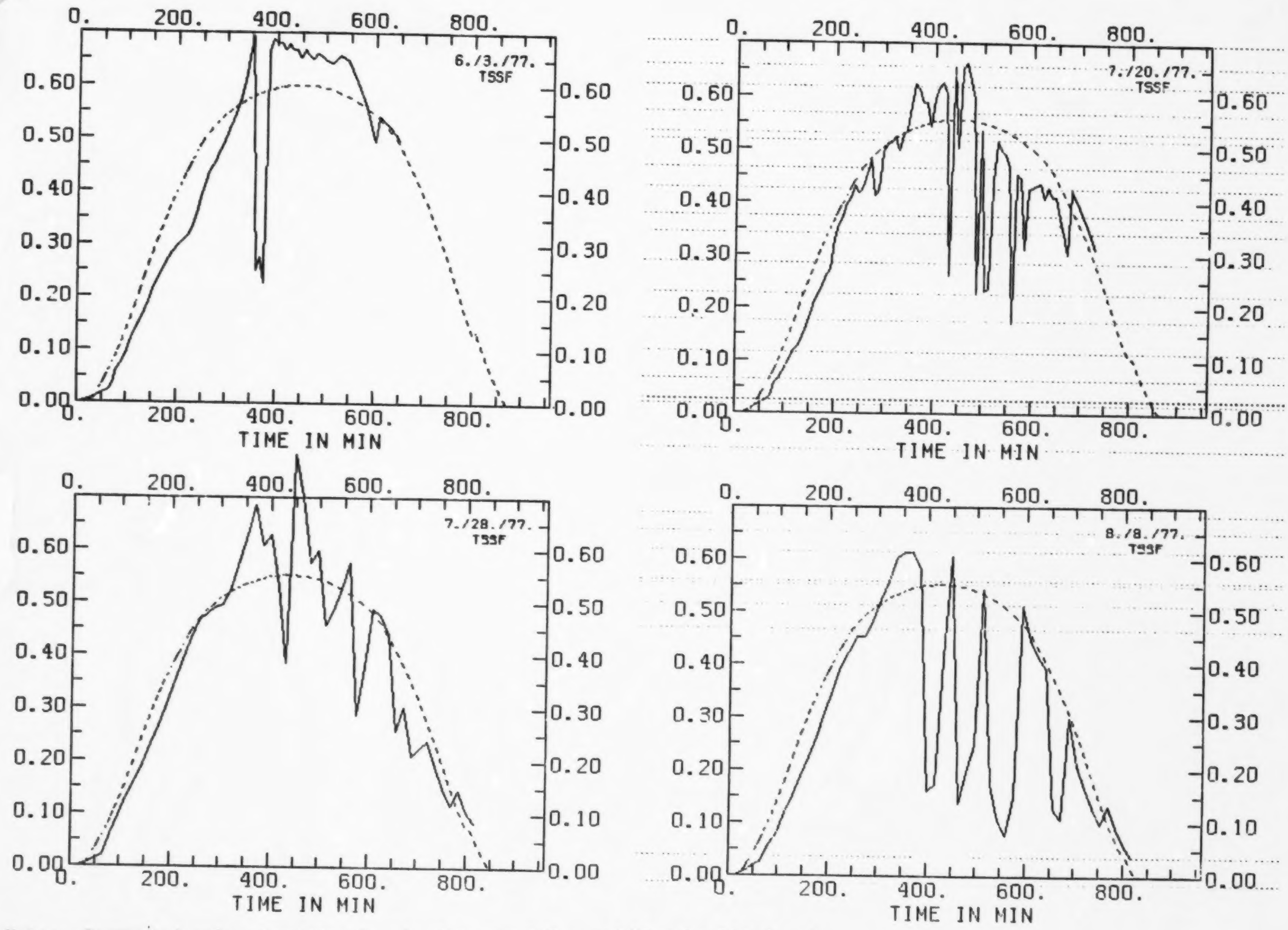

Note: Corrected solar function (---); data used for modeling by SAI (—).

FIGURE 61. DIURNAL NO_2 PHOTOLYSIS FOR THE UNC SMOG CHAMBER

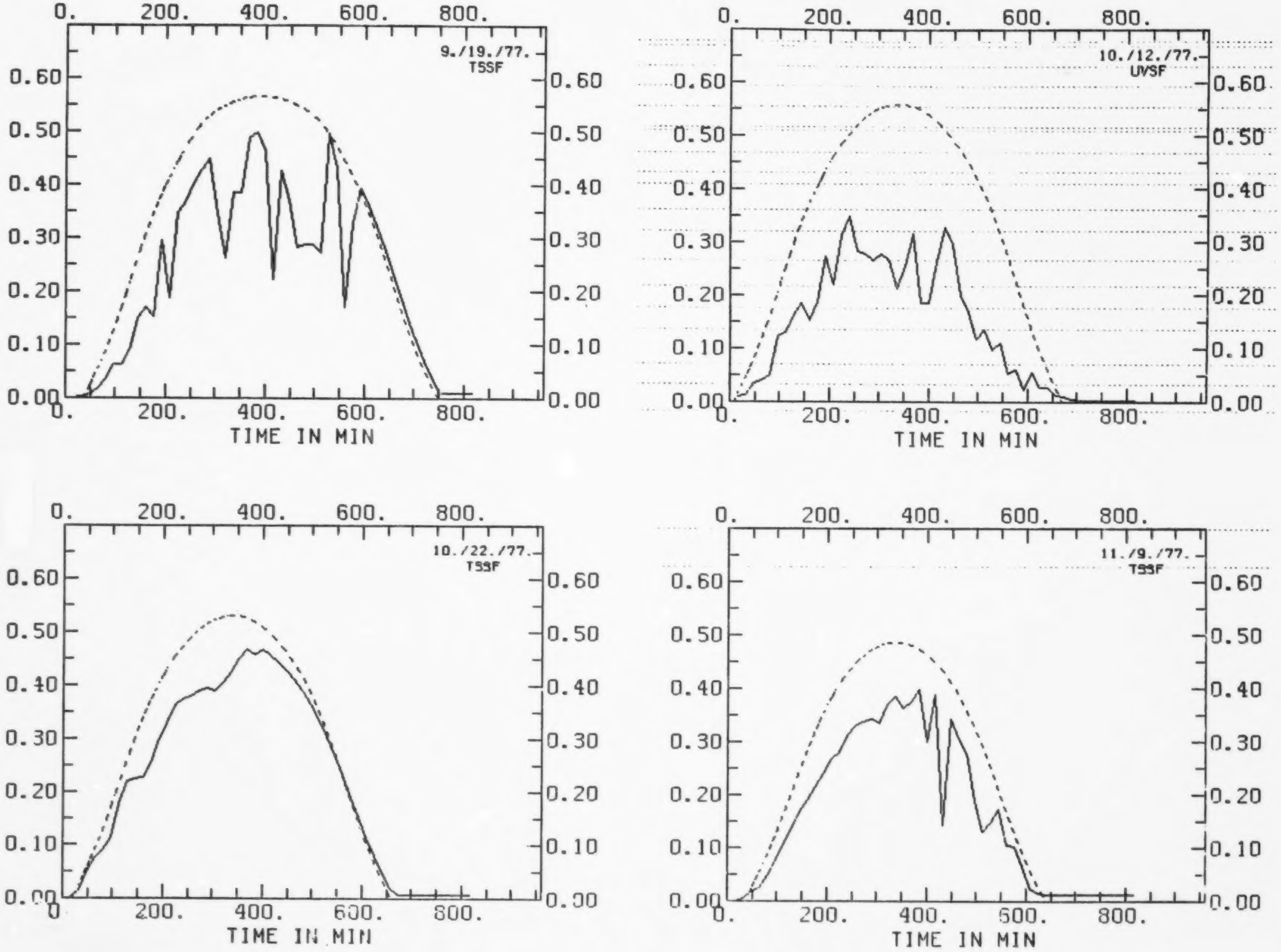

FIGURE 61. (Continued)

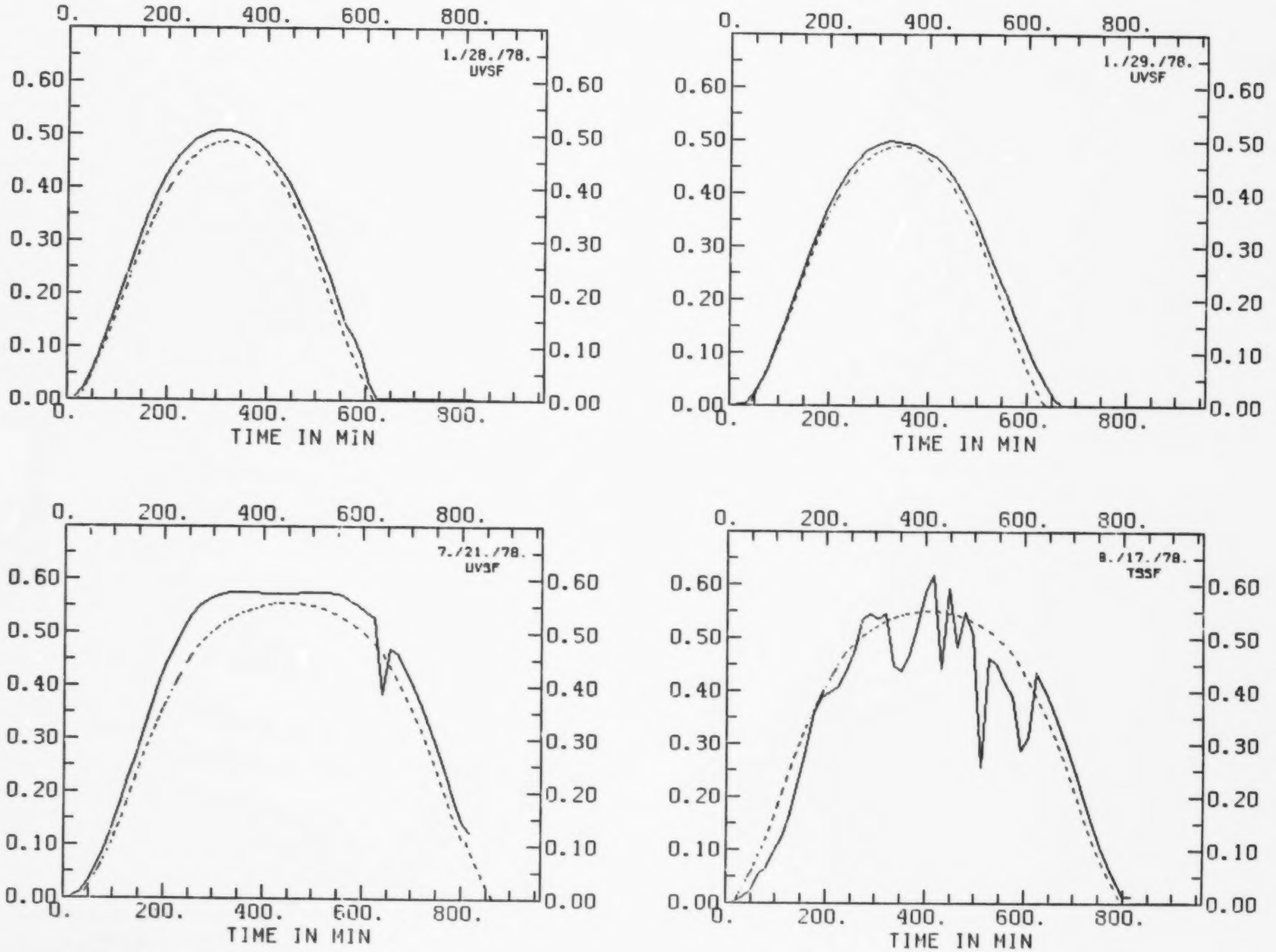

FIGURE 61. (Continued)

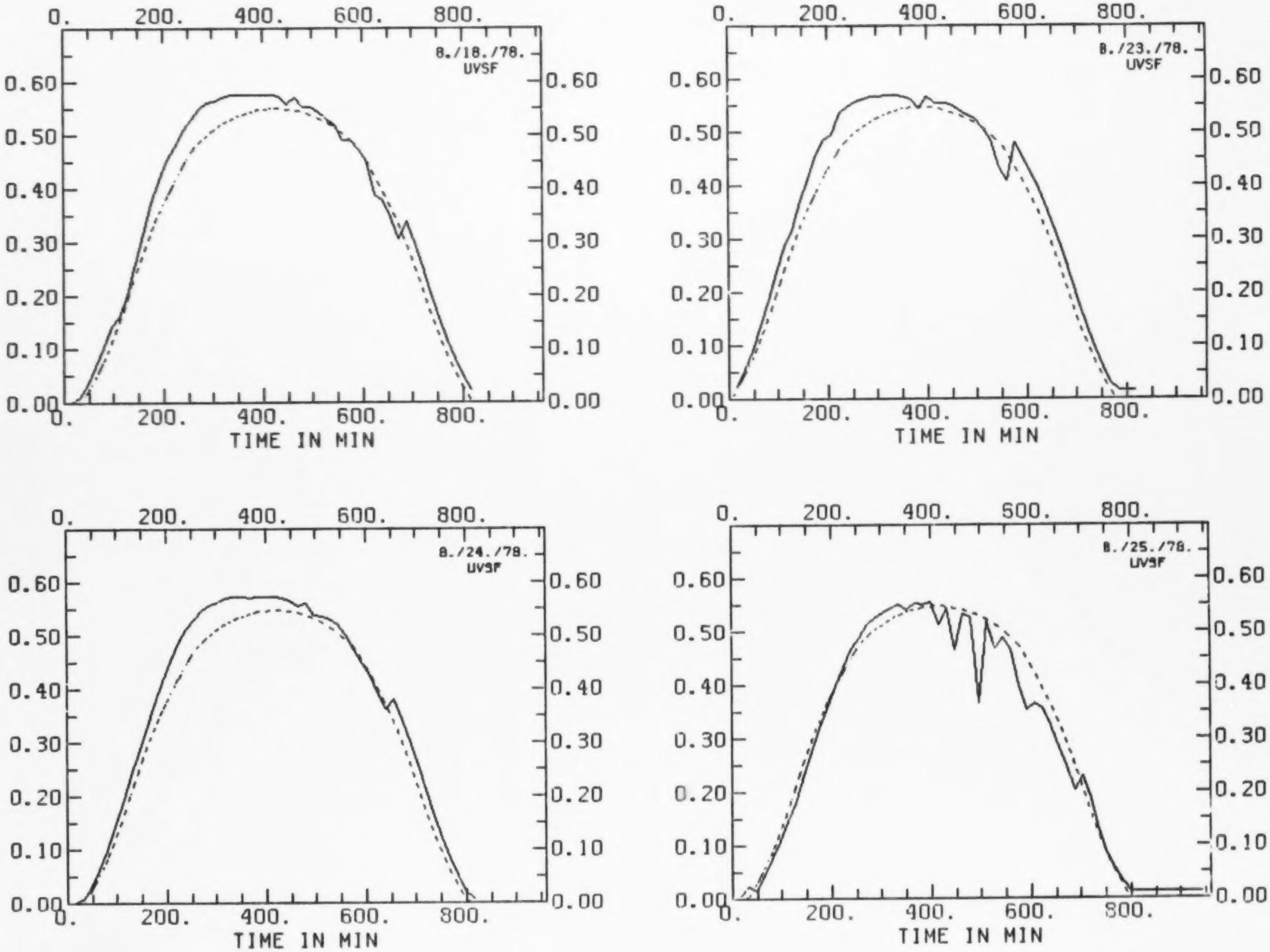

FIGURE 61. (Continued)

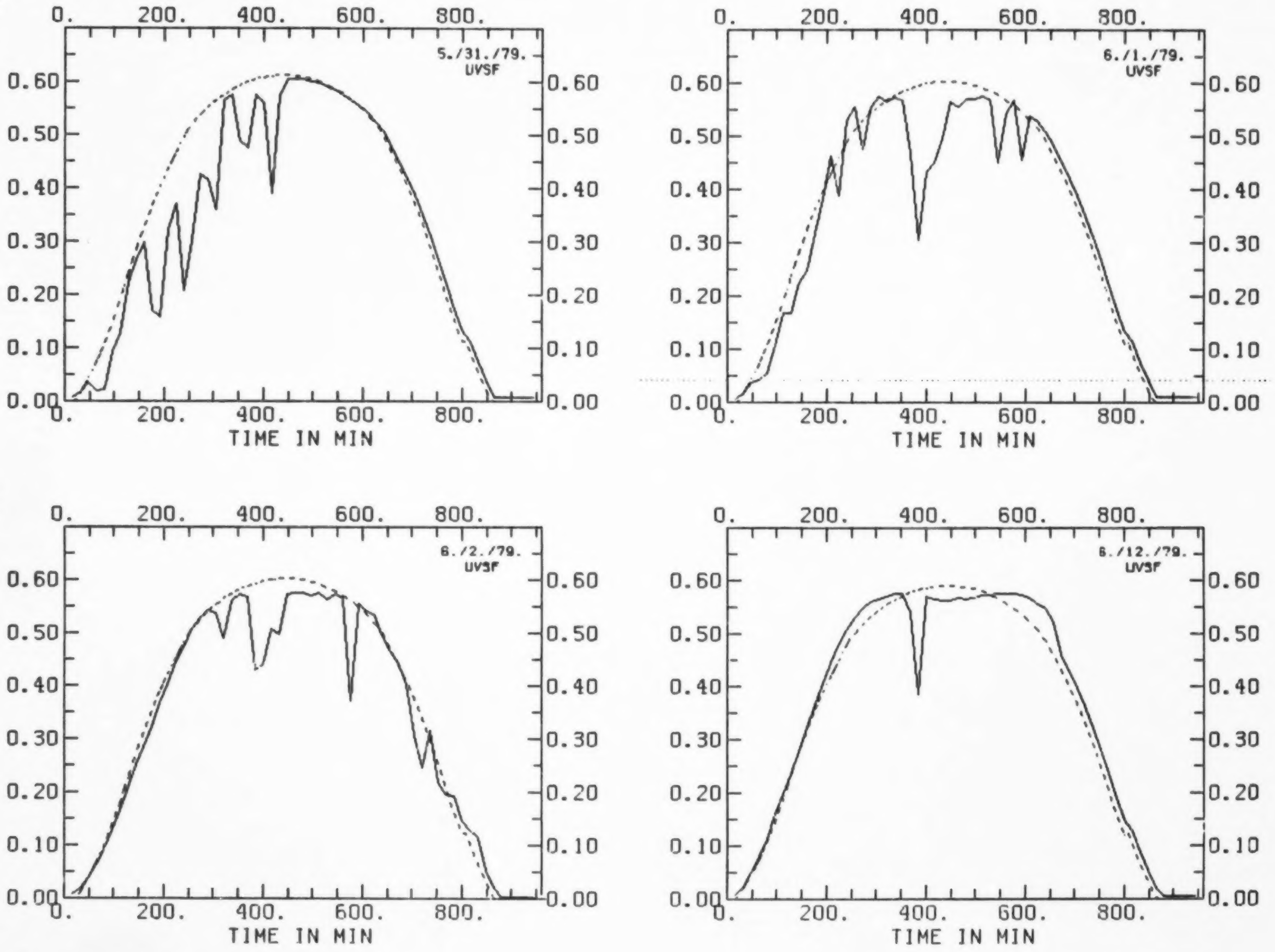

FIGURE 61. (Continued)

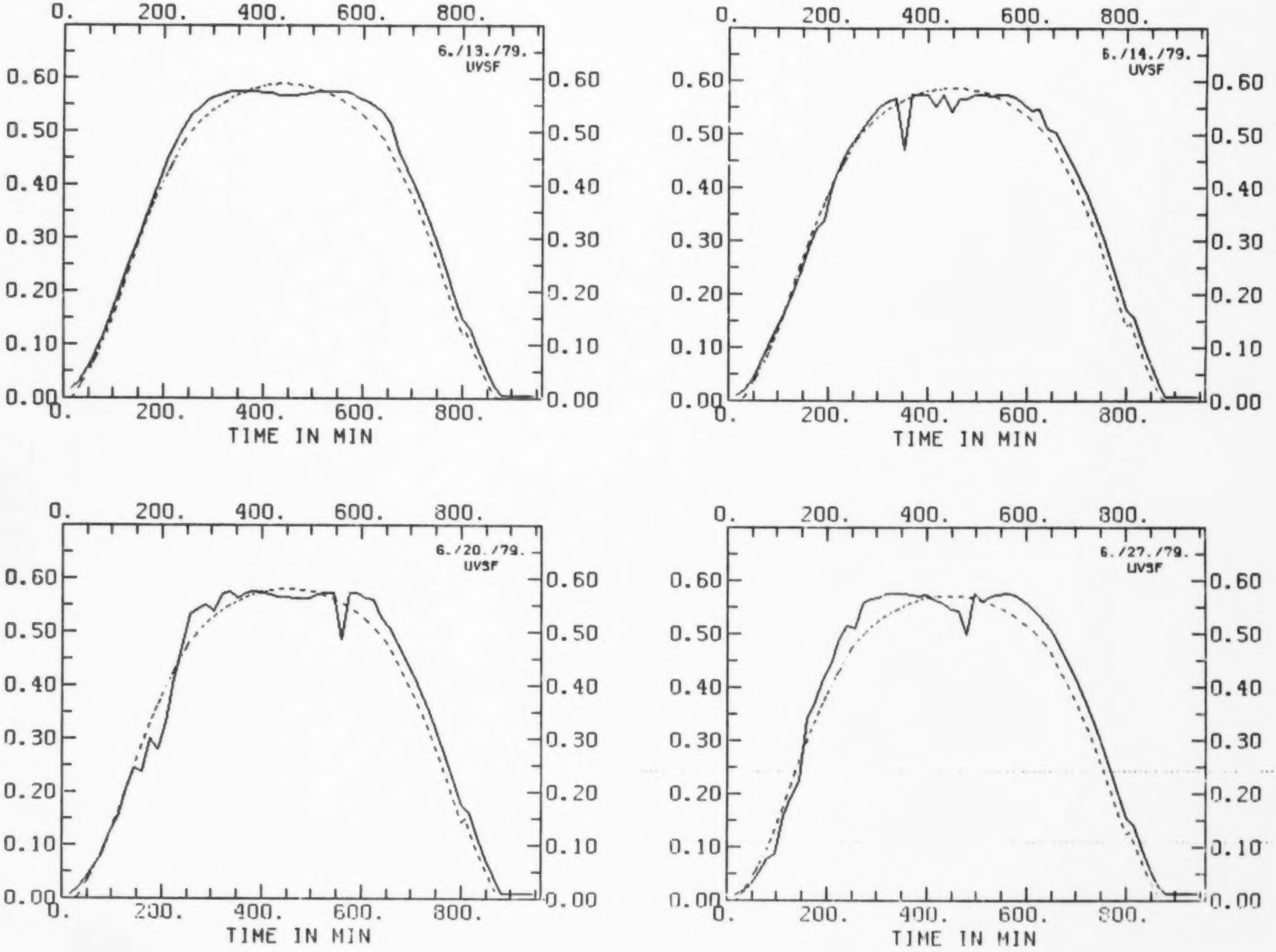

FIGURE 61. (Continued)

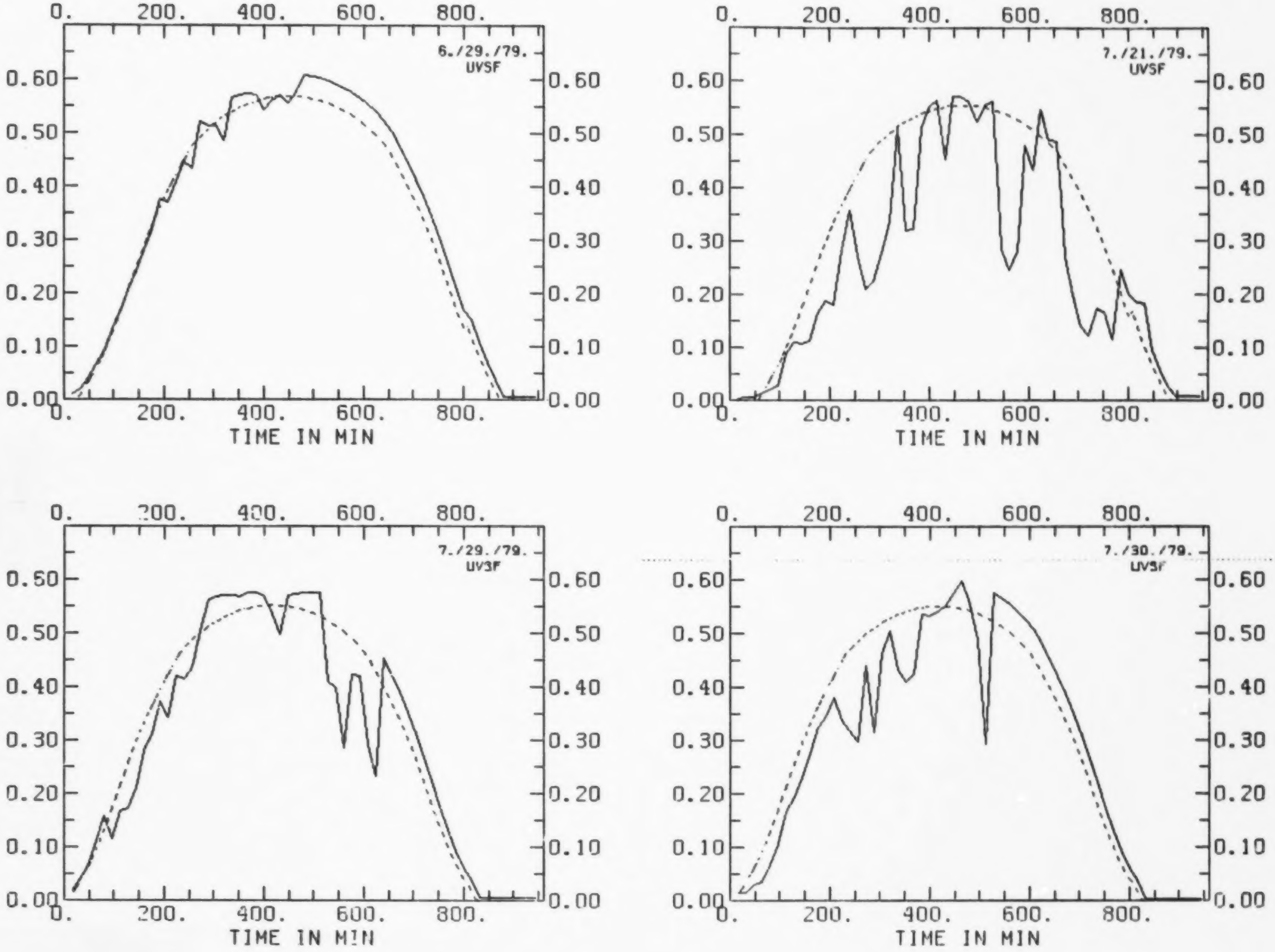

FIGURE 61. (Continued)

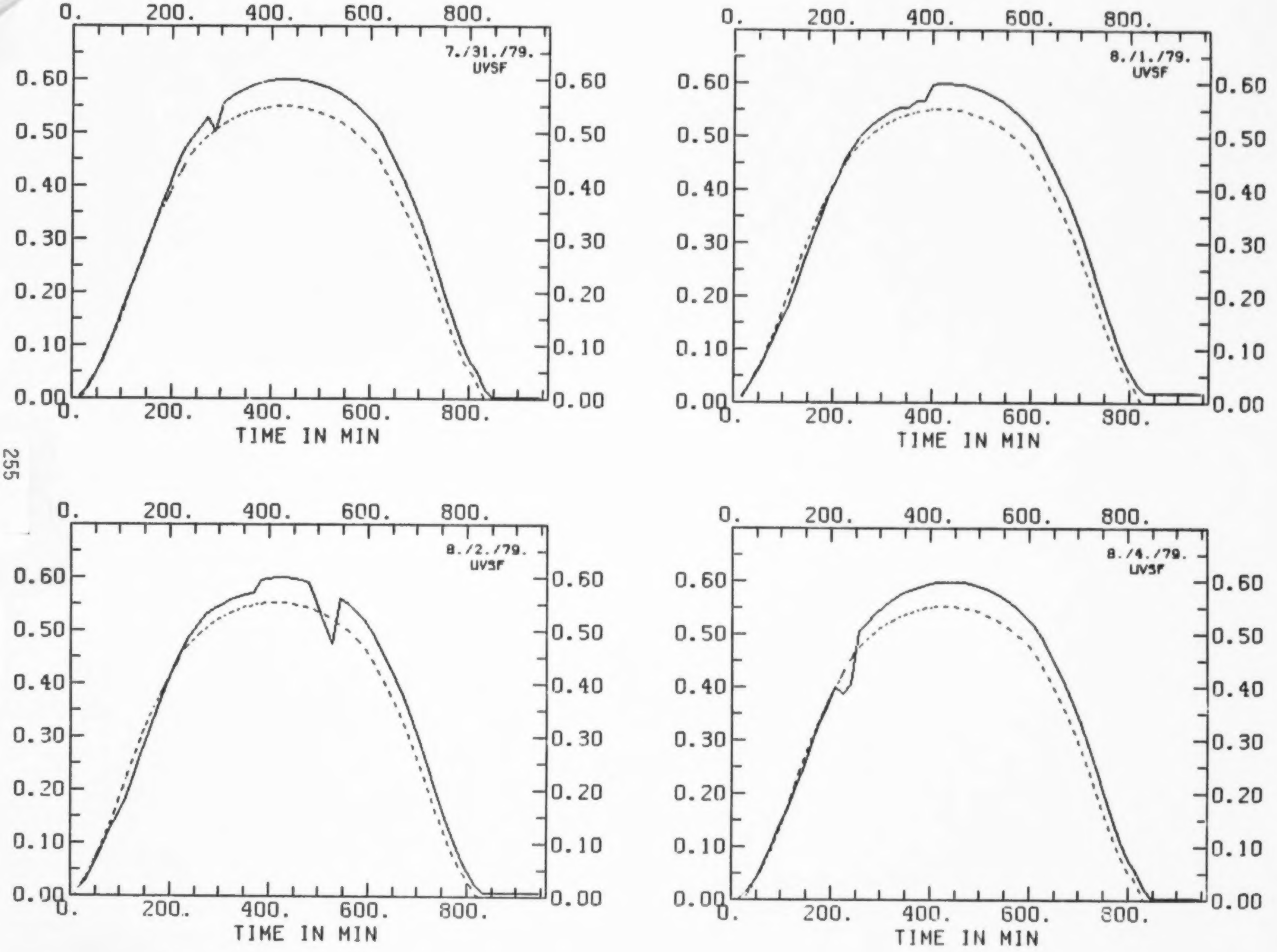

FIGURE 61. (Continued)

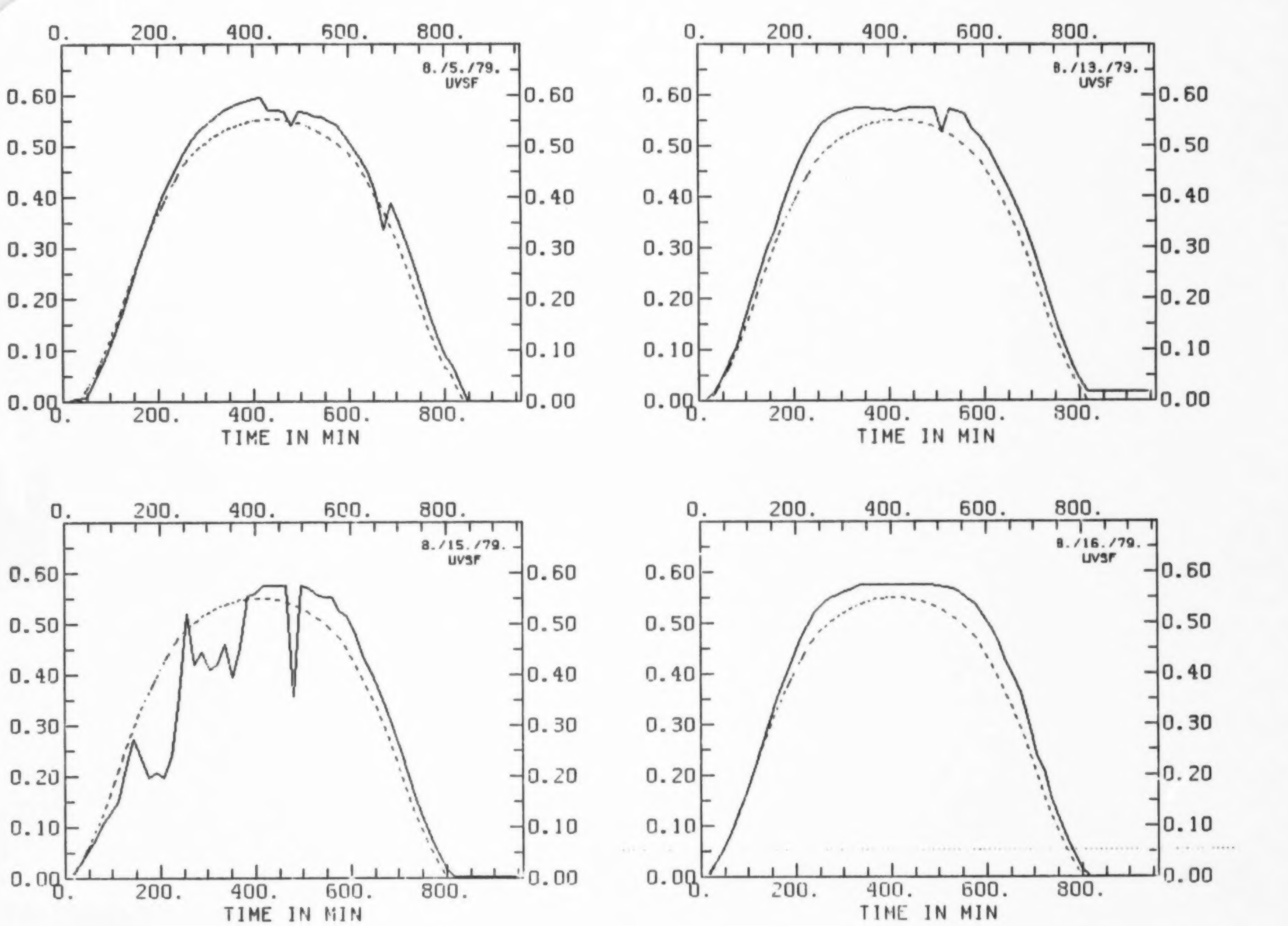

FIGURE 61. (Continued)

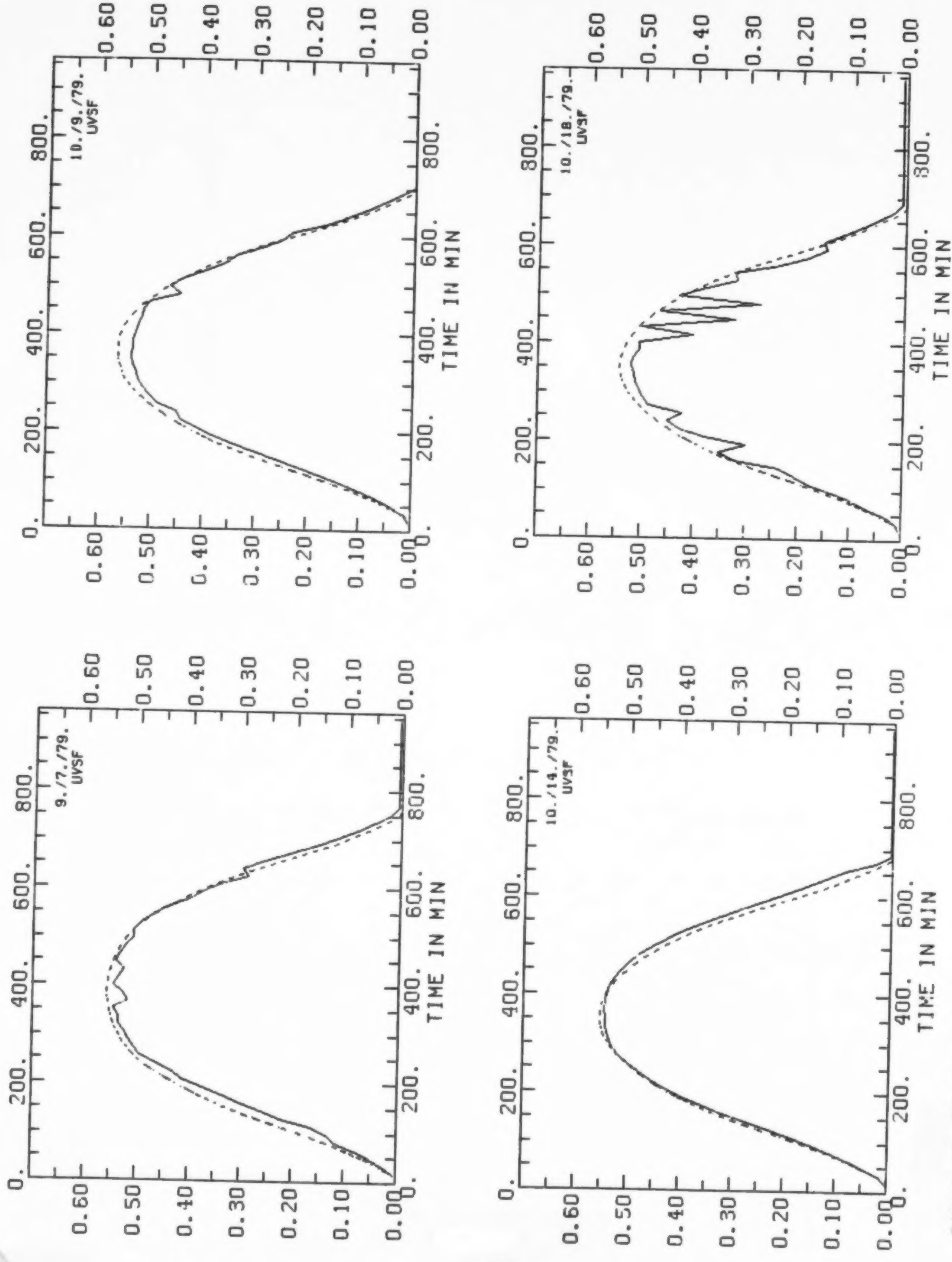

FIGURE 61. (Continued)

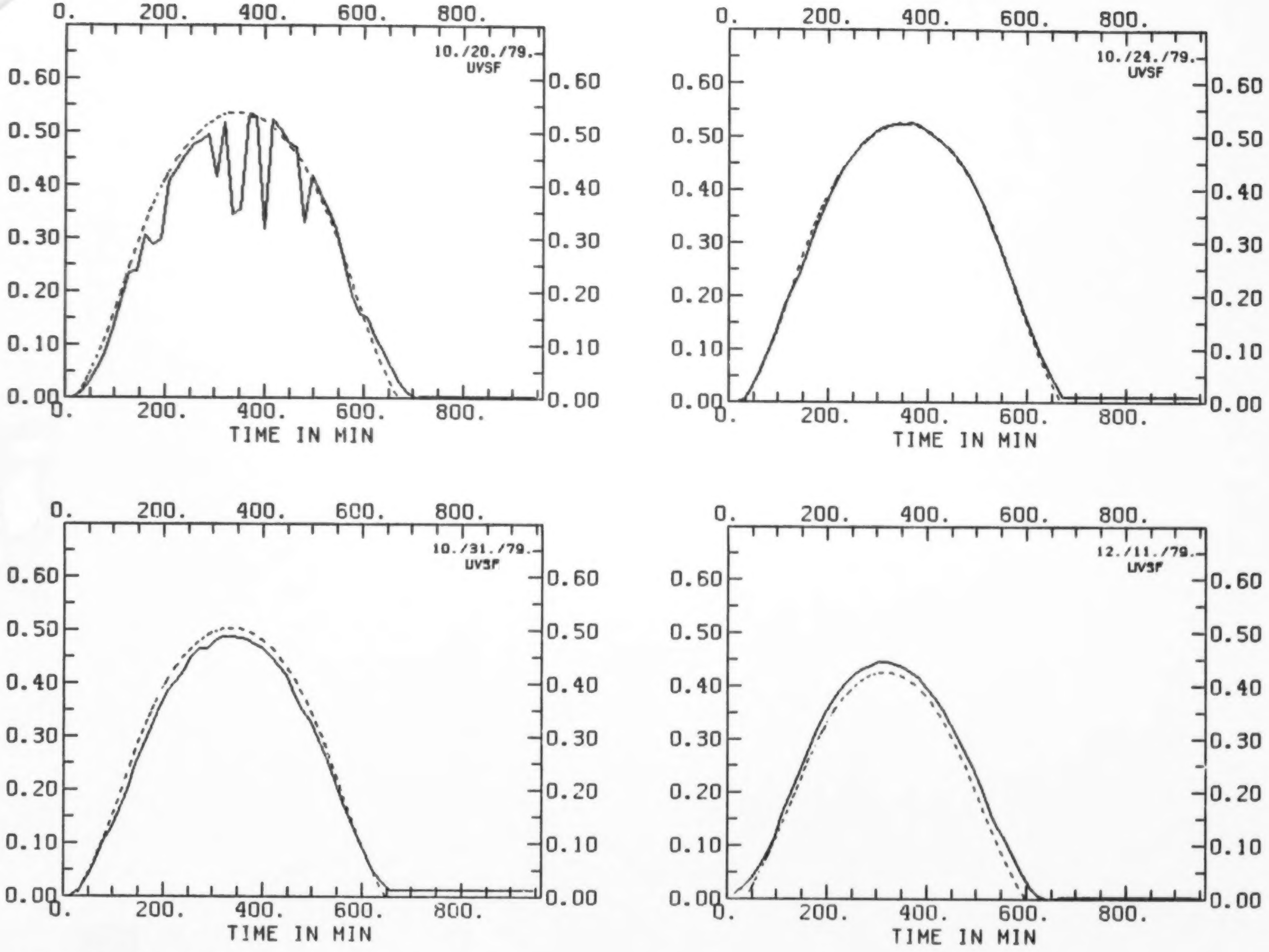

FIGURE 61. (Concluded)

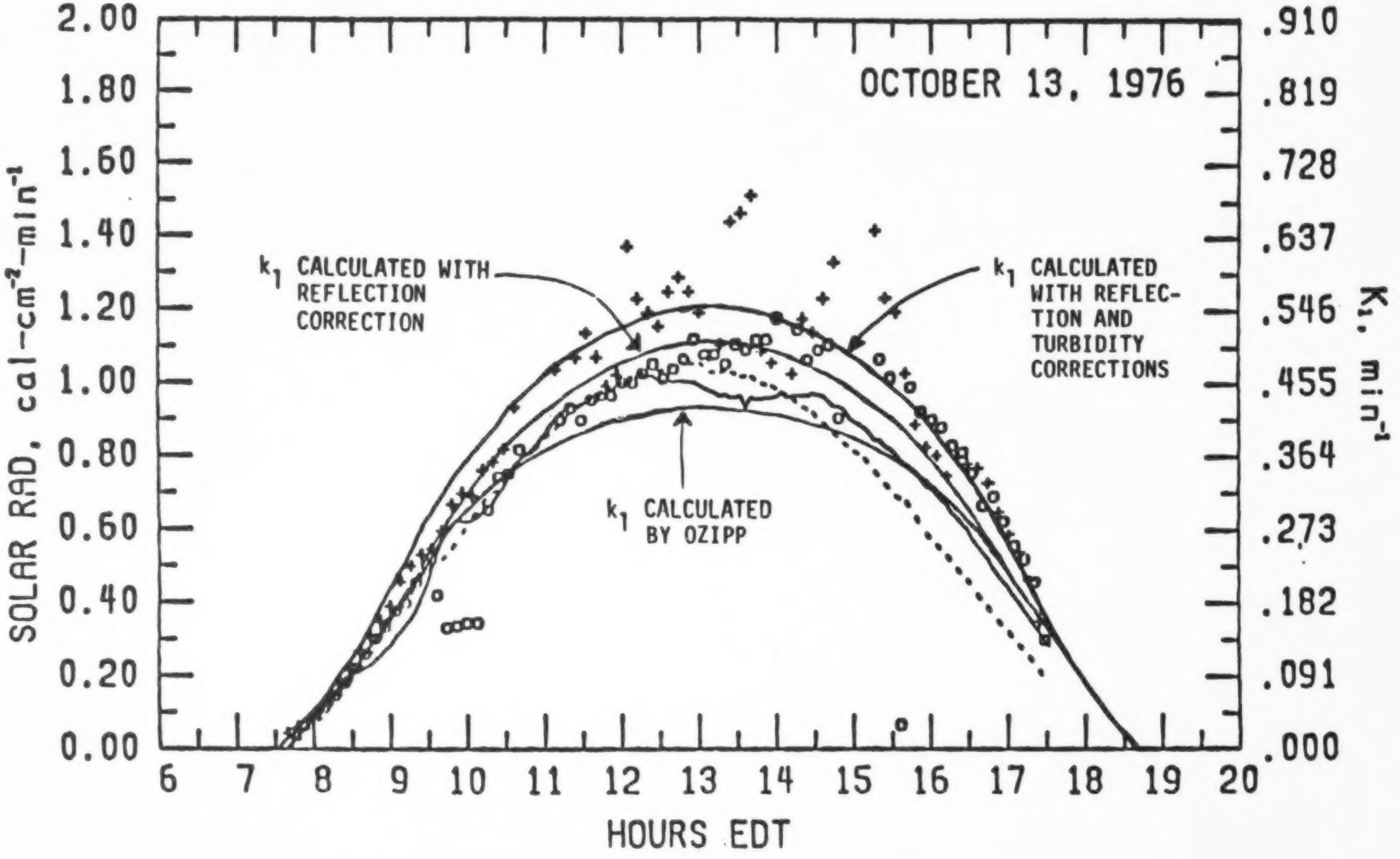

Source: **Private communication from H. E. Jeffries (1978).**

FIGURE 62. SPECIFIC PHOTOLYSIS RATE OF NITROGEN DIOXIDE AND INCIDENT TOTAL SOLAR RADIATION AND ULTRAVIOLET RADIATION AS A FUNCTION OF TIME FOR 13 OCTOBER 1976. SOLID LINE IS TOTAL SOLAR RADIATION; DASHED LINE IS ULTRAVIOLET RADIATION (FULL SCALE IS 64.64 x 10^{-3} al-cm-2-min-1); O ARE AMBIENT k_1, + k_1 INSIDE THE SMOG CHAMBER. SKY CONDITIONS WERE CLEAR.

REFERENCES

Addison, M. C., J. P. Burrows, R. A. Cox, and R. Patrick (1980), "Absorption Spectrum and Kinetics of the Acetylperoxy Radical," *Chem. Phys. Lett.*, Vol. 73, pp. 283-287.

Akimoto, H., M. Hoshino, G. Inoue, F. Kakamaki, N. Washida, and M. Okuda (1979), "Design and Characterization of the Evaluable and Bakable Photochemical Smog Chamber," *Environ. Sci. Technol.*, Vol. 13, No. 4, pp. 471-475.

Altwicker, E., and F. Dicesare (1979), "Relationship between Specific NonMethane Hydrocarbons and Ozone in Urban Air and Their Role in Transportation Control Strategies," DOT/RSPA/DPB-SO/79/25, U.S. Department of Transportation, Research and Special Projects Administration, Office of University Research, Washington, D.C. 20590.

Atkinson, R., S. M. Aschmann, W.P.L. Carter, A. M. Winer, J. N. Pitts Jr. (1982), "Alkyl Nitrate Formation from the NO_x-Air Photooxidation of C_2-C_8 N-Alkanes," presented at the XVth Informal Conference on Photochemistry, 27 June-1 July, 1982, Stanford, California.

Atkinson, R., and A. C. Lloyd (1982), "Evaluation of Kinetic and Mechanistic Data for Modeling of Photochemical Smog," P-A040, Environmental Research and Technology, Incorporated, Westlake Village, California, Submitted to *J. Phys. Chem. Ref. Data*.

Atkinson, R., W.P.L. Carter, K. R. Darnall, A. M. Winer, and J. N. Pitts, Jr. (1980), "A Smog Chamber and Modeling Study of the Gas-Phase NO_x-air Photooxidation of Toluene and the Cresols," *Int. J. Chem. Kinet.*, Vol. 12, pp. 779-836.

Atkinson, R., K. R. Darnall, A. C. Lloyd, A. M. Winer, and J. N. Pitts, Jr. (1979), "Kinetics and Mechanisms of the Reaction of the Hydroxyl Radical with Organic Compounds in the Gas Phase," *Adv. Photochem.*, Vol. 11, pp. 375-488.

Bahta, A., R. Simonaitis, and J. Heicklen (1982), "Thermal Decomposition Kinetics of $CH_3O_2NO_2$," J. Phys. Chem., Vol. 86, pp. 1849-1853.

Baulch, D. L., R. A. Cox, R. F. Hampson Jr., J. A. Kerr, J. Troe, and R. T. Watson (1980), "Evaluated Kinetic and Photochemical Data for Atmospheric Chemistry," reprint No. 159 from J. Phys. Chem. Ref. Data, Vol. 9, No. 2, pp. 295-471.

Becker, U., M. Y. Ben-Sira, S. Fritz, F. Möller, W. Schüepp, G. Yamamoto, and N. Robinson (1966), Solar Radiation, N. Robinson, ed. (Elsevier Publishing Company, New York, New York).

Boller, T., and H. Kende (1980), "Regulation of Wound Ethylene Synthesis in Plants" Nature, Vol. 286.

Calvert, J. G. (1976), "Hydrocarbon Involvement in Photochemical Smog Formation in Los Angeles Atmosphere," Environ. Sci. Technol., Vol. 10, No. 3, p. 257.

Carter, W.P.L., R. Atkinson, A. M. Winer, and J. N. Pitts Jr. (1981), "Evidence for Chamber-Dependent Radical Sources: Impact on Kinetic Computer Models for Air Pollution," Int. J. Chem. Kinet., Vol. 13, p. 735.

Carter, W.P.L., A.C. Lloyd, J. L. Sprung, and J. N. Pitts, Jr. (1979), "Computer Modeling of Smog Chamber Data: Progress in Validation of a Detailed Mechanism for the Photooxidation of Propene and n-Butane in Photochemical Smog," Int. J. Chem. Kinet., Vol. 11, pp. 45-103.

Carter, W.P.L., R. Atkinson, A. M. Winer, and J. N. Pitts Jr. (1982), "An Experimental Investigation of Chamber-Dependent Radical Sources," Int. J. Chem. Kinet., in press.

Cox, R. A., K. F. Patrick, and S. A. Chant (1981), "Mechanisms of Atmospheric Photooxidation of Organic Compounds. Reactions of Alkoxy Radicals in Oxidation of n-butane and Simple Ketones," Environ. Sci. Technol., Vol. 15, p. 587.

Darnall, K. R., R. Atkinson, and J. N. Pitts, Jr. (1979), "Observation of Biacetyl from the Reaction of OH Radicals with o-xylene: Evidence for Ring Cleavage," J. Phys. Chem., Vol. 83, p. 1943.

Dawson, G. A., J. C. Farmer, and J. L. Moyers (1980), "Formic and Acetic Acids in the Southwestern U.S.A.," Geo. Res. Lett., Vol. 7, No. 9, pp. 725-728.

Demerjian, K. L., K. L. Schere, and J. T. Peterson (1980), "Theoretical Estimates of Active (Spherically Integrated) Flux and Photolytic Rate Constants of Atmospheric Species in the Lower Troposphere," Adv. Environ. Sci. Technol., Vol. 9.

Dimitriades, B. (1976), "Smog Chamber Conference Proceedings," EPA-600/3-76-029, U.S. Environmental Protection Agency, Research Triangle Park, North Carolina.

EPA (1976), "1973 National Emissions Report," EPA-450/2-76-007, U.S. Environmental Protection Agency, Research Triangle Park, North Carolina.

Fishman, J., and P. Crutzen (1978), "The Origin of Ozone in the Troposphere," Nature, Vol. 274, pp. 855-858, 31 August 1978.

Fushimi, K., and Y. Miyake (1980), "Contents of Formaldehyde above the Surface of the Ocean," J. Geo. Res., Vol. 85, No. C12, December 20, 1980.

Gill, R. J., W. D. Johnson, and G. H. Atkinson (1981), "The Formation and Decay Mechanisms of HCO in the Photodissociation of Gas Phase Acetaldehyde," Chemical Physics (North-Holland), Vol. 58, pp. 29-44.

Grosjean, D. (1980), "Measurements in Support of a Photochemical Oxidant Model: Hydrocarbons, Aldehydes, and Ozone Formation in Teflon Tents. Vol. II Appendices. ERT Document P-A029-800

Heidt, L. E., J. P. Krasnec, K. H. Lueb, W. H. Pollock, B. E. Henry, and P. J. Crutzen (1980), Latitudinal Distributions of CO and CH_4 over the Pacific," J. Geophys. Res., Vol. 85, No. C12, 20 December 1980.

Hendry, D. G. (1979), "Reactions of Aromatic Compounds in the Atmosphere," invited paper presented at the symposium on Chemical Kinetic Data Needs for Modeling the Lower Troposphere, 15-17 May 1978, Reston, Virginia, sponsored by the U.S. Environmental Protection Agency and the National Bureau of Standards.

Hernon, J. T., R. I. Martinez, and R. E. Huie (1982), "Kinetics and Energetics of the Criegee Intermediate in the Gas Phase. I. The Criegee Intermediate in Ozone-Alkene Reactions," Int. J. Chem. Kinet., Vol. 14, pp. 201-224.

Hernon, J. T., and R. E. Huie (1977), "Stopped-Flow Studies of the Mechanisms of Ozone-Alkene Reactions in the Gas Phase: Ethylene," J. Am. Chem. Soc., Vol. 99, pp. 5430-5435.

Jeffries, H., D. Fox, and R. Kamens (1976), "Outdoor Smog Chamber Studies: Light Effects Relative to Indoor Chambers," Environ. Sci. Technol., Vol. 10, No. 10, pp. 1006-1011.

Kamens, R. M., H. E. Jeffries, K. G. Sexton, and A. A. Gerhardt (1981), "Smog Chamber Experiments to Test Oxidant Related Control Strategy Issues," Draft Report, Department of Environmental Sciences and Engineering, School of Public Health, University of North Carolina, Chapel Hill, North Carolina.

Kan, C. S., J. C. Calvert, and J. H. Shaw (1980), "Reactive Channels of the CH_3O_2-CH_3O_2 Reaction," Department of Chemistry and Department of Physics, Ohio State University, Columbus, Ohio.

Kan, C. S., F. Su, J. C. Calvert, and J. H. Shaw (1981), "Mechanism of the Ozone-Ethene Reaction in Dilute N_2/O_2 Mixtures Near 1-atm Pressure," J. Phys. Chem., pp. 2359-2363.

Kelly, T. J., D. H. Stedman, J. A. Ritter, and R. B. Harvey (1980), "Measurements of Oxides of Nitrogen and Nitric Acid in Clean Air," J. Geophys. Res., Vol. 85, No. C12, 20 December 1980.

Killus, J. P., and G. Z. Whitten (1982a), "A Mechanism Describing the Photochemical Oxidation of Toluene in Smog," Atmos. Environ. , Vol. 16, pp. 1973-1988.

Killus, J. P., and G. Z. Whitten, (1982b), "A New Carbon-Bond Mechanism for Air Quality Simulation Modeling," EPA 600/3-82-041, U.S. Environmental Protection Agency, Research Triangle Park, North Carolina.

Magnotta, F., and H. S. Johnston (1980), "Absolute Photodissociation Quantum Yields for the NO_3 Free Radical," Geophys. Res. Lett., Vol. 7, pp. 769-772.

Mayrsohn H., and T. H. Crabtree (1976), "Source Reconciliation of Atmospheric Hydrocarbons" Atmos. Environ., Vol. 10, 1976, p. 137.

Miller, D. F., A. J. Alxezweeny, J. M. Hales, and R. N. Lee (1978), "Ozone Formation Related to Power Plant Emissions" Science, Vol. 202, pp. 1186-1188.

Nadar, J. S., and N. White (1969), "Volumetric Measurement of Ultraviolet Energy in an Urban Atmosphere," Environ. Sci. Technol., Vol. 3, pp. 848-854.

NASA (1981), "Chemical Kinetic and Photochemical Data for Use in Stratospheric Modeling," JPL Publication 81-3, Evaluation Number 4, Jet Propulsion Laboratory, Pasadena, California.

Nelson, H. H., W. J. Marinelli, and H. S. Johnston (1981), "The Kinetics and Product Yield of the Reaction of HO with HNO_3," Chem. Phys. Lett., Vol. 78, pp. 495-499.

Niki, H., P. D. Maker, C. M. Savage, and L. P. Beitenbach (1981a), "A FTIR Study of Mechanisms for the HO Radical Initiated Oxidation of C_2H_4 in the Presence of NO: Detection of Glycoladehyde," Chem. Phys. Lett., Vol. 80, pp. 499-503.

Niki, H., P. D. Maker, C. M. Savage, and L. P. Beitenbach (1981b), "A FTIR Study of a Transitory Product in the Gas-Phase Ozone-Ethylene Reaction," J. Phys. Chem., Vol. 85, pp. 1024-1027.

Niki, H., P. D. Maker, C. M. Savage, and L. P. Beitenbach (1981c), "Fourier Transform Infrared Studies of the Self-Reaction of CH_3O_2 Radicals," Engineering and Research Staff, Ford Motor Company, Dearborn, Michigan.

Noxon, J. F. (1978), "Tropospheric NO_x," J. Geophys. Res., Vol. 83, p. 3051.

Noxon, J. F., R. B. Norton, and E. Marovich (1980), "NO_3 in the Troposphere," Geophys. Res. Lett., February 1980, Vol. 7, No. 2, pp. 125-128.

Petersen, J. T., E. C. Flowers, G. J. Berri, C. L. Reynolds, and J. H. Rudsill (1981), "Atmospheric Turbidity over Central North Carolina," J. Appl. Meteorol., Vol. 20, pp. 229-241.

Pitts, J. N., Jr. K. R. Darnall, W.P.L. Carter, A. M. Winer, and R. Atkinson (1979), "Mechanisms of Photochemical Reactions in Urban Air," EPA-600/3-79-110, U.S. Environmental Protection Agency, Research Triangle Park, North Carolina.

Pitts, J. N., Jr., K. R. Darnall, A. M. Winer, and J. M. McAfee (1977), "Mechanisms of Photochemical Reactions in Urban Air: Volume II. Chamber Studies," Statewide Air Pollution Research Center and Department of Chemistry, University of California, Riverside, California.

Platt, U., and D. Perner (1980), "Direct Measurements of Atmospheric CH_2O, HNO_2, O_3, NO_2 and SO_2 by Differential Optical Absorption in the Near UV," J. Geo. Res., Vol. 85, No. C12, December 20, 1980.

Rasmussen R. A., and F. W. Went (1965), "Volatile Organic Material of Plant Origin in the Atmosphere" Proc. N.A.S, Vol. 53, pp. 215-220.

Rasmussen, R. A., R. B. Chatfield, and M. W. Holdren (1977), "Hydrocarbon Species in Urban Air," Washington State University, Pullman Washington, January 1977.

Ross, D. (1979), Grant Proposal from SRI Submitted to Harold M. Barnes, U.S. Environmental Protection Agency, Research Triangle Park, North Carolina.

Routhier, F., K. Dennett, D. D. Davis, H. Wartburg, P. Haagenson, and H. C. Delany (1980), "Free Troposphere and Boundary Layer Airborne Measurements of Ozone Over the Latitude Range of 58°S to 70°N," Journal of Geophysical Res., Vol. 85, No. C12, 20 December 1980.

Sakamaki, F., H. Akimoto, and Michio Okuda (1981), "Photochemical Reactivity and Ozone Formation in 1-Olefin-Nitrogen-Oxide Air Systems," National Institute for Environmental Studies, Ibaraki, Japan, Amer. Chem. Soc., Vol. 15, p. 665.

Sander, S. P., and R. T. Watson (1981), "Temperature Dependence of the Self-Reaction of CH_3O_2 Radicals," J. Phys. Chem., Vol. 85, pp. 2960-2964.

Schere, K. L., and K. L. Demerjian (1977), "Calculation of Selected Photolytic Rate Constants over a Diurnal Range," EPA-600/4-77-015, U.S. Environmental Protection Agency, Research Triangle Park, North Carolina.

Scott Research Laboratories (1970), "1969 Atmospheric Reaction Studies in the Los Angeles Basin," APRAC Project CABA-7-68 for CRL Inc., and NAPCA (contract No. CPA 70-6), SRL Inc., P.O. Box D-11, Plumsteadville, Pennsylvania 18949. Vol. II. Commerce Ground Data, Vol. III. El Monte Ground Data, Vol. IV. Airborne Data; ESSA Cooperative Data.

Seiler, W. (1974), The Cycle of Atmospheric CO," Tellus, XXVI 1974 (1-2), pp. 116-135.

Seiler, W., and C. Junge (1970), "Carbon Monoxide in the Atmosphere" J. Geophys. Res., Vol. 75, pp. 2217-2226.

Singh, H. B., W. Viezee, W. B. Johnson, and F. L. Ludwig (1980), "The Impact of Stratospheric Ozone on Tropospheric Air Quality," JAPCA, Vol. 30, No. 9.

Stedman, D. H., R. B. Harvey, and R. R. Dickerson (1977), "Measurement of Photons Involved in Photochemical Oxidant Formation," EPA-600/3-77-0016, Int. Conf. on Photopchem. Oxidant Pollution and Its Control, Proceedings, Vol. 2, pp. 753-762.

Stevens, C. M., L. Krout, D. Walling, A. Venters, A. Engelkemeir, and L. E. Ross (1972) "The Isotope Composition of Atmospheric Carbon Monoxide" Meeting on Source, Sinks, and Concentrations of Carbon Monoxide and Methane in the Earth's Environment, St. Petersburg, Florida.

Stewart, D. A., and M. K. Liu (1980), "Development and Application of a Reactive Plume Model," Atmos. Environ., Vol. 15, pp. 2377-2393.

Su, F., J. G. Calvert, and J. H. Shaw (1980), "A FTIR Spectorscopic Study of the Ozone-Ethene Reaction Mechanism in O_2-Rich Mixtures," J. Phys. Chem., Vol. 84, pp. 239-246.

Whitten, G. Z., J. P. Killus, and H. Hogo (1980), "Modeling Simulated Photochemical Smog with Kinetic Mechanisms: Final Report," EPA-600/3-80-028a, U.S. Environmental Protection Agency, Research Triangle Park, North Carolina.

Whitten, G. Z., and H. Hogo (1978), "User's Manual for a Kinetic Model and Ozone Isopleth Plotting Package," EPA-600/8-78-014a, July 1978, U.S. Environmental Protection Agency, Research Triangle Park, North Carolina.

Whitten, G. Z., H. Hogo, M. J. Meldgin, J. P. Killus, and P. J. Bekowies (1979), "Modeling of Simulated Photochemical Smog with Kinetic Mechanisms. Vol. 1. Interim Report," EPA-600/3-79-001a, U.S. Environmental Protection Agency, Research Triangle Park, North Carolina.

Wilson, D. F., Swinnerton, J. W. and Lamontagne, R. A. (1970), "Production of Carbon Monoxide and Gaseous Hydrocarbons in Seawater: Relation to Dissolved Organic Carbon," Science, Vol. 168, pp. 1577-1579.

Zafiriou, O. C., J. Alford, M. Herrera, E. T. Pelltzer, and R. B. Gagosian (1980), "Formaldehyde in Remote Marine Air and Rain: Flux Measurements and Estimates," Geo. Res. Lett., Vol. 7, No. 5, pp. 341-344.

Zafonte, L., P. L. Rieger, and J. R. Holmes (1976), "Nitrogen Dioxide Photolysis in the Los Angeles Atmosphere," Publication No. DTS-76-18, California Air Resources Board, El Monte, California.

Zimmerman, P. (1977), "Procedures for Conducting Hydrocarbon Emission Inventories of Biogenic Sources and Some Results of Recent Investigations," presented at the 1977 EPA Emission Inventory/Emission Factor Workshop, Raleigh, North Carolina.

Appendix

USE OF STEADY-STATE APPROXIMATIONS IN THE NUMERICAL SOLUTION OF CHEMICAL KINETIC EQUATIONS

In the design and implementation of a photochemical kinetic mechanism for atmospheric applications, considerable thought should be given to the question of computational efficiency. The computational time required to integrate the ordinary differential equations representing the kinetic mechanism used to simulate photochemistry is principally affected by two factors: the number of state variables (chemical species) involved and the stiffness of the equations representing them. Of these two related concerns, the stiffness problem is the more critical.

Stiffness is most easily described for linear systems. For example, consider the system $\dot{y} = My$, where M is a constant matrix whose eigenvalues are all negative but of widely different magnitudes. Classical methods of solution to ordinary differential euqations require a time step small enough to avoid instability of solution for the most rapid time constant. Thus they may require so many time steps that completion of the calculation is not feasible. The situation is analogous, though more complex, for nonlinear systems.

For the solution of chemical kinetic equations not involving atmospheric transport, we use a numerical algorithm based on the method of Gear (1971). Although the Gear algorithms can be used for the kinetic calculations in an airshed model (as they are in the LIRAQ model developed by the Lawrence Livermore Laboratory), they have certain shortcomings. The Gear method is designed for a system in which the solution asymptotically decays to a smooth function. The introduction of discontinuities--such as boundary conditions and hourly changes in input files--into the forcing function of a

Gear solution causes major inefficiencies in computation. These inefficiencies, together with the additional storage requirements of a high-order predictor-corrector method, make such a scheme unattractive for complex, input-driven models.

The numerical method we chose for photochemical dispersion modeling applications is a lower-order method (Crank-Nicholson), which is coupled with the utilization of steady-state approximations to reduce both the number of state variables and the stiffness of the equations of solution. These are complementary goals because the species for which the steady-state approximation is valid are those with the smallest time constants of asymptotic decay--i.e., those whose elimination reduces the stiffness of the ordinary differential equations.

The validity of the steady-state approximation for the concentration of species y is related to the terms in the ordinary differential equation for that species:

$$\dot{y} = P - yD \quad ,$$

where $\dot{y}$ is the time rate of change in the concentration of y, P is the rate of production of y, and yD is the rate of destruction. A steady-state approximation is valid if $P \approx yD >> \dot{y}$. Algebraically, the steady-state concentration is:

$$y_{ss} = \frac{P - \dot{y}}{D} \quad . \qquad (1)$$

Since $P >> \dot{y}$, the above equation is usually written as:

$$y_{ss} = \frac{P}{D} \quad . \qquad (2)$$

Note that $\dot{y}$ need not be zero, but its absolute value must be insignificant compared with either P or yD.

The complexity of an algebraic solution increases as steady-state species that react with each other are added to a mechanism. For example, if species y reacts with itself, then:

$$y_{ss} = \frac{P}{f(y)} \quad , \tag{3}$$

and the solution for y_{ss} becomes quadratic. Similar but more complex situations exist when two or more steady-state species react with each other. The Carbon-Bond Mechanism I, for example, requires a quartic solution. The numerical solution of higher-order algebraic equations can be quite time-consuming, which poses a constraint on mechanism design: the minimization of reactions between steady-state species.

Invoking the steady-state relationship for a species also in effect removes that species from mass balance considerations; i.e., the steady-state expression assumes that $\dot{y} \approx 0$. If $\int|\dot{y}|$ is very small, then removal of this species does not matter. If, however, $\int|\dot{y}|$ is sufficiently different from zero to affect the overall mass balance, then the steady-state assumption produces invalid results.

1. STEADY-STATE RELATIONSHIPS IN THE CARBON-BOND MECHANISM I (CBM-I)

The Carbon-Bond Mechanism I (CBM-I) is listed in table 1. The species we wish to approximate via steady-state relationships are O, OH·, $MeO_2^{\cdot}$, $HCO_3^{\cdot}$, $HO_2^{\cdot}$, $HSO_5^{\cdot}$, $HSO_4^{\cdot}$, and $NO_3^{\cdot}$.

The steady-state approximations for the first and the last of these species are easily obtained, being simply:

$$[O] = \frac{k_1[NO_2]}{k_2[O_2][M] + k_4[NO_2] + k_{18}[OLE] + k_{21}[PAR] + k_{25}[ARO]} \quad , \tag{4}$$

$$[NO_3] = \frac{k_5[O_3][NO_2]}{k_6[NO] + k_7[NO_2][H_2O]} \quad . \tag{5}$$

TABLE 1. THE ORIGINAL FORMULATION OF THE CARBON-BOND MECHANISM

	Reaction	Rate Constant ($ppm^{-1}min^{-1}$)
1	$NO_2 + h\nu \rightarrow NO + O$	*†
2	$O + O_2\ (+ M) \rightarrow O_3\ (+ M)$	2.08×10^{-5}
3	$O_3 + NO \rightarrow NO_2 + O_2$	25.2
4	$O + NO_2 \rightarrow NO + O_2$	1.34×10^{4}
5	$O_3 + NO_2 \rightarrow NO_3 + O_2$	5×10^{-2}
6	$NO_3 + NO \rightarrow NO_2 + NO_2$	1.3×10^{4}
7	$NO_3 + NO_2 + H_2O \rightarrow 2HNO_3$	1.66×10^{-3}§**
8	$NO + NO_2 + H_2O \rightarrow 2HNO_2$	2.2×10^{-9}§
9	$HNO_2 + h\nu \rightarrow NO + OH$	†
10	$NO_2 + OH\cdot \rightarrow HNO_3$	9×10^{3}
11	$NO + OH\cdot \rightarrow HNO_2$	9×10^{3}
12	$CO + OH\cdot \rightarrow CO_2 + HO_2^{\bullet}$	2.06×10^{2}
13	$OLE + OH\cdot \xrightarrow{O_2} HCHO + CH_3O_2^{\bullet}$	3.8×10^{4}
14	$PAR + OH\cdot \xrightarrow{O_2} CH_3O_2^{\bullet} + H_2O$	1.3×10^{3}
15	$ARO + OH\cdot \xrightarrow{O_2} HCHO + CH_3O_2^{\bullet}$	8×10^{3}
16	$OLE + O \xrightarrow{2O_2} HC(O)O_2^{\bullet} + CH_3O_2^{\bullet}$	5.3×10^{3}
17	$PAR + O \xrightarrow{O_2} CH_3O_2^{\bullet} + OH\cdot$	20
18	$ARO + O\cdot \xrightarrow{2O_2} HC(O)O_2^{\bullet} + CH_3O_2^{\bullet}$	37
19	$OLE + O_3 \xrightarrow{O_2} HC(O)O_2^{\bullet} + HCHO + OH\cdot$	0.01

(continued)

TABLE 1

	Reaction	Rate Constant ($ppm^{-1}min^{-1}$)
20	$ARO + O_3 \xrightarrow{O_2} HC(O)O_2^{\bullet} + HCHO + OH\cdot$	0.002
21	$OLE + O_3 \rightarrow Ozonide$	0.005
22	$HCHO + h\nu \xrightarrow{2O_2} HC(O)O_2^{\bullet} + HO_2^{\bullet}$	†
23	$HCHO + h\nu \rightarrow CO + H_2$	4×10^{-4}*
24	$HCHO + OH\cdot \xrightarrow{O_2} HC(O)O_2^{\bullet} + H_2O$	1×10^{4}
25	$HO_2^{\bullet} + NO \rightarrow OH\cdot + NO_2$	2×10^{3}
26	$CH_3O_2^{\bullet} + NO \rightarrow NO_2 + HCHO + HO_2^{\bullet}$	2×10^{3}
27	$HC(O)O_2^{\bullet} + NO \rightarrow NO_2 + CO_2 + HO_2^{\bullet}$	2×10^{3}
28	$H_2O_2 + h\nu \rightarrow OH\cdot + OH\cdot$	†
29	$HO_2^{\bullet} + HO_2^{\bullet} \rightarrow H_2O_2 + O_2$	4×10^{3}
30	$CH_3O_2^{\bullet} + HO_2^{\bullet} \rightarrow H_3COOH + O_2$	4×10^{3}
31	$HC(O)O_2^{\bullet} + HO_2 \rightarrow HC(O)OOH + O_2$	1×10^{4}
32	$HC(O)O_2^{\bullet} + NO_2 \rightarrow PAN$	50
33	$PAN \rightarrow HC(O)O_2^{\bullet} + NO_2$	0.02*
34	$ARO + NO_3 \rightarrow Products$	50
35	$HO_2^{\bullet} + NO_2 \rightarrow HNO_2$	20

---

* Units of min^{-1}.

† Light-dependent.

§ Units of $ppm^{-2}min^{-1}$.

** Rate constant is for the computer simulations of UCR smog-chamber experiments.

(concluded)

TABLE 1. THE ORIGINAL FORMULATION OF THE CARBON-BOND MECHANISM

	Reaction	Rate Constant ($ppm^{-1}min^{-1}$)
1	$NO_2 + h\nu \rightarrow NO + O$	*†
2	$O + O_2\ (+ M) \rightarrow O_3\ (+ M)$	2.08×10^{-5}
3	$O_3 + NO \rightarrow NO_2 + O_2$	25.2
4	$O + NO_2 \rightarrow NO + O_2$	1.34×10^{4}
5	$O_3 + NO_2 \rightarrow NO_3 + O_2$	5×10^{-2}
6	$NO_3 + NO \rightarrow NO_2 + NO_2$	1.3×10^{4}
7	$NO_3 + NO_2 + H_2O \rightarrow 2HNO_3$	1.66×10^{-3}§**
8	$NO + NO_2 + H_2O \rightarrow 2HNO_2$	2.2×10^{-9}§
9	$HNO_2 + h\nu \rightarrow NO + OH$	†
10	$NO_2 + OH\cdot \rightarrow HNO_3$	9×10^{3}
11	$NO + OH\cdot \rightarrow HNO_2$	9×10^{3}
12	$CO + OH\cdot \rightarrow CO_2 + HO_2^{\cdot}$	2.06×10^{2}
13	$OLE + OH\cdot \xrightarrow{O_2} HCHO + CH_3O_2^{\cdot}$	3.8×10^{4}
14	$PAR + OH\cdot \xrightarrow{O_2} CH_3O_2^{\cdot} + H_2O$	1.3×10^{3}
15	$ARO + OH\cdot \xrightarrow{O_2} HCHO + CH_3O_2^{\cdot}$	8×10^{3}
16	$OLE + O \xrightarrow{2O_2} HC(O)O_2^{\cdot} + CH_3O_2^{\cdot}$	5.3×10^{3}
17	$PAR + O \xrightarrow{O_2} CH_3O_2^{\cdot} + OH\cdot$	20
18	$ARO + O\cdot \xrightarrow{2O_2} HC(O)O_2^{\cdot} + CH_3O_2^{\cdot}$	37
19	$OLE + O_3 \xrightarrow{O_2} HC(O)O_2^{\cdot} + HCHO + OH\cdot$	0.01

(continued)

TABLE 1

	Reaction	Rate Constant ($ppm^{-1}min^{-1}$)
20	$ARO + O_3 \xrightarrow{O_2} HC(O)O_2^{\bullet} + HCHO + OH\cdot$	0.002
21	$OLE + O_3 \rightarrow$ Ozonide	0.005
22	$HCHO + h\nu \xrightarrow{2O_2} HC(O)O_2^{\bullet} + HO_2^{\bullet}$	†
23	$HCHO + h\nu \rightarrow CO + H_2$	4×10^{-4}*
24	$HCHO + OH\cdot \xrightarrow{O_2} HC(O)O_2^{\bullet} + H_2O$	1×10^{4}
25	$HO_2^{\bullet} + NO \rightarrow OH\cdot + NO_2$	2×10^{3}
26	$CH_3O_2^{\bullet} + NO \rightarrow NO_2 + HCHO + HO_2^{\bullet}$	2×10^{3}
27	$HC(O)O_2^{\bullet} + NO \rightarrow NO_2 + CO_2 + HO_2^{\bullet}$	2×10^{3}
28	$H_2O_2 + h\nu \rightarrow OH\cdot + OH\cdot$	†
29	$HO_2^{\bullet} + HO_2^{\bullet} \rightarrow H_2O_2 + O_2$	4×10^{3}
30	$CH_3O_2^{\bullet} + HO_2^{\bullet} \rightarrow H_3COOH + O_2$	4×10^{3}
31	$HC(O)O_2^{\bullet} + HO_2 \rightarrow HC(O)OOH + O_2$	1×10^{4}
32	$HC(O)O_2^{\bullet} + NO_2 \rightarrow PAN$	50
33	$PAN \rightarrow HC(O)O_2^{\bullet} + NO_2$	0.02*
34	$ARO + NO_3 \rightarrow$ Products	50
35	$HO_2^{\bullet} + NO_2 \rightarrow HNO_2$	20

* Units of min^{-1}.

† Light-dependent.

§ Units of $ppm^{-2}min^{-1}$.

** Rate constant is for the computer simulations of UCR smog-chamber experiments.

(concluded)

Solving for the other species is a more complicated task, since they are interdependent:

$$[HO_2^{\cdot}] = \frac{k_{12}[CO][OH\cdot] + \alpha k_{23}[HCHO] + k_{27}[MeO_2^{\cdot}][NO] + k_{28}[HCO_3^{\cdot}][NO] + k_{36}[SO_2][MeO_2^{\cdot}]}{k_8[NO_2] + k_{13}[NO] + 2k_{14}[HO_2^{\cdot}] + k_{30}[MeO_2^{\cdot}] + k_{31}[HCO_3^{\cdot}] + k_{34}[HSO_4^{\cdot}] + k_{35}[SO_2]} \tag{6}$$

$$[OH\cdot] = \frac{k_{10}[HNO_2] + k_{13}[HO_2^{\cdot}][NO] + 2k_{16}[H_2O_2] + k_{19}[OLE][O_3] + k_{21}[PAR][O] + k_{26}[ARO][O] + k_{35}[SO_2][HO_2^{\cdot}]}{k_9[NO_2] + k_{11}[NO] + k_{12}[CO] + k_{17}[OLE] + k_{20}[PAR] + k_{22}[HCHO] + k_{24}[ARO] + k_{32}[SO_2]} \tag{7}$$

$$[HCO_3^{\cdot}] = \frac{k_{15}[PAN] + k_{18}[OLE][O] + k_{19}[OLE][O_3] + k_{22}[HCHO][OH\cdot] + \alpha k_{23}[HCHO] + k_{25}[ARO][O] + k_{26}[ARO][O_3]}{k_{28}[NO] + k_{29}[NO_2] + k_{31}[HO_2^{\cdot}]} \tag{8}$$

$$[MeO_2^{\cdot}] = \frac{k_{17}[OLE][OH\cdot] + k_{18}[OLE][O] + k_{20}[PAR][OH\cdot] + k_{21}[PAR][O] + k_{24}[ARO][OH\cdot] + k_{25}[ARO][O]}{k_{27}\,[NO] + k_{30}[HO_2^{\cdot}] + k_{36}[SO_2]} \tag{9}$$

$$[HSO_5^{\cdot}] = \frac{k_{32}[SO_2][OH\cdot]}{k_{33}[NO]} \tag{10}$$

$$[HSO_4^{\cdot}] = \frac{k_{33}[HSO_5^{\cdot}][NO]}{k_{34}[HO_2^{\cdot}]} \tag{11}$$

Note, for example, that the concentration of $HO_2^{\cdot}$ depends upon the concentration of OH·, and vice versa. Moreover,the denominator for $HO_2^{\cdot}$ contains not only $HO_2^{\cdot}$, thus creating a quadratic form for the solution of $HO_2^{\cdot}$, but also the species $MeO_2^{\cdot}$ and $HCO_3^{\cdot}$, creating a quartic.

Obtaining a solvable set of equations is elementary algebra, though somewhat tedious. First, we solve for all species in terms of $HO_2^{\cdot}$.

For the species OH· we have:

$$[OH\cdot] = A_2 + B_2[HO_2^{\cdot}] \quad , \tag{12}$$

where

$$A_2 = \frac{k_{10}[HNO_2] + 2k_{16}[H_2O_2] + k_{19}[OLE][O_3] + k_{21}[PAR][O] + k_{26}[ARO][O_3]}{DENOM_2} ,$$

$$B_2 = \frac{k_{13}[NO] + k_{35}[SO_2]}{DENOM_2} ,$$

$$DENOM_2 = k_9[NO_2] + k_{11}[NO] + k_{12}[CO] + k_{17}[OLE] + k_{20}[PAR] + k_{22}[HCHO] + k_{24}[ARO] + k_{32}[SO_2].$$

For $HCO_3^{\cdot}$, we have

$$[HCO_3^{\cdot}] = \frac{A_3' + B_3'[OH\cdot]}{C_3 + D_3[HO_2^{\cdot}]} = \frac{A_3' + B_3'(A_2 + B_2[HO_2^{\cdot}])}{C_3 + D_3[HO_2^{\cdot}]}$$

$$= \frac{A_3 + B_3[HO_2^{\cdot}]}{C_3 + D_3[HO_2^{\cdot}]} \quad , \tag{13}$$

where

$$A_3 = k_{15}[PAN] + k_{18}[OLE][O] + k_{19}[OLE][O_3] + k_{22}[HCHO]A_2 + \alpha k_{23}[HCHO] + k_{25}[ARO] + [O] + k_{26}[ARO] + [O_3],$$

$$B_3 = k_{22}[HCHO]B_2 ,$$

$$C_3 = k_{28}[NO] + k_{29}[NO_2],$$

$$D_3 = k_{31}.$$

Solving for $MeO_2^{\cdot}$ in terms of $HO_2^{\cdot}$ yields:

$$[MeO_2^{\cdot}] = \frac{A_4' + B_4'[OH\cdot]}{C_4 + D_4[HO_2^{\cdot}]} = \frac{A_4' + B_4'(A_2 + B_2[HO_2^{\cdot}])}{(C_4 + D_4)[HO_2^{\cdot}]} = \frac{A_4 + B_4[HO_2^{\cdot}]}{C_4 + D_4[HO_2^{\cdot}]} \quad , \tag{14}$$

where

$$A_4' = k_{18}[OLE][O] + k_{21}[PAR][O] + k_{25}[ARO][O],$$
$$A_4 = A_4' + B_4'A_2,$$
$$A_4 = [O](k_{18}[OLE] + k_{21}[PAR] + k_{25}[ARO]) + B_4'A_2,$$
$$B_4' = k_{17}[OLE] + k_{20}[PAR] + k_{24}[ARO],$$
$$B_4 = B_4'B_2,$$
$$C_4 = k_{27}[NO] + k_{36}[SO_2],$$
$$D_4 = k_{30}.$$

It then remains to solve for $[HO_2^{\cdot}]$:

$$\begin{aligned} 0 = {} & 2k_{14}[HO_2^{\cdot}]^2 + k_8[NO_2][HO_2^{\cdot}] + k_{13}[NO][HO_2^{\cdot}] + k_{35}[SO_2][HO_2^{\cdot}] + k_{30}[MeO_2^{\cdot}][HO_2^{\cdot}] \\ & + k_{31}[HCO_3^{\cdot}][HO_2^{\cdot}] - \alpha k_{23}[HCHO] - k_{12}[CO][OH\cdot] + k_{32}[SO_2][OH\cdot] \\ & - k_{27}[NO][MeO_2^{\cdot}] - k_{36}[SO_2][MeO_2^{\cdot}] \overset{-}{+} k_{28}[NO][HCO_3^{\cdot}] \quad . \end{aligned} \tag{15}$$

Rearranging terms, we obtain:

$$2k_{14}[HO_2^{\cdot}]^2 + [HO_2^{\cdot}]\left(A_1' + B_1'[MeO_2^{\cdot}] + C_1'[HCO_3^{\cdot}]\right) + D_1'[OH\cdot] + E_1'[MeO_2^{\cdot}]$$

$$+ F_1'[HCO_3^{\cdot}] + G_1' = 0 \quad , \qquad (16)$$

where

$A_1' = k_8[NO_2] + k_{13}[NO] + k_{35}[SO_2]$,
$B_1' = k_{30}$,
$C_1' = k_{31}$,
$D_1' = -k_{12}[CO] + k_{32}[SO_2]$,
$E_1' = -k_{27}[NO] - k_{36}[SO_2]$,
$F_1' = -k_{28}[NO]$,
$G_1' = -\alpha k_{23}[HCHO]$.

Substituting for $[MeO_2^{\cdot}]$, $[HCO_3^{\cdot}]$, and $[OH\cdot]$ in the above equation, we get:

$$2k_{14}[HO_2^{\cdot}]^2 + [HO_2^{\cdot}] \quad A_1' + B_1'\frac{A_4 + B_4[HO_2^{\cdot}]}{C_4 + D_4[HO_2^{\cdot}]} + C_1'\frac{A_3 + B_3[HO_2^{\cdot}]}{C_3 + D_3[HO_2^{\cdot}]}$$

$$+ D_1'\left(A_2 + B_2[HO_2^{\cdot}]\right) + E_1'\frac{A_4 + B_4[HO_2^{\cdot}]}{C_4 + D_4[HO_2^{\cdot}]} + F_1'\frac{A_3 + B_3[HO_2^{\cdot}]}{C_3 + D_3[HO_2^{\cdot}]}$$

$$+ G_1' = 0 \quad , \qquad (17)$$

which can be rewritten as:

$$\begin{aligned}
&2k_{14}[HO_2^{\cdot}]^2(C_4 + D_4[HO_2^{\cdot}])(C_3 + D_3[HO_2^{\cdot}]) \\
&\quad + [HO_2^{\cdot}]\Big[A_1'(C_3 + D_3[HO_2^{\cdot}])(C_4 + D_4[HO_2^{\cdot}]) \\
&\quad + B_1'(C_3 - D_3[HO_2^{\cdot}])(A_4 + C_4[HO_2^{\cdot}]) \\
&\quad + C_1'(A_3 + B_3[HO_2^{\cdot}])(C_4 + D_4[HO_2^{\cdot}])\Big] \\
&\quad + D_1'(A_2 + B_2[HO_2^{\cdot}])(C_3 + D_3[HO_2^{\cdot}])(C_4 + D_4[HO_2^{\cdot}]) \\
&\quad + E_1'(A_4 + B_4[HO_2^{\cdot}])(C_3 + D_3[HO_2^{\cdot}]) \\
&\quad + F_1'(A_3 + B_3[HO_2^{\cdot}])(C_4 + D_4[HO_2^{\cdot}]) \\
&\quad + G_1'(C_3 + D_3[HO_2^{\cdot}])(C_4 + D_4[HO_2^{\cdot}]) = 0 \quad . \qquad (18)
\end{aligned}$$

By collecting terms we obtain:

$$\begin{aligned}
&[HO_2^{\cdot}]^4(2k_{14}D_4D_3) \\
&+ [HO_2^{\cdot}]^3\,[2k_{14}(C_3D_4 + C_4D_3) + A_1'D_3D_4 + B_1'D_3B_4 + C_1'B_3D_4 + D_1'B_2D_3D_4] \\
&+ [HO_2^{\cdot}]^2[2k_{14}C_4C_3 + A_1'(C_4D_3 + C_3D_4) + B_1'(A_4D_3 + B_4C_3) + C_1'(A_3D_4 + B_3C_4) \\
&\qquad + D_1'\left\{B_2C_4D_3 + D_4(B_2C_3 + A_2D_3)\right\} + E_1'B_4D_3 + F_1'B_3D_4 \\
&\qquad + G_1'D_3D_4] \\
&\qquad + [HO_2^{\cdot}][A_1'C_3C_4 + B_1'A_4C_3 + C_1'A_3C_2 + D_1'\ \ A_2C_3D_4 \\
&\qquad + C_4(B_2C_3 + A_2D_3) + E_1'(B_4C_3 + A_4D_3) + F_1'(A_3D_4 + B_3C_4) \\
&\qquad + G_1'(C_3D_4 + C_4D_3)] \\
&\qquad + D_1'A_2C_3C_4 + E_1'A_4C_3 + F_1'A_3C_4 + G_1'C_3C_4 = 0 \quad . \qquad (19)
\end{aligned}$$

This is admittedly a messy equation; one can see why we suggest that the kinetic mechanism be designed to eliminate higher order terms if possible. However, the above equation may be solved via the Newton-Raphson approximation. For $g(x) = 0$

$$x_{n+1} = x_n - \frac{g(x_n)}{g'(x_n)} \quad . \qquad (20)$$

For the equation for $HO_2^{\cdot}$, we can define:

$$g = E + [HO_2^{\cdot}]\Big[D + [HO_2^{\cdot}]\ \{C + [HO_2^{\cdot}](B + A[HO_2^{\cdot}])\}\Big] \quad , \qquad (21)$$

$$g' = D + [HO_2^{\cdot}]\ \Big[2C + [HO_2^{\cdot}](3B + 4A[HO_2^{\cdot}])\Big] \quad . \qquad (22)$$

Once the concentration of OH has been calculated $[HSO_5^{\cdot}]$ and $[HSO_4^{\cdot}]$ can be calculated from Eqs. (10) and (11).

2. ADDITIONAL ALTERATIONS IN THE SOLUTION OF THE CARBON-BOND MECHANISM

a. Nighttime Chemistry

Simulation of the chemical reactions occurring as the sun sets and at night presents computational problems that are not immediately apparent. As the sun sets, the rates of production of many radicals approach zero. At night the production rates are zero. Hence the steady-state approximations for those radicals become indeterminate. Moreover, all of the reactions in the Carbon-Bond Mechanism that produce nitric oxide (NO) are photolytic; therefore, the production rate of NO becomes zero at night. In the presence of O_3, the predicted concentration of NO at night tends rapidly toward zero because of Reaction (23).

$$NO + O_3 \rightarrow NO_2 \quad . \qquad (23)$$

Finite difference solutions become inefficient when predicting a rapid zero asymptote. The time step required for avoiding negative concentrations becomes small. In addition, because the destruction rates of some radicals (e.g., the radicals produced by ozone-olefin reactions) are principally dependent upon the concentrations of NO, the concentrations of those radicals, as calculated using the steady-state approximation, become large. These concentrations force the NO concentration to zero even faster.

It should be mentioned that Gear-type calculations also have some difficulty with nighttime chemistry. LIRAQ, for example, requires a significant amount of extra computational time to simulate sunset. Our CHEMK routine, which uses a Gear calculation, checks for species with very low concentrations (those asymptotically approaching zero) and sets them identically equal to zero in order to maintain computational efficiency.

To solve the problems in simulating nighttime chemistry, we chose to truncate the chemical reaction set. In other words, we produced a special reaction set for the nighttime case. The Nighttime Chemistry Module consists of the following reactions:

$$O_3 + NO \rightarrow NO_2 \tag{24}$$

$$O_3 + OLE \rightarrow 2HCHO \tag{25}$$

$$NO + NO + O_2 \rightarrow NO_2 \tag{26}$$

$$PAN + NO \rightarrow 2NO_2 + HO_2^{\cdot} + HCHO \tag{27}$$

$$HO_2^{\cdot} + NO \rightarrow NO_2 + OH\cdot \tag{28}$$

$$OH\cdot + NO_2 \rightarrow HNO_3 \tag{29}$$

$$OH\cdot + NO \rightarrow HNO_2 \tag{30}$$

One reaction sequence from SO_2 chemistry is also included:

$$SO_2 + OH\cdot \rightarrow HSO_5 \qquad (31)$$

$$HSO_5^{\cdot} + NO \rightarrow NO_2 + HSO_4^{\cdot} \qquad (32)$$

$$HSO_4^{\cdot} + NO_2 \rightarrow H_2SO_4 + HNO_3 \qquad (33)$$

Reaction (24) is assumed to be instantaneous; the actual time constant for the reaction is about a minute. Note that Reactions (26) through (33) depend on the presence of NO. At low concentrations of NO these reactions become negligible.

The rate of Reaction (27) is calculated from the ratio of NO to total NO_x. The actual reaction sequence is

$$PAN \rightleftarrows RCO_3^{\cdot} + NO_2 \quad , \qquad (34)$$

$$RCO_3^{\cdot} + NO \rightarrow NO_2 + HO_2^{\cdot} + RCHO + CO_2 \quad . \qquad (35)$$

The rate at which PAN decomposes depends upon the ratio of the reactions of $RCO_3^{\cdot}$ with NO and with NO_2. In the absence of NO, PAN is stable.

The ozone/olefin reaction [Reaction (25) in the nighttime set] cannot result in NO-to-NO_2 conversions because O_3 and NO cannot coexist at night. Thus, any radical products formed in ozone/olefin reactions must take other pathways. We assume that the end products of the ozone/olefin reaction are aldehydes and ignore the intermediate steps.

The mechanism described here accounts for the following features of nighttime chemistry:

> The O_3 + NO scavenging reaction
> The self-oxidation of NO at high concentrations

- > The oxidation of olefins by ozone
- > The decay of PAN in the presence of NO.

The Nighttime Chemistry Module also has the attractive feature that for the nighttime hours, when the rates of change of pollutant concentrations are low, computation is very fast, two to three times as fast as for the daytime.

b. Elimination of the Species H_2O_2 and HNO_2

Hydrogen peroxide (H_2O_2) affects the predictions of the Carbon-Bond Mechanism only through its photolysis via the reaction:

$$H_2O_2 + h\nu \rightarrow OH\cdot + OH\cdot \quad .$$

The rate constant for this reaction is low, and the reaction typically provides less than 10 percent of the number of radicals supplied by aldehyde photolysis. The photolysis of H_2O_2 may therefore be omitted from simulations without significantly affecting predictions. This omission allows the elimination of H_2O_2 as a state variable with the attendant computational savings. The reaction of $HO_2^{\cdot}$ with itself:

$$HO_2^{\cdot} + HO_2^{\cdot} \rightarrow \quad , \tag{36}$$

then becomes a permanent radical sink.

HNO_2 presents a slightly more complex situation than H_2O_2. The HNO_2 concentration is determined by the reactions:

$$HNO_2 + h\nu \rightarrow NO + OH\cdot \quad , \tag{37}$$

$$NO + OH\cdot \rightarrow HNO_2 \quad . \tag{38}$$

In smog chamber experiments with a constant irradiation flux, the photolysis of HNO_2 may be an important initial radical source. In simulations in which the irradiation flux changes slowly (like the diurnal variation in sunlight), the initial radical source is less important, and so the need to include HNO_2 in the mechanism is questionable. Similarly, the action of HNO_2 as a temporary radical sink in the morning and a radical source in the afternoon is probably much less important than the similar role played by PAN.

Figures 1 and 2 show isopleths of ozone concentrations produced by the Carbon-Bond Mechanism with and without the inclusion of H_2O_2 and HNO_2. The close similarity of those plots indicates the feasibility of omitting those species from the mechanism.

c. The Steady-State Estimation of NO, NO_2, and O_3 Concentrations

As noted previously, invoking a steady-state approximation for a chemical species removes that species from mass balance considerations. This limitation presents a problem in the use of the steady-state relationship for major species such as NO, NO_2, and O_3. It is well known that those three species are in a dynamic equilibrium with a time constant much lower than those of the rest of the nonradical chemical kinetic system. The dynamic equilibrium established very nearly satisfies the equation:

$$k_3[O_3][NO] = k_1[NO_2] \quad . \qquad (39)$$

Unfortunately, the NO, NO_2, and O_3 concentrations are all important to the mass balance, and the use of any two of those concentrations to calculate the third leads to erroneous results. [For a discussion of this, see Anderson et al. (1977, Appendix A, p. 246).] Since late 1976, we have been using the correction factor approach to the calculation of equilibrium concentrations for the NO, NO_2, O_3 triad. This factor can be determined from the fact that a certain quantity of NO_2 must photolyze to produce NO and O_3 for nonequilibrium concentrations of NO_2, NO, and O_3 to reach equilibrium:

$$K_3(O_3 + \Delta_{ss})(NO + \Delta_{ss}) = k_1(NO_2 - \Delta_{ss}) \quad . \qquad (40)$$

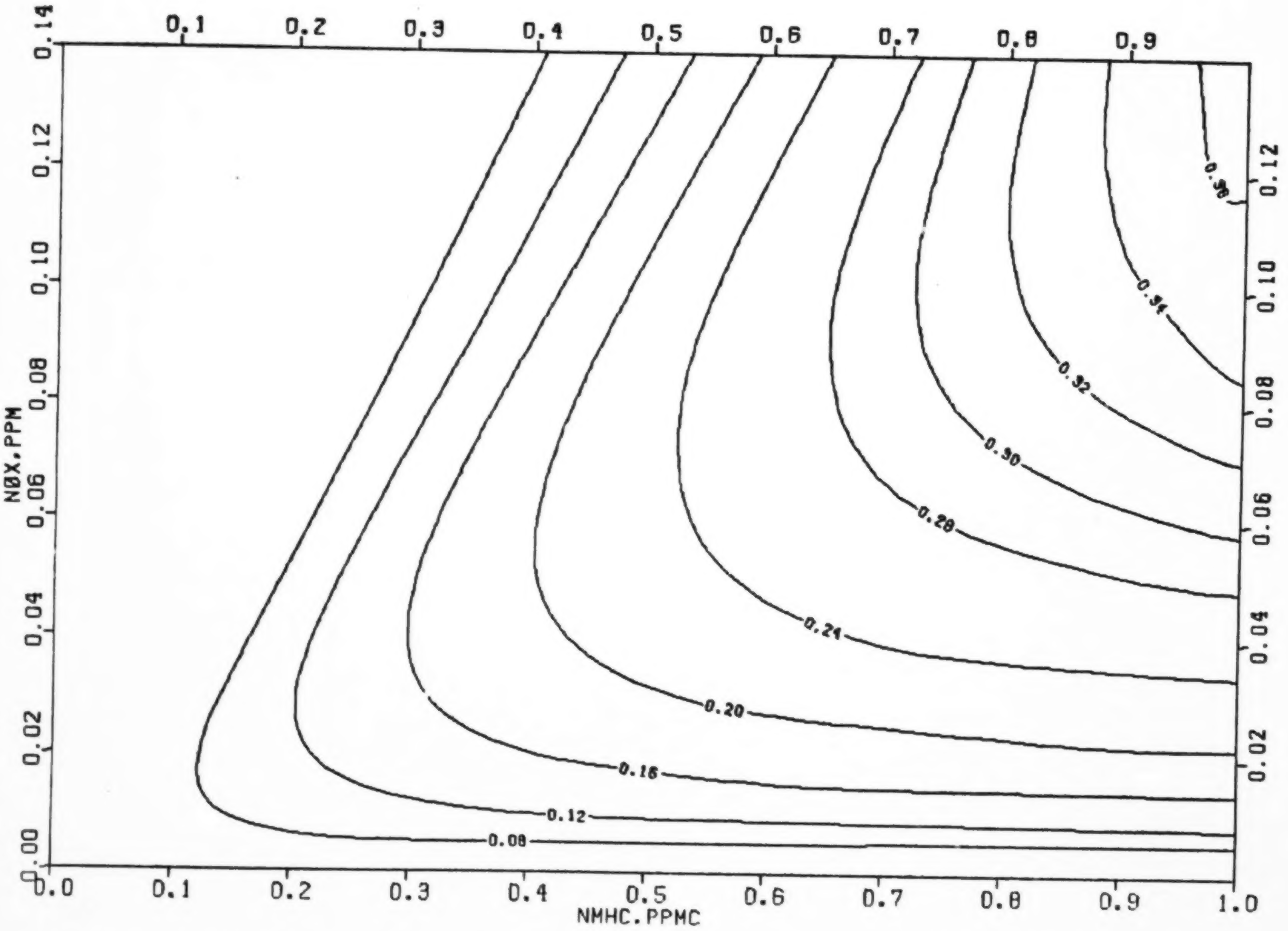

FIGURE 1. ISOPLETHS OF MAXIMUM ONE-HOUR-AVERAGE OZONE CONCENTRATIONS (ppm) IN SIMULATIONS USING THE CARBON-BOND MECHANISM I WITH HNO_2 AND H_2O_2 CHEMISTRY

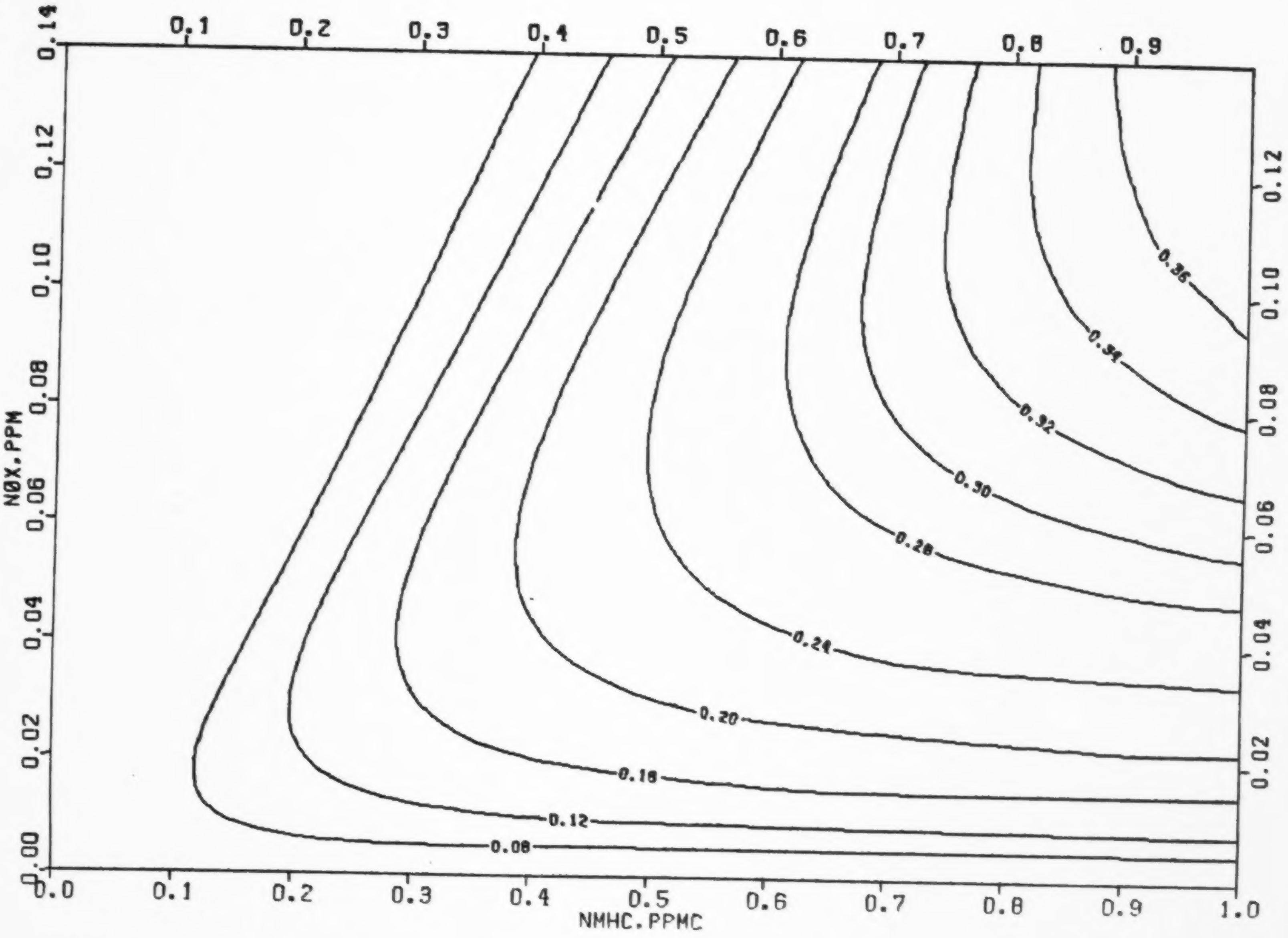

FIGURE 2. ISOPLETHS OF MAXIMUM ONE-HOUR-AVERAGE OZONE CONCENTRATIONS (ppm) IN SIMULATIONS USING THE CARBON-BOND MECHANISM I WITHOUT HNO_2 AND H_2O_2 CHEMISTRY

Therefore,

$$k_3\left\{(O_3)(NO) + \Delta_{ss}[(NO) + (O_3)] + \Delta_{ss}^2\right\} = k_1(NO_2) = k_1\Delta_{ss} \quad , \qquad (41)$$

and from the quadratic formula we obtain:

$$\begin{aligned}\Delta_{ss} = &- \frac{1}{2}\left([O_3] + [NO] + \frac{k_1}{k_3}\right)\\ &+ \frac{1}{2}\left\{\left([O_3] + [NO] + \frac{k_1}{k_3}\right)^2\right.\\ &\left.- 4\left([NO][O_3] - \frac{k_1}{k_3}[NO_2]\right)\right\}^{1/2} \quad , \qquad (42)\end{aligned}$$

so that

$$[NO_2]_{ss} = [NO_2] - \Delta_{ss} \qquad (43)$$

$$[NO]_{ss} = [NO] + \Delta_{ss} \qquad (44)$$

$$[O_3]_{ss} = [O_3] + \Delta_{ss} \qquad (45)$$

If we were to redefine our state variables as NO_x and unpaired oxygen (O_x), where $NO_x = NO + NO_2$ and $O_x = NO_2 + O_3$, then the correction factor equation becomes:

$$\begin{aligned}\Delta_{ss} = &- \frac{1}{2}\left([O_x] + [NO_x] + \frac{k_1}{k_3}\right)\\ &+ \frac{1}{2}\left\{\left([O_x] + [NO_x] + \frac{k_1}{k_3}\right)^2\right.\\ &\left.- 4\,[NO_x][O_x]\right\}^{1/2} \quad , \qquad (A\text{-}46)\end{aligned}$$

and NO-to-NO_2 conversions now become the creators of unpaired oxygen.

Thus, by mapping the three species--O_3, NO, and NO_2--into two species, we eliminate one species and reduce the stiffness of the system by eliminating the differential solution of the three-species equilibrium.

We should point out here that the algebraic estimate of the triad described above is only an estimate. If we include in the calculations the reactions of oxidizing radicals that convert NO to NO_2:

$$NO + HO_2^{\cdot} \rightarrow NO_2 + OH\cdot \quad , \tag{47}$$

$$NO + MeO_2^{\cdot} \rightarrow NO_2 + HCHO + HO_2^{\cdot} \quad , \tag{48}$$

$$NO + HCO_3^{\cdot} \rightarrow NO_2 + HO_2^{\cdot} \quad , \tag{49}$$

the steady-state approximation of the equilibrium becomes nearly exact, but the steady-state equations then become impossibly cumbersome. In the following section we attempt to demonstrate that the triad approximation given above is sufficiently accurate for our purposes.

Figure 3 presents the predicted concentrations in simulations of a smog chamber experiment using the program CHEMK (with Gear-type numerics) for the Carbon-Bond Mechanism. We present results for the Carbon-Bond Mechanism both with and without HNO_2 and H_2O_2 as state variables. Since the experiment used a constant irradiation flux, the differences between predictions are larger than one would expect for simulations of experiments using diurnal sunlight, as noted previously. Even so, the maximum difference is only about 20 percent, and less than that if a small initial concentration of HNO_2 is assumed in the simulations.

We present the simulations in Figure 3 as a baseline for comparison with simulations based on finite difference solution methods. The HC/NO_x ratio used, 6.25, is near that of typical urban simulations. A moderate

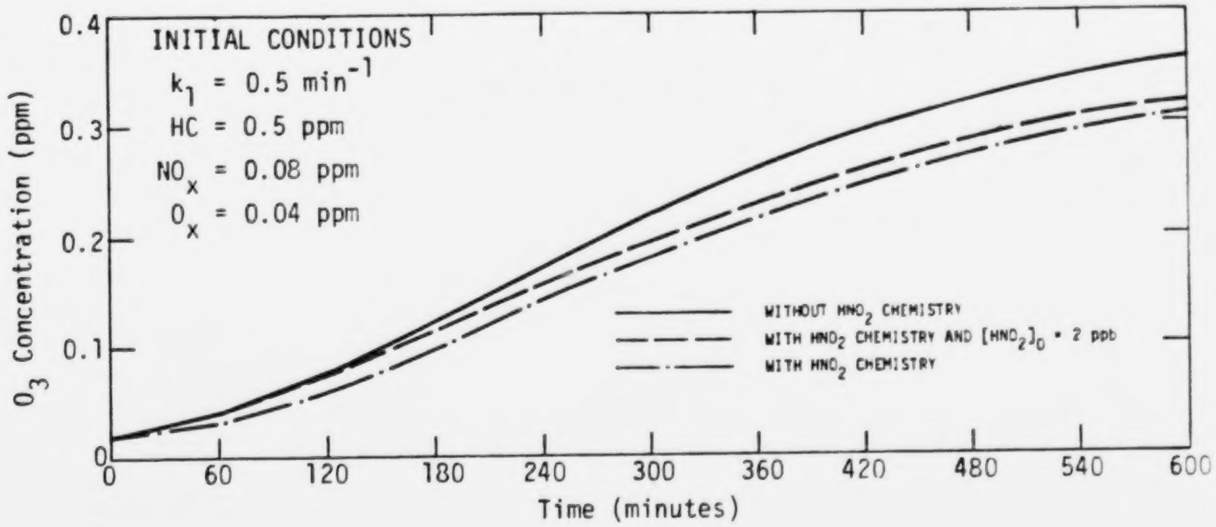

FIGURE 3. OZONE CONCENTRATIONS CALCULATED WITH THE CARBON-BOND MECHANISM (CBM-I) WITH AND WITHOUT HNO_2 CHEMISTRY

concentration of ozone is generated in the simulations. We know from previous experience that the differences between ozone concentrations calculated using different numerical computation schemes under these circumstances are similar to the maximum that one might expect.

Figure 4 shows the results obtained using the Carbon-Bond Mechanism with CHEMK and with the finite difference scheme presently used in the SAI Airshed Model. Five-minute time steps were used. The figure shows results for the Carbon-Bond Mechanism both with and without HNO_2 and H_2O_2 chemistry. Note that the difference between the CHEMK and finite difference calculations, for the same mechanism, does not exceed 5 percent.

Figure 5 shows the same simulations made with the $NO/NO_2/O_3$ triad in a steady-state equilibrium. The differences between the CHEMK and finite difference calculations are slightly greater when the steady-state triad is assumed (about 10 percent early in the run), but the overall comparison is favorable. Table 2 gives the computational times required for finite difference simulations such as those in Figures 4 and 5. As may be seen, assuming a steady-state triad for NO, NO_2, and O_3 markedly decreases the computational time. Simulations with and without the steady-state triad give essentially the same results even with 30-minute time steps, but the simulation with the steady-state for NO, NO_2, and O_3 requires only one-third of the computing time for any time step $\leq$ 30 minutes. The standard scheme (without the steady-state triad) has degraded accuracy at 15-minute time steps and will not converge for longer time steps.

Our conclusions are as follows:

- The Carbon-Bond Mechanism with the steady-state triad for NO, NO_2, and O_3 has three fewer species than the standard mechanism and requires correspondingly lower computation and storage costs (about 20 percent lower).
- The steady-state triad permits the use of a time step of 30 minutes or more. Computational costs for time steps

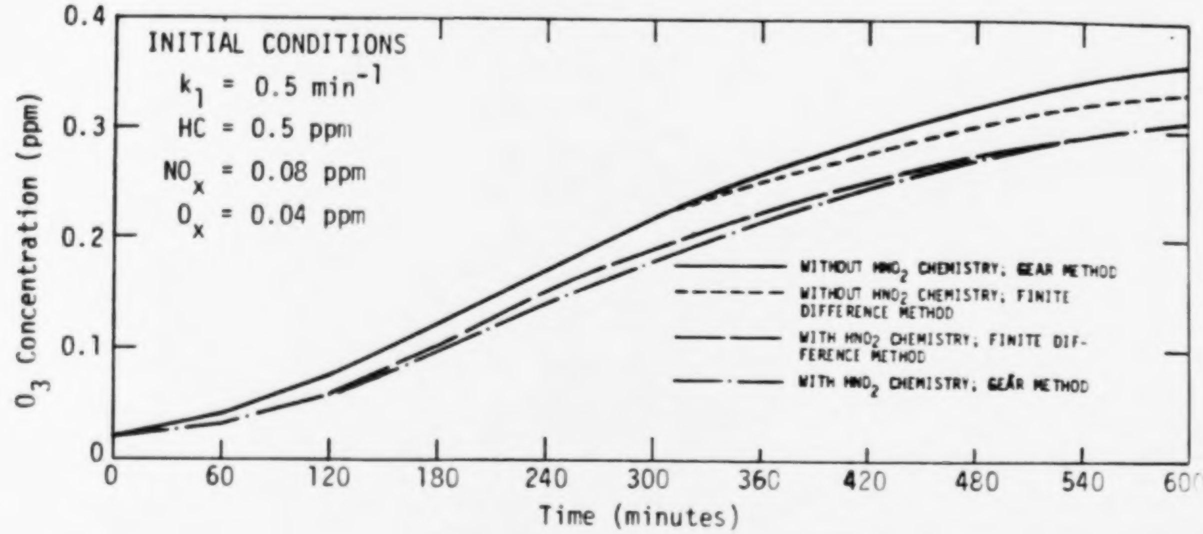

FIGURE 4. OZONE CONCENTRATIONS CALCULATED WITH THE CARBON-BOND MECHANISM (CBM-I) USING GEAR AND FINITE DIFFERENCE SOLUTION METHODS

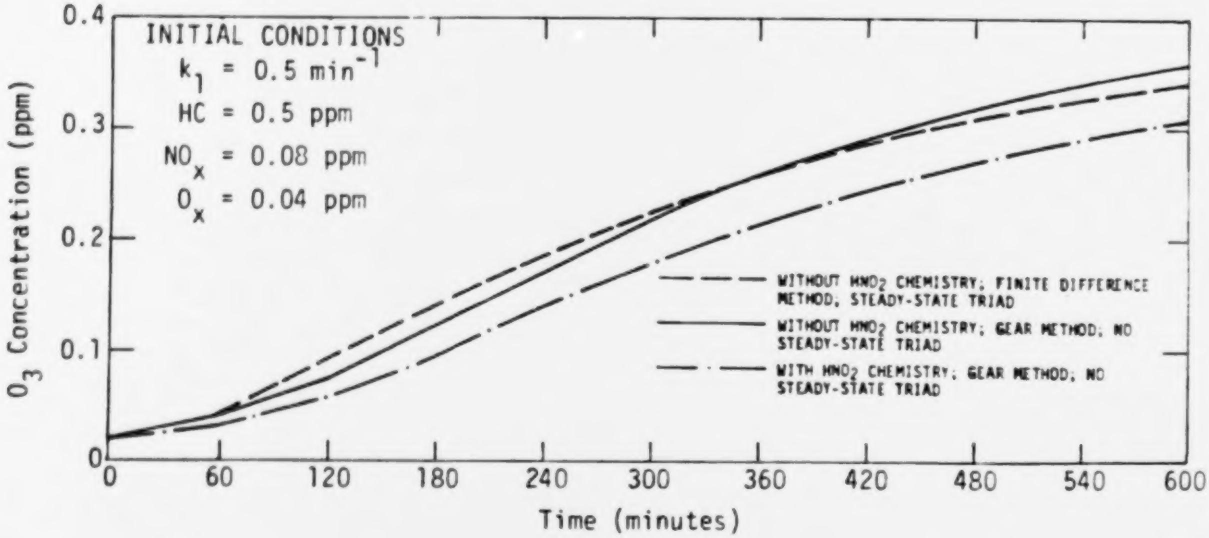

FIGURE 5. OZONE CONCENTRATIONS CALCULATED WITH THE CARBON-BOND MECHANISM (CBM-I) WITH AND WITHOUT THE STEADY-STATE NO, NO_2, O_3 TRIAD

TABLE 2. COMPUTATION TIMES REQUIRED TO SIMULATE A SIX-HOUR CONSTANT IRRADIATION SMOG CHAMBER EXPERIMENT WITH THE CARBON-BOND MECHANISM

(seconds)

Time Step (minutes)	Standard Finite Difference Solution (with HNO_2 and H_2O_2 Chemistry)	Standard Finite Difference Solution (without HNO_2 and H_2O_2 Chemistry)	Steady-State Triad Solution
5	0.402	0.368	0.259
15	--	0.185	0.095
30	--*	--*	0.055

---

* Solution does not converge.

up to 30 minutes are roughly inversely proportional to the time step.

> Use of longer time steps degrades the results from the standard chemistry but not those from the chemistry with the steady-state triad. Therefore, the time step used should be made as long as is permitted by the transport scheme.

3. STEADY-STATE RELATIONSHIPS IN CARBON-BOND MECHANISM-II

Algebraic steady-state approximations have been utilized in the implementation of CBM-II in both the SAI Urban Airshed Model and the SAI Reactive Plume Model (RPM). Two versions of the Reactive Plume Model are the same except for the numerical solution of the chemical kinetics scheme. RPM-2B uses the Gear-Hindemarsh method, and RPM-26 uses the same finite difference (plus steady-state approximations) used in the Urban Airshed Model. Thus, a comparison of RPM-2B and RPM-2C can be made to test the validity of the finite difference and steady-state approximation.

4. COMPARISON OF THE RPM-2B AND RPM-2C MODELS

Since large-scale fossil-fuel-burning power plants are typically very efficient combustion devices, emissions from such major point sources consist of large quantities of nitrogen oxides (NO_x), whereas the emissions of hydrocarbon are usually not significant. It is well known that ozone in excess of ambient levels can be formed in the atmosphere only when both nitrogen oxides and hydrocarbons are present under conditions of sunlight. Thus, the formation of ozone downwind of fossil-fuel-burning power plants, as observed by Davis et al. (1974) and Miller et al. (1978), is dependent on the presence of concentrations of ambient hydrocarbons outside of the plume. Generally, ambient nonmethane hydrocarbon concentrations range from 0.04 ppm to 1.0 ppm, with values as high as 2.0 ppm found in the Los Angeles basin. For this reason, four comparisons of the RPM-2B and RPM-2C models were run using ambient levels of nonmethane hydrocarbons of 0.01, 0.15, 0.52, and 1.04 ppm. The hydrocarbon splits and the emissions from a typical fossil-fuel burning plant for these runs are displayed in Tables 3 and 4, respectively.

The comparison of results for the RPM-2B and RPM-2C models at the four levels of ambient hydrocarbons for the three species NO, NO_2, and O_3 are displayed in Figures 6, 7, and 8, respectively. Under conditions of low ambient hydrocarbon concentrations, the results for the two models are in close agreement. As the ambient hydrocarbon level is raised, the difference in results for the two models increases; this is caused by the increasing importance of the radical reactions at high levels of hydrocarbon concentrations. As expected, the steady-state chemistry in the RPM-2C model tends to act more rapidly; thus, the conversion rates of NO to NO_2, and of NO_2 to O_3 are faster, resulting in more rapid formation of ozone. It should be noted that in all cases the peak ozone concentrations are about the same for both versions, with the RPM-2C model reaching a peak ozone concentration about ten minutes earlier than the RPM-2B model. The RPM-2C model also tends to predict more rapid ozone decay, as is evident in the high ambient-level hydrocarbon tests runs. The maximum difference in the results of the two models for the three species of NO_2, NO, and O_3 is displayed in Table 5.

TABLE 3.

RELATIVE HYDROCARBON COMPOSITION OF TEST RUNS

Hydrocarbon Species	Percentage (by Volume)
Paraffins	63.5
Olefins	2.1
Ethylenes	2.1
Carbonyls	5.4
Aromatics	26.9
BZA	0.002
PAN	0.0001

TABLE 4.

EMISSIONS USED IN TEST RUNS

Species	Emissions Rate (gms/sec)
NO_2	41
NO	238
SO_2	238

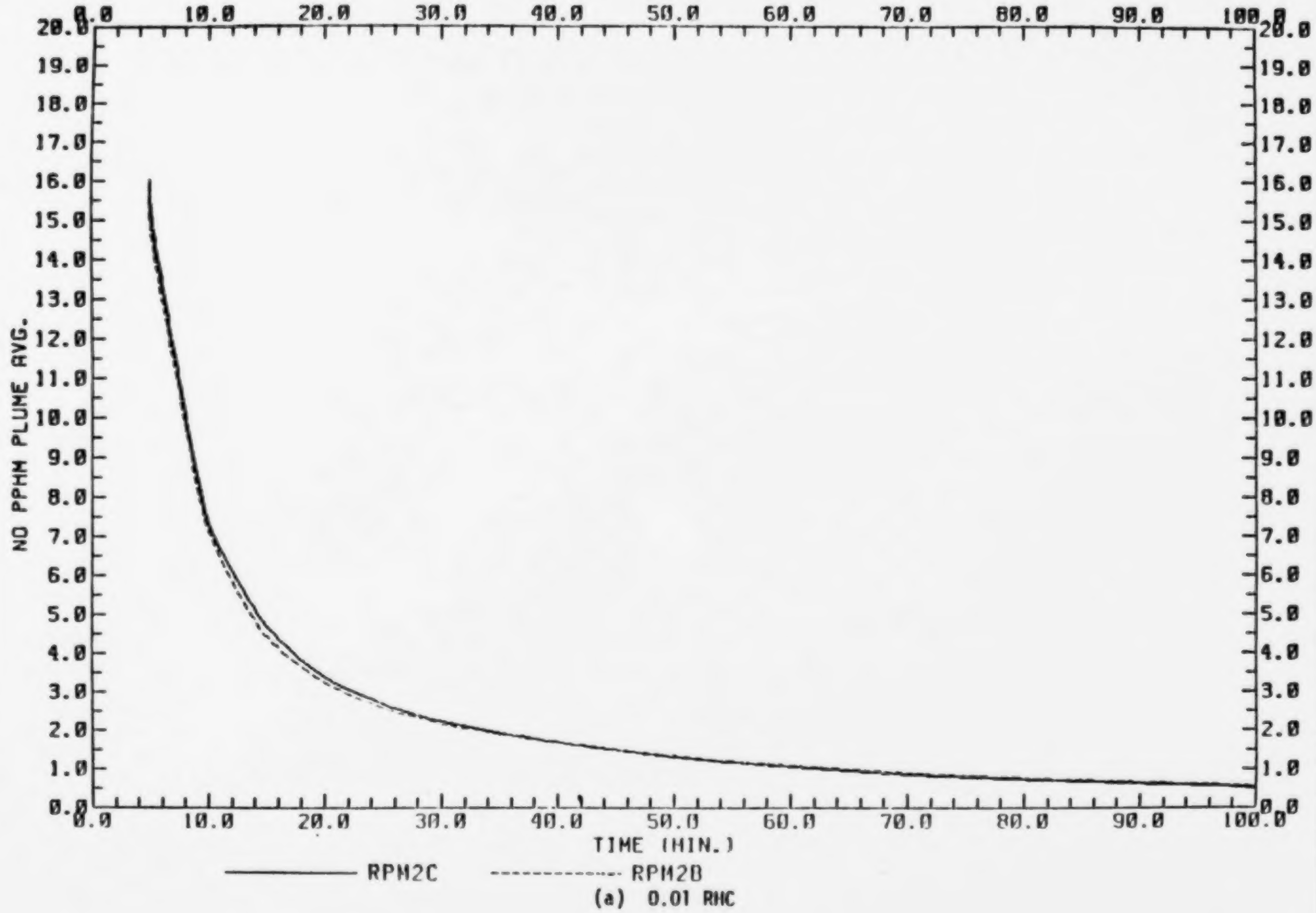

FIGURE 6. **Comparison of NO predictions for the RPM2C and RPM2B models.**

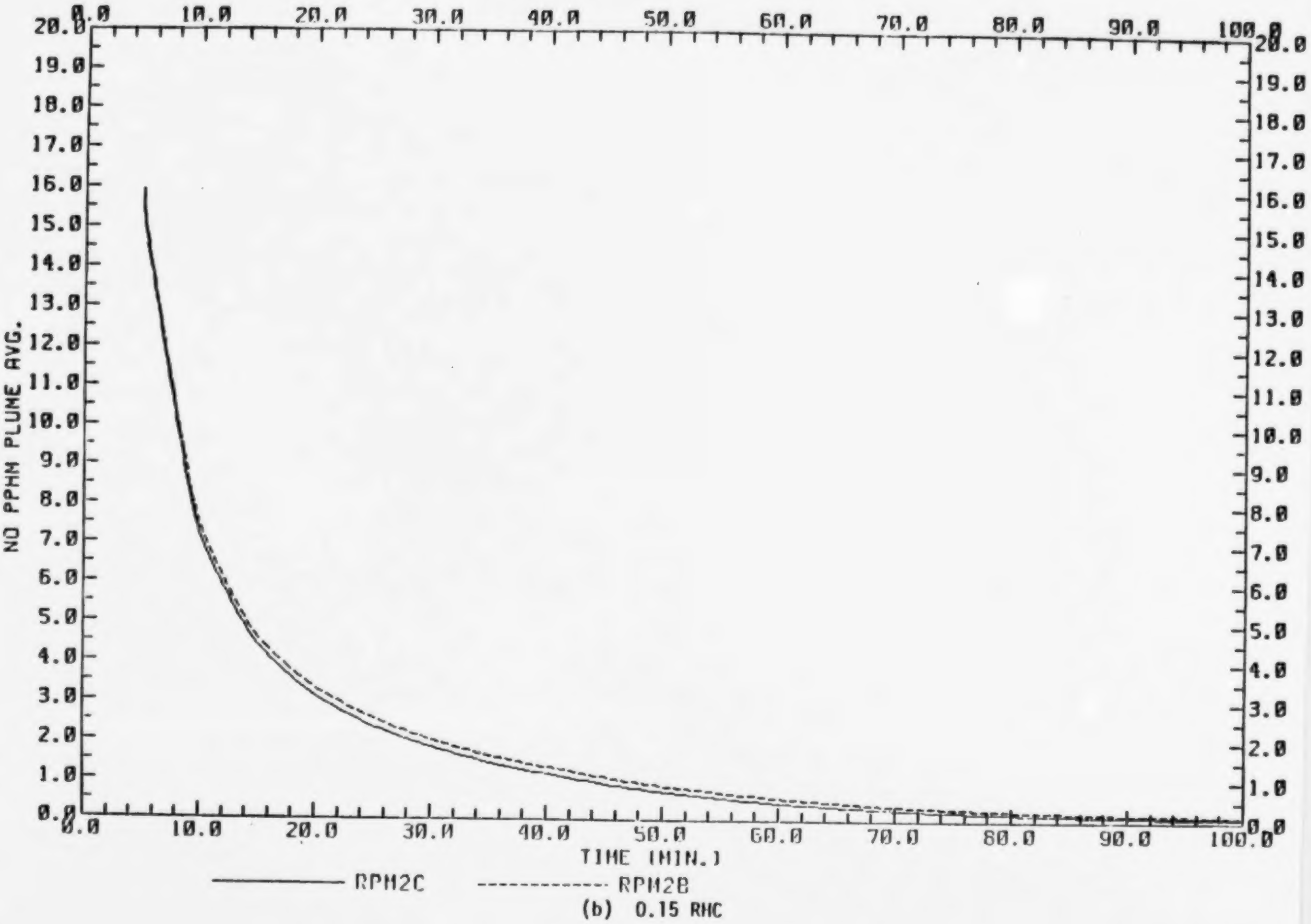

(b) 0.15 RHC

FIGURE 6. **(continued).**

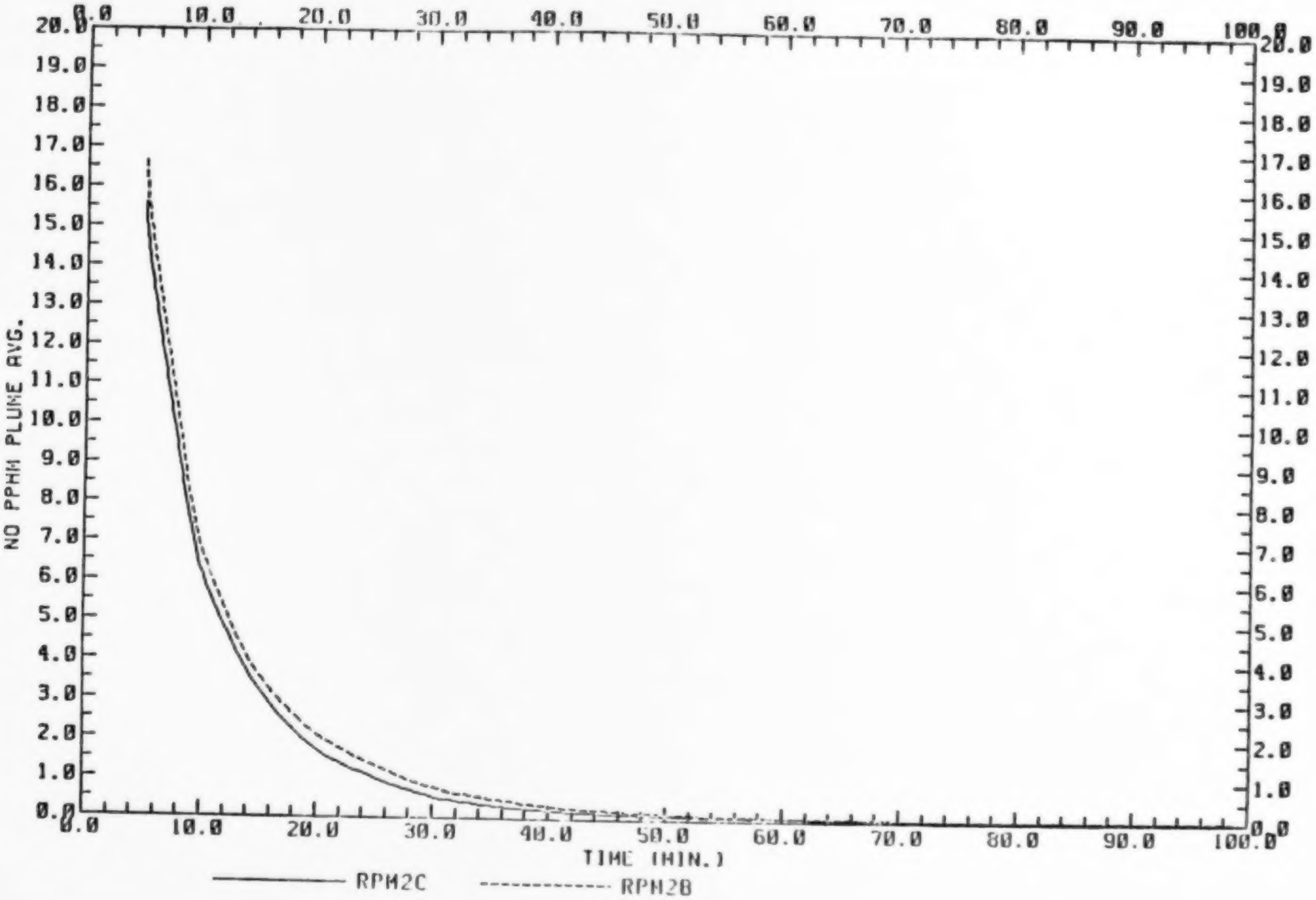

(c) 0.52 RHC

FIGURE 6. **(continued).**

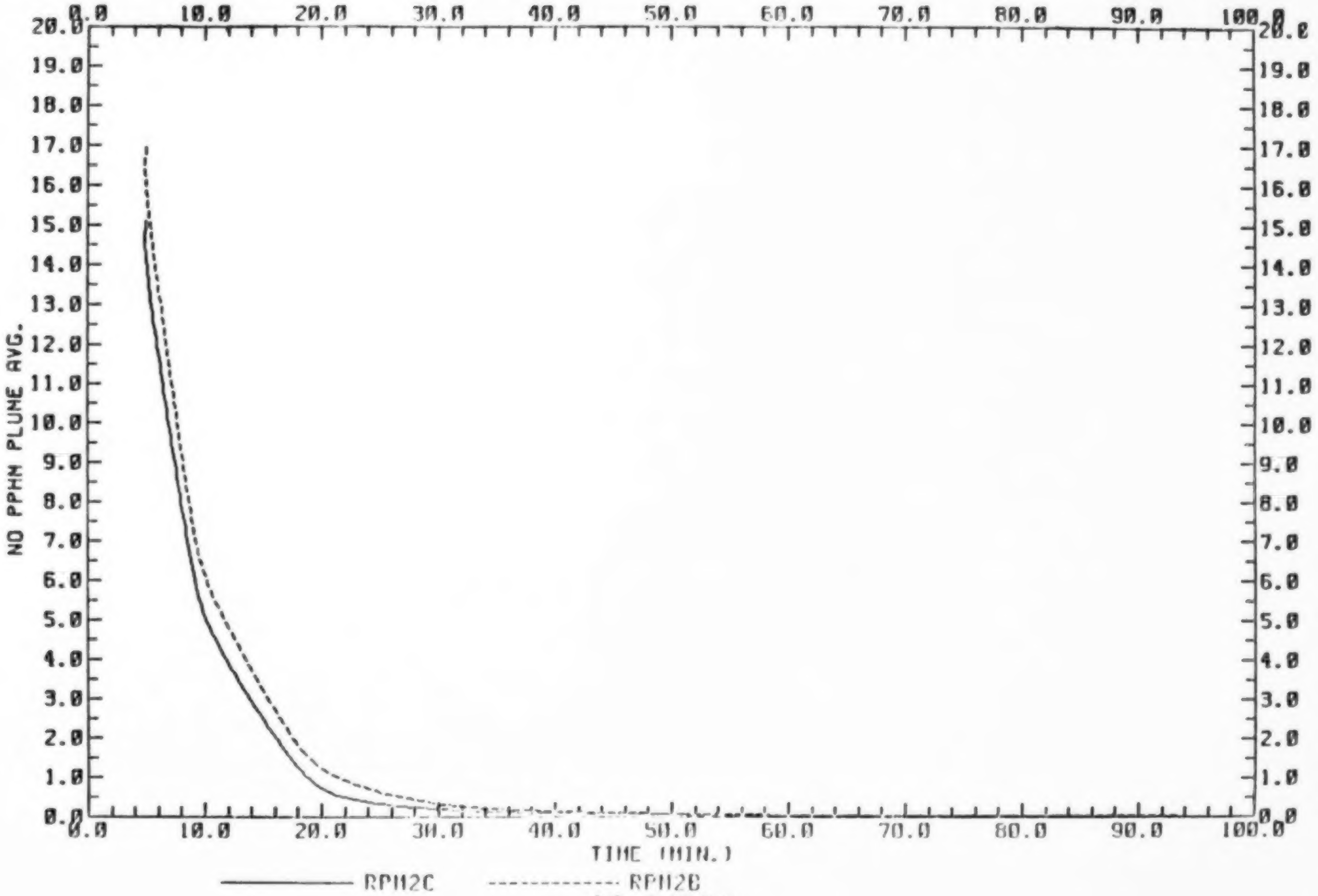

(d) 1.04 RHC

FIGURE 6. **(concluded).**

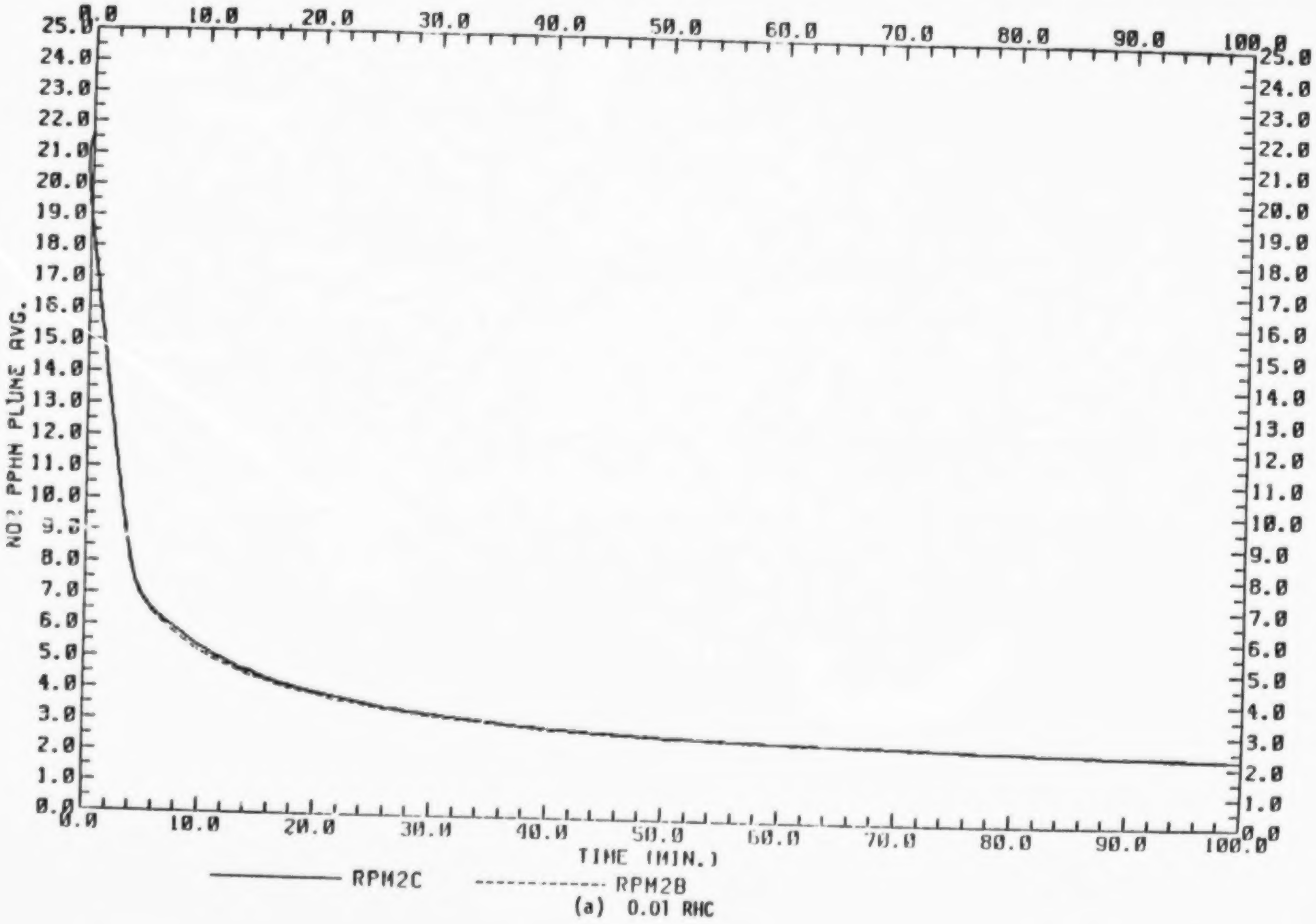

FIGURE 7. Comparison of NO_2 predictions for the RPM2C and RPM2B models.

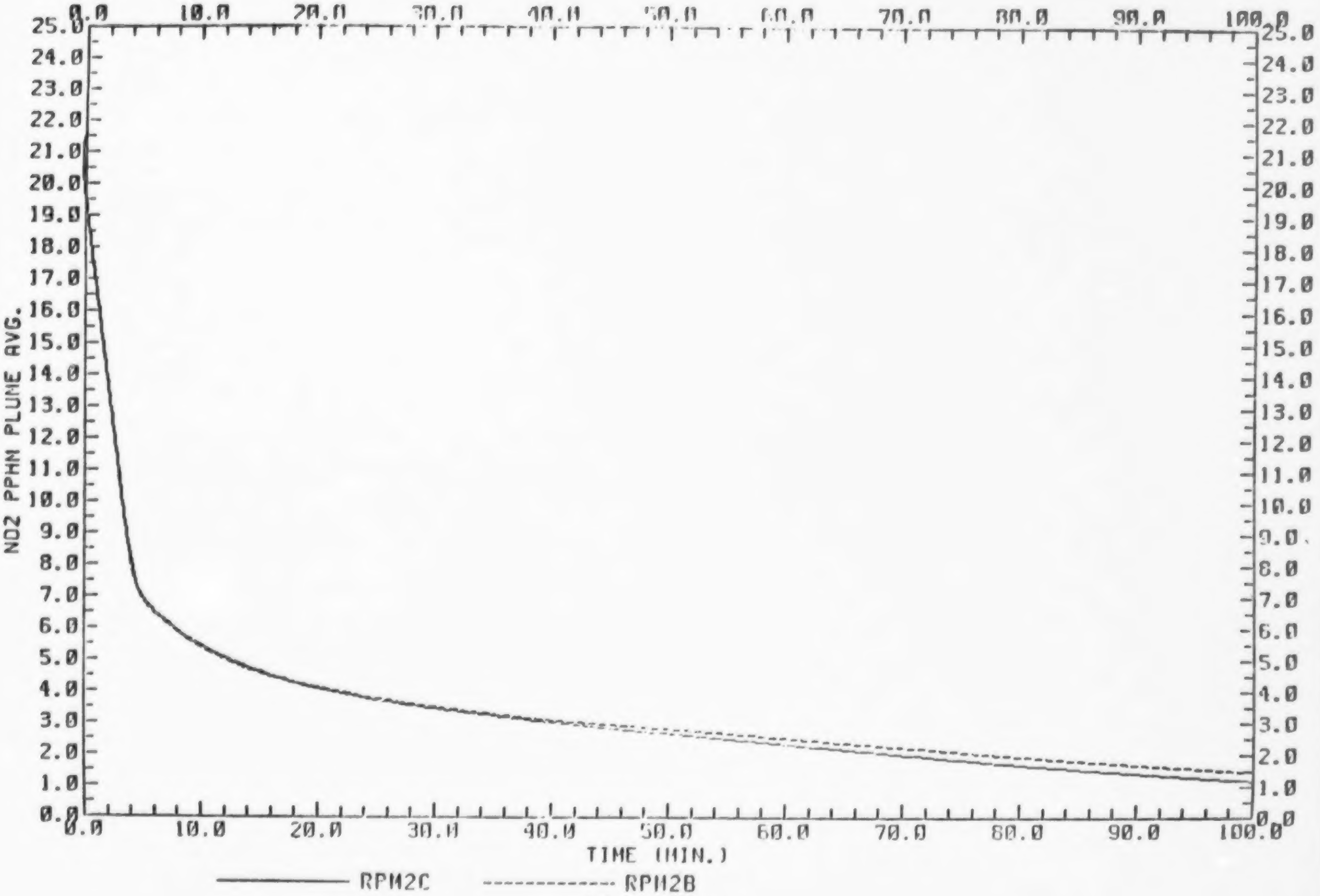

(b) 0.15 RHC

FIGURE 7. **(continued).**

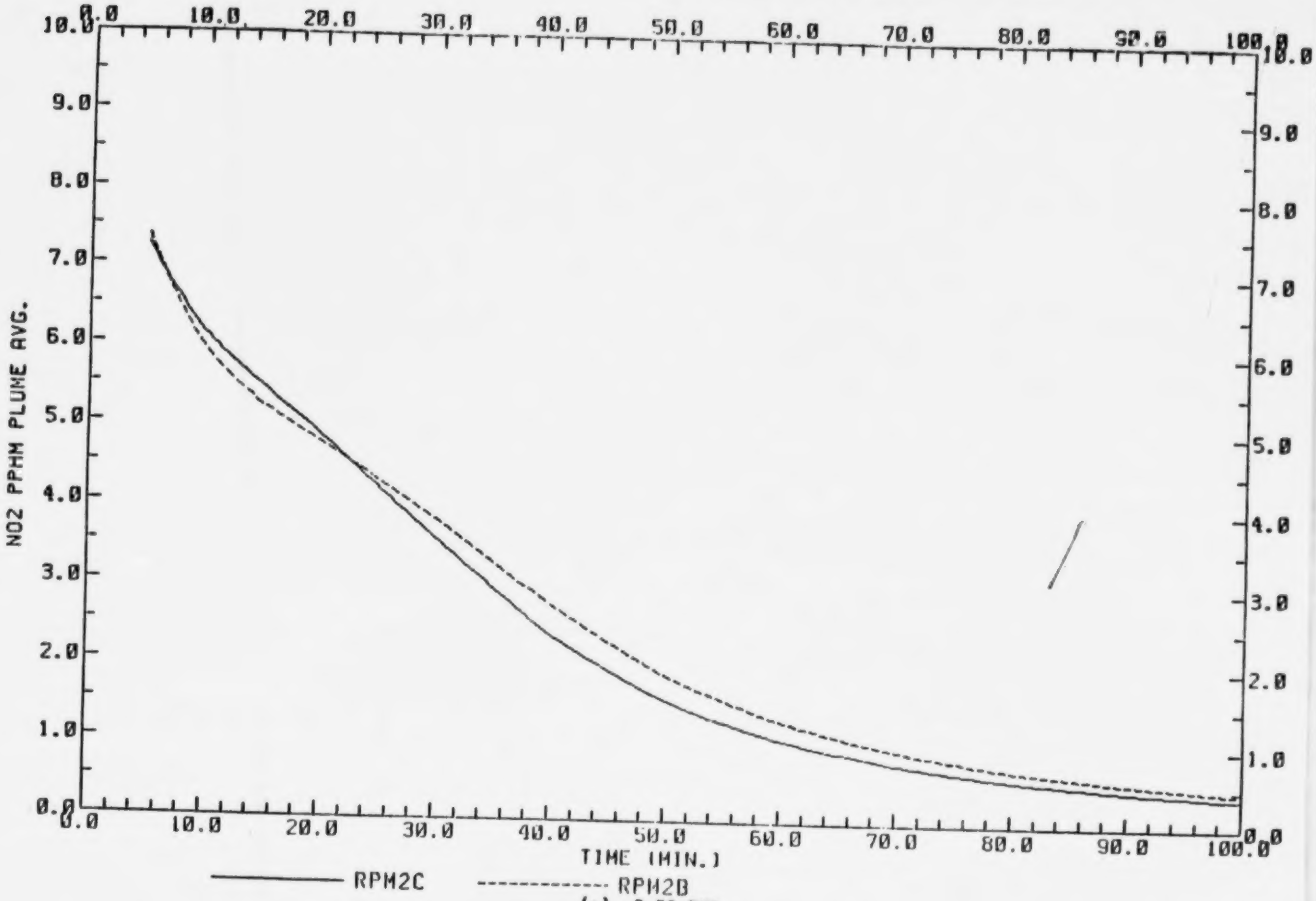

(c) 0.52 RHC

FIGURE 7. **(continued).**

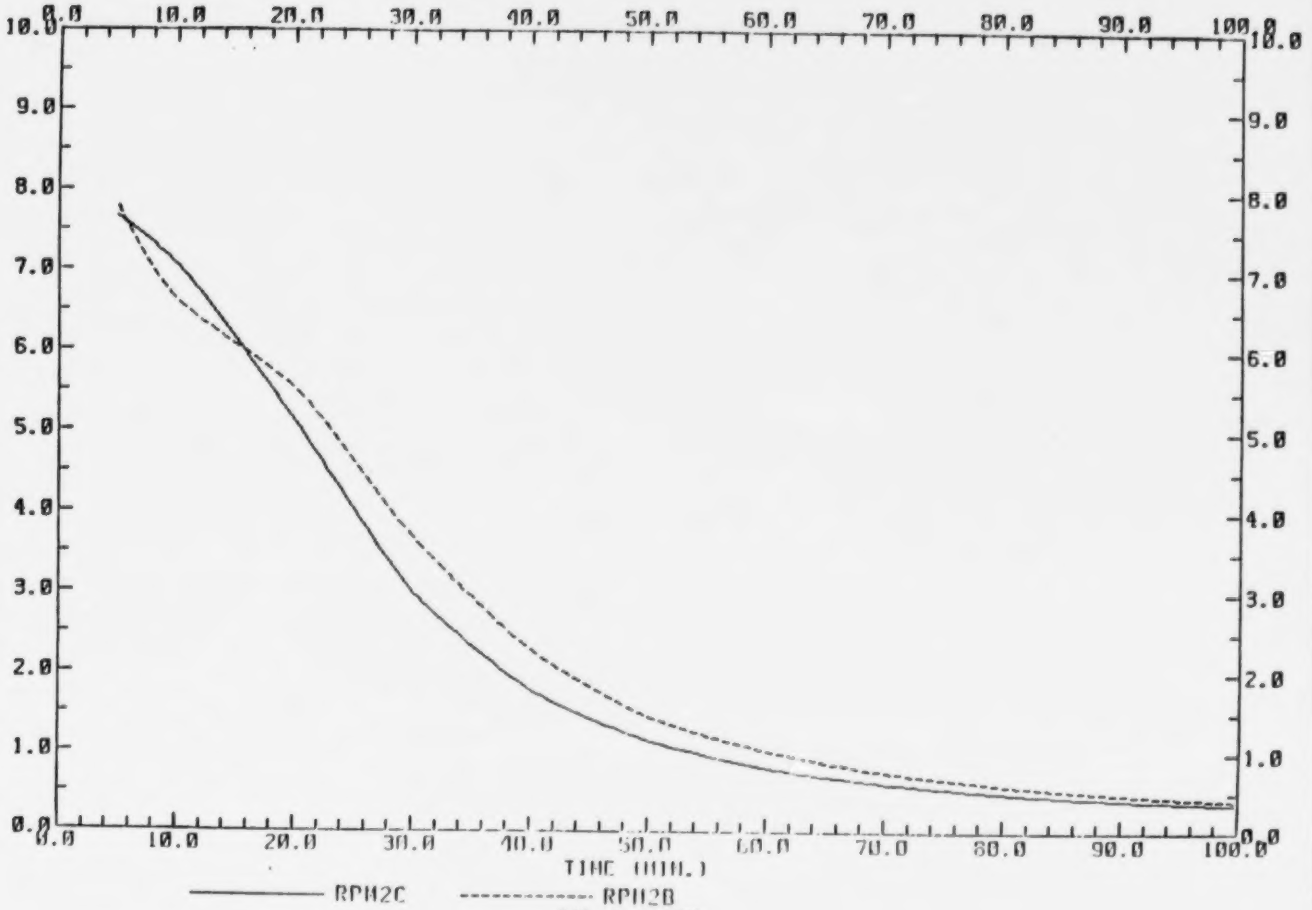

(d) 1.04 RHC

FIGURE 7. **(concluded).**

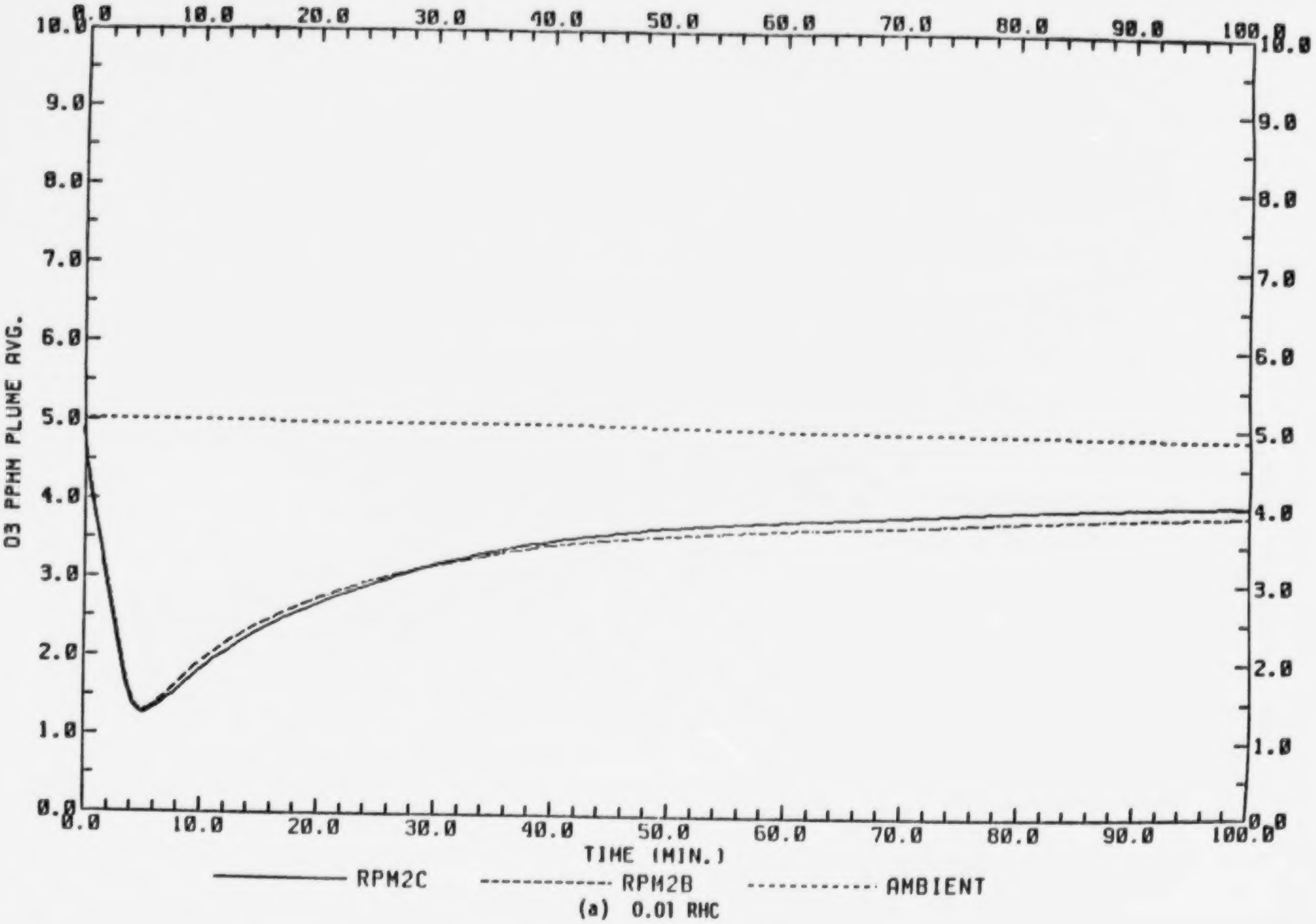

FIGURE 8. **Comparison of O_3 predictions for the RPM2C and RPM2B models.**

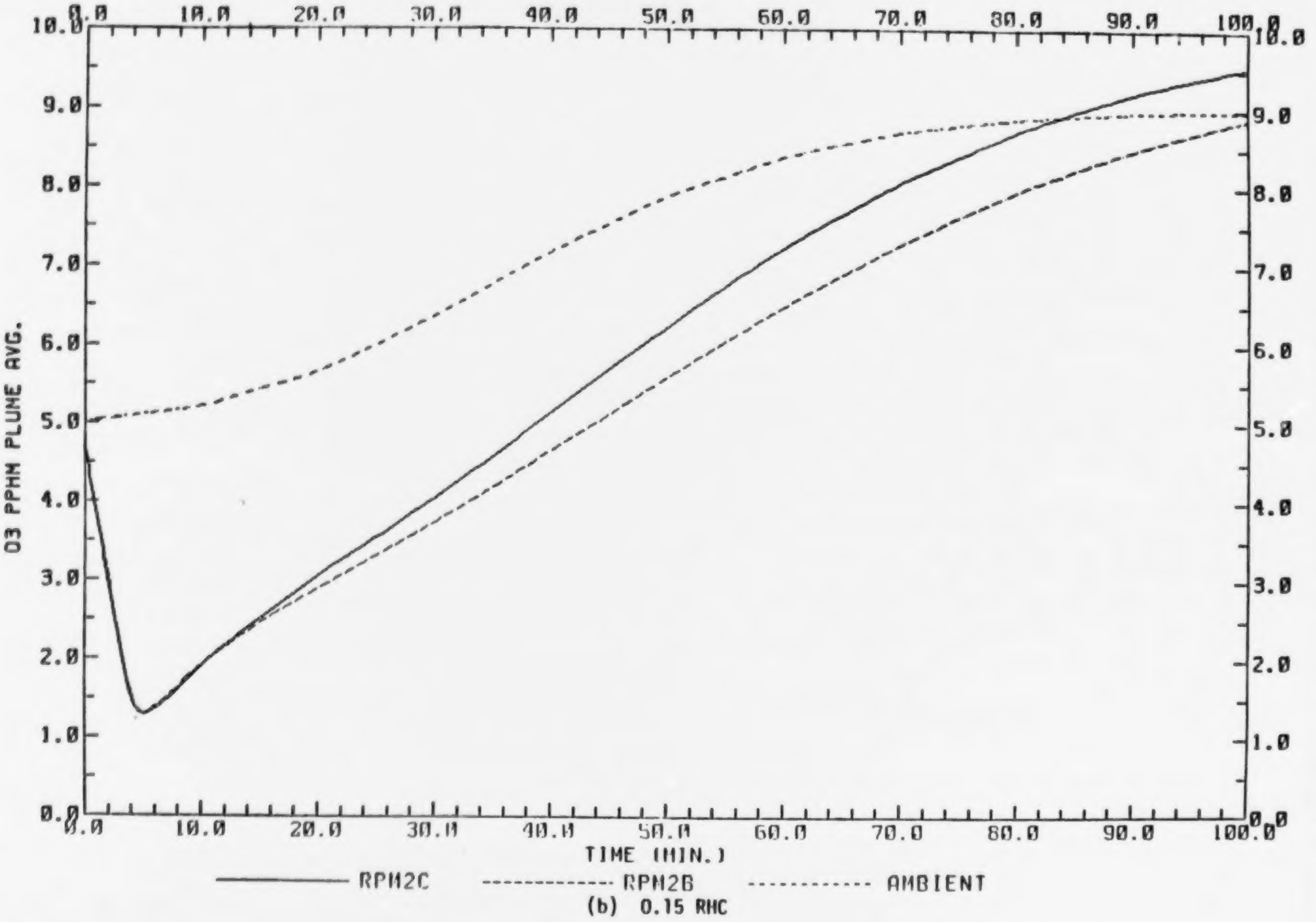

(b) 0.15 RHC

FIGURE 8. **(continued).**

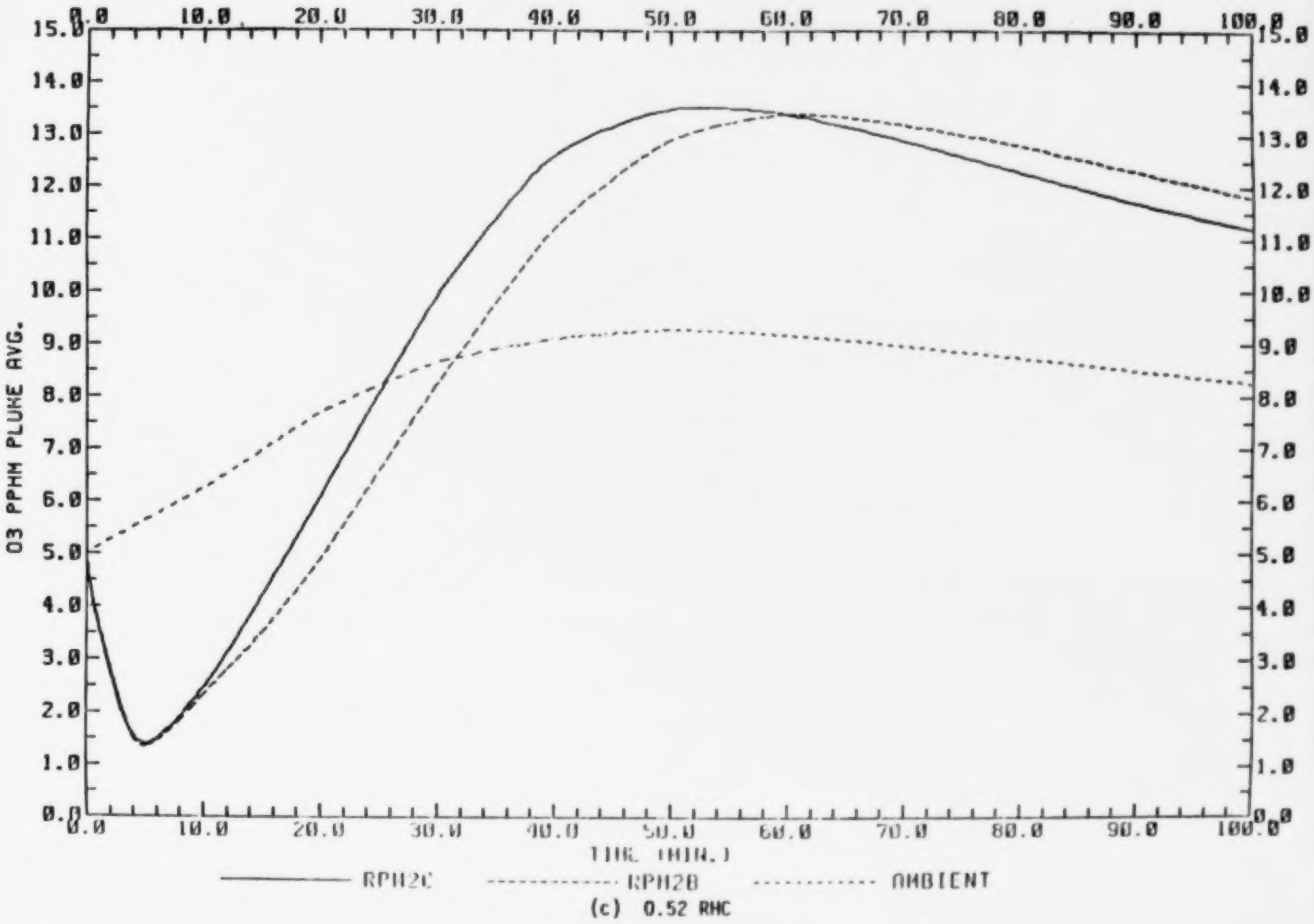

(c) 0.52 RHC

FIGURE 8. **(continued).**

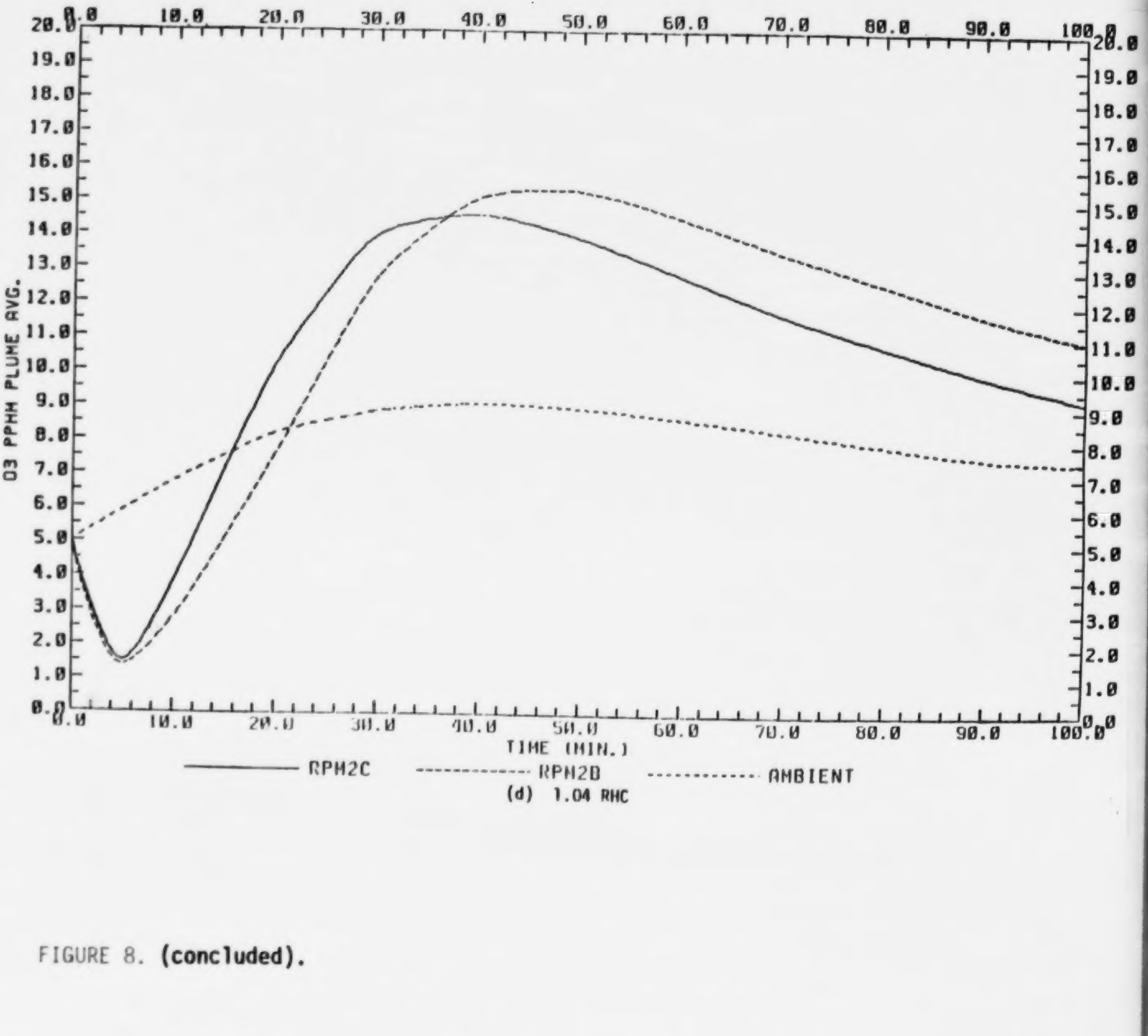

(d) 1.04 RHC

FIGURE 8. **(concluded).**

TABLE 5.

MAXIMUM DIFFERENCES BETWEEN PREDICTIONS OF THE RPM-2C AND RPM-2B MODELS FOR THE FOUR AMBIENT LEVELS OF HYDROCARBONS*

Chemical Species	Ambient Level of Reactive Hydrocarbons (ppm)			
	0.01	0.15	0.52	1.04
NO				
Absolute difference	0.005	-0.0024	-0.011	-0.019
Relative difference	0.03	-0.03	-0.06	-0.11
Time of occurrence (min.)	5	10	5	5
NO_2				
Absolute difference	0.0013	-0.0027	-0.0038	-0.0068
Relative difference	0.03	-0.18	-0.13	-0.19
Time of occurrence (min.)	10	100	40	30
O_3				
Absolute difference	0.0014	0.0078	0.0169	0.0261
Relative difference	0.04	0.11	0.21	0.40
Time of occurrence (min.)	100	70	30	20

---

* Differences expressed as [RPM-2C] - [RPM-2B] (absolute difference) and ([RPM-2C] - [RPM-2B])/[RPM-2B] (relative difference).